THE STATIC AND MAGNUS AERODYNAMIC CHARACTERISTICS OF THE M823 RESEARCH STORE EQUIPPED WITH FIXED AND FREELY SPINNING STABILIZERS

Frank J. Regan, et al

Naval Ordnance Laboratory
White Oak, Maryland

1 December 1972

NOLTR 72-291

THE STATIC AND MAGNUS AERODYNAMIC CHARACTERISTICS OF THE M823 RESEARCH STORE EQUIPPED WITH FIXED AND FREELY SPINNING STABILIZERS

By
Frank J. Regan
Mary E. Falusi

1 DECEMBER 1972

NOL

NAVAL ORDNANCE LABORATORY, WHITE OAK, SILVER SPRING, MARYLAND

UNCLASSIFIED

Security Classification

DOCUMENT CONTROL DATA - R & D

(Security classification of title, body of abstract and indexing annotation must be entered when the overall report is classified)

1 ORIGINATING ACTIVITY (Corporate author) Naval Ordnance Laboratory White Oak, Silver Spring, Maryland 20910	2a. REPORT SECURITY CLASSIFICATION UNCLASSIFIED 2b. GROUP

3 REPORT TITLE

The Static and Magnus Aerodynamic Characteristics of the M823 Research Store Equipped with Fixed and Freely Spinning Stabilizers

4 DESCRIPTIVE NOTES (Type of report and inclusive dates)

5 AUTHOR(S) (First name, middle initial, last name)

Frank J. Regan
Mary E. Falusi

6 REPORT DATE 1 December 1972	7a. TOTAL NO. OF PAGES 154	7b. NO. OF REFS 9
8a. CONTRACT OR GRANT NO. b. PROJECT NO. c. A320-320C/WF32-323-201 d. RMMO-42-005/212-1/F008-09-001	9a. ORIGINATOR'S REPORT NUMBER(S) NOLTR 72-291 9b. OTHER REPORT NO(S) (Any other numbers that may be assigned this report)	

10. DISTRIBUTION STATEMENT

APPROVED FOR PUBLIC RELEASE; DISTRIBUTION UNLIMITED.

11. SUPPLEMENTARY NOTES	12. SPONSORING MILITARY ACTIVITY Naval Air Systems Command Washington, D. C. 20360

13. ABSTRACT

This report is the first in a two-part series of technical reports on the dynamics and aerodynamics of free-fall stores using freely spinning stabilizers. Presented herein are the results of recent wind-tunnel measurements of the normal force, pitching moment and Magnus force and moment on the M823 Research Store in transonic flow. Comparisons are made between configurations equipped with fixed and freely spinning stabilizers, with regard to sign and relative magnitude of the Magnus force and moment. A method is presented and applied whereby the Magnus force and moment are corrected for flow angularity.

DD FORM 1 NOV 1473 (PAGE 1)

S/N 0101-807-6801

UNCLASSIFIED

Security Classification

14 KEY WORDS	LINK A		LINK B		LINK C	
	ROLE	WT	ROLE	WT	ROLE	WT
Bombs Magnus Testing Freely Spinning Stabilizers						

THE STATIC AND MAGNUS AERODYNAMIC CHARACTERISTICS OF THE M823 RESEARCH STORE EQUIPPED WITH FIXED AND FREELY SPINNING STABILIZERS

Prepared by:

Frank J. Regan
Mary E. Falusi

ABSTRACT: This report is the first in a two-part series of technical reports on the dynamics and aerodynamics of free-fall stores using freely spinning stabilizers. Presented herein are the results of recent wind-tunnel measurements of the normal force, pitching moment and Magnus force and moment on the M823 Research Store in transonic flow. Comparisons are made between configurations equipped with fixed and freely spinning stabilizers, with regard to sign and relative magnitude of the Magnus force and moment. A method is presented and applied whereby the Magnus force and moment are corrected for flow angularity.

NAVAL ORDNANCE LABORATORY
WHITE OAK, MARYLAND

NOLTR 72-291 1 December 1972

THE STATIC AND MAGNUS AERODYNAMIC CHARACTERISTICS OF THE M823 RESEARCH STORE EQUIPPED WITH FIXED AND FREELY SPINNING STABILIZERS

The purpose of this report is to present wind-tunnel measurements of the static and Magnus aerodynamic characteristics of the freely spinning cruciform stabilizers.

The authors wish to acknowledge the assistance given by the 4-T wind-tunnel staff, particularly Mr. R. W. Butler, of the Arnold Engineering Development Center. Also much appreciated is a critical review by Mr. Anders Platou (U. S. Army's Ballistics Research Laboratories) of the Magnus data reduction. Mr. Platou's comments and analyses have been responsible in particular for the inclusion of the flow angularity corrections to these data.

This project was sponsored by the Naval Air Systems Command under A320-320C/WF32-323-201, RMMO-42-005-212-1/F008-09-001.

ROBERT WILLIAMSON II
Captain, USN
Commander

Leon H. Schindel

LEON H. SCHINDEL
By direction

CONTENTS

ILLUSTRATIONS

ILLUSTRATIONS (Cont'd)

INTRODUCTION

Free-fall stores with conventional cruciform panel stabilizers have at times evidenced erratic behavior when subjected to high angles of attack. This anomalistic performance has often been attributed to the large yawing and rolling moments which vary periodically with roll angle (see Refs. (1) and (2)). It is common practice to refer to these moments as being "roll induced." Another source of errant flight behavior with dynamic origin is the somewhat related problem of roll-pitch resonance (see Ref. (2)). This latter difficulty becomes evident when the pitch and roll frequencies are nearly equal. Yaw-roll resonance becomes precipitous when the pitch frequency and roll rate become nearly equal and remain so for an extended period of time.

The freely spinning stabilizer is a demonstrated practical means for reducing these induced moments and minimizing the likelihood of yaw-pitch resonance. In the freely spinning stabilizer the panels are permitted to spin about the body's longitudinal axis. The forebody, on the other hand, has little or no spin rate. Ballistic advantages of this type of stabilizer are as follows. First, the effects of roll-induced forces and moments can be minimized or eliminated. Secondly, the moment of inertia in roll of the tail cone is an order of magnitude less than that of the complete configuration. Since only the fins rotate they rapidly accelerate after release to a roll rate well above the bomb's pitch frequency. In addition, the freely spinning tail offers a tactical advantage in that it can be used as an environmental sensor by replacing the commonly used air-arming vane.

During the past few years an investigation has been carried out at the Naval Ordnance Laboratory to determine the dynamic and aerodynamic properties of typical free-fall stores with freely spinning stabilizers. Toward this end, a series of wind-tunnel investigations have measured static, pitch damping and Magnus characteristics of freely spinning stabilizers (see Refs. (3), (4) and (5)). The present report documents the results of a series of comparative measurements of the fixed and freely spinning stabilizers on the basis of static and Magnus forces and moments. A subsequent report will combine these aerodynamic measurements with an analytic study of the dynamics of the freely spinning stabilizer; the goal of this second effort will be to establish the effect of spin rate (fin cant) and forebody and stabilizer associated asymmetries on store stability.

Portions of the data used in this report are also available in Reference (6), although the data in Reference (6) has not been corrected for flow angularity.

SYMBOLS

a	magnitude of a vector
A	corrected angle of attack
C_ℓ	section lift coefficient
C_ℓ	rolling moment, M_x/QSd
C_{ℓ_α}	sectional lift curve slope
C_{ℓ_δ}	rolling moment due to fin cant, $\partial C_\ell/\partial\delta$
C_{ℓ_p}	roll-damping moment derivative, $\partial C_\ell/\partial(pd/2V)$
C_m	pitching-moment coefficient, M_y/QSd
C_{m_α}	pitching-moment derivative, $\partial C_m/\partial\alpha$
C_N	normal-force coefficient, $-F_z/QS$
C_{N_α}	normal-force derivative, $\partial C_N/\partial\alpha$
C_n	yawing-moment coefficient, M_z/QSd
C_y	side-force coefficient, F_y/QS
d	reference length, body diameter
F_x	uncorrected load component along the x axis
F_y	uncorrected load component along the y axis
F_z	uncorrected load component along the z axis
G_x	corrected load component along the x axis
G_y	corrected load component along the y axis
G_z	corrected load component along the z axis

SYMBOLS (Cont'd)

I_x	pitch moment of inertia
$\bar{i}$	unit vector along the x axis
$\bar{j}$	unit vector along the y axis
$\bar{k}$	unit vector along the z axis
$\bar{\ell}$	unit vector along the velocity vector
K_x	axial radius of gyration, $\sqrt{I_x/md^2}$
M_x	component of aerodynamic moment about x axis
M_y	component of aerodynamic moment about y axis
M_z	component of aerodynamic moment about z axis
M_∞	free-stream Mach number
p	spin rate, radians per second
$\tilde{p}$	reduced spin rate, pd/2V
Re	Reynolds number per unit length
S	model reference area, $\pi d^2/4$
V	free-stream airspeed
$\vec{V}$	free-stream velocity
X,Y,Z	conventional fixed-body axes
y	coordinate of spanwise station
α	nominal angle of attack
$\{\alpha_o, \beta_o\}$	flow angularity variables
δ	fin cant
δ_J	designated fin cant angle with J = 1, 2, 3, 4, 5 degrees
$\bar{\eta}$	unit vector normal to angle-of-attack plane

SYMBOLS (Cont'd)

$\bar{\xi}$	unit vector in angle-of-attack plane normal to $\bar{i}$
ρ	density of the air
ρ_B	density of the bomb
c	indicates correction for flow angularity (used as superscript)

TEST FACILITY

The Magnus tests were carried out exclusively at the Aerodynamic Wind Tunnel (4T) of the Arnold Engineering Development Center. This facility is a recirculating, continuous flow, variable density tunnel capable of being operated at Mach numbers from 0.2 to 1.3. At all Mach numbers the stagnation pressure can be varied from 200 to 400 psfa. The test section is four feet square and 12.5 feet long. The wind tunnel is completely enclosed in a plenum chamber from which the air can be evacuated, allowing part of the air flow to be removed through the perforated walls of the test section. A more complete description of the wind tunnel may be found in Reference (7).

WIND-TUNNEL MODEL

The model used in these tests is the M823 Research Store. This configuration has a long history as the standard shape in an extensive free-fall weapons dynamics research program participated in by the United States, the United Kingdom and Australia. In this tripartite effort the M823 was used in several free-fall trials and subjected to exhaustive wind-tunnel measurements. It has also served as a model in numerous six-degree-of-freedom computer flight simulations (Ref. (8)).

The full-scale M823 is illustrated in Figure 1. In its standard form the M823 is a 7.7-caliber-long free-fall store with a cruciform conical stabilizer. For the tests reported herein, the M823 was modified in that the conical stabilizer was mounted on a bearing-supported shaft and was free to rotate about the longitudinal axis of the body. A dimensional sketch of the wind-tunnel model is given in Figure 2 with details of stabilizer geometry given in Figure 3. In these tests the stabilizer had fin cants of 1, 2, 3, 4 and 5 degrees. The model was tested with stabilizer decoupled and free to spin about the longitudinal axis of the store. Tests were also conducted with the rigidly fixed to the forebody to form a configuration with a conventional fixed stabilizer.

INSTRUMENTATION

The aerodynamic loads on the model were measured by means of a four-component (C_N, C_y, C_m and C_n) strain-gage balance. To measure the rotational rate of the model or stabilizer, a magnetic tachometer is located in the tail assembly. A magnetic pick-up coil was embedded in the sting.

CORRECTIONS FOR FLOW ANGULARITY

In a succeeding section the salient features of the wind-tunnel measurements will be pointed out. Before doing this, however, it is of some value to discuss how the measurements were made and what special corrections were applied. In the freely spinning stabilizer tests, the model's forebody is rigidly fixed to the balance with only the stabilizer free to spin, being supported on a bearing shaft and driven in spin by means of fin cant.

The model was rigidly fixed to the balance with only the stabilizer allowed to spin during the freely spinning tail tests; during the fixed-stabilizer tests, the stabilizer was locked to the forebody and the whole configuration was allowed to spin about the balance. The model is shown mounted on the balance and installed in the wind tunnel in Figure 4. The model is then rotated through the angle of range with load measurements made at several discrete angular positions. At the completion of each angle-of-attack span, the model is brought to zero angle of attack and the Mach number is changed. The angle-of-attack range is again spanned while holding the Mach number fixed. There seems to be a source of error in bringing the model to the nominally zero angle of attack. The model would thus be experiencing a slightly different angle of attack from the nominal value, the difference being represented by the symbol, α_o. Since the model was rotated in a vertical plane, there was the additional possibility that the plane of rotation would not at any time contain the velocity vector. Stated alternately, the vertical plane of rotation of the model was not coincident with a vertical plane containing the velocity vector. The angle between these two vertical planes is designated as β_o. Thus, to define the velocity vector at a nominal angle of attack of zero requires two variables, α_o, the vertical coordinate, and β_o, the horizontal coordinate. $\{\alpha_o, \beta_o\}$ might also be thought of as the directional angles of the velocity vector in the $\{X_o, Y_o, Z_o\}$ coordinate frame.

Because of the way α_o and β_o occur it might be expected that α_o would change more readily than β_o because the zero value of the nominal angle of attack changes with each Mach number change, but the plane of rotation should not move until model changes are made. In Appendix A, Equations (A-26) and (A-29) provide a means for

calculating the trim angles α_o and β_o, respectively. These trim angles are shown plotted versus Mach number in Figure 5 for the configuration with a freely spinning stabilizer with a four-degree fin cant. The angle β_o is less than α_o, but not sufficiently so, it seems, to support the above reasoning. Also, it might be expected that β_o would not vary much with Mach number, but apparently it evidences as much variation as does α_o. In showing α_o and β_o versus Mach number in Figure 5, a compressibility effect is not necessarily implied. Mach number in Figure 5 is intended to act more as a "counter" to indicate the completion of an angle-of-attack span.

In making use of Equations (A-26) and (A-29) the question that must be faced is how well can the wind-tunnel balance make small-load measurements. One way of assessing balance accuracy is to measure C_{N_α} in the simple finite difference method suggested by Equation (A-28). Since normal loads were measured at -1, 0, +1 and +2 degrees angle of attack, it was decided to obtain the normal-force derivative, C_{N_α}, by use of the following formulae and then to compare the results

$$C_{N_\alpha} = \frac{(C_{N_1} - C_{N_{-1}})57.3}{2} \tag{1a}$$

$$C_{N_\alpha} = \frac{(C_{N_1} - C_{N_o})57.3}{1} \tag{1b}$$

$$C_{N_\alpha} = \frac{(C_{N_2} - C_{N_o})57.3}{2} \tag{1c}$$

where the subscripts indicate the angle at which the measurements were made. Reasoning would go somewhat as follows: If there exists a time-dependent ramdom error large in proportion to the measurement made at small angles, than the calculation of C_{N_α} by means of Equations (1) should indicate considerable scatter. Figure 6 is a plot of C_{N_α} versus Mach number as obtained from Equations (1). Quite obviously there is little scatter in the measurements of the individual values of C_{N_α}. Of course the data depicted in Figure 6 do not support the contention that there is small error in the measurements of $C_{N_{-1}}$, C_{N_o}, C_{N_1} and C_{N_2}, but rather that the time-dependent ramdom or noise type of error must be small. Without confidence in the freedom of the balance measurements at small angles of attack from noise-type errors, there could be no confidence in the measurements of α_o and β_o from Equations (A-26) and (A-29).

It is now a relatively straightforward procedure to make corrections to wind-tunnel Magnus measurements. In reducing the wind-tunnel side-force data, Equation (1a) was used to calculate the normal-force derivative. The normal-force derivative and the trim forces, C_{N_o} and C_{y_o}, were used in Equations (A-26) and (A-29), respectively, to calculate the flow angularity variables $\{\alpha_o, \beta_o\}$ as,

$$\alpha_o \cong C_{N_o} / C_{N_\alpha} \tag{2a}$$

$$\beta_o \cong - C_{Y_o} / C_{N_\alpha} \tag{2b}$$

These quantities are then used, together with the nominal angle of attack, α, to calculate h and k from Equations (A-19).

$$h = \mathrm{Cos}\alpha_o \mathrm{Cos}\beta_o \mathrm{Sin}\alpha + \mathrm{Sin}\alpha_o \mathrm{Cos}\alpha \tag{3a}$$

$$k = \mathrm{Cos}\alpha_o \mathrm{Sin}\beta_o \tag{3b}$$

The above quantities are substituted in Equations (A-24a) and (A-25b) to obtain the corrected side-force and yawing-moment coefficients

$$C_y^c = \frac{C_y h + C_N K}{\sqrt{h^2 + k^2}} \tag{4a}$$

$$C_n^c = \frac{C_n h + C_m k}{\sqrt{h^2 + k^2}} \tag{4b}$$

Next, the corrected angle of attack is calculated from Equation (A-12).

$$A = \mathrm{Tan}^{-1}\left[\frac{\left\{\left[\mathrm{Cos}\alpha_o \mathrm{Cos}\beta_o \mathrm{Sin}\alpha + \mathrm{Sin}\alpha_o \mathrm{Cos}\alpha\right]^2 + \left[\mathrm{Cos}\alpha_o \mathrm{Sin}\beta_o\right]^2\right\}^{\frac{1}{2}}}{\left[\mathrm{Cos}\alpha_o \mathrm{Cos}\beta_o \mathrm{Cos}\alpha - \mathrm{Sin}\alpha_o \mathrm{Sin}\alpha\right]}\right] \tag{5}$$

In discussing flow angularity one final problem must be addressed. Alternate expressions for the flow angularity variables might be used, that is computations based upon the measured "trim" moments, C_{m_o} and C_{n_o}, rather than the trim forces, C_{y_o} and C_{N_o}. Thus rather than having expressions for $\{\alpha_o, \beta_o\}$ given in Equations (2), the following alternate expressions might be used:

$$\alpha_o \cong C_{m_o} / C_{m_\alpha} \tag{6a}$$

$$\beta_o \cong -C_{n_o} / C_{m_\alpha} \tag{6b}$$

The question that must then be considered is the quality of agreement between Equations (2) and (6). If the variables $\{\alpha_o, \beta_o\}$, after having been calculated separately from Equations (2) and (6), are not in agreement then there must be a variation of flow angularity along the body. In the extreme case where $\{\alpha_o, \beta_o\}$ are zero from Equations (2) and nonzero from Equations (6), the conclusion would have to be that the flow angularity varies along the body in sign such that there is a couple on the body (C_{m_o} and/or C_{n_o} are nonzero) and yet the net force is zero. This is somewhat at odds with the assumption of Appendix A in that the flow angularity, $\{\alpha_o, \beta_o\}$, was assumed constant along the body. In reducing the Magnus data contained in this report it was found that $\{\alpha_o, \beta_o\}$, as calculated from Equations (2), differed between 10 and 50 percent from $\{\alpha_o, \beta_o\}$ as calculated from Equations (6). The procedure that was followed was to use Equations (2) to correct force data (Eq. (4a)) and to use Equations (6) to correct moment data (Eq. (4b)). As pointed out in Appendix A, no corrections were made to the normal-force measurements since such corrections must be of third order.

TEST PROCEDURE*

All configurations were tested at Mach numbers of 0.6 to 1.2 at a constant Reynolds number per foot of 3 million. The variation of wind-tunnel dynamic pressure with Mach number is given in Figure 7. The stream total temperature was maintained at 90 degrees Fahrenheit. The model angle of attack was swept between -1 and +12 degrees.

PRECISION OF MEASUREMENTS*

Errors arising from free-stream test conditions were determined from wind-tunnel calibration data. Since the other data obtained in this report were determined from single-sample measurements, the

---

* This section was taken from Reference (6).

uncertainties for these data are estimated, based on instrument precision and calibration curve fit deviation at a 95 percent confidence level. The uncertainties in the coefficients presented in this report are as follows:

ΔC_N	ΔC_m	ΔC_y	ΔC_n	$\Delta\alpha$
±0.01	±0.01	±0.002	±0.002	±0.1

DISCUSSION OF RESULTS

In the wind-tunnel program the yawing and pitching moments and the side and normal forces were measured. In addition, the spin rate of the tail (freely spinning stabilizer) or the entire configuration (fixed stabilizer) were also measured. Figures 8 through 42 present the normal-force and pitching-moment coefficients of the fixed and freely spinning configurations having fin-cant angles of two and four degrees. It was found that fin-cant angles within the range of one to five degrees had little effect on the normal-force and pitching-moment characteristics of the body. Therefore, normal-force and pitching-moment data for only two of the five fin cants are presented.

It will be noted in examining Figures 16 through 24 and again Figures 34 through 42 that the fixed stabilizer has a slightly greater pitching moment at a given angle of attack than does the freely spinning stabilizer. Both the fixed and freely spinning configurations at both fin cants given evidence of a nonlinearity in the pitching moment about zero angle of attack. This effect may be due to sting interference. The sting diameter-to-base ratio is 0.5. Unfortunately, a large sting diameter was required because the Magnus balance was designed for spin-stabilized models where air conduits for the drive system are required. These conduits are provided by internal passageways internal to the balance.

Before considering the Magnus measurements, it is necessary to justify to some extent the experimental technique used and the method chosen for data presentation. First, it must be appreciated that in its linear formulation the Magnus effect (force or moment) is a unique function of a quantity which will be designated herein as the reduced spin rate, $\tilde{p}$, or $pd/2V^*$. One physical interpretation of $\tilde{p}$ might be as the ratio of the linear velocity of a surface element due to advance. Within the restriction of small values, $\tilde{p}$ is approximately the angle of the flow "seen" by a surface element. For a finned body, if the reference length were the fin span, then $\tilde{p}$ might be identified as the helix angle of the fin tip. Since $\tilde{p}$ is an indication of the flow angularity or distortion at a surface element

---

* The reduced spin rate, $\tilde{p}$, is identical to the Strouhal number that is used in hydrodynamics as a similarity parameter in unsteady flow.

due to spin, the Magnus loads should be thought of as a function of the reduced frequency and not the spin rate alone. The sketch below indicates the flow angularity at a surface element caused by spin.

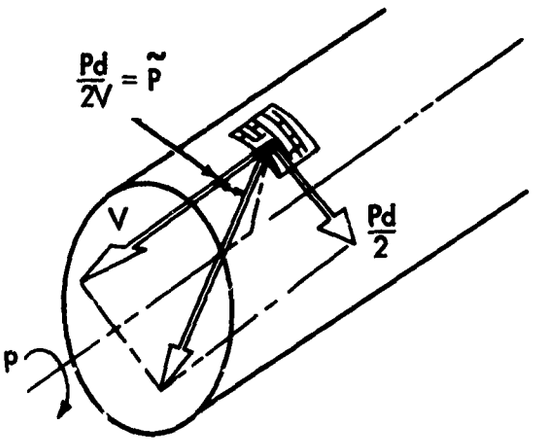

In making Magnus measurements on bodies of revolution (usually spin stabilized) the usual procedure is to spin or to permit spin decay of the body through a fairly wide range of spin rates. Side loads and yawing-moment measurements are made continuously and presented as functions of reduced spin rate, $\tilde{p}$. The reason for doing this is that the reduced spin rate enjoyed by a body of revolution depends upon the value of the initial spin rate (which in turn can be related to the gun rifling) and to some extent the roll damping; in addition, the reduced frequency also depends upon the trajectory flown by the body. One encounters, for example, the situation where the reduced spin rate often increases with downrange distance, for while the spin rate decreases somewhat the airspeed, V, decreases much more quickly.

For a finned body the situation is somewhat different. In Appendix B the reduced spin rate is obtained from the integration of a single-degree-of-freedom equation. The steady-state reduced frequency is shown in Equation (B-2) to be

$$\tilde{p}_s = -\frac{C_{\ell_\delta}\delta}{C_{\ell_p}} \tag{7}$$

where C_{ℓ_δ} is the rolling-moment derivative due to fin cant, δ, the fin-cant angle in radians and C_{ℓ_p} the roll-damping moment derivative.

The Magnus effect is a function of the angle of attack and the similarity parameters: Mach number, Reynolds number and the reduced spin rate. Equation (7) indicates that for a given shape, Mach number and Reynolds number, the reduced spin rate is fixed since C_{ℓ_δ}, δ and C_{ℓ_p} are determined by shape and Mach number and Reynolds number. It might be reasoned further that the reduced spin rate, $\tilde{p}$, is a weak function of Mach number since both C_{ℓ_δ} and C_{ℓ_p} should vary in nearly the same manner with Mach number and both appear in Equation (7) in a ratio. Measurements of the reduced spin rate in these tests indicate that the reduced spin rate does vary little with Mach number for a given shape.

Figures 43 through 47 present the reduced spin rate versus angle of attack for all five angles of fin cant. It will be noted that for fins having cant angles of 1, 2 and 3 degrees, the reduced spin rate is nearly invariant with angle of attack (up to 12 degrees). The five-degree fin cant indicates the greatest variation with angle of attack, changing about 15 percent over the angle range of 12 degrees. It will also be noted that the variation of reduced spin rate with Mach number is small. For example, the value of $\tilde{p}$ for the four-degree fin cant is 0.076 at a Mach number of 0.59 and 0.078 at a Mach number of 1.20, supporting the earlier made conjecture on the small influence of Mach number on reduced spin rate.

The only question that remains to be settled is how quickly the store reaches the steady-state value of the reduced spin rate. Equation (B-5) expresses the relationship between the initial difference between actual and steady-state reduced spin rates, $\tilde{p}_o - \tilde{p}_s$, and the difference, $\tilde{p} - \tilde{p}_s$, at a later time, t*. The quantity t* is a nondimensional time, having for units the time for the passage of one body length. The half life of the spin rate difference, $\tilde{p} - \tilde{p}_s$, means that,

$$t^* \left(\frac{\rho}{\rho_B}\right)\left(\frac{C_{\ell_p}}{4K_x^2}\right) = -.69 \tag{8}$$

assuming the following values,

$$\frac{\rho}{\rho_B} = 10^{-3} \qquad C_{\ell_p} = -1.0 \qquad K_x^2 = 0.0875 \tag{9}$$

Equation (8) may be solved for t* to give

$$t^* = 242 \tag{10}$$

The above value of t* means that the body moves through 242 lengths (about 3 to 4 seconds) before the reduced spin rate would be one-half

way to the steady-state value. This result indicates that to study initial motion after release, a wind-tunnel test must be carried out in which the model is driven in spin over a range of reduced spin rates from zero to the steady-state value. Data, as presented in this report, would appear to be inadequate for analyzing the initial motion. However, beyond the first five or six seconds after release it would seem a safe assumption that the configuration has attained the steady-state value of reduced spin rate. From that time onward the reduced spin rate is nearly constant over the remainder of the trajectory. The conclusion is then that once the Mach number and the angle of attack are set, the reduced spin rate is automatically set (by Eq. (7)). Thus, the side-force and yawing-moment coefficients will be directly applicable to the full-scale configuration. Magnus loads can then be treated like conventional static loads and the reduced spin rate is not a separate independent variable.

The Magnus forces and moments are given as functions of angle of attack and Mach number in Figures 48 through 124. With the exception of the configuration having a one-degree fin cant, all Magnus data are presented for both the fixed and freely spinning stabilizers.

Platou's qualitative theory of the Magnus effect on finned bodies can be used with limited success to explain these data. Platou's theory was originally set forth in Reference (9). This theory centers around the effect of the body wake impinging upon the leeward fin. The resulting decrease in fin lift is felt first in the region of the root; it then propagates towards the tip as the body angle of attack increases. The essentials of the concept may be seen in the sketch below:

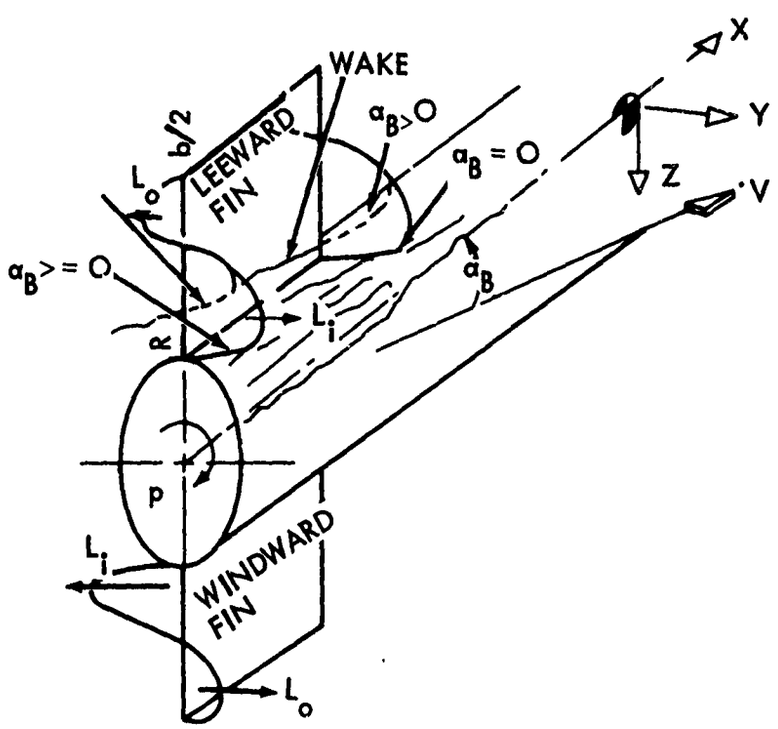

In the above sketch the fins normal to the angle-of-attack plane have been omitted for clarity. It will be noted that the lift distribution changes sign across the fin, both at zero and nonzero angles of attack. For a body rolling at the steady-state value of the reduced spin rate, the lift distribution must satisfy the condition that the net rolling moment is zero, i.e.,

$$\int_{R}^{b/2} q C_{\ell_\alpha} Q c(y) \left[\alpha_B + \delta - 2\hat{p}\frac{y}{d}\right] dy = 0 \qquad (11)$$

where C_{ℓ_α}, Q, C(y), α_B, δ and y are the sectional lift coefficient slope, the dynamic pressure, the panel chord as a function of the spanwise station, the body angle of attack, the fin-cant angle and the spanwise station, respectively.

It will be noted in the above sketch that at zero angle of attack, α_B, the net force in the Y direction is zero. However, as the angle of attack increases the decrease in the lift at the root of the most leeward fin results in an imbalance in the side force. Thus, with increasing angle of attack there will be a net side force in the negative Y direction (to the left looking forward along the direction of positive spin). Since the stabilizers are usually located well aft of the center of gravity, the Magnus force in the negative Y direction will result in a positive Magnus or yawing moment about the Z axis.

The qualitative value of Platou's theory may now be evaluated by comparing its predictions with some measurements. Consider the fixed-stabilized configuration for the moment. It may be seen in Figure 58 that for a fin having a two-degree fin cant the side force is negative. The corresponding moment, presented in Figure 66, is shown to be positive. However, it will be noted that with increasing Mach number the yawing moment initially becomes zero. Compare, for example, Figures 66 and 71. The same trend of decreasing yawing moment with Mach number is in evidence for the four- and five-degree fin cants. Compare Figures 100 and 106 for the four-degree fin cant and Figures 117 and 123 for the five-degree fin cant. It should be pointed out that this decrease in positive yawing moment cannot be explained by including forebody force contributions. If the Magnus moment on the forebody is identified with that on a body of revolution, the trend would be for the Magnus center of pressure to move aft with increasing Mach number. The result should be a contribution to the total Magnus moment that increases with Mach number.

Platou's theory deals directly with the Magnus force and predicts that this force should be negative for positive spin rate, although not necessarily linear with increasing angle of attack. It may be of interest to examine how a typical Magnus force varies with angle of attack and Mach number. For both the fixed and freely spinning configurations having a four-degree fin cant the side-force coefficient is negative for small angles of attack (see Fig. 91 for example).

The freely spinning configuration has a smaller side-force coefficient, presumably because the forebody contribution is absent. In Figure 91 both fixed and freely spinning configurations have side forces which reach a maximum at about six degrees angle of attack and then become increasingly negative. As the Mach number increases the negative peak diminishes. At a Mach number of 0.84 the freely spinning stabilizer has a positive Magnus force for angles of attack greater than seven degrees; the fixed stabilizer has a positive Magnus force above 11 degrees. A further increase in the Mach number results in a further positive trend in the Magnus force. For example, at a Mach number of 1.11 (Fig. 97) the Magnus force is entirely positive. A similar trend is recognizable for all fin-cant angles except one degree. The measurements made on the one-degree fin, either fixed or freely spinning, are only a few times greater than the uncertainty of ±0.002 in the measurement of the force coefficient.

One final consideration is the relative size of the Magnus effect on the fixed and freely spinning stabilizers. For the two-degree fin cant both configurations (fixed and freely spinning) have positive Magnus moments which tend to increase with angle of attack to a peak value of about seven degrees angle of attack at low Mach numbers (see Figs. 64 and 65). Both configurations have Magnus moments of nearly the same magnitude. Where the free stream becomes supersonic, the Magnus or yaw moment decreases from its positive subsonic peak of about 0.04 to a slightly negative value (see Fig. 106). The magnitude of the moment is comparable for both configurations.

At a fin cant of four degrees the trend is roughly that observed at two degrees, although the maximum positive value is about 0.05. It does appear that the fixed stabilizer has a slightly less positive or a slightly greater negative moment than does the freely spinning configuration.

Increasing the fin cant to five degrees increases the positive Magnus moment with increasing subsonic Mach numbers (compare Fig. 119 with 116). However, the differences between the fixed and freely spinning configurations, as noted above for the four-degree fin cant, become more evident. At Mach number of 0.94 (Fig. 122) the freely spinning stabilizer has a positive yawing moment up to eight degrees angle of attack, but the fixed stabilizer has a negative moment over the whole of the angle-of-attack range. For supersonic Mach numbers, both configurations have negative Magnus moments, although the magnitude of the moment applied to the fixed stabilizer is greater.

REFERENCES

(1) Nicolaides, J. D., "An Hypothesis for Catastrophic Yaw," Ballistics Technical Note, Bureau of Ordnance, Dept. of Navy, 1955

(2) Nicolaides, J. D., "On the Free-Flight Motion of Missiles Having Slight Configurational Asymmetries," BRL Report 858, 1953

(3) Regan, F. J., "Preliminary Static Wind-Tunnel Measurements on the M823 Research Store with a Monoplane Stabilizer," Wind-Tunnel Report No. 49, NOL, Jan 1971

(4) Regan, F. J., "Preliminary Pitch-Damping Wind-Tunnel Measurements on the M823 Research Store with a Monoplane Stabilizer," Wind-Tunnel Report No. 55, NOL, Oct 1971

(5) Regan, F. J., "Preliminary Static and Magnus Measurements on the M823 Research Store with a Monoplane Stabilizer," Wind-Tunnel Report No. 51, NOL, Jun 1971

(6) Butler, R. W., "Aerodynamic Characteristics of a 0.187-Scale M823 Research Bomb with a Free-Spinning Tail and a Free-Spinning Body-Tail Combination at Transonic Mach Numbers," AEDC Report TR-71-82, Apr 1971

(7) Test Facilities Handbook (Eighth Edition) Arnold Engineering Development Center, Dec 1969

(8) Regan, F. J., Shannon, J. H. W. and Tanner, F. J., "The Joint NOL/RAE/WRE Research Program on Bomb Dynamics. Part II A Low-Drag Bomb with Split-Skirt Stabilizers," NOLTR 69-232, Dec 1969

(9) Platou, A. S., "The Magnus Force on a Finned Body," BRL Report No. 1193, Mar 1963

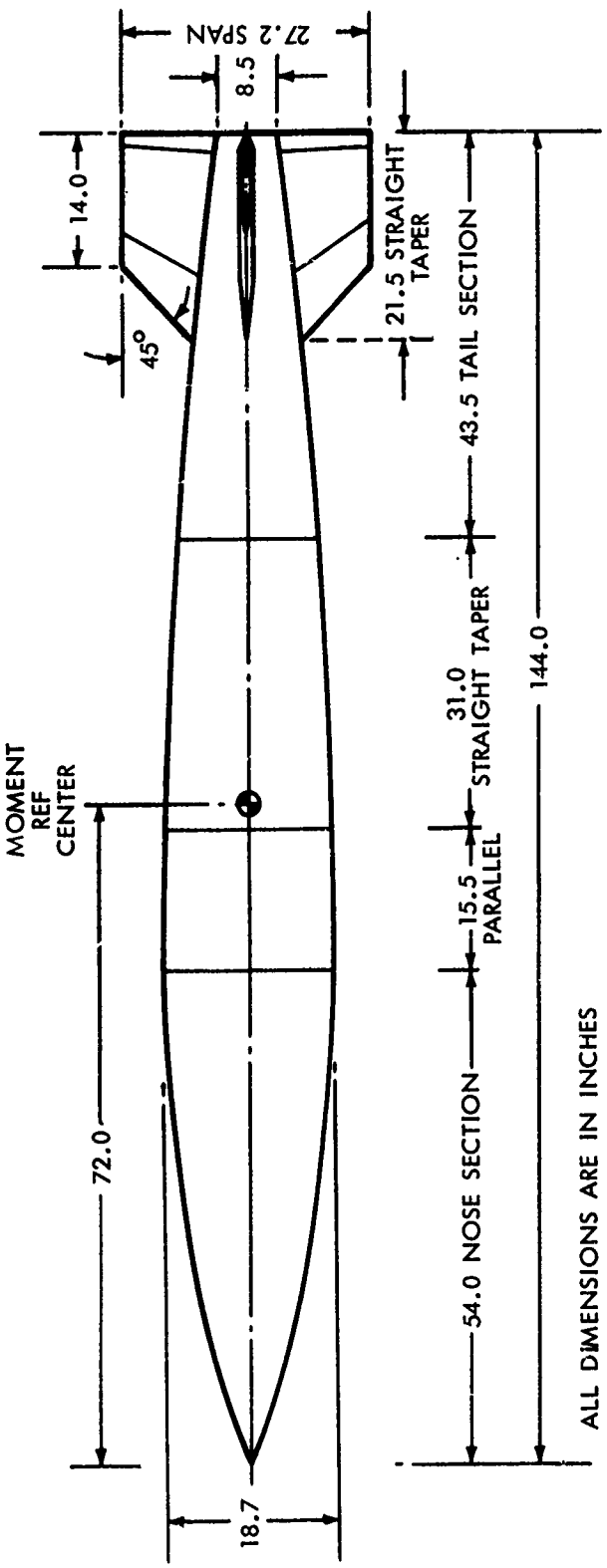

FIG. 1 M823 FREE-FALL RESEARCH STORE WITH CRUCIFORM STABILIZER

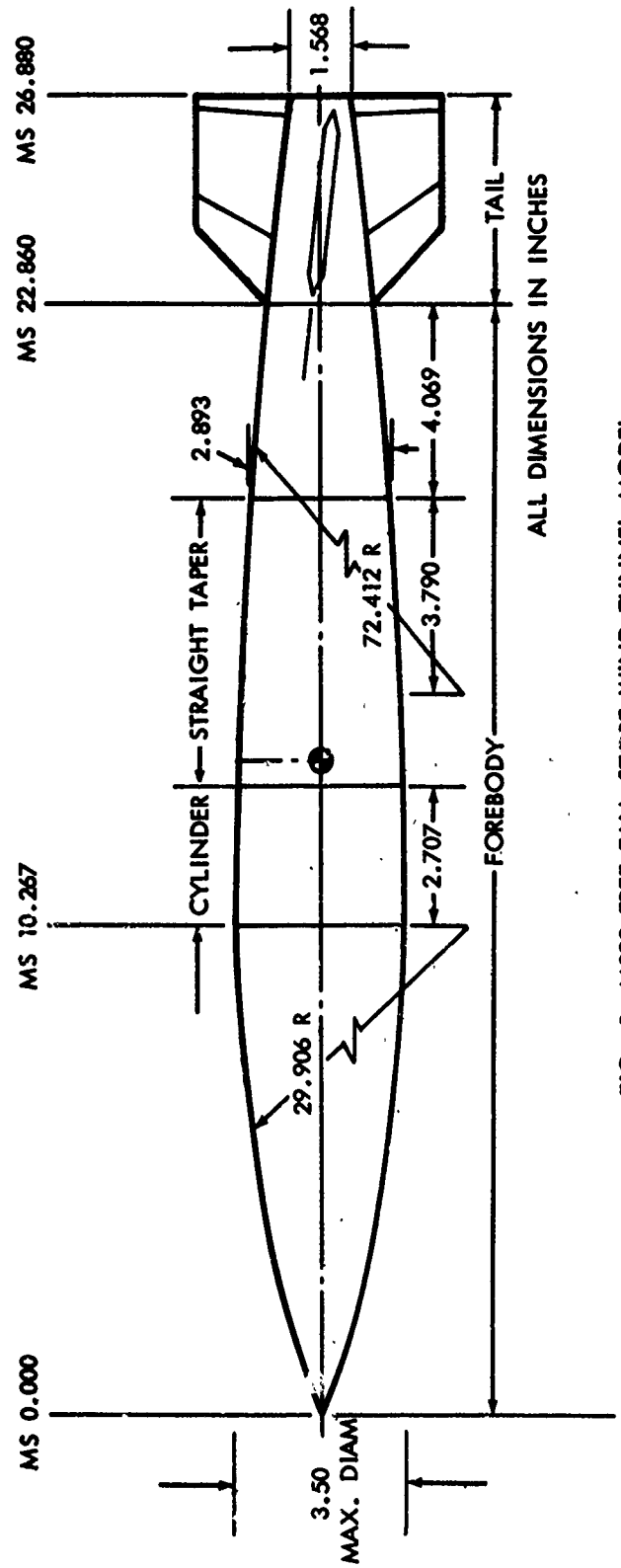

FIG. 2 M823 FREE FALL STORE WIND-TUNNEL MODEL

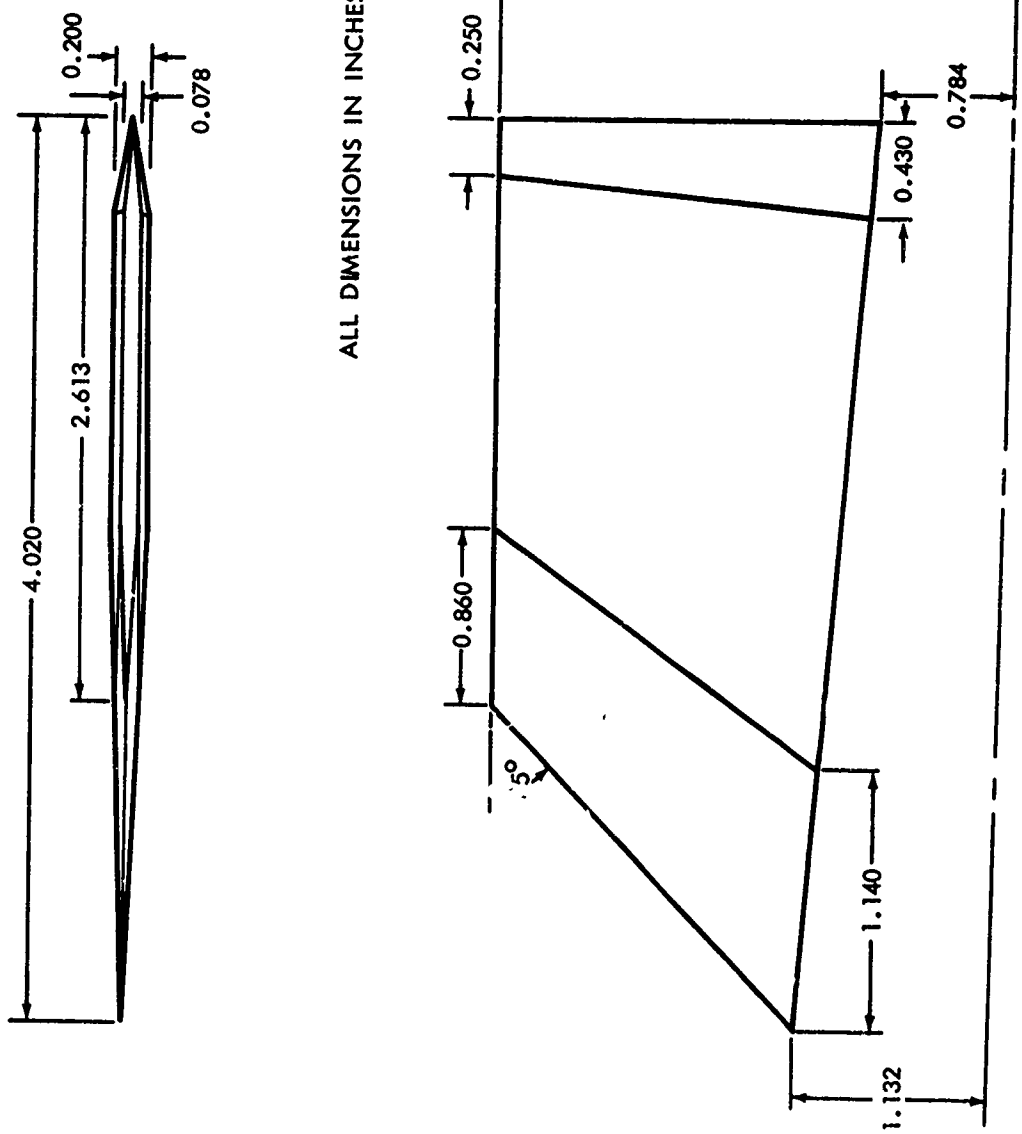

FIG. 3 GEOMETRIC DETAILS OF WIND-TUNNEL MODEL FIN

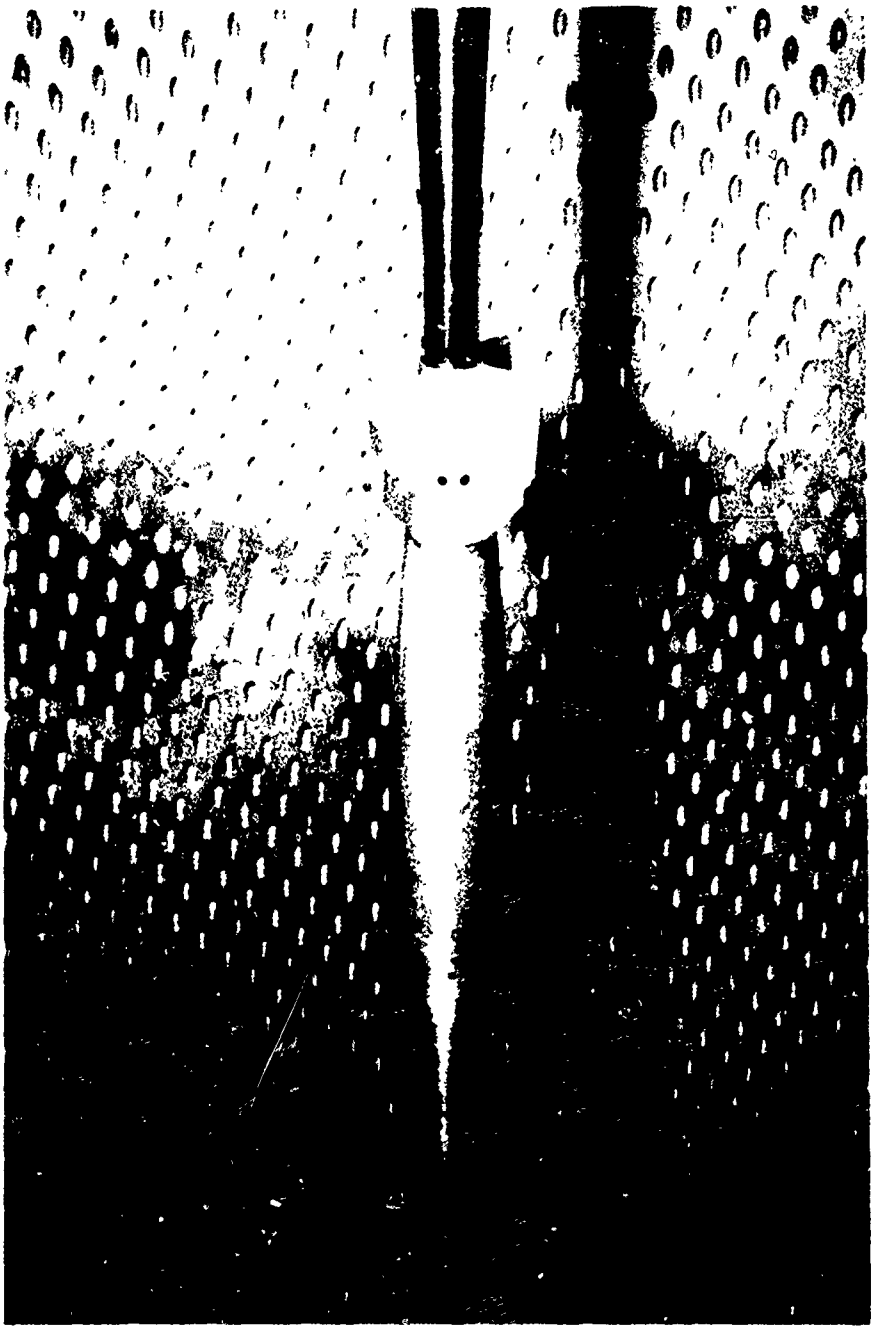

FIG. 4 MODEL OF M823 FREE FALL STORE MOUNTED IN THE WIND-TUNNEL

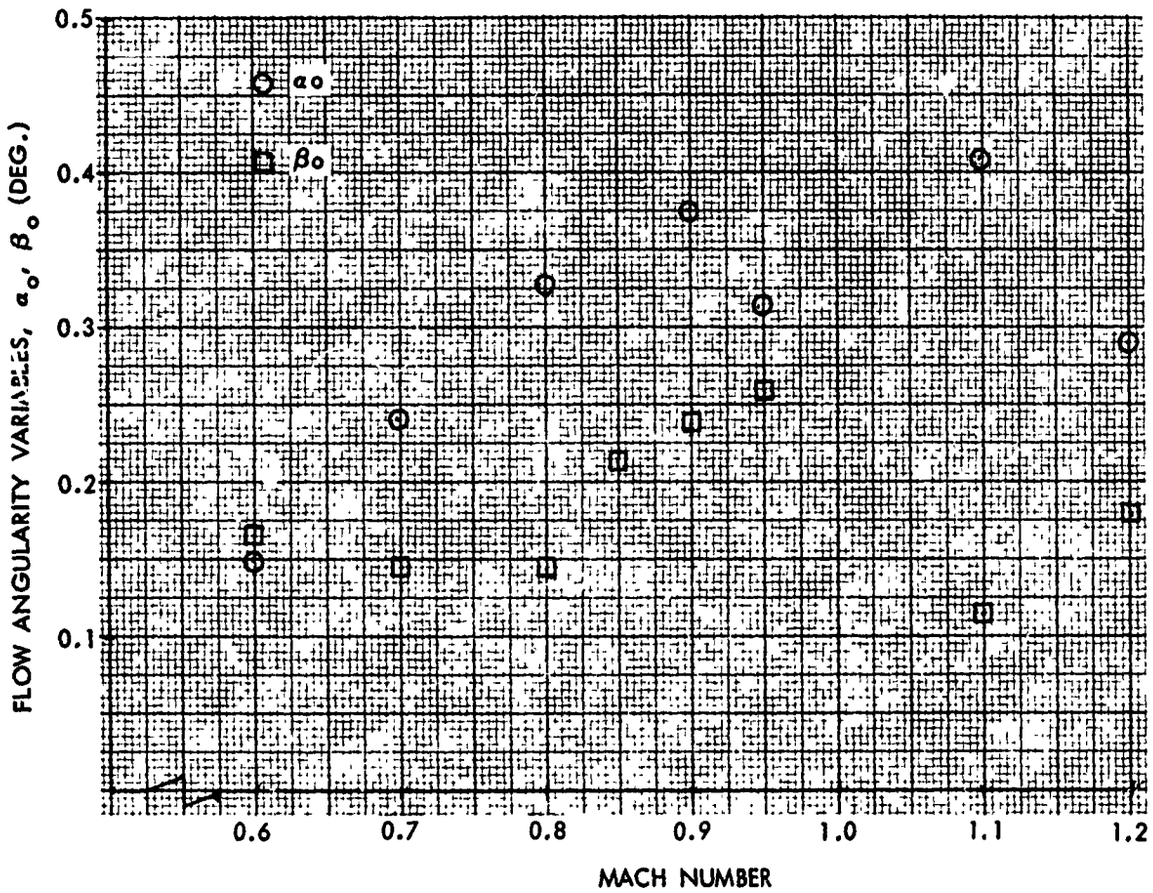

FIG. 5 FLOW ANGULARITY VARIABLES VERSUS MACH NUMBER FOR THE FREELY SPINNING STABILIZER WITH A FIN CANT OF 4 DEGREES

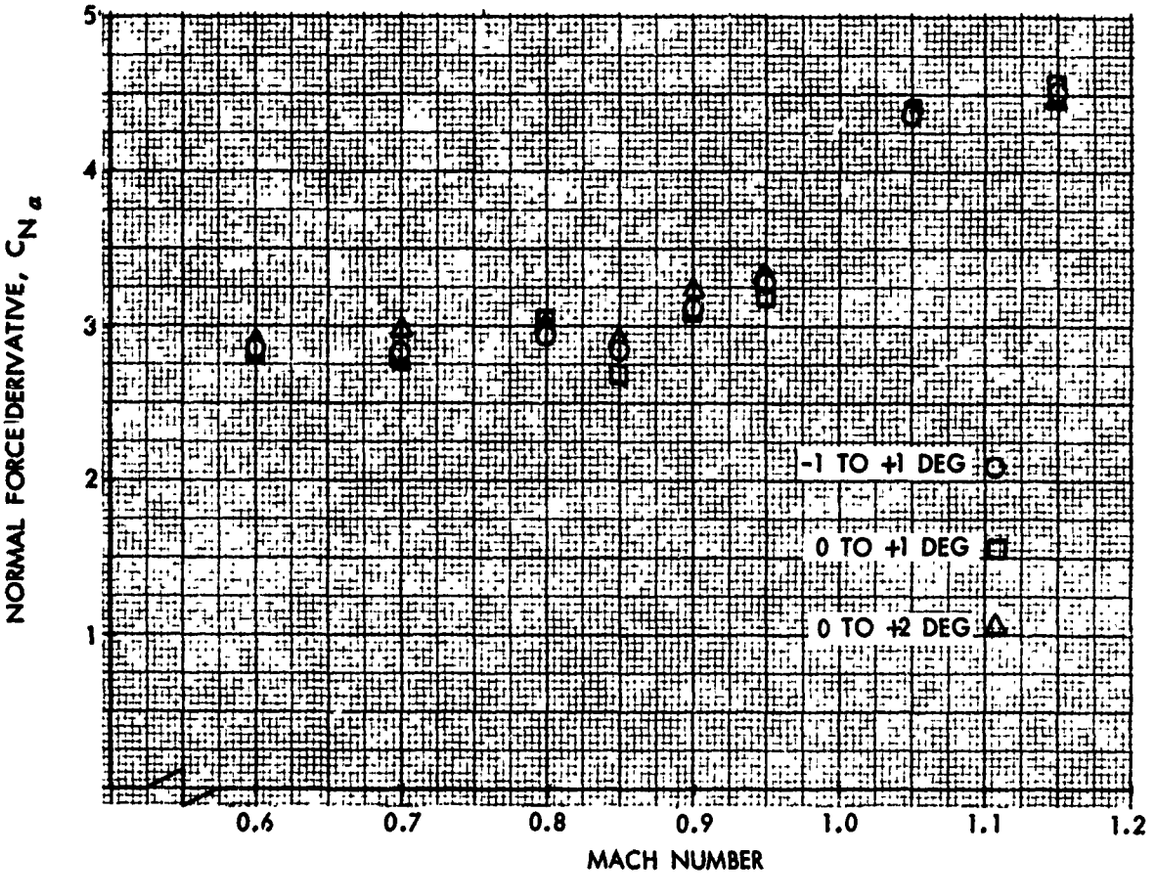

FIG. 6 NORMAL FORCE DERIVATIVE VERSUS MACH NUMBER FOR THE FREELY SPINNING STABILIZER WITH A FIN CANT OF 4 DEGREES

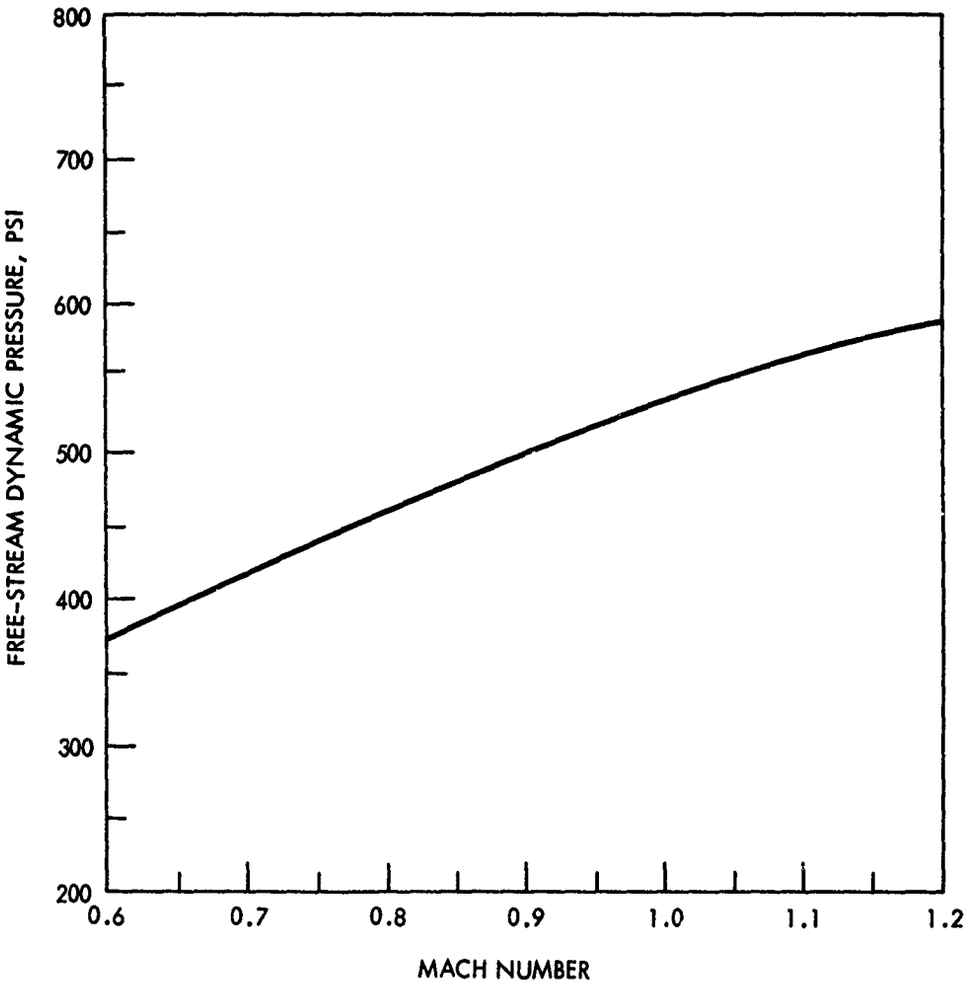

FIG. 7 VARIATION OF WIND-TUNNEL DYNAMIC PRESSURE WITH MACH NUMBER AT A REYNOLDS NUMBER OF 3.0 MILLION PER FOOT

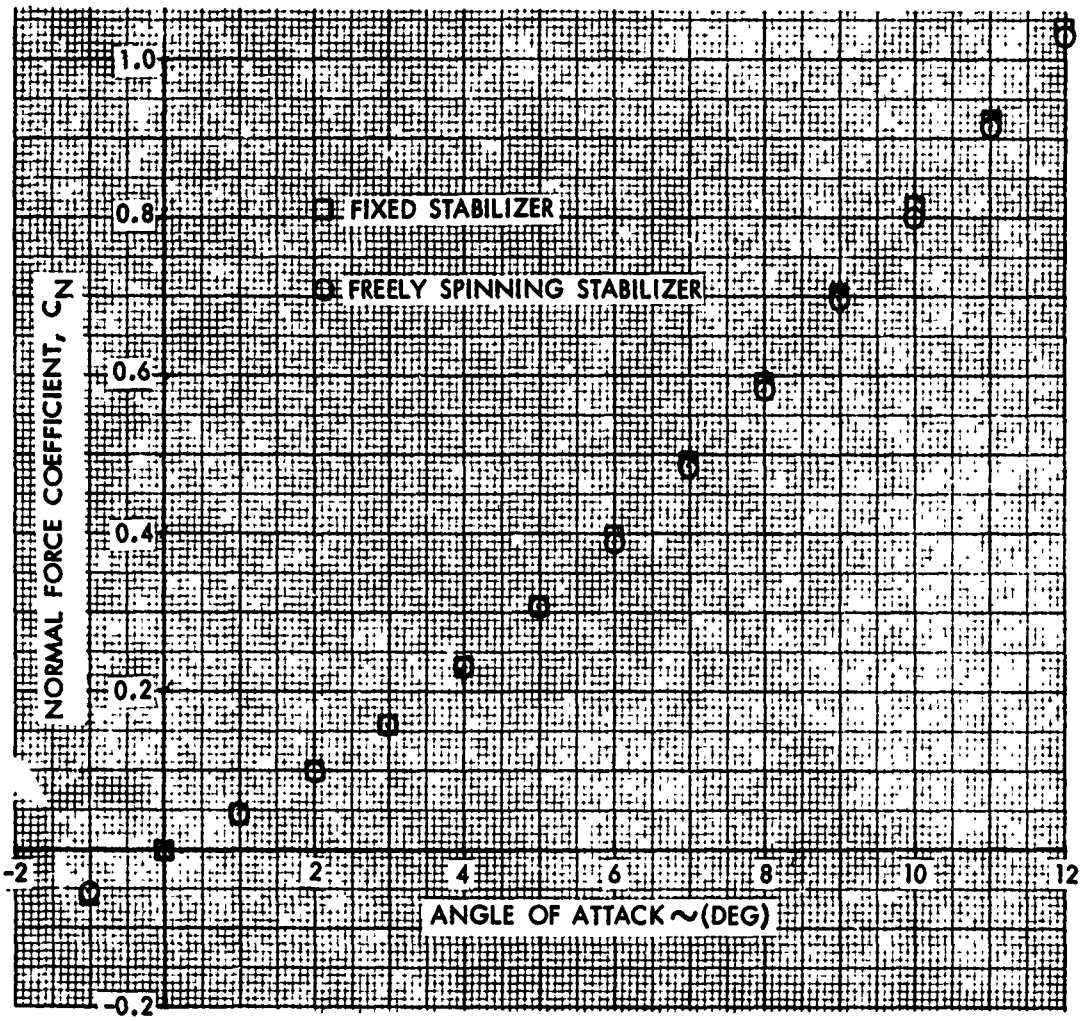

FIG. 8 NORMAL FORCE COEFFICIENT VERSUS ANGLE OF ATTACK FOR THE FIXED AND FREELY SPINNING STABILIZERS AT A FIN CANT OF 2 DEGREES AND A MACH NUMBER OF 0.59

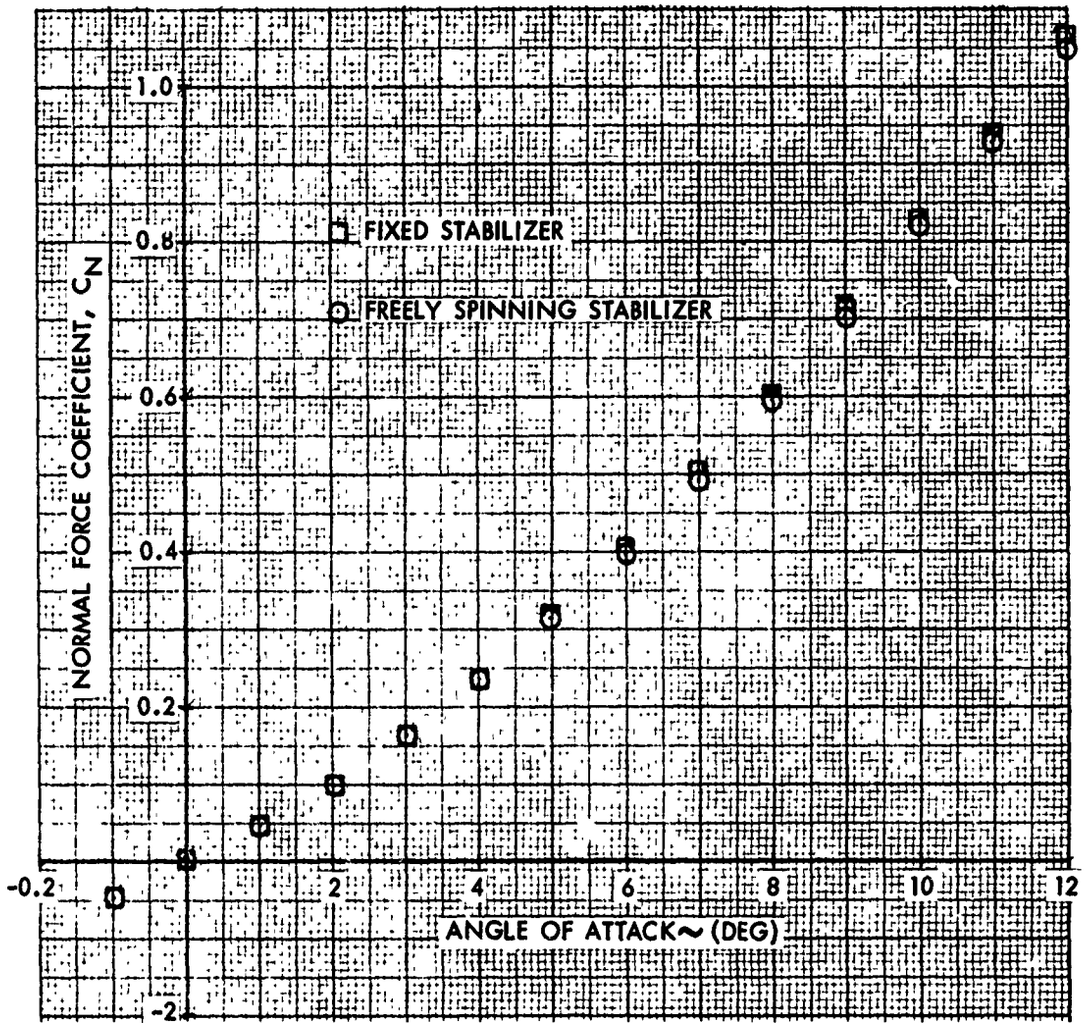

FIG. 9 NORMAL FORCE COEFFICIENT VERSUS ANGLE OF ATTACK FOR THE FIXED AND FREELY SPINNING STABILIZERS AT A FIN CANT OF 2 DEGREES AND A MACH NUMBER OF 0.74

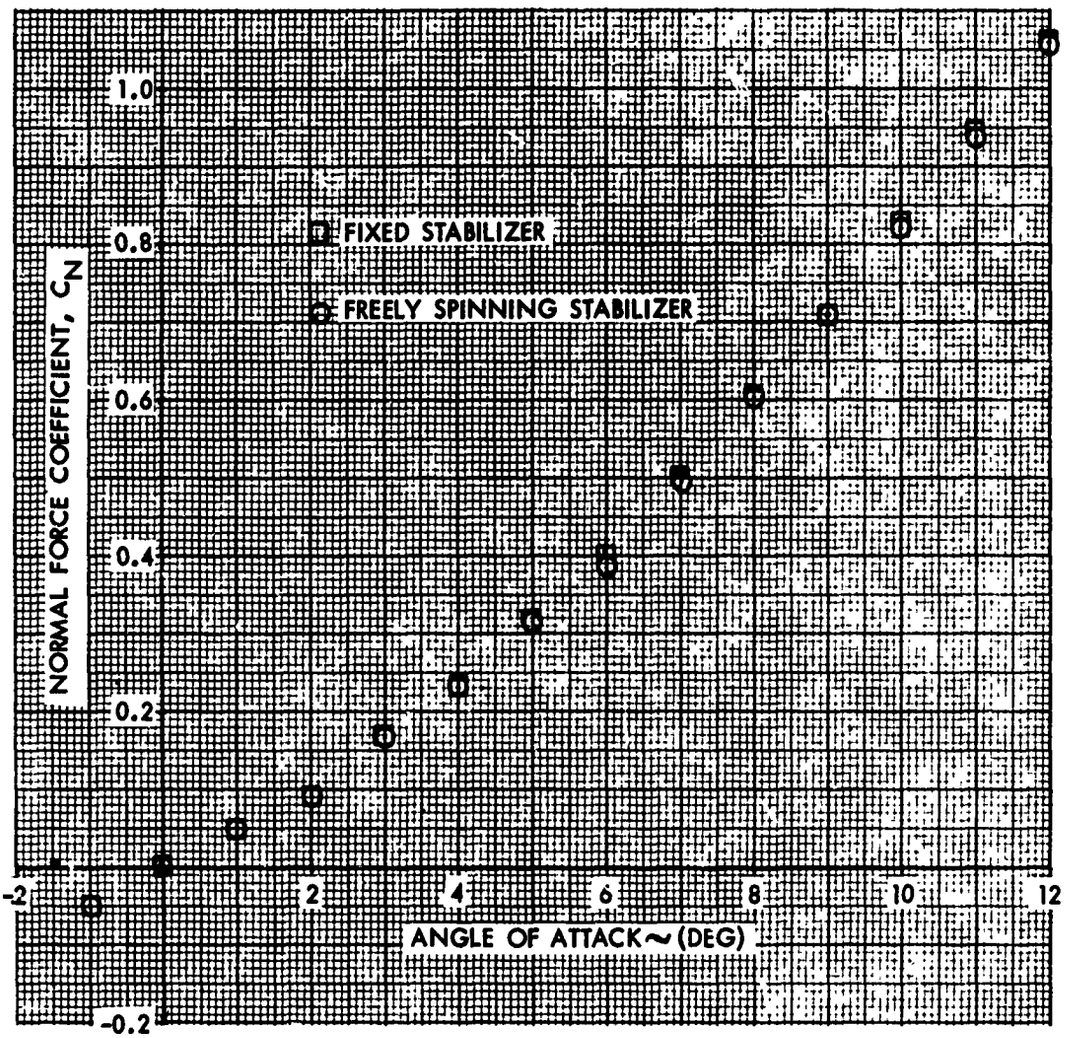

FIG. 10 NORMAL FORCE COEFFICIENT VERSUS ANGLE OF ATTACK FOR THE FIXED AND FREELY SPINNING STABILIZERS AT A FIN CANT OF 2 DEGREES AND A MACH NUMBER OF 0.79

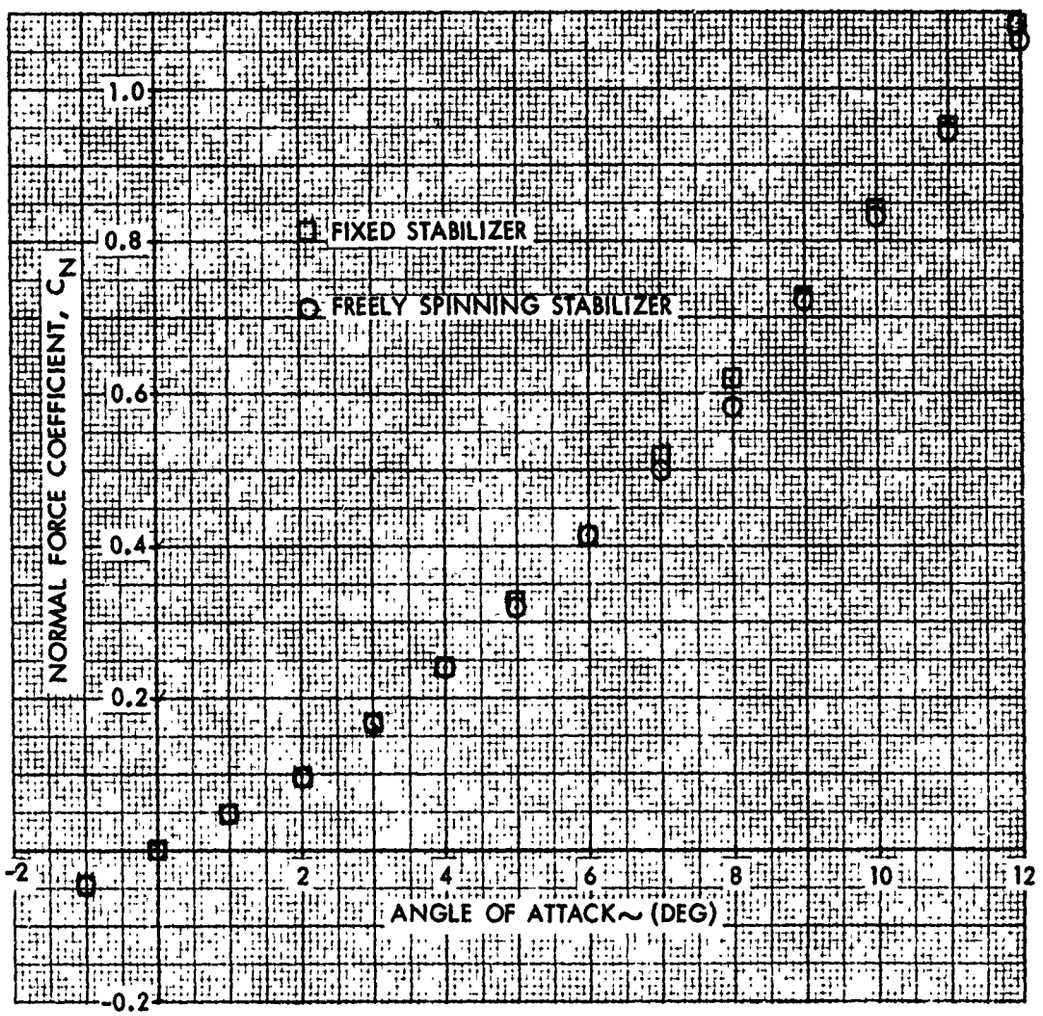

FIG. 11 NORMAL FORCE COEFFICIENT VERSUS ANGLE OF ATTACK FOR THE FIXED AND FREELY SPINNING STABILIZERS AT A FIN CANT OF 2 DEGREES AND A MACH NUMBER OF 0.84

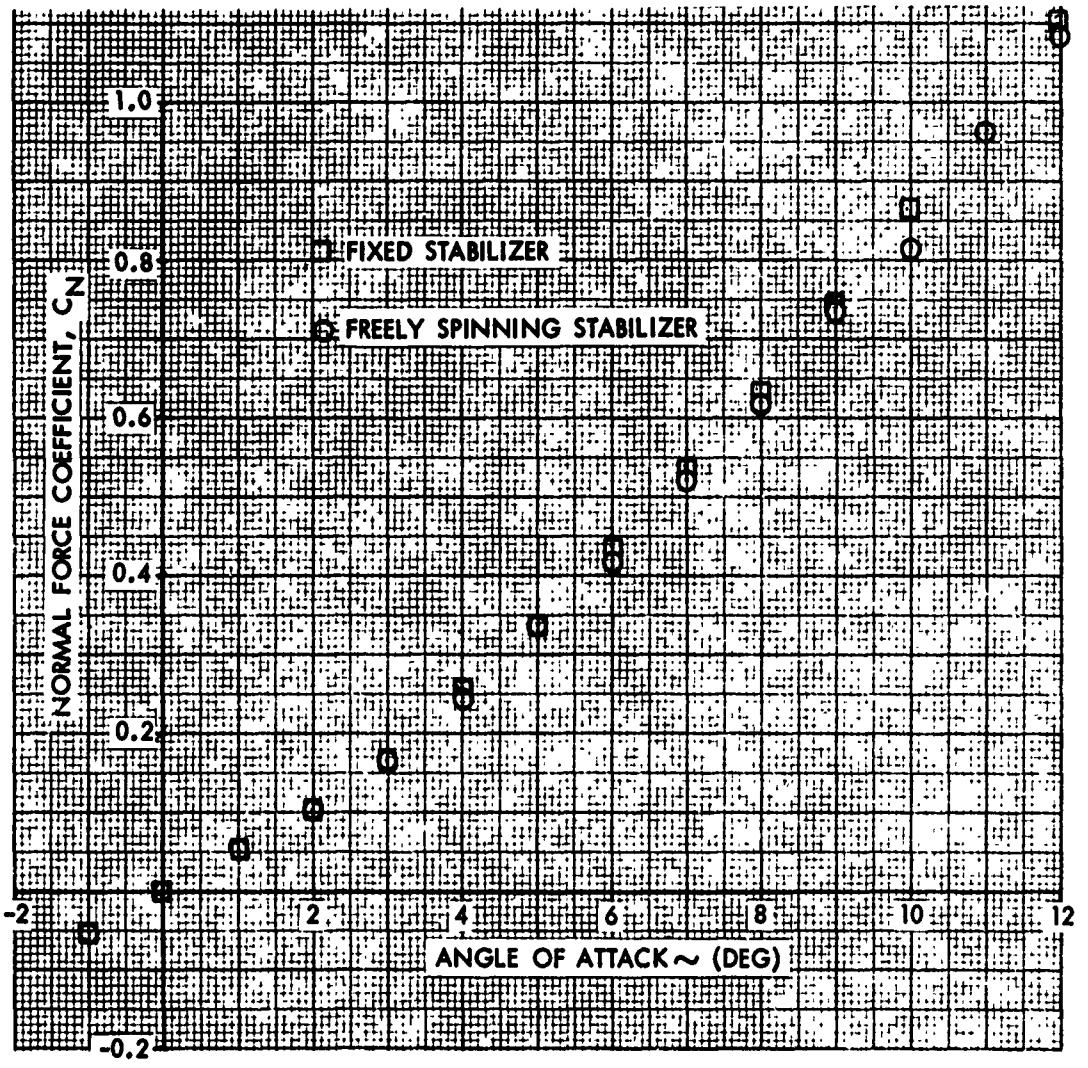

FIG. 12 NORMAL FORCE COEFFICIENT VERSUS ANGLE OF ATTACK FOR THE FIXED AND FREELY SPINNING STABILIZERS AT A FIN CANT OF 2 DEGREES AND A MACH NUMBER OF 0.89

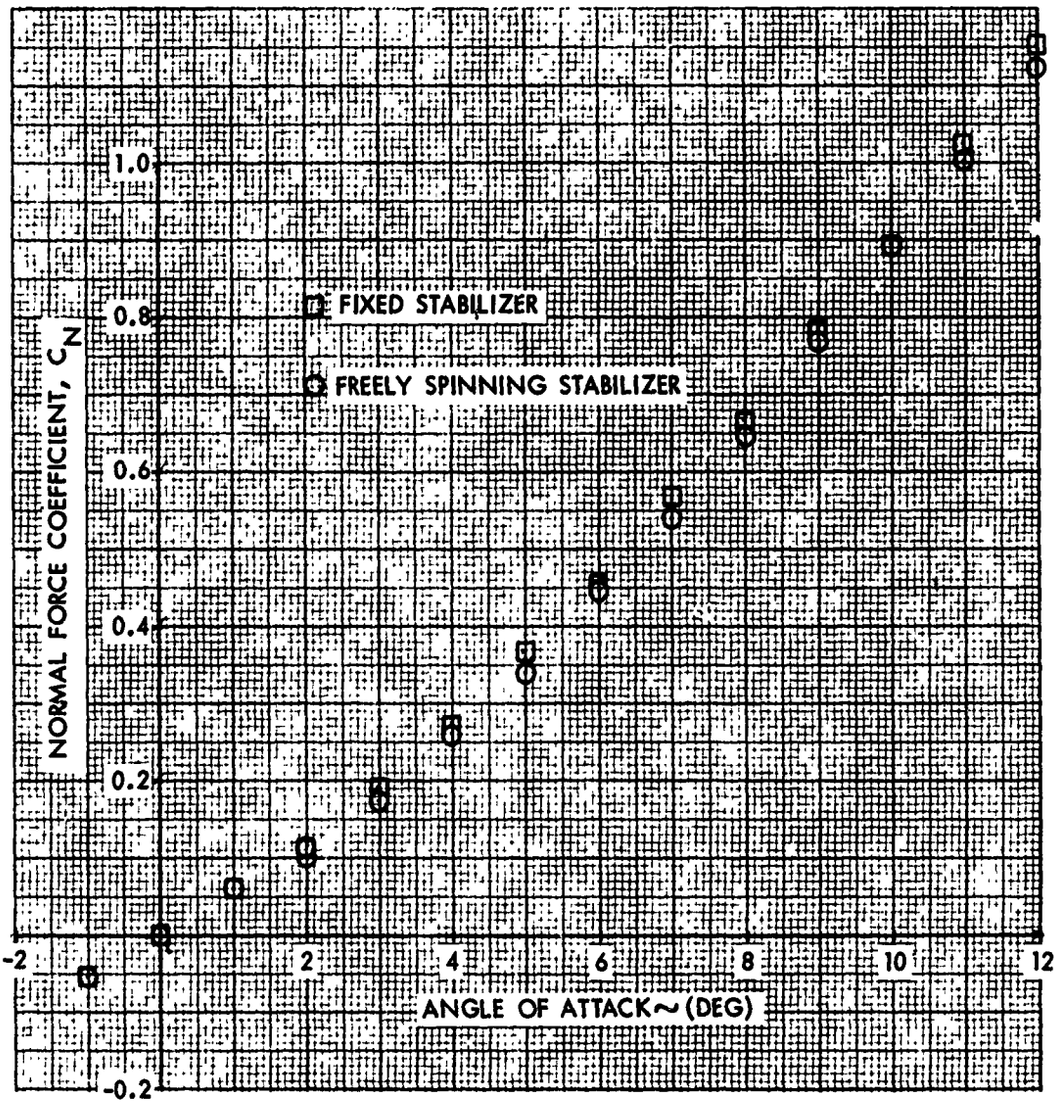

FIG. 13 NORMAL FORCE COEFFICIENT VERSUS ANGLE OF ATTACK FOR THE FIXED AND FREELY SPINNING STABILIZERS AT A FIN CANT OF 2 DEGREES AND A MACH NUMBER OF 0.94

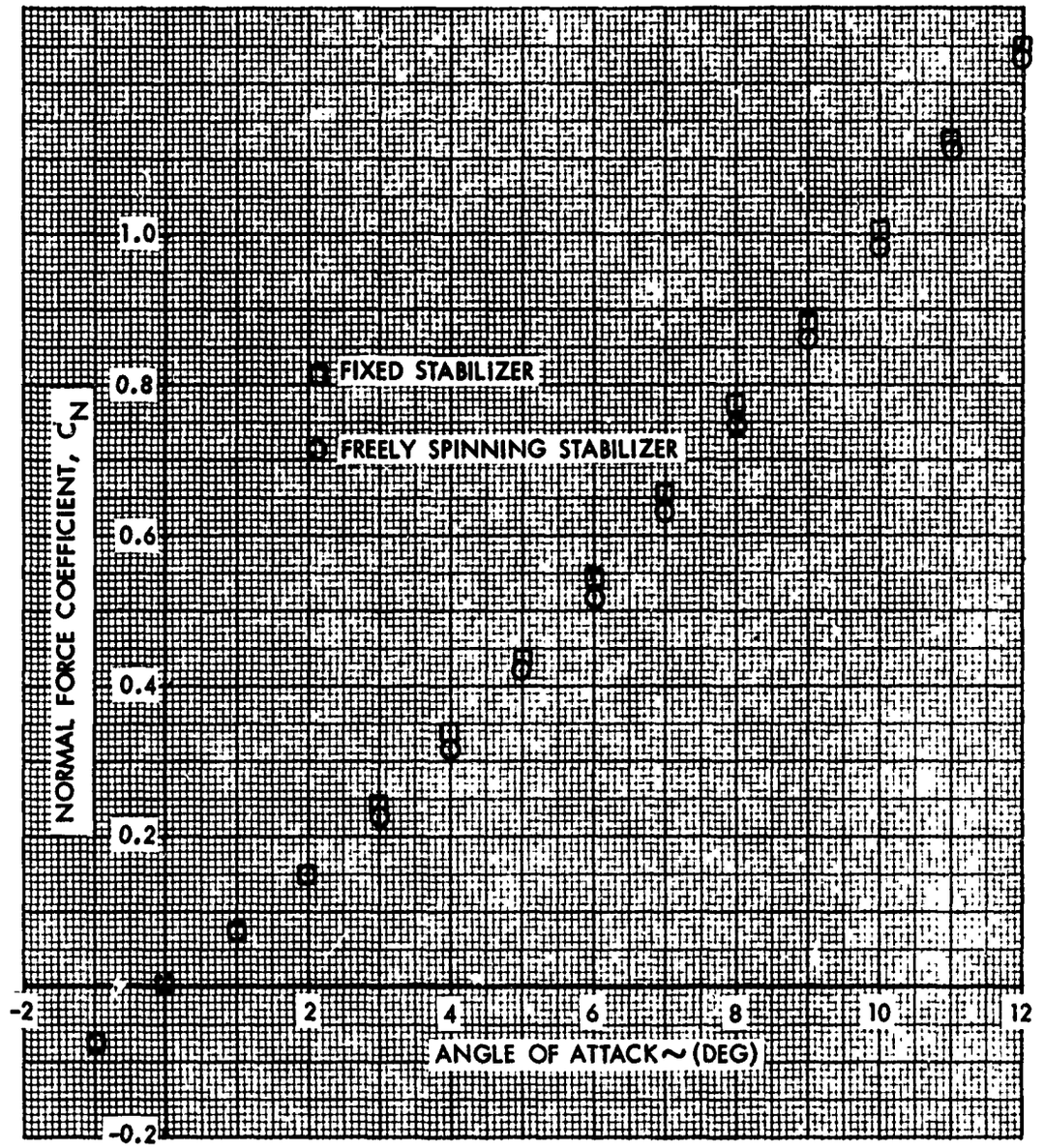

FIG. 14 NORMAL FORCE COEFFICIENT VERSUS ANGLE OF ATTACK FOR THE FIXED AND FREELY SPINNING STABILIZERS AT A FIN CANT OF 2 DEGREES AND A MACH NUMBER OF 1.11

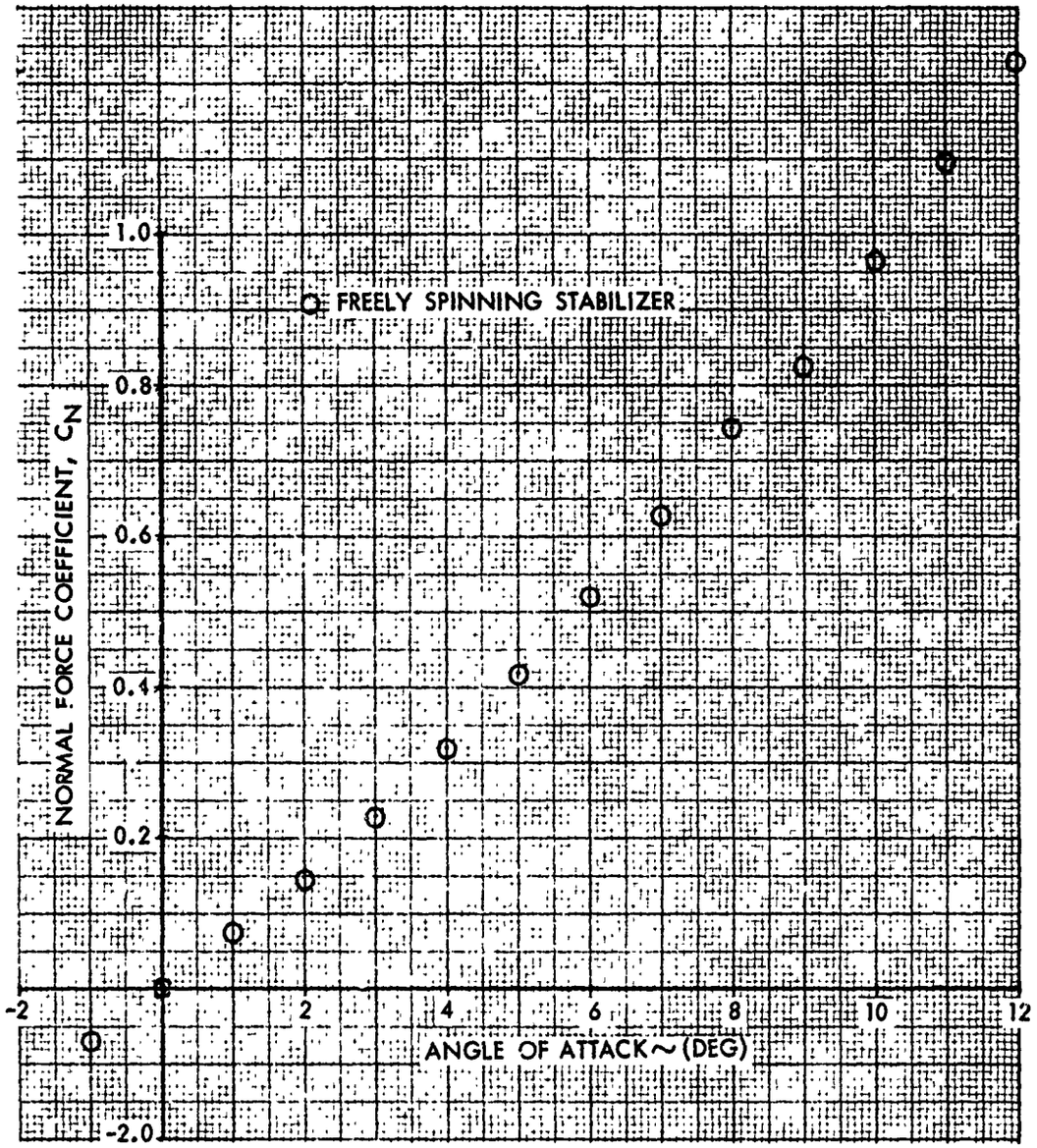

FIG. 15 NORMAL FORCE COEFFICIENT VERSUS ANGLE OF ATTACK FOR THE FIXED AND FREELY SPINNING STABILIZERS AT A FIN CANT OF 2 DEGREES AND A MACH NUMBER OF 1.19

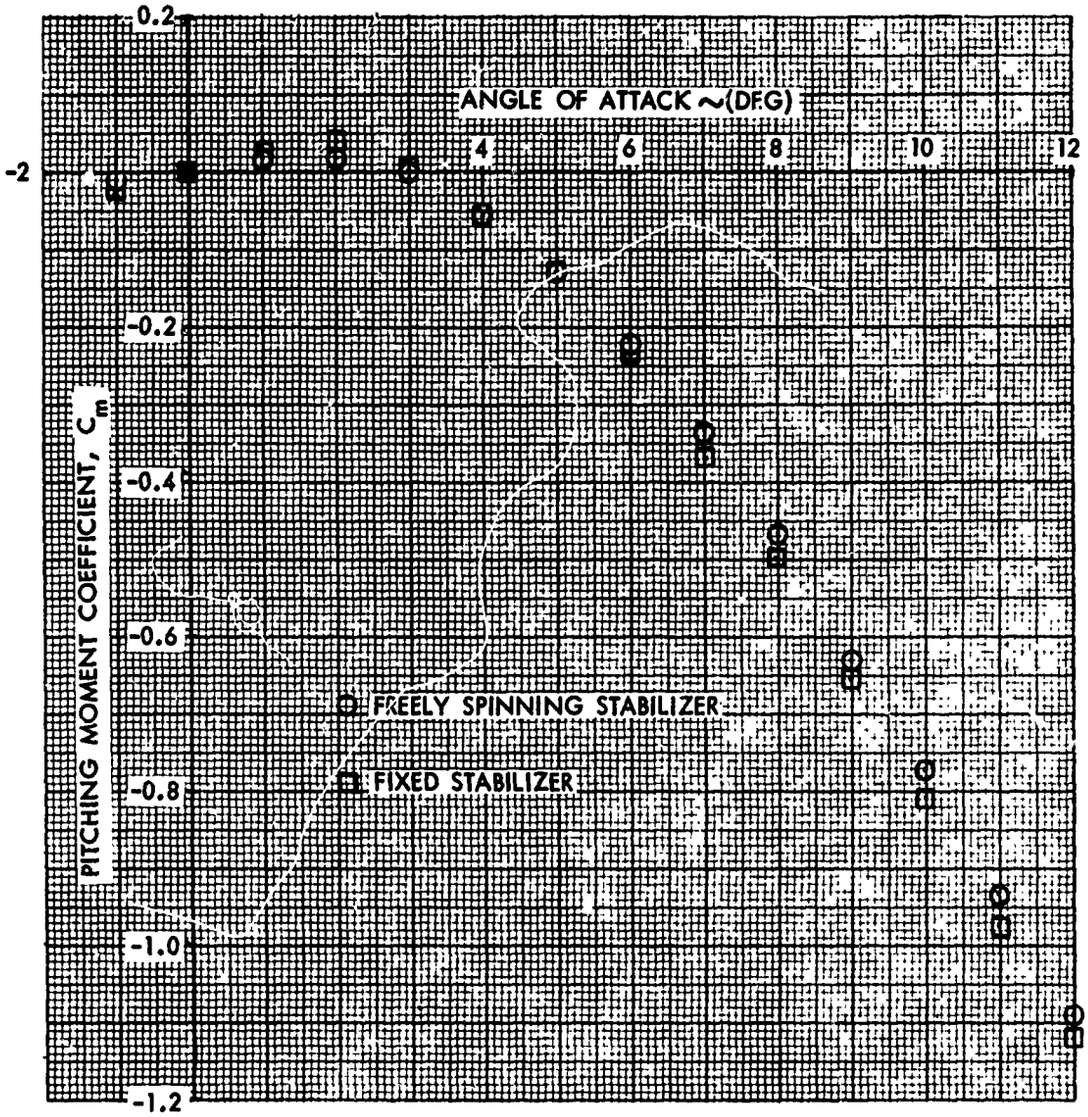

FIG. 16 PITCHING MOMENT COEFFICIENT VERSUS ANGLE OF ATTACK FOR THE FIXED AND FREELY SPINNING STABILIZER AT A FIN CANT OF 2 DEGREES AND A MACH NUMBER OF 0.59

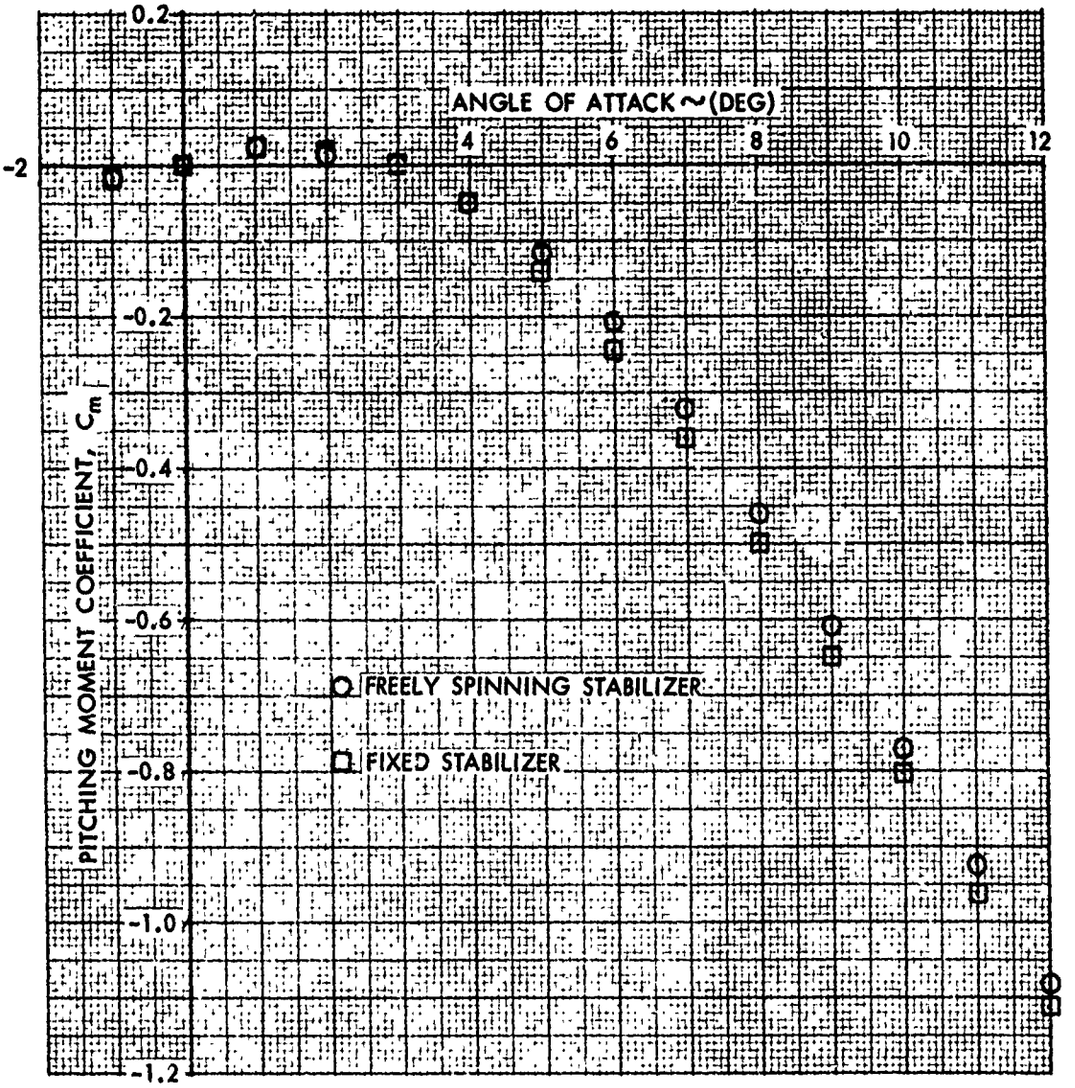

FIG. 17 PITCHING MOMENT COEFFICIENT VERSUS ANGLE OF ATTACK FOR THE FIXED AND FREELY SPINNING STABILIZER AT A FIN CANT OF 2 DEGREES AND A MACH NUMBER OF 0.69

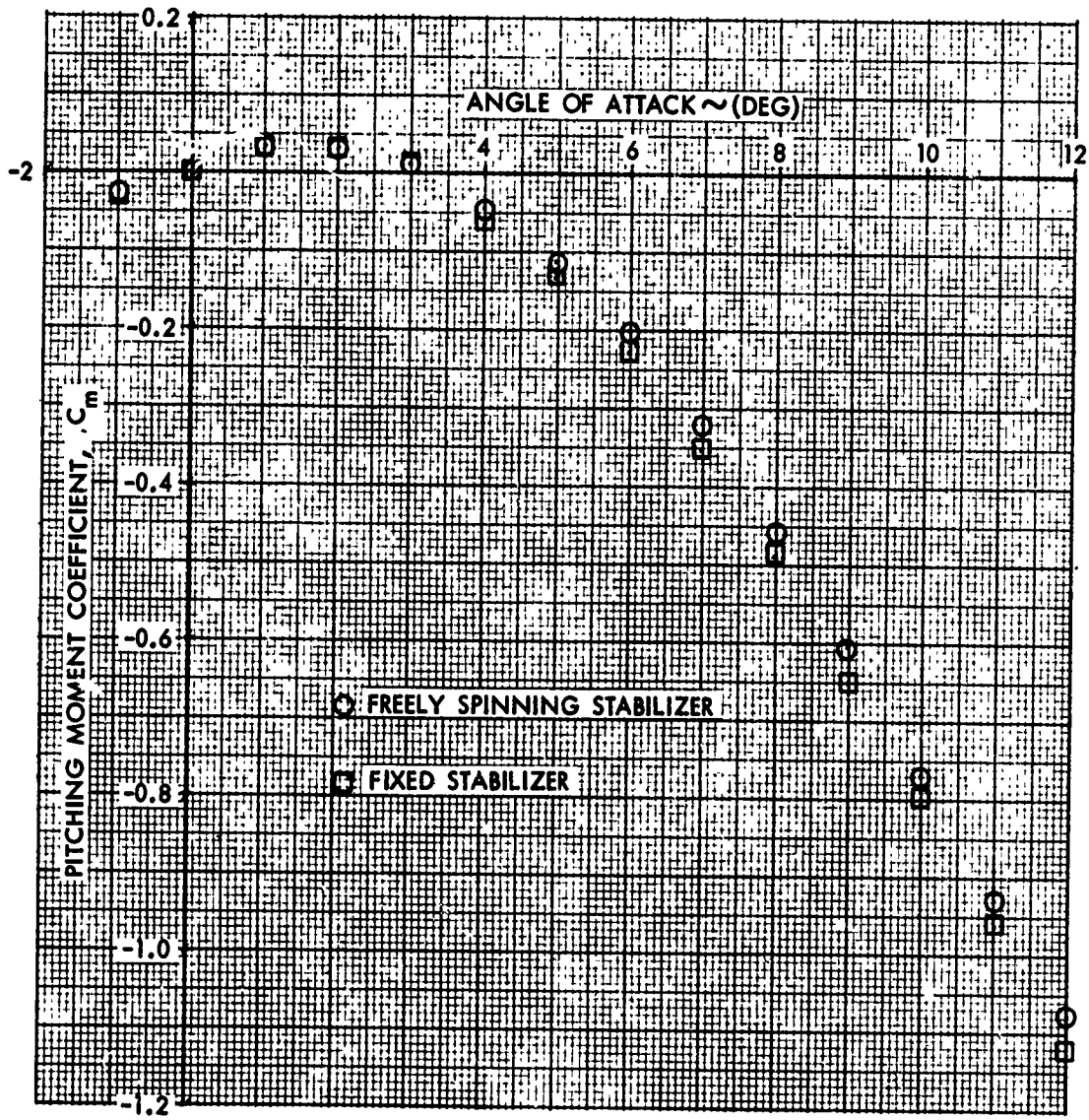

FIG. 18 PITCHING MOMENT COEFFICIENT VERSUS ANGLE OF ATTACK FOR THE FIXED AND FREELY SPINNING STABILIZER AT A FIN CANT OF 2 DEGREES AND A MACH NUMBER OF 0.74

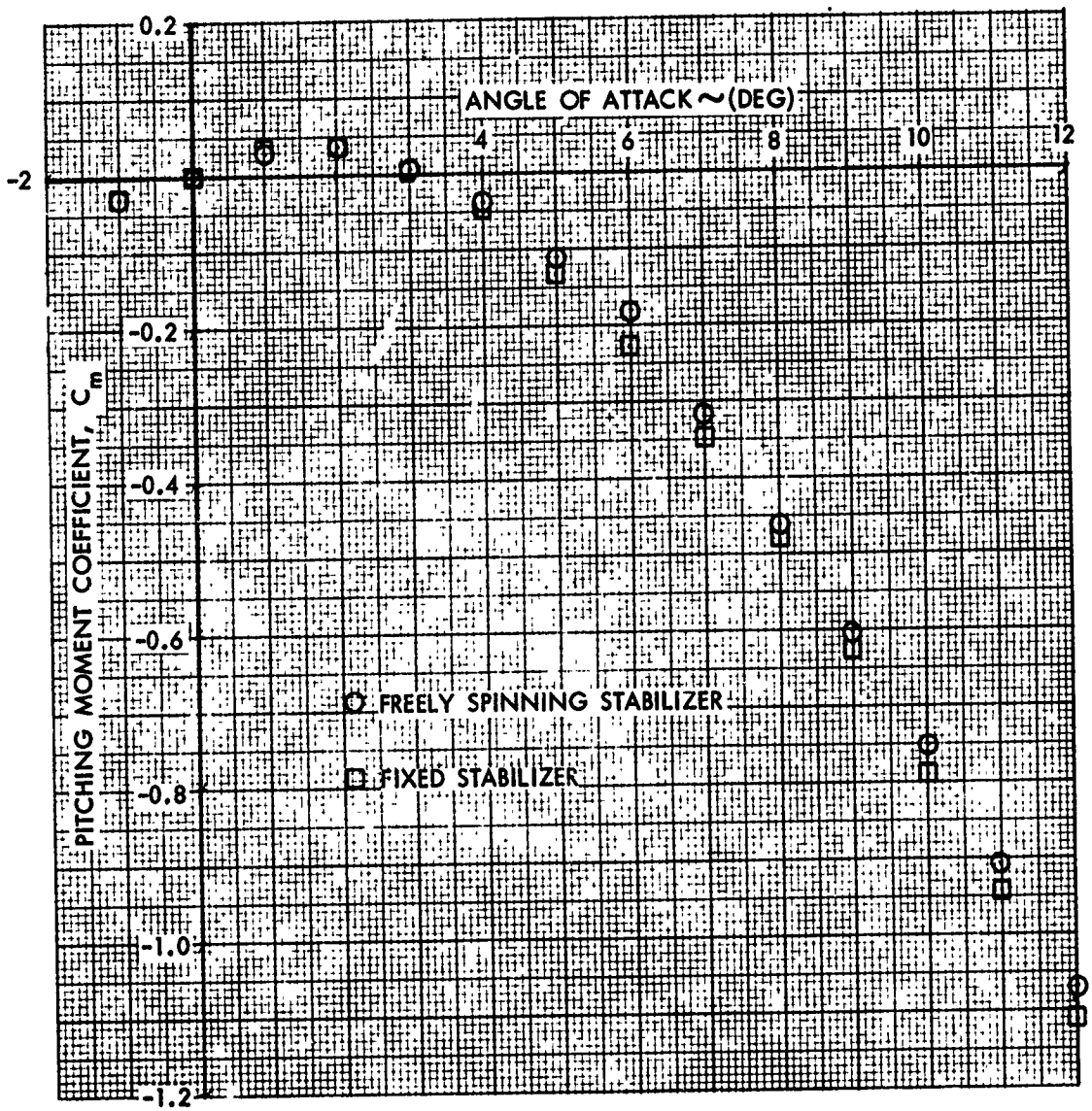

FIG. 19 PITCHING MOMENT COEFFICIENT VERSUS ANGLE OF ATTACK FOR THE FIXED AND FREELY SPINNING STABILIZER AT A FIN CANT OF 2 DEGREES AND A MACH NUMBER OF 0.79

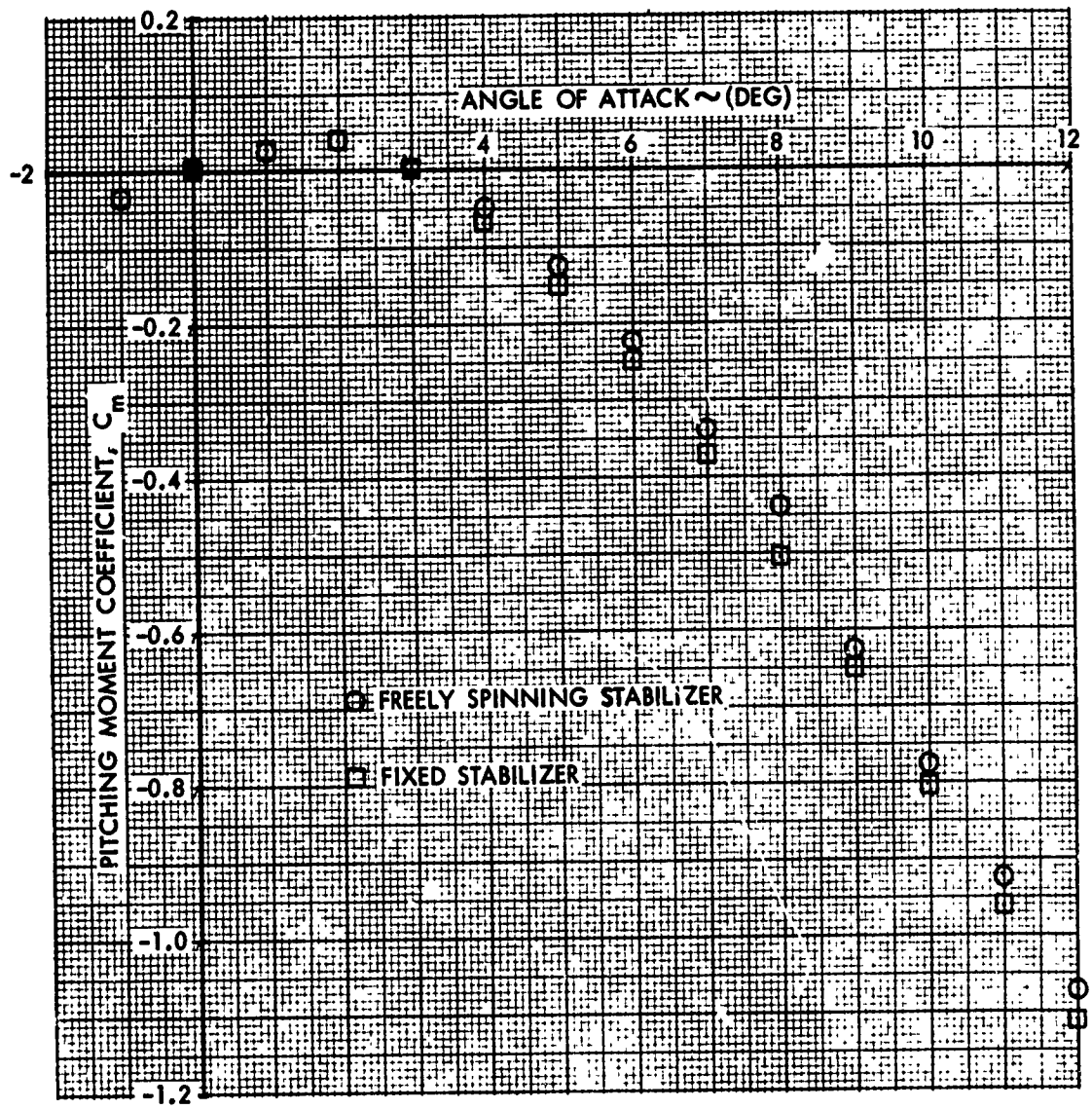

FIG. 20 PITCHING MOMENT COEFFICIENT VERSUS ANGLE OF ATTACK FOR THE FIXED AND FREELY SPINNING STABILIZER AT A FIN CANT OF 2 DEGREES AND A MACH NUMBER OF 0.84

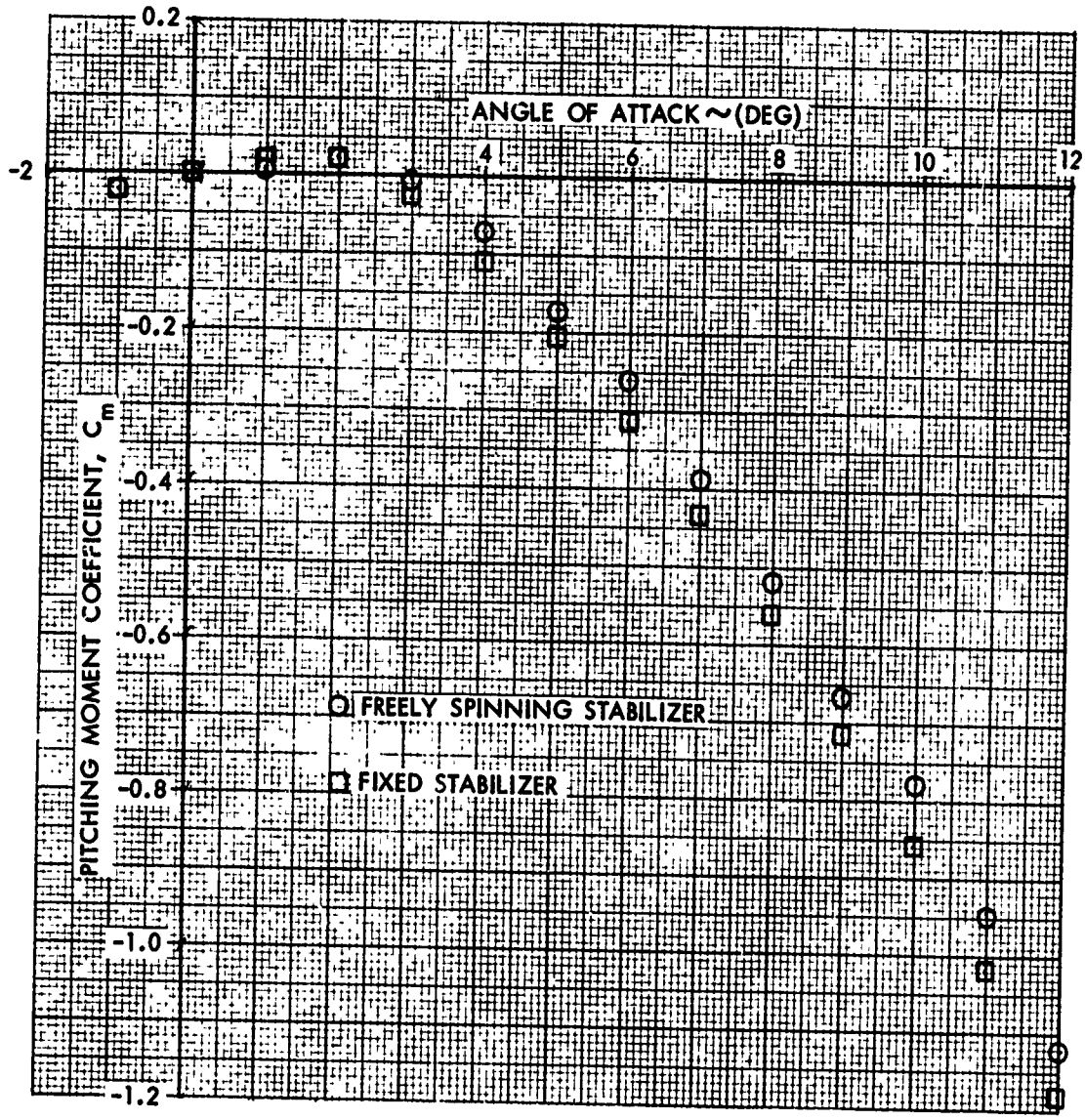

FIG. 21 PITCHING MOMENT COEFFICIENT VERSUS ANGLE OF ATTACK FOR THE FIXED AND FREELY SPINNING STABILIZER AT A FIN CANT OF 2 DEGREES AND A MACH NUMBER OF 0.89

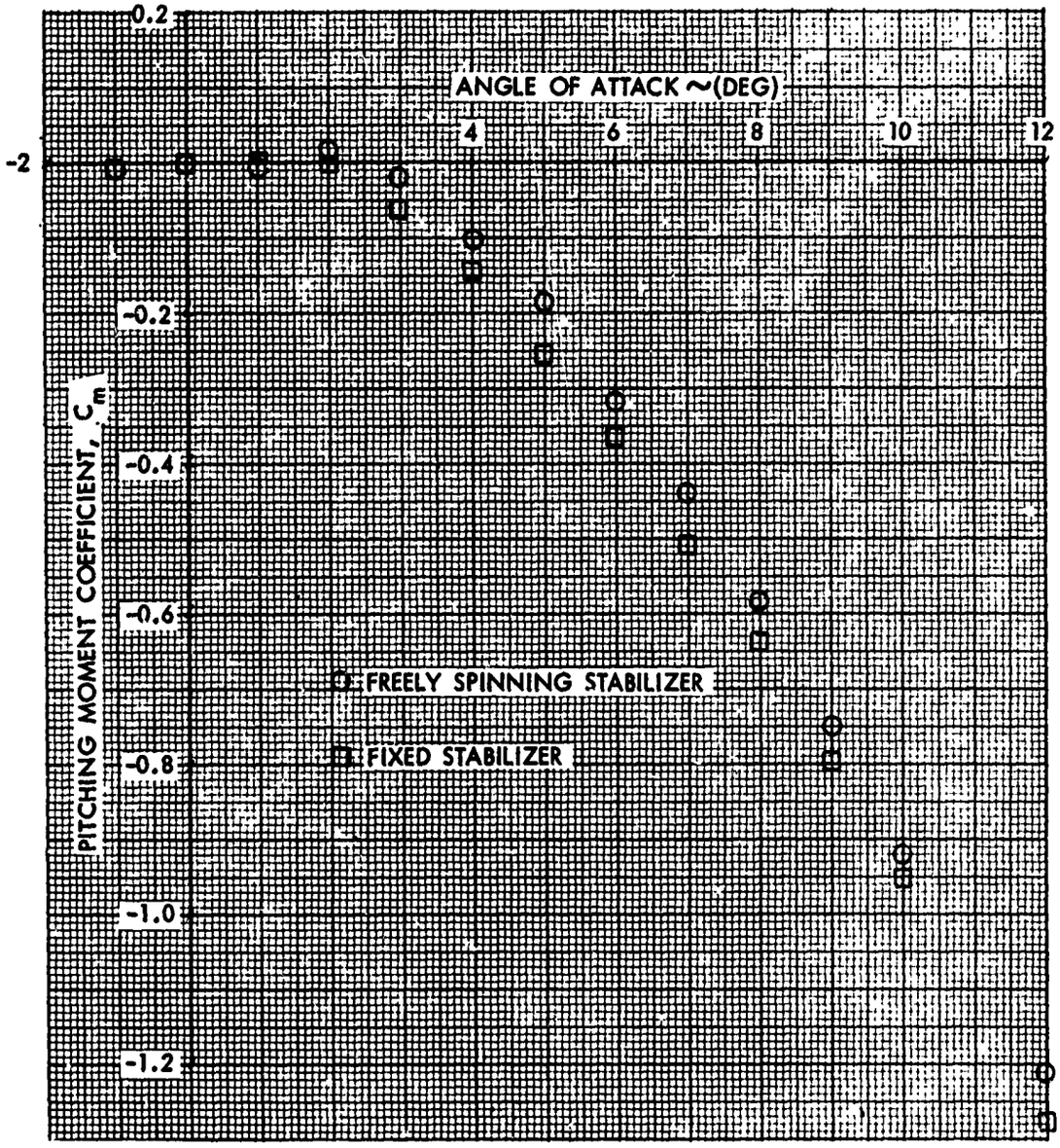

FIG. 22 PITCHING MOMENT COEFFICIENT VERSUS ANGLE OF ATTACK FOR THE FIXED AND FREELY SPINNING STABILIZER AT A FIN CANT OF 2 DEGREES AND A MACH NUMBER OF 0.94

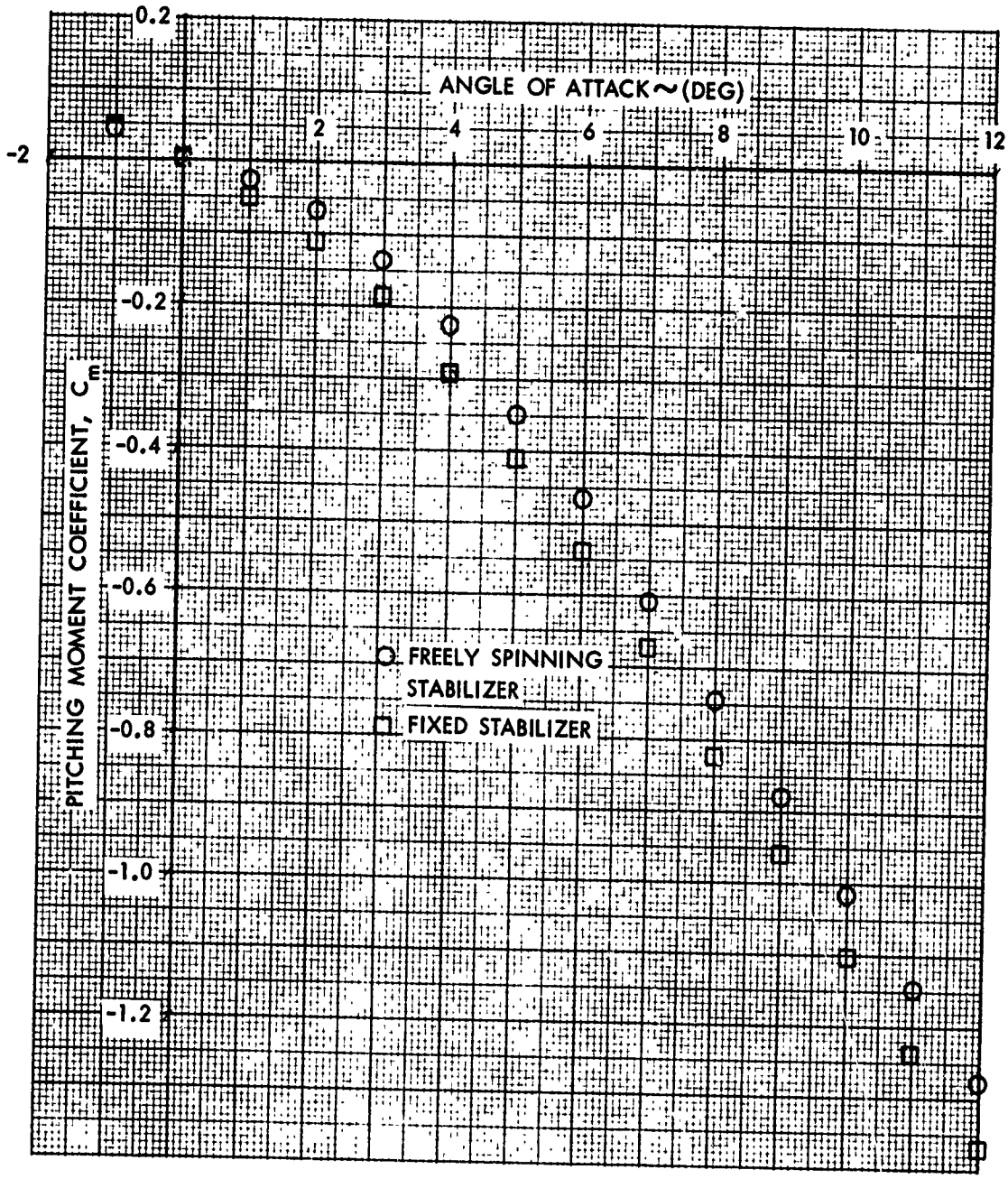

FIG. 23 PITCHING MOMENT COEFFICIENT VERSUS ANGLE OF ATTACK FOR THE FIXED AND FREELY SPINNING STABILIZER AT A FIN CANT OF 2 DEGREES AND A MACH NUMBER OF 1.10

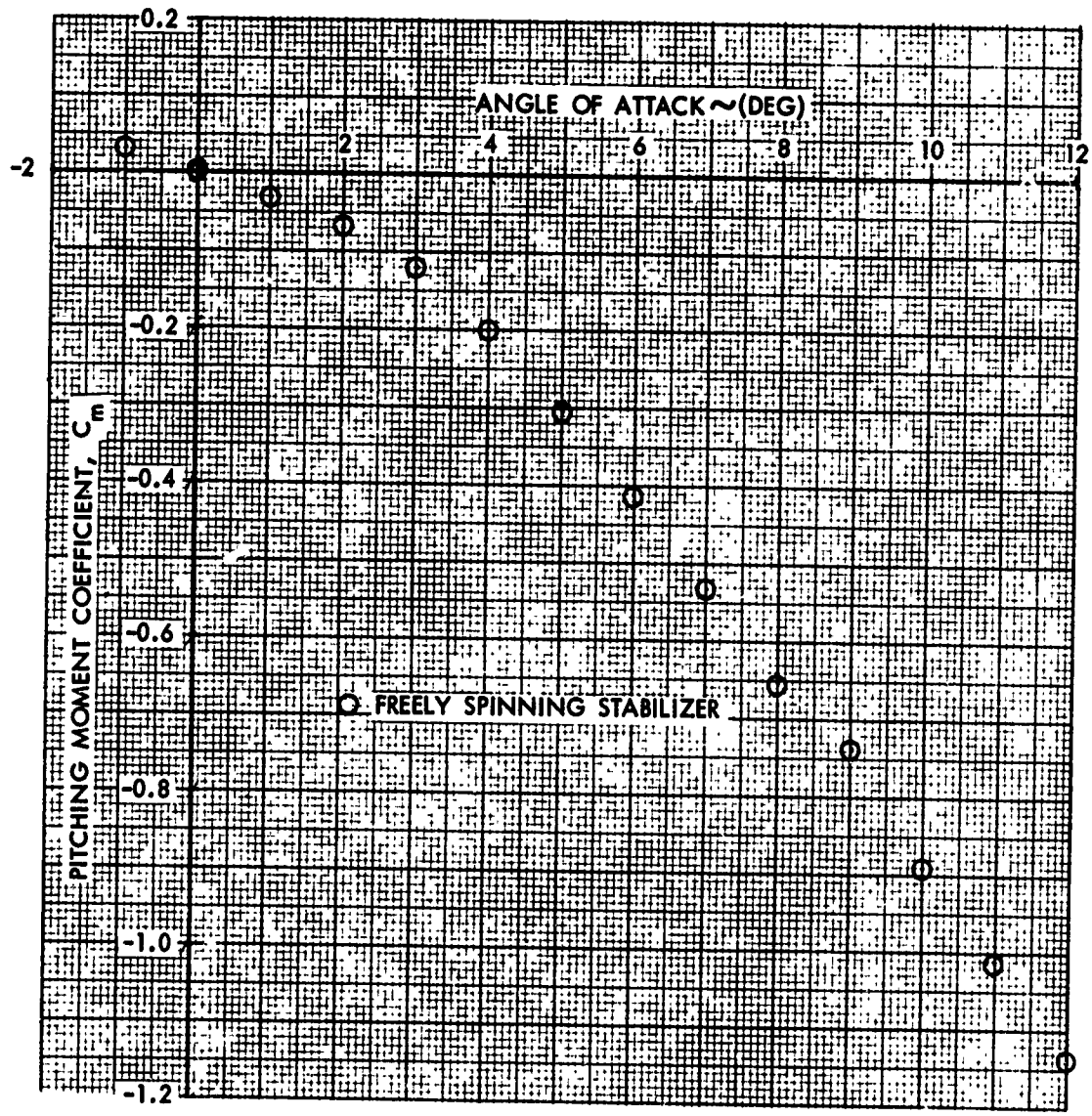

FIG. 24 PITCHING MOMENT COEFFICIENT VERSUS ANGLE OF ATTACK FOR THE FIXED AND FREELY SPINNING STABILIZER AT A FIN CANT OF 2 DEGREES AND A MACH NUMBER OF 1.20

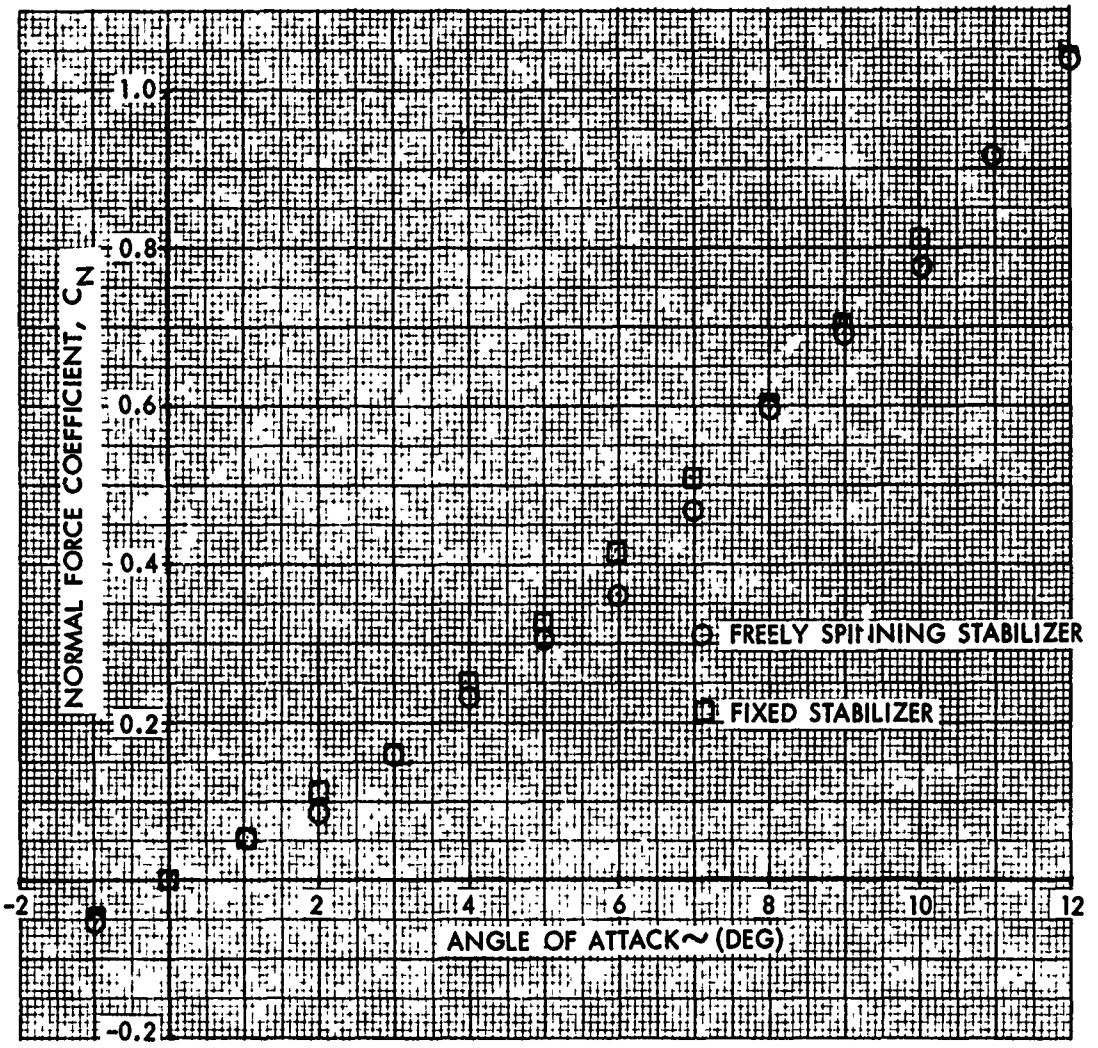

FIG. 25 NORMAL FORCE COEFFICIENT VERSUS ANGLE OF ATTACK FOR THE FIXED AND FREELY SPINNING STABILIZERS AT A FIN CANT OF 4 DEGREES AND A MACH NUMBER OF 0.59

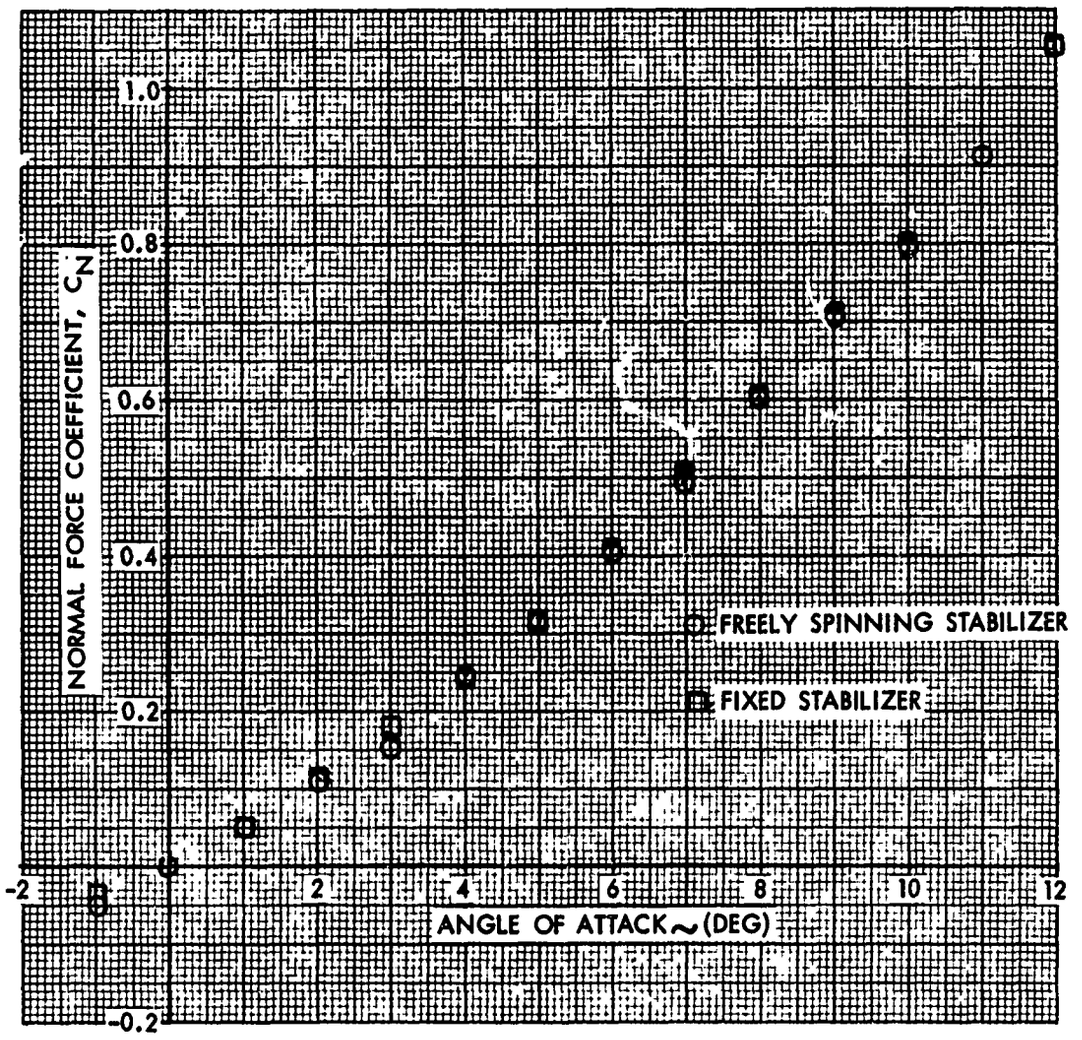

FIG. 26 NORMAL FORCE COEFFICIENT VERSUS ANGLE OF ATTACK FOR THE FIXED AND FREELY SPINNING STABILIZERS AT A FIN CANT OF 4 DEGREES AND A MACH NUMBER OF 0.69

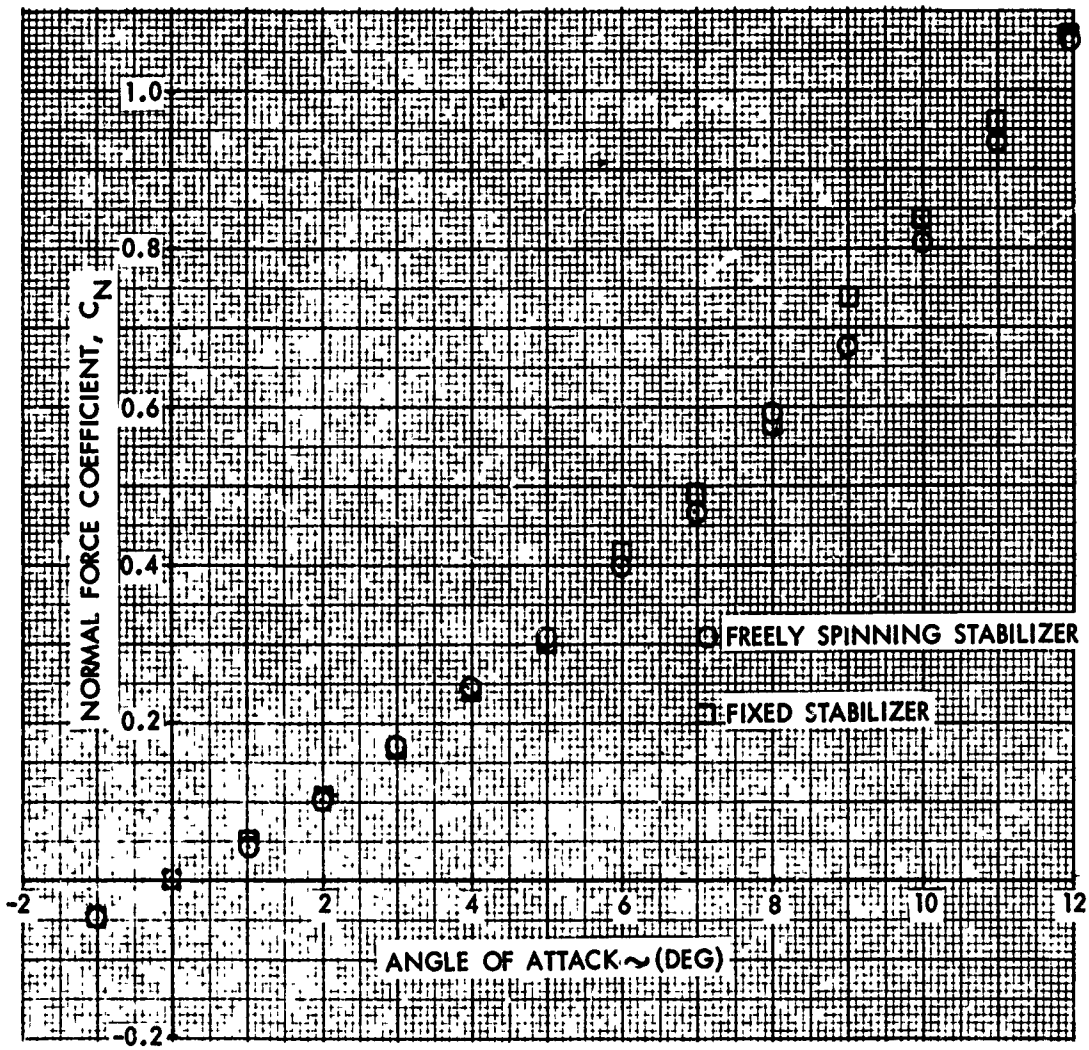

FIG. 27 NORMAL FORCE COEFFICIENT VERSUS ANGLE OF ATTACK FOR THE FIXED AND FREELY SPINNING STABILIZERS AT A FIN CANT OF 4 DEGREES AND A MACH NUMBER OF 0.74

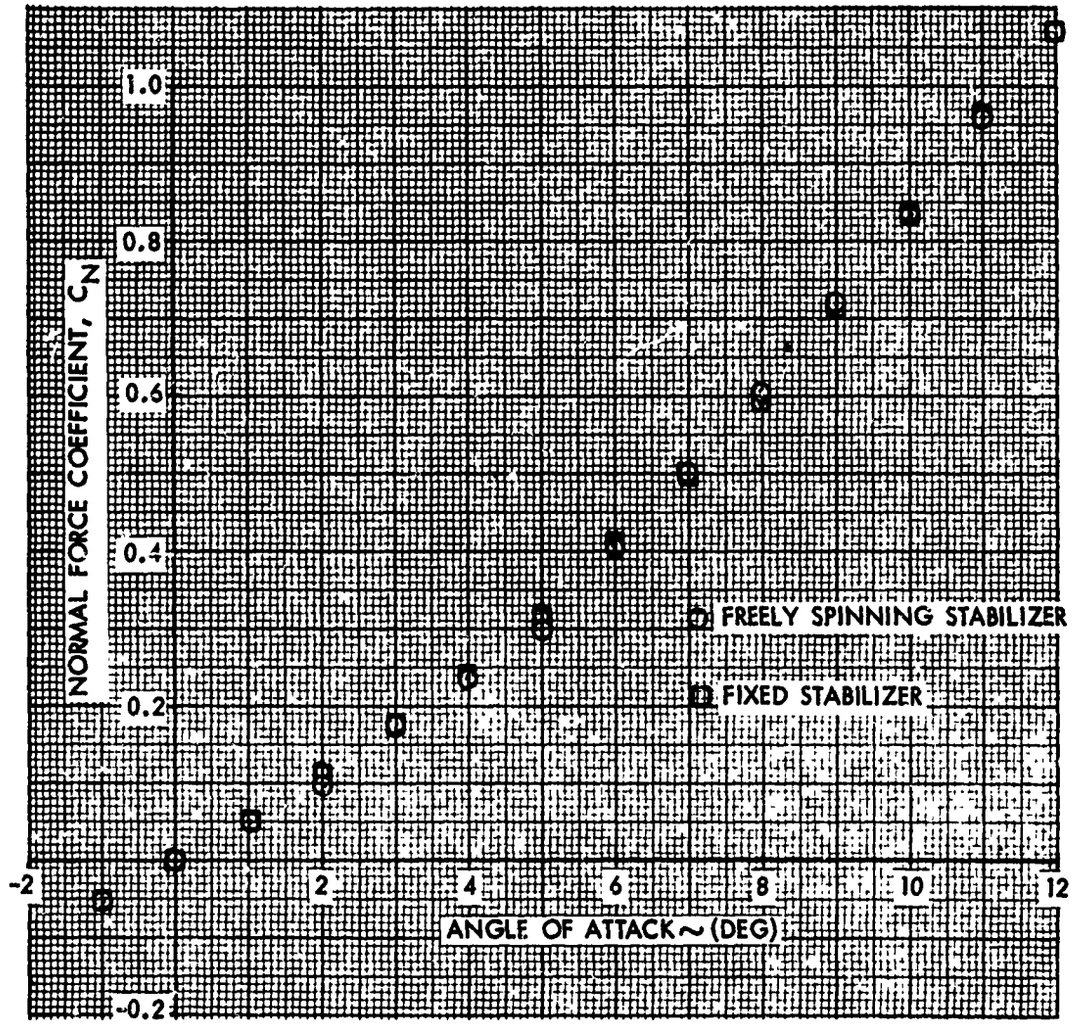

FIG. 28 NORMAL FORCE COEFFICIENT VERSUS ANGLE OF ATTACK FOR THE FIXED AND FREELY SPINNING STABILIZERS AT A FIN CANT OF 4 DEGREES AND A MACH NUMBER OF 0.79

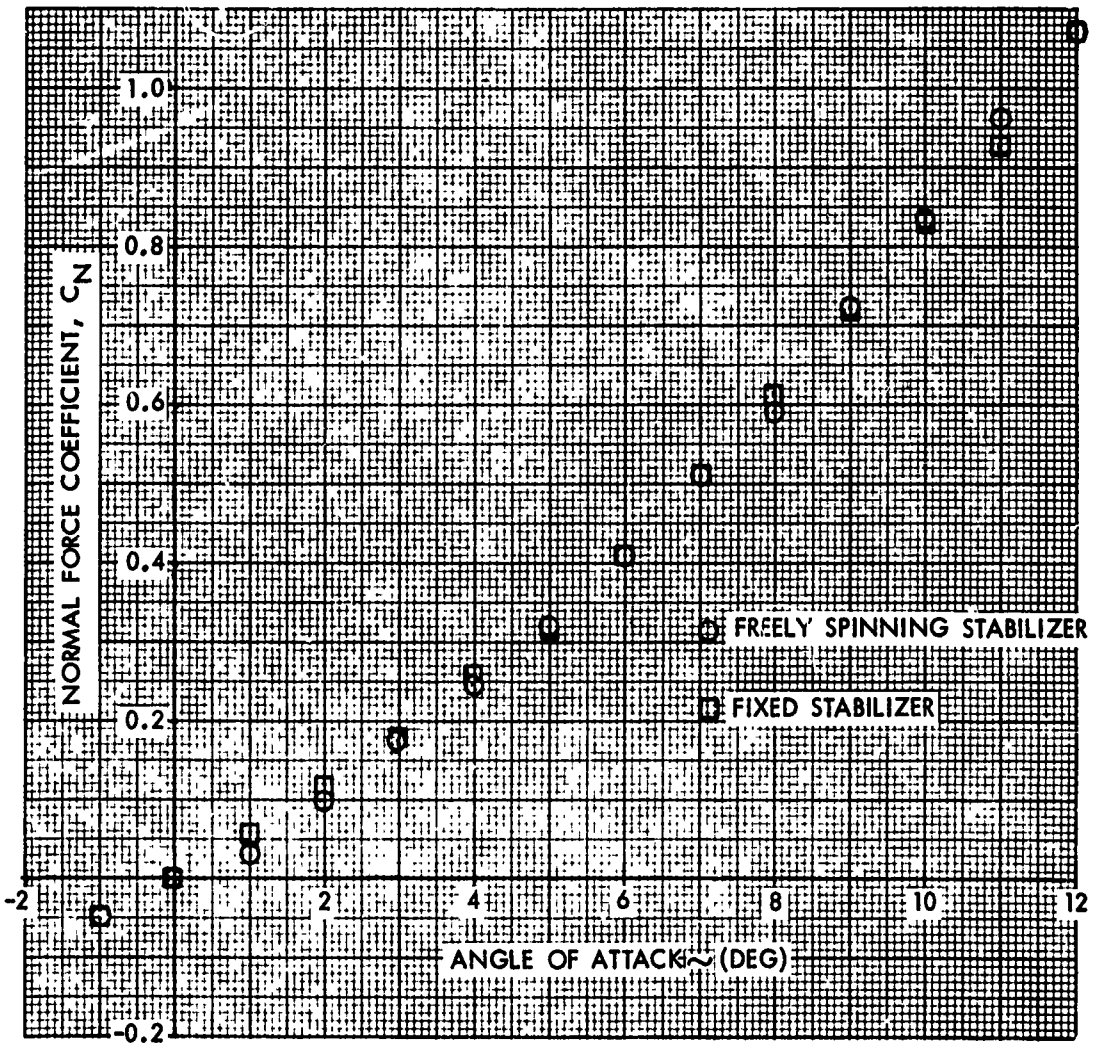

FIG. 29 NORMAL FORCE COEFFICIENT VERSUS ANGLE OF ATTACK FOR THE FIXED AND FREELY SPINNING STABILIZERS AT A FIN CANT OF 4 DEGREES AND A MACH NUMBER OF 0.84

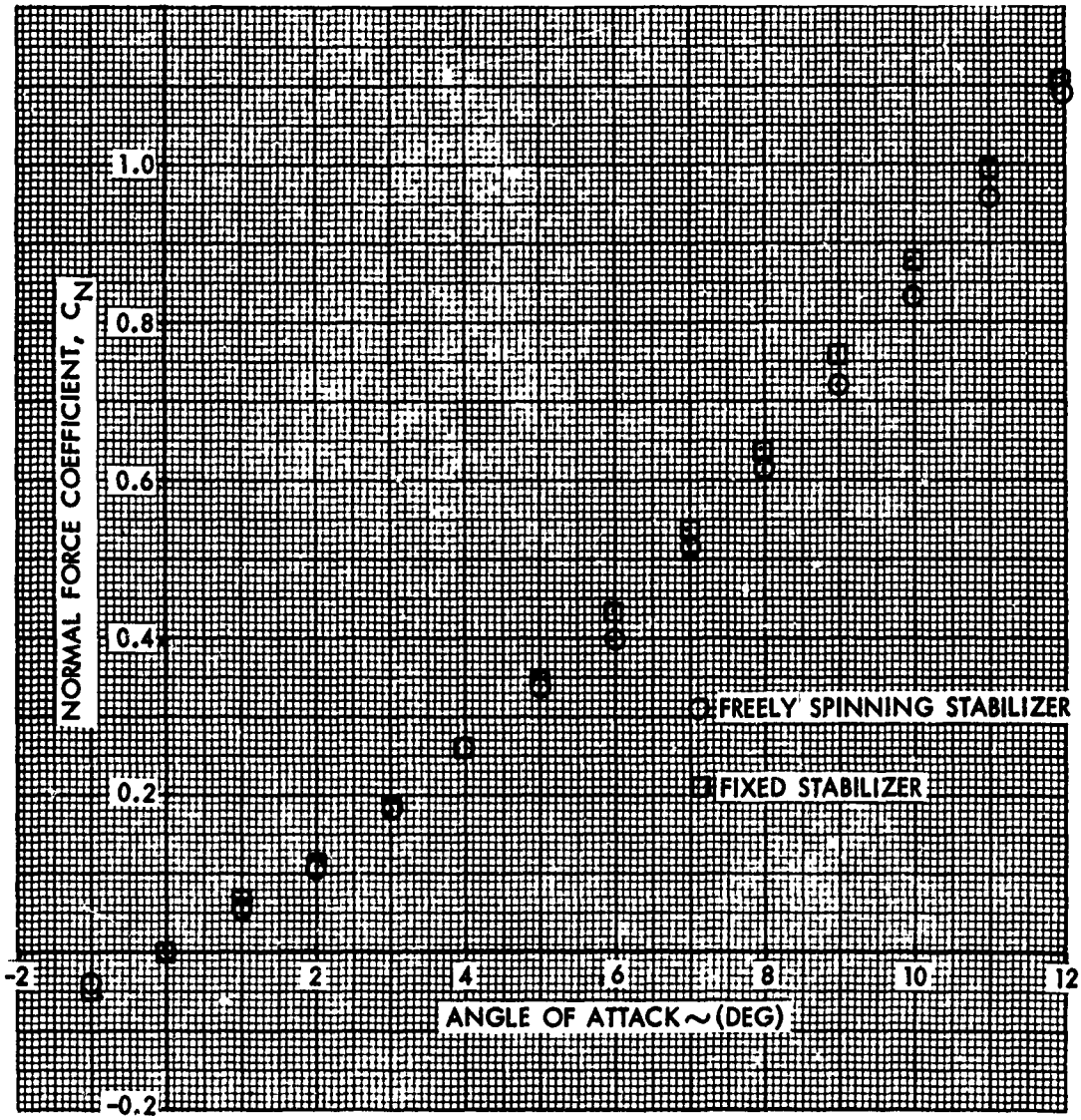

FIG. 30 NORMAL FORCE COEFFICIENT VERSUS ANGLE OF ATTACK FOR THE FIXED AND FREELY SPINNING STABILIZERS AT A FIN CANT OF 4 DEGREES AND A MACH NUMBER OF 0.89

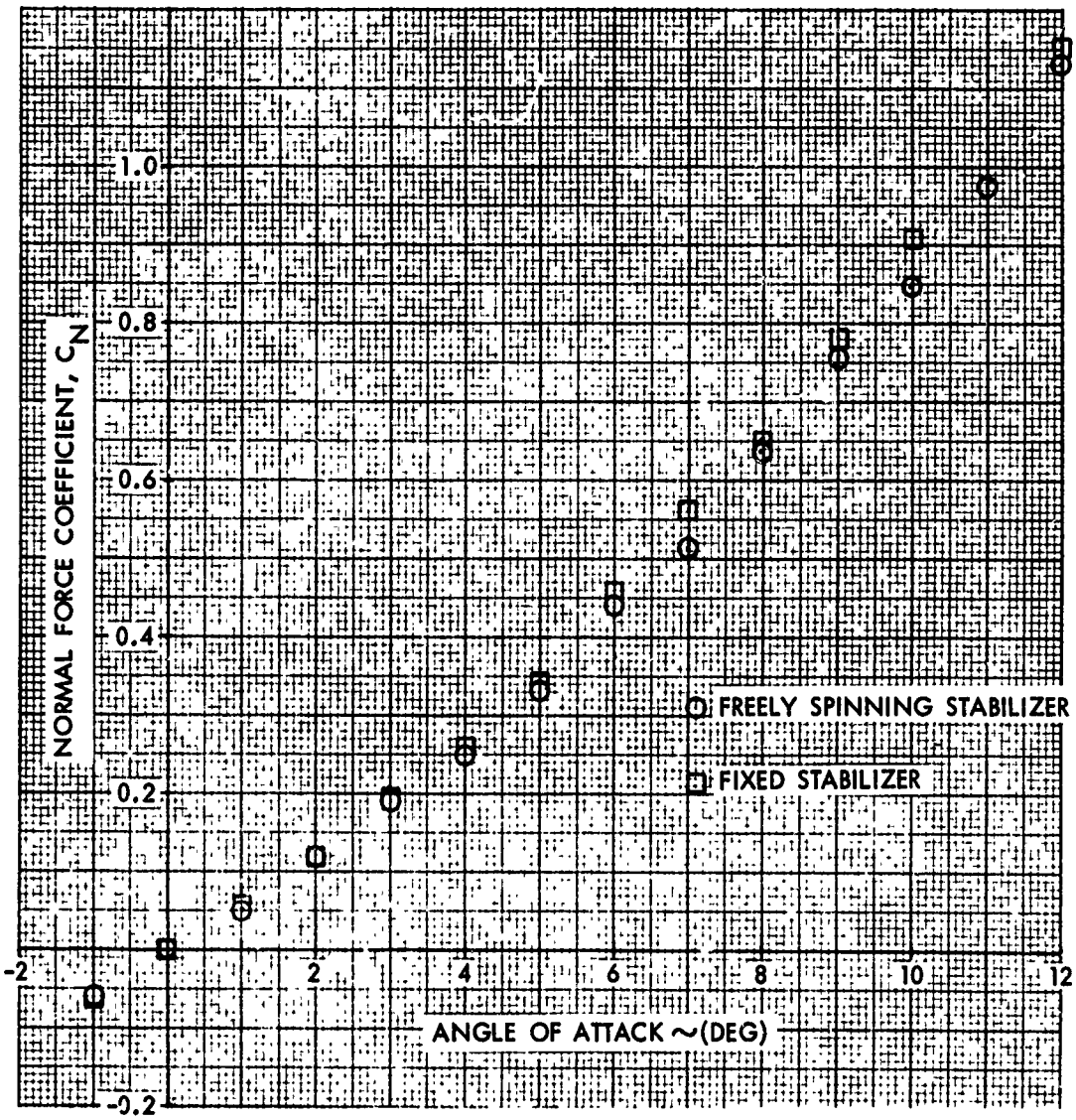

FIG. 31 NORMAL FORCE COEFFICIENT VERSUS ANGLE OF ATTACK FOR THE FIXED AND FREELY SPINNING STABILIZERS AT A FIN CANT OF 4 DEGREES AND A MACH NUMBER OF 0.94

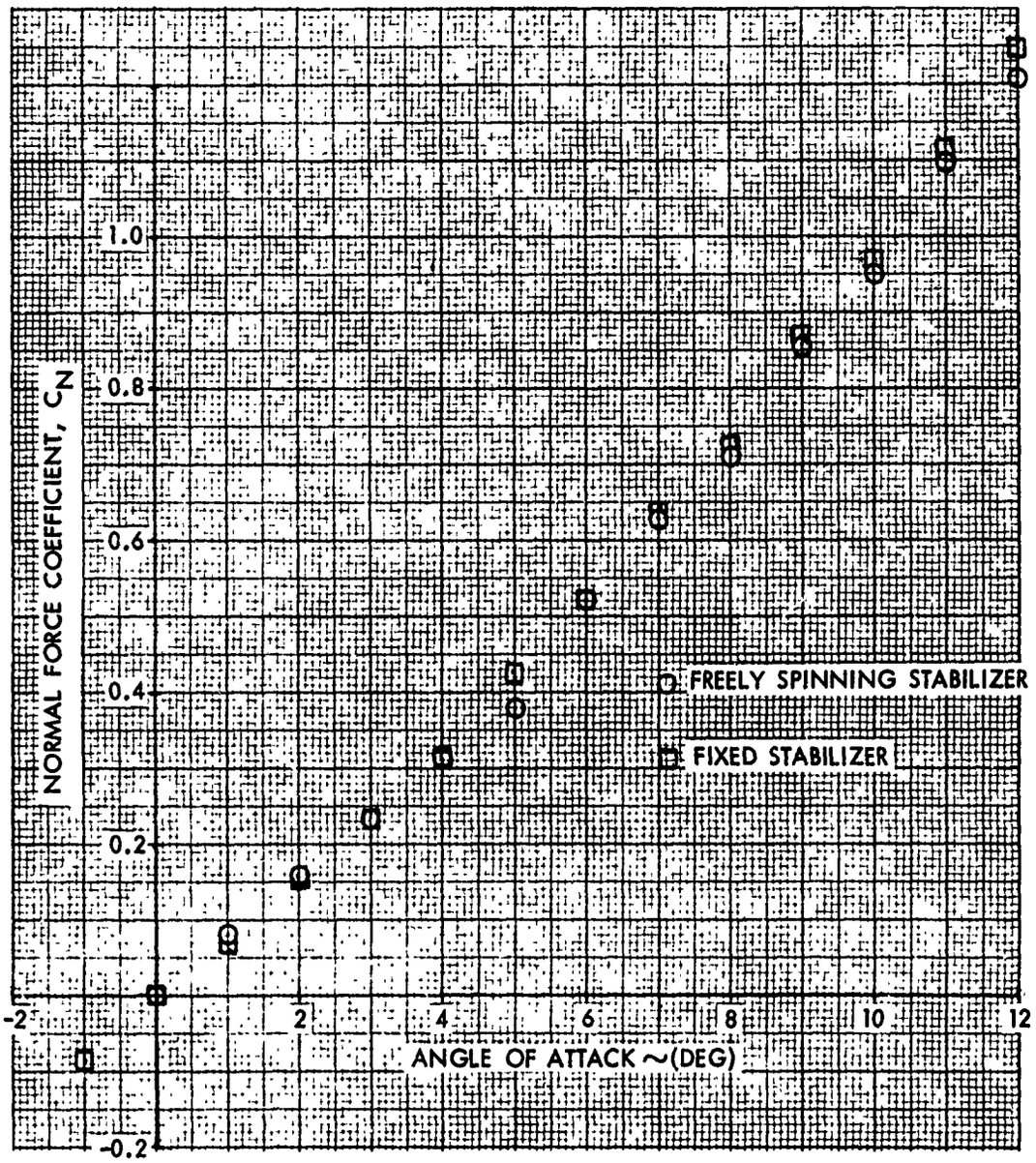

FIG. 32 NORMAL FORCE COEFFICIENT VERSUS ANGLE OF ATTACK FOR THE FIXED AND FREELY SPINNING STABILIZERS AT A FIN CANT OF 4 DEGREES AND A MACH NUMBER OF 1.11

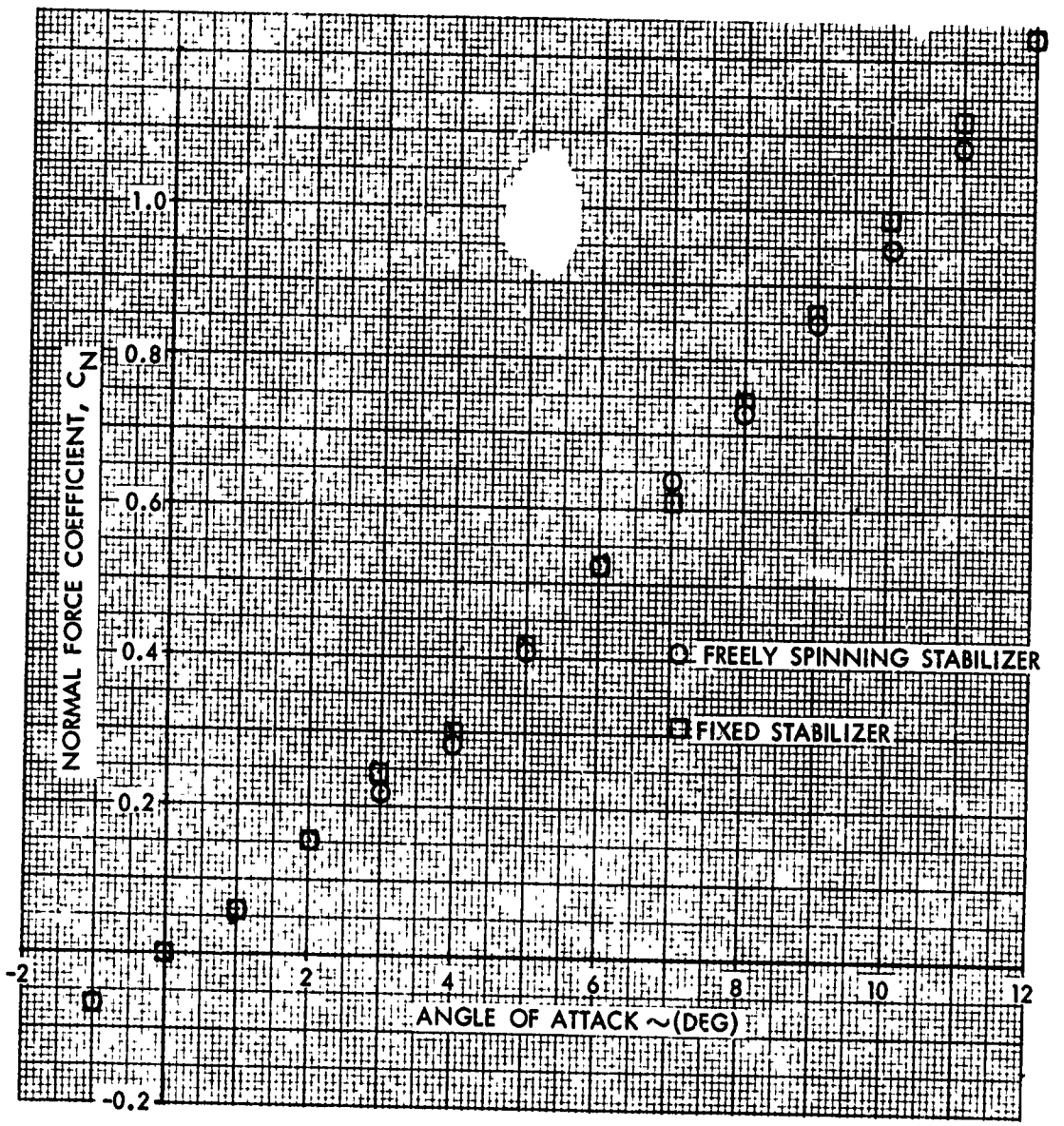

FIG. 33 NORMAL FORCE COEFFICIENT VERSUS ANGLE OF ATTACK FOR THE FIXED AND FREELY SPINNING STABILIZERS AT A FIN CANT OF 4 DEGREES AND A MACH NUMBER OF 1.19

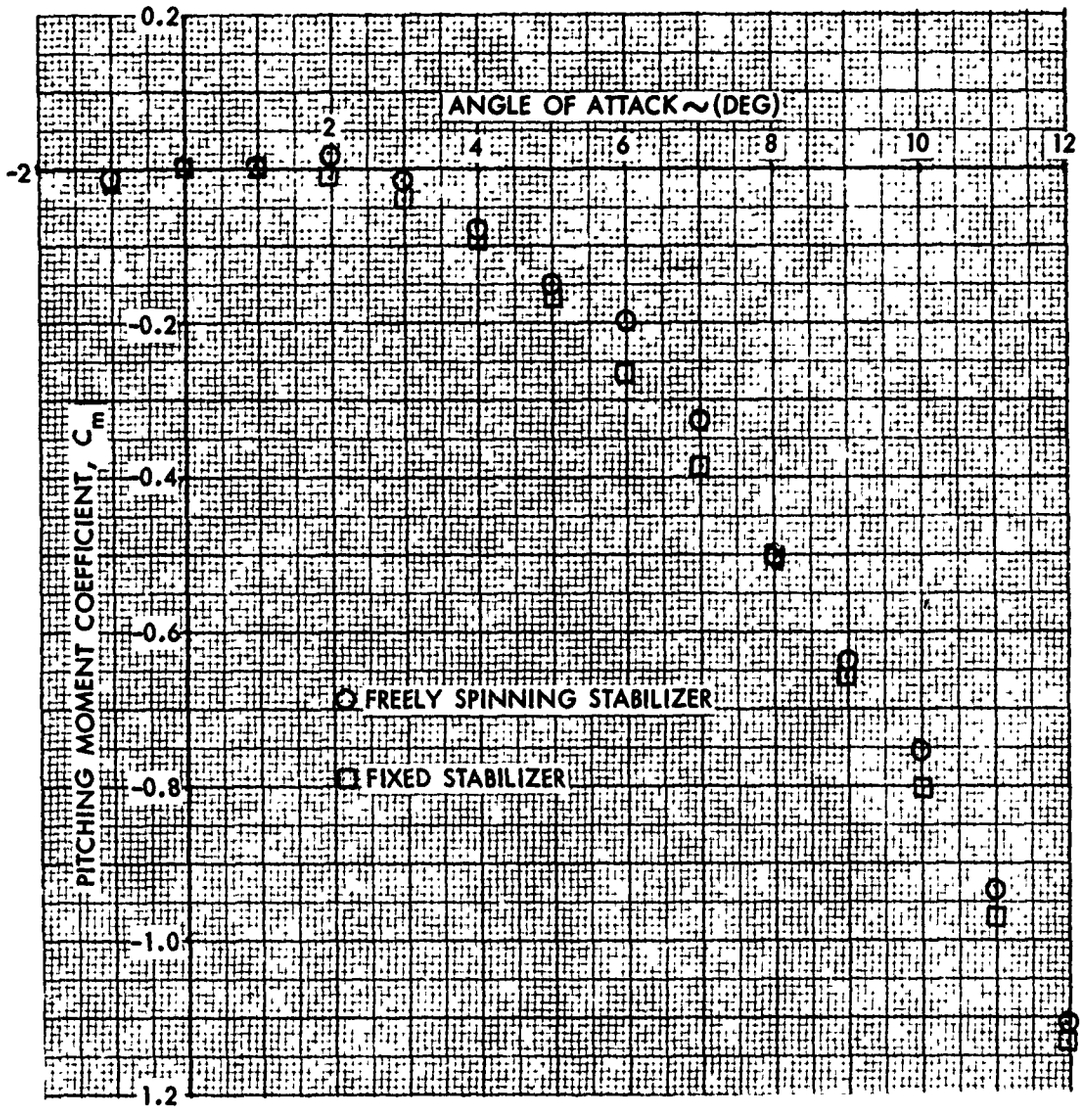

FIG. 34 PITCHING MOMENT COEFFICIENT VERSUS ANGLE OF ATTACK FOR THE FIXED AND FREELY SPINNING STABILIZERS AT A FIN CANT OF 4 DEGREES AND A MACH NUMBER OF 0.59

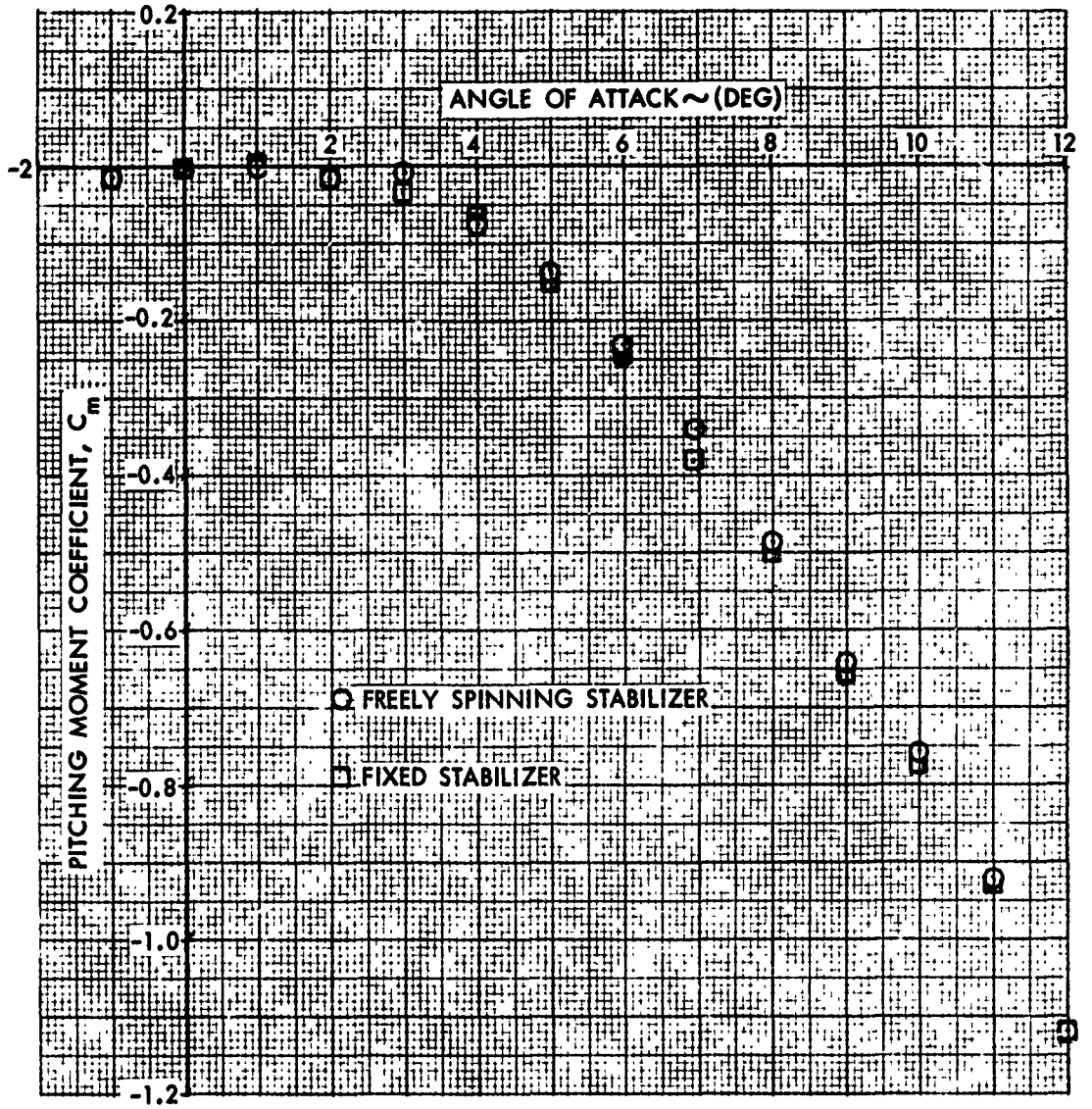

FIG. 35 PITCHING MOMENT COEFFICIENT VERSUS ANGLE OF ATTACK FOR THE FIXED AND FREELY SPINNING STABILIZERS AT A FIN CANT OF 4 DEGREES AND A MACH NUMBER OF 0.69

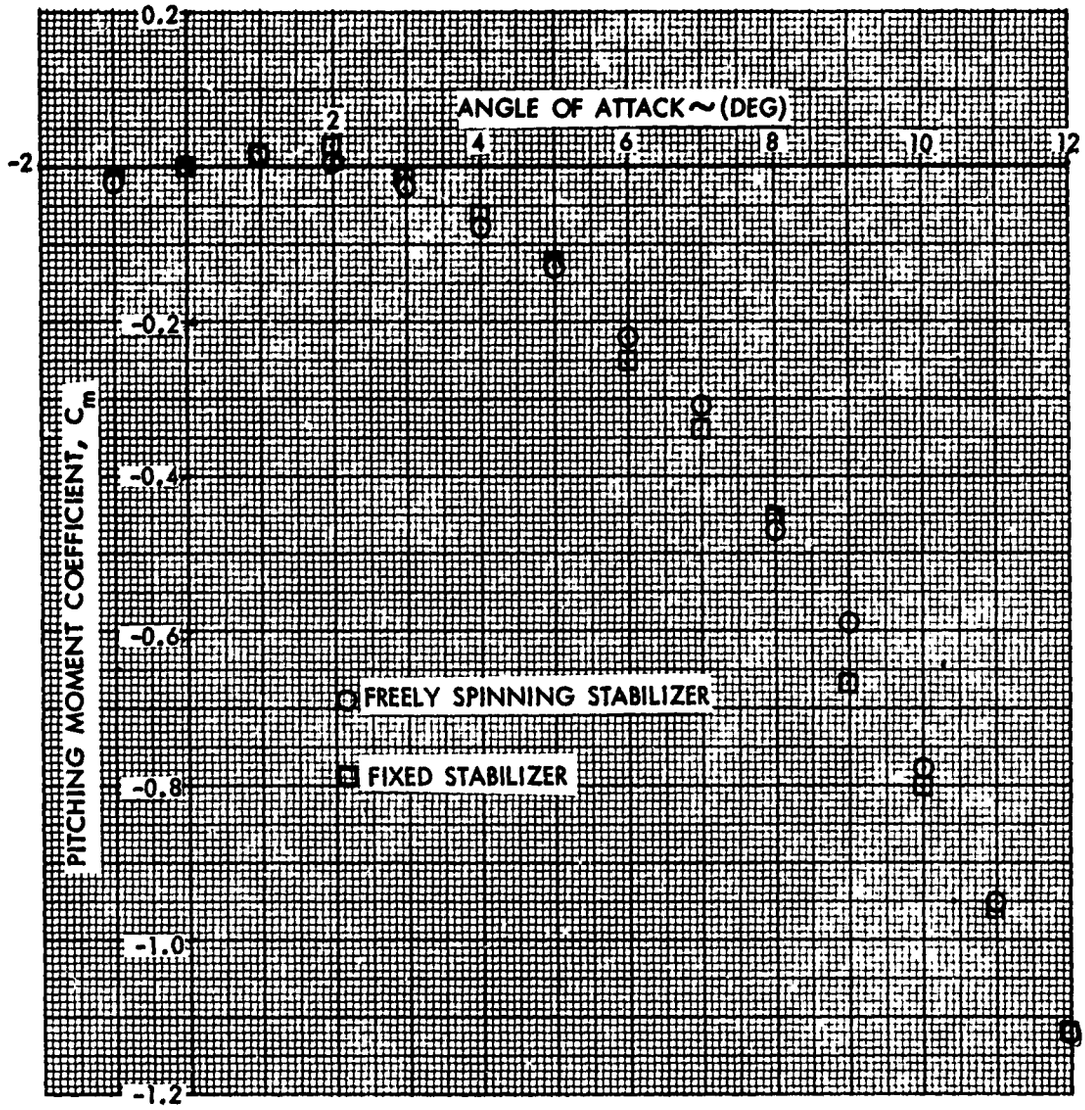

FIG. 36 PITCHING MOMENT COEFFICIENT VERSUS ANGLE OF ATTACK FOR THE FIXED AND FREELY SPINNING STABILIZERS AT A FIN CANT OF 4 DEGREES AND A MACH NUMBER OF 0.74

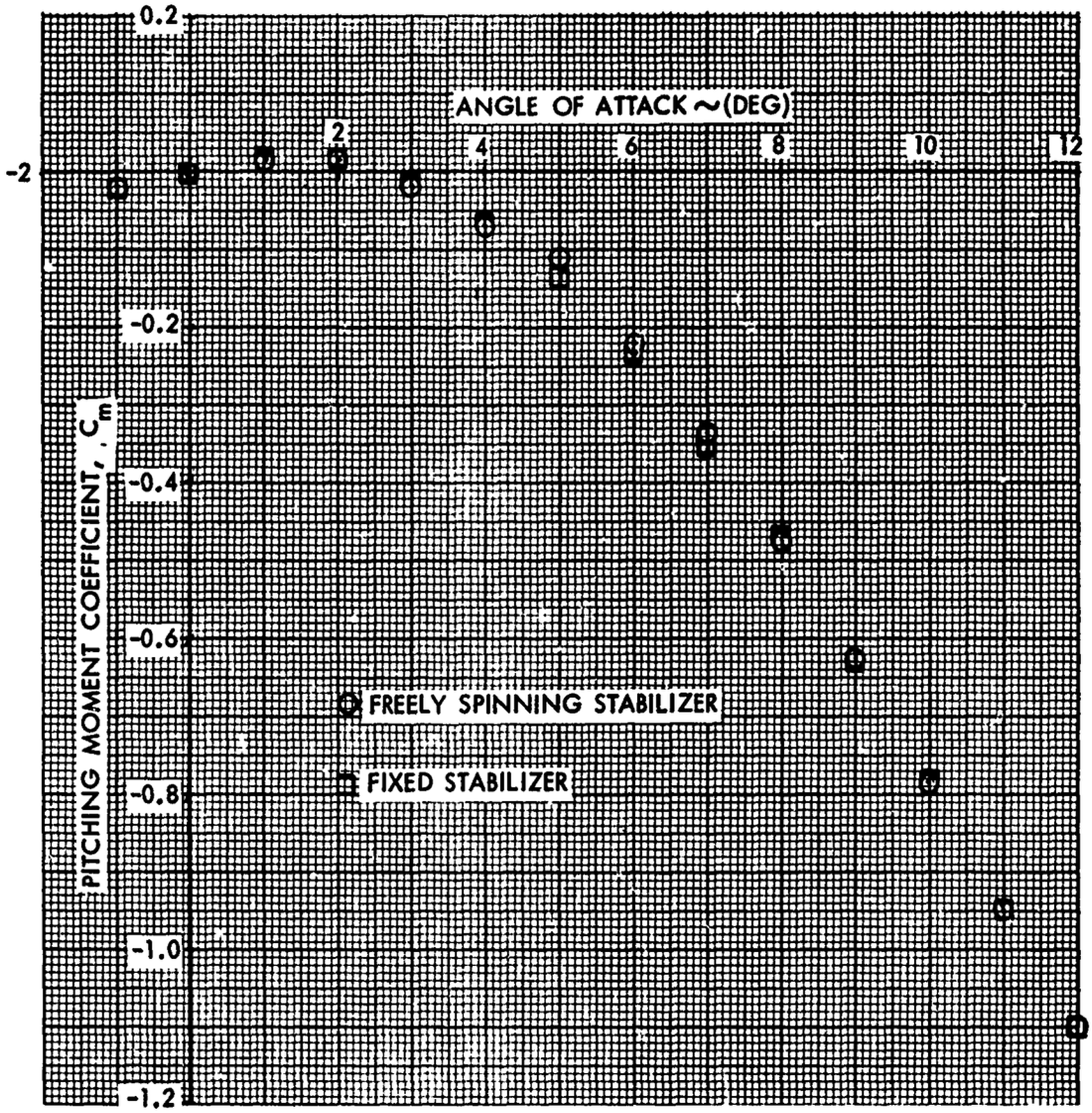

FIG. 37 PITCHING MOMENT COEFFICIENT VERSUS ANGLE OF ATTACK FOR THE FIXED AND FREELY SPINNING STABILIZERS AT A FIN CANT OF 4 DEGREES AND A MACH NUMBER OF 0.79

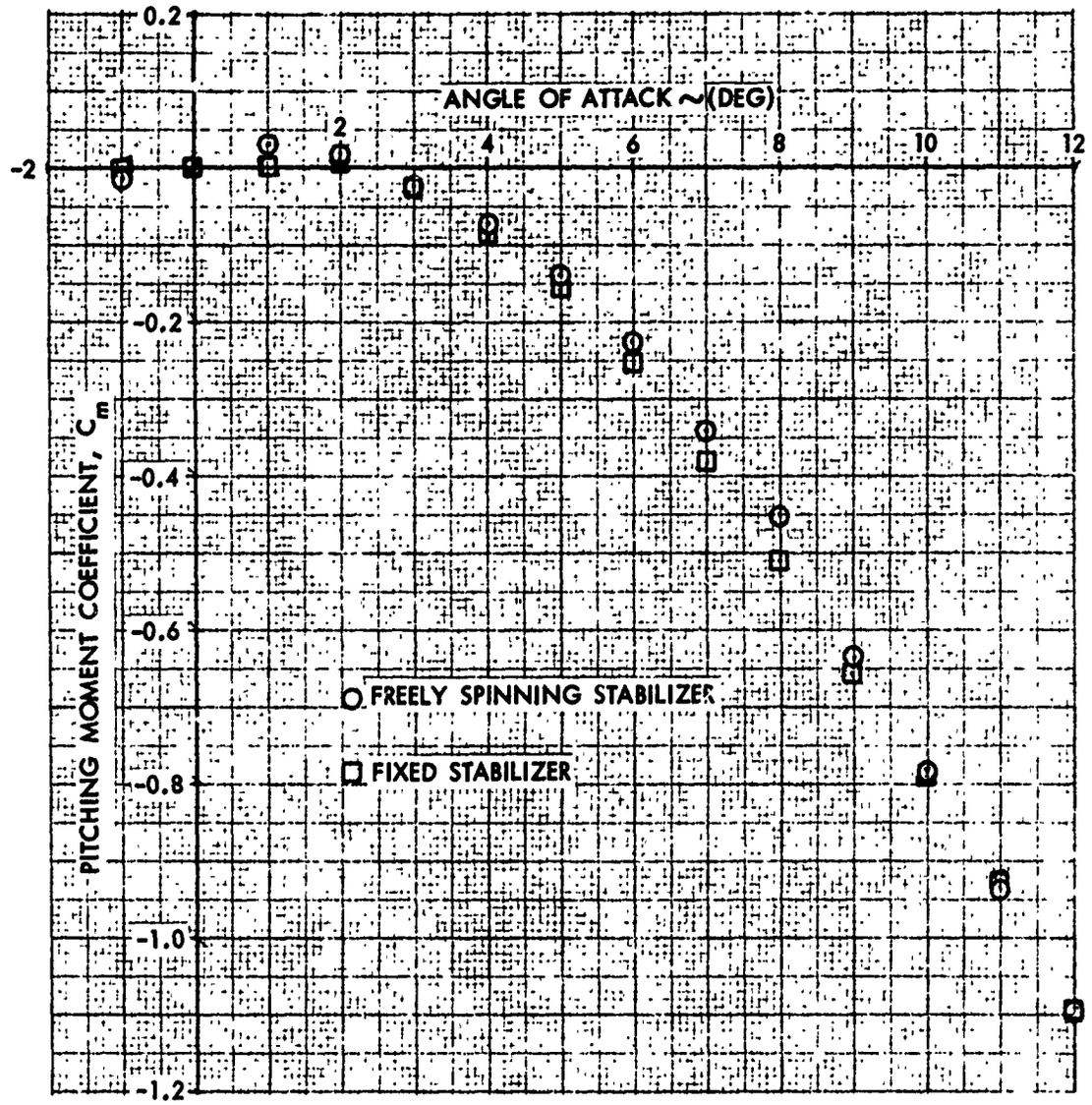

FIG. 38 PITCHING MOMENT COEFFICIENT VERSUS ANGLE OF ATTACK FOR THE FIXED AND FREELY SPINNING STABILIZERS AT A FIN CANT OF 4 DEGREES AND A MACH NUMBER OF 0.84

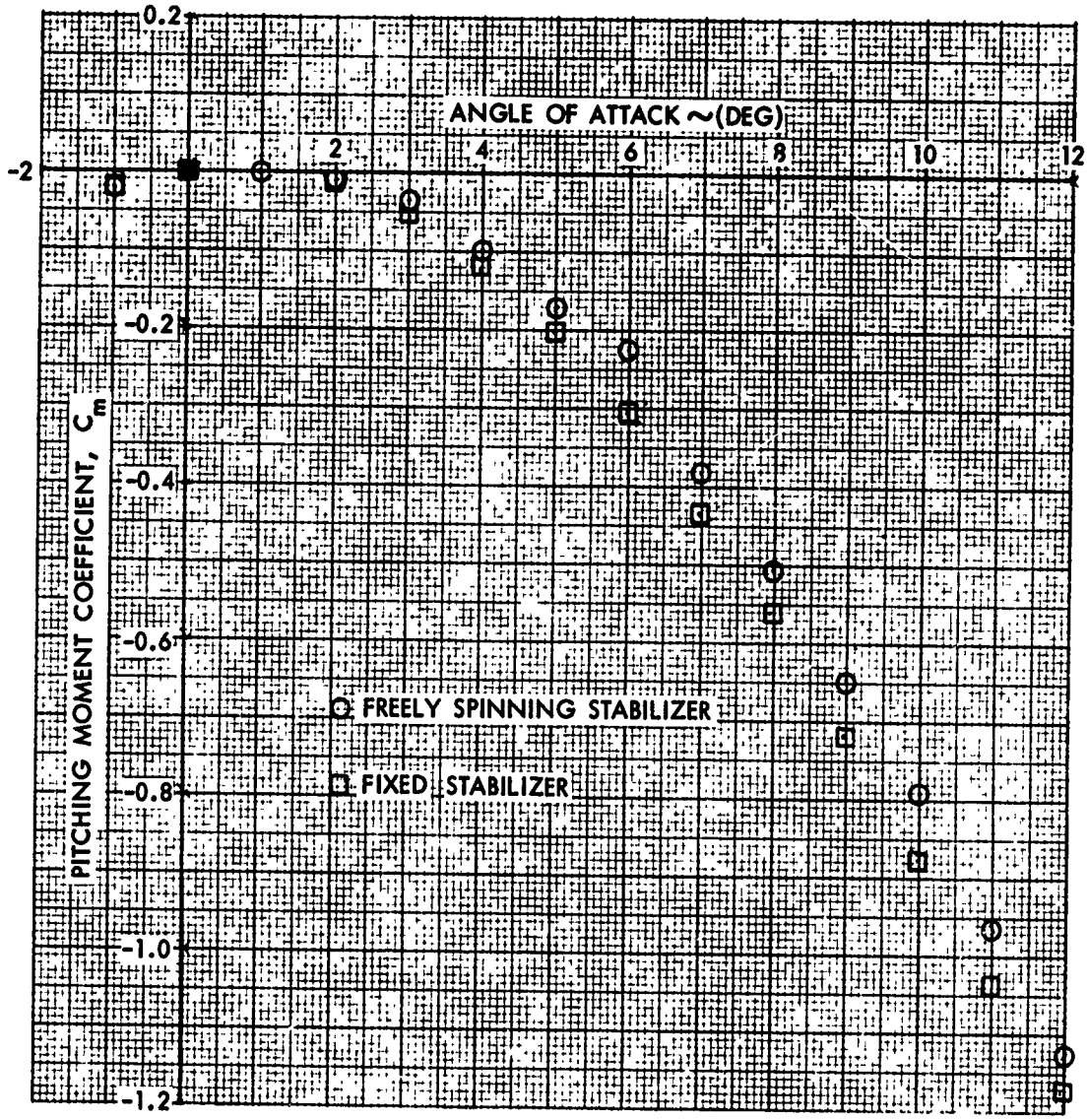

FIG. 39 PITCHING MOMENT COEFFICIENT VERSUS ANGLE OF ATTACK FOR THE FIXED AND FREELY SPINNING STABILIZERS AT A FIN CANT OF 4 DEGREES AND A MACH NUMBER OF 0.89

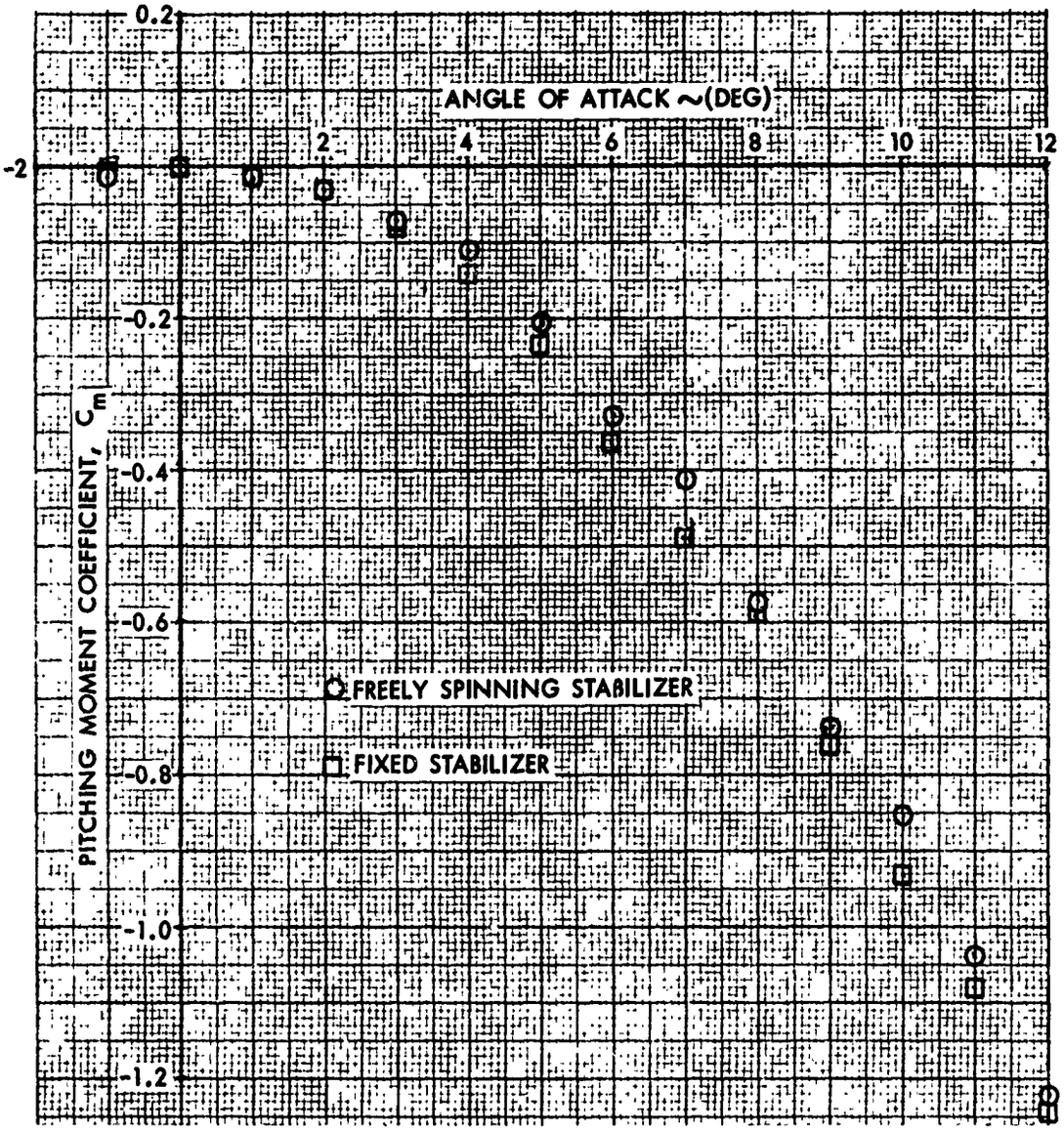

FIG. 40 PITCHING MOMENT COEFFICIENT VERSUS ANGLE OF ATTACK FOR THE FIXED AND FREELY SPINNING STABILIZERS AT A FIN CANT OF 4 DEGREES AND A MACH NUMBER OF 0.94

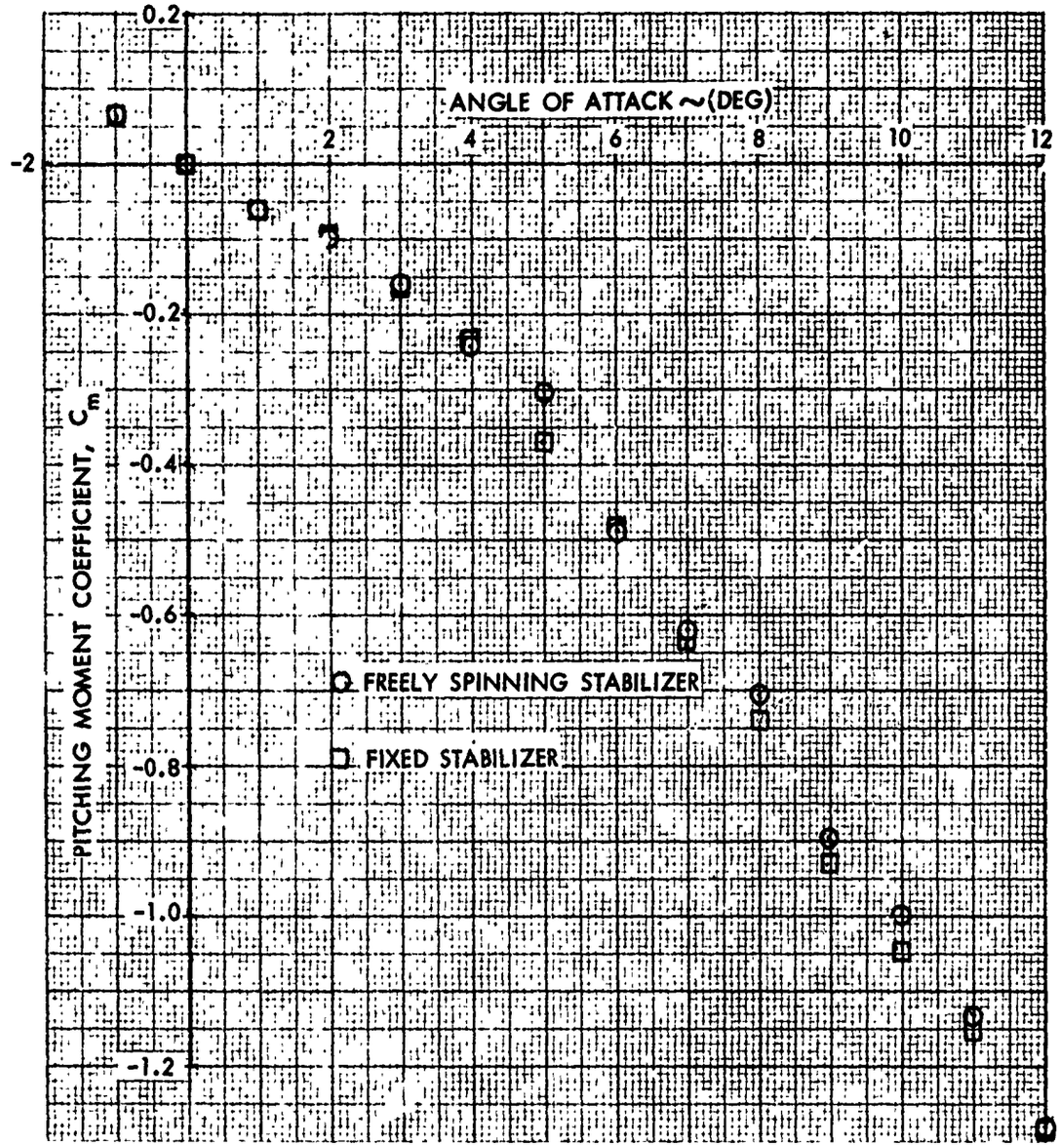

FIG. 41 PITCHING MOMENT COEFFICIENT VERSUS ANGLE OF ATTACK FOR THE FIXED AND FREELY SPINNING STABILIZERS AT A FIN CANT OF 4 DEGREES AND A MACH NUMBER OF 1.12

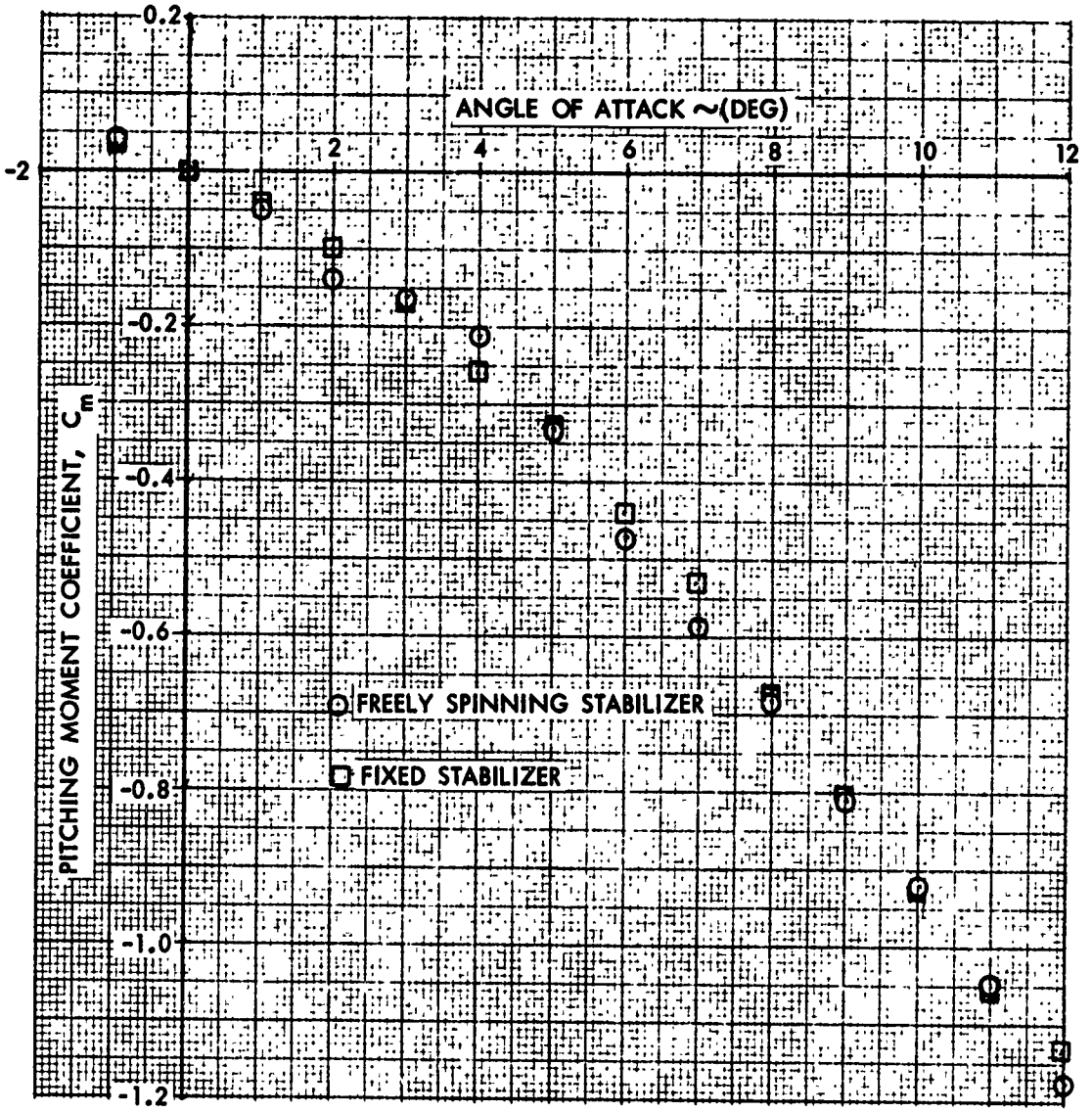

FIG. 42 PITCHING MOMENT COEFFICIENT VERSUS ANGLE OF ATTACK FOR THE FIXED AND FREELY SPINNING STABILIZERS AT A FIN CANT OF 4 DEGREES AND A MACH NUMBER OF 1.20

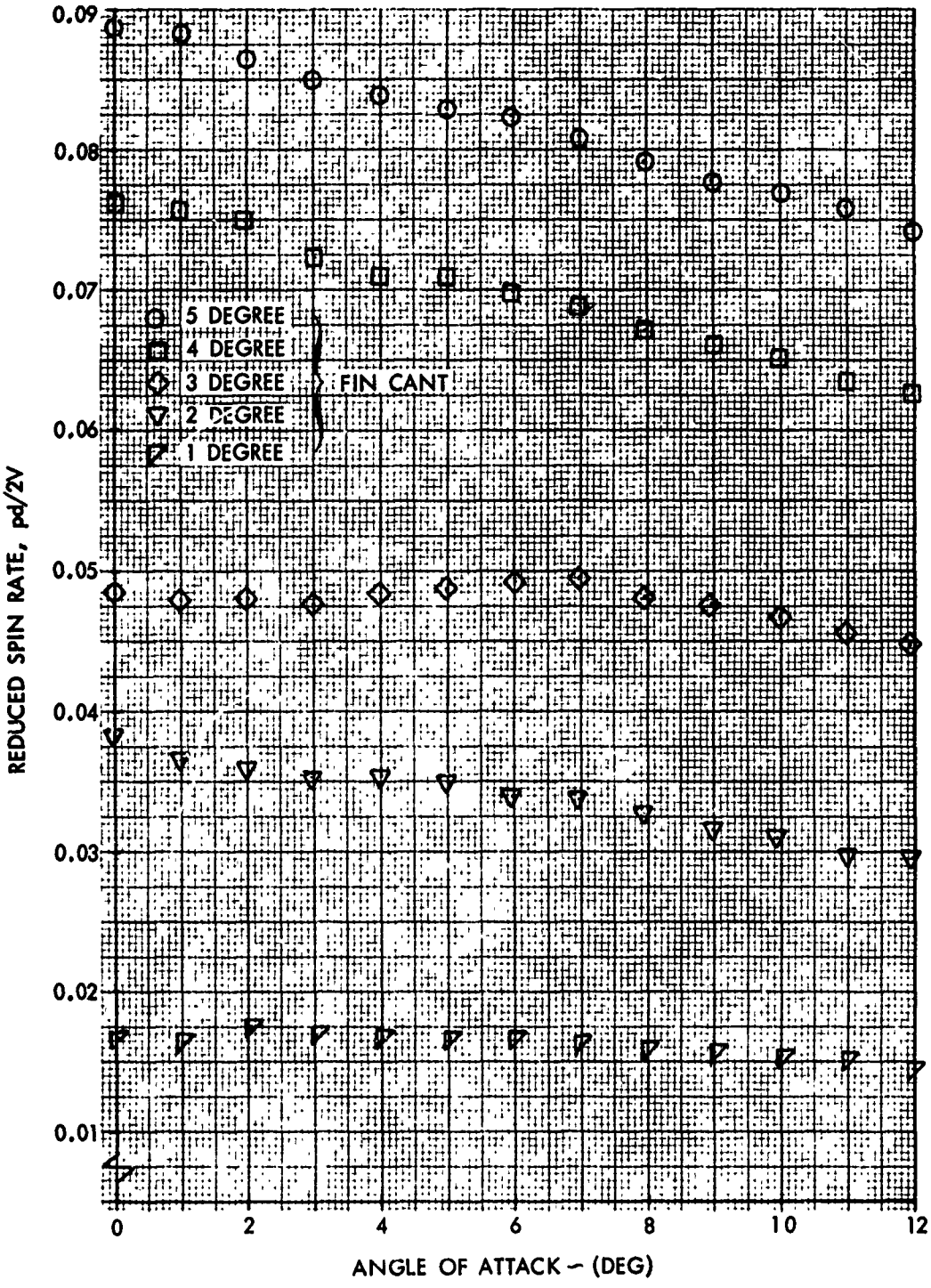

FIG. 43 REDUCED SPIN RATE VERSUS ANGLE OF ATTACK FOR THE FREELY SPINNING STABILIZER AT FIN CANTS OF 1, 2, 3, 4 AND 5 DEGREES AND A MACH NUMBER OF 0.59

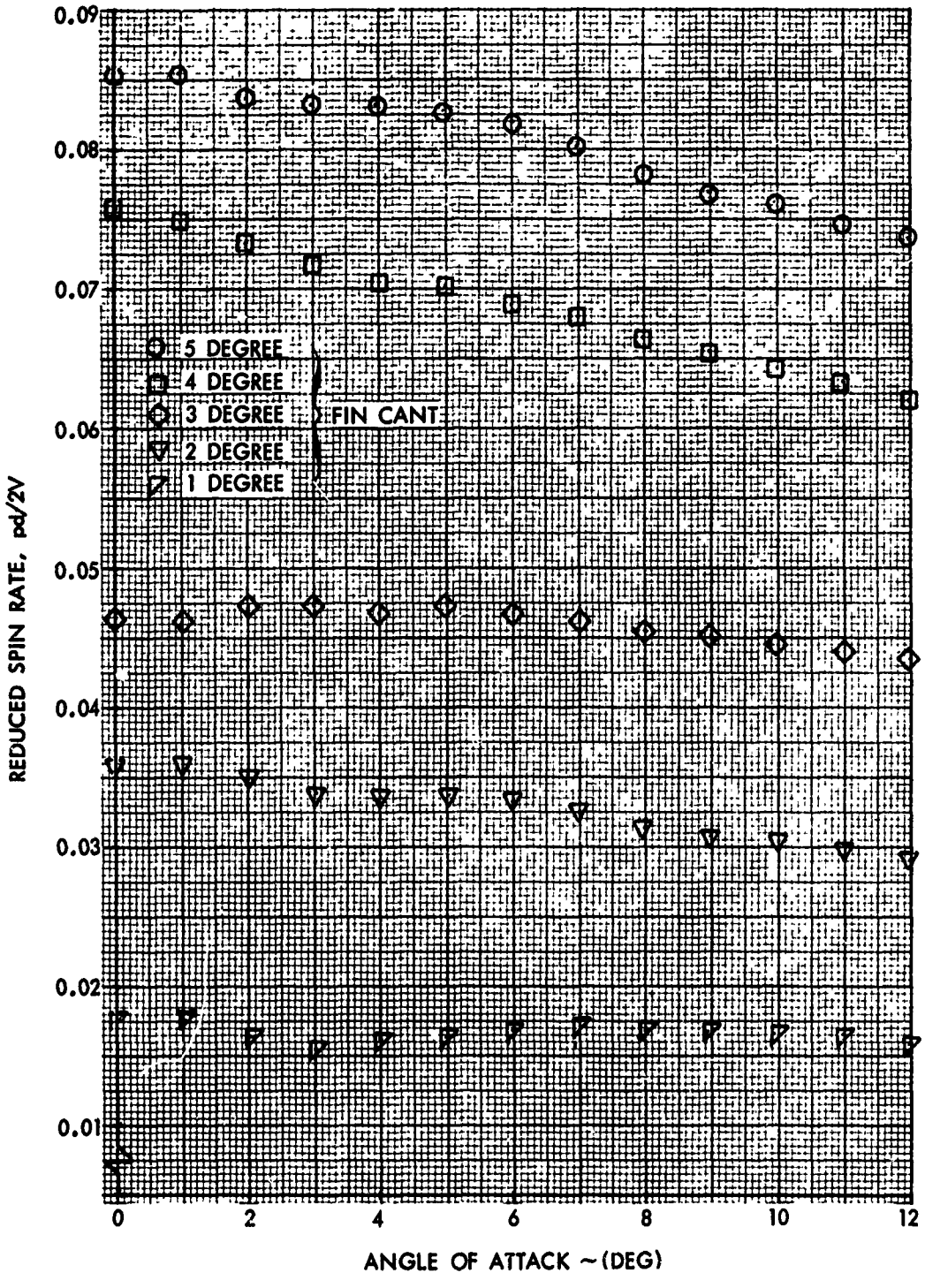

FIG. 44 REDUCED SPIN RATE VERSUS ANGLE OF ATTACK FOR THE FREELY SPINNING STABILIZER AT FIN CANTS OF 1, 2, 3, 4 AND 5 DEGREES AND A MACH NUMBER OF 0.79

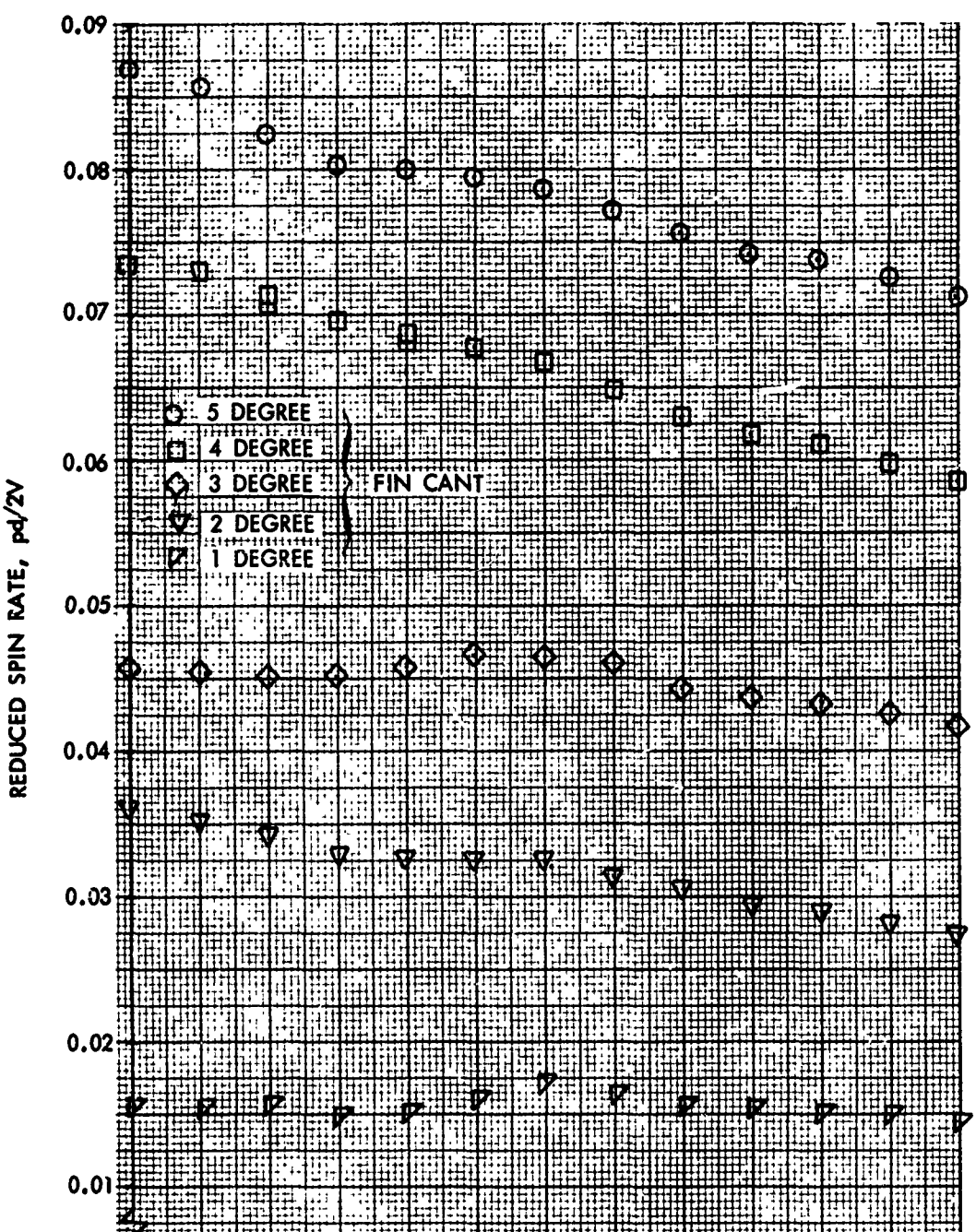

FIG. 45 REDUCED SPIN RATE VERSUS ANGLE OF ATTACK FOR THE FREELY SPINNING STABILIZER AT FIN CANTS OF 1, 2, 3, 4, AND 5 DEGREES AND A MACH NUMBER OF 0.94

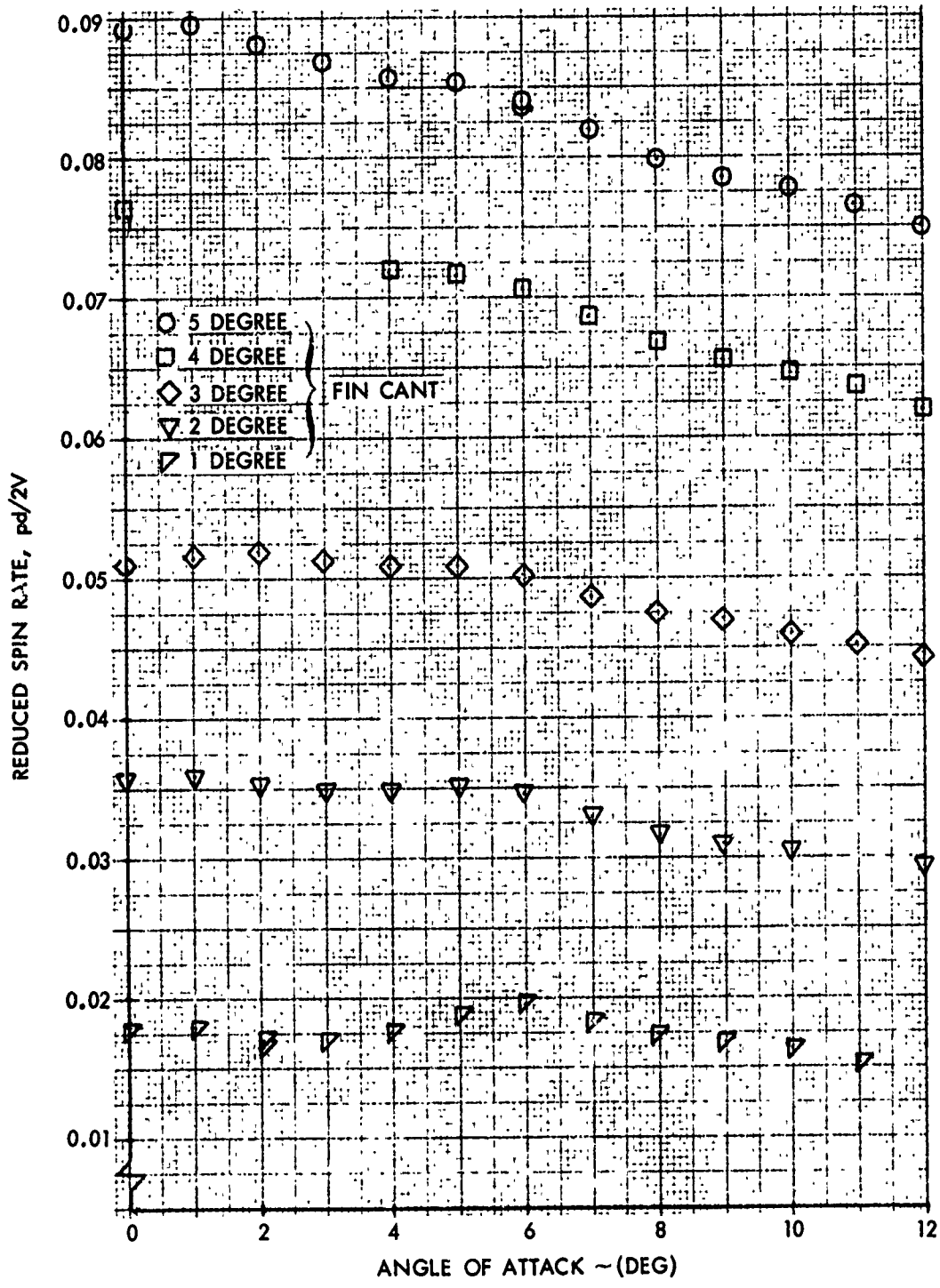

FIG. 46 REDUCED SPIN RATE VERSUS ANGLE OF ATTACK FOR THE FREELY SPINNING STABILIZER AT FIN CANTS OF 1, 2, 3, 4 AND 5 DEGREES AND A MACH NUMBER OF 1.10

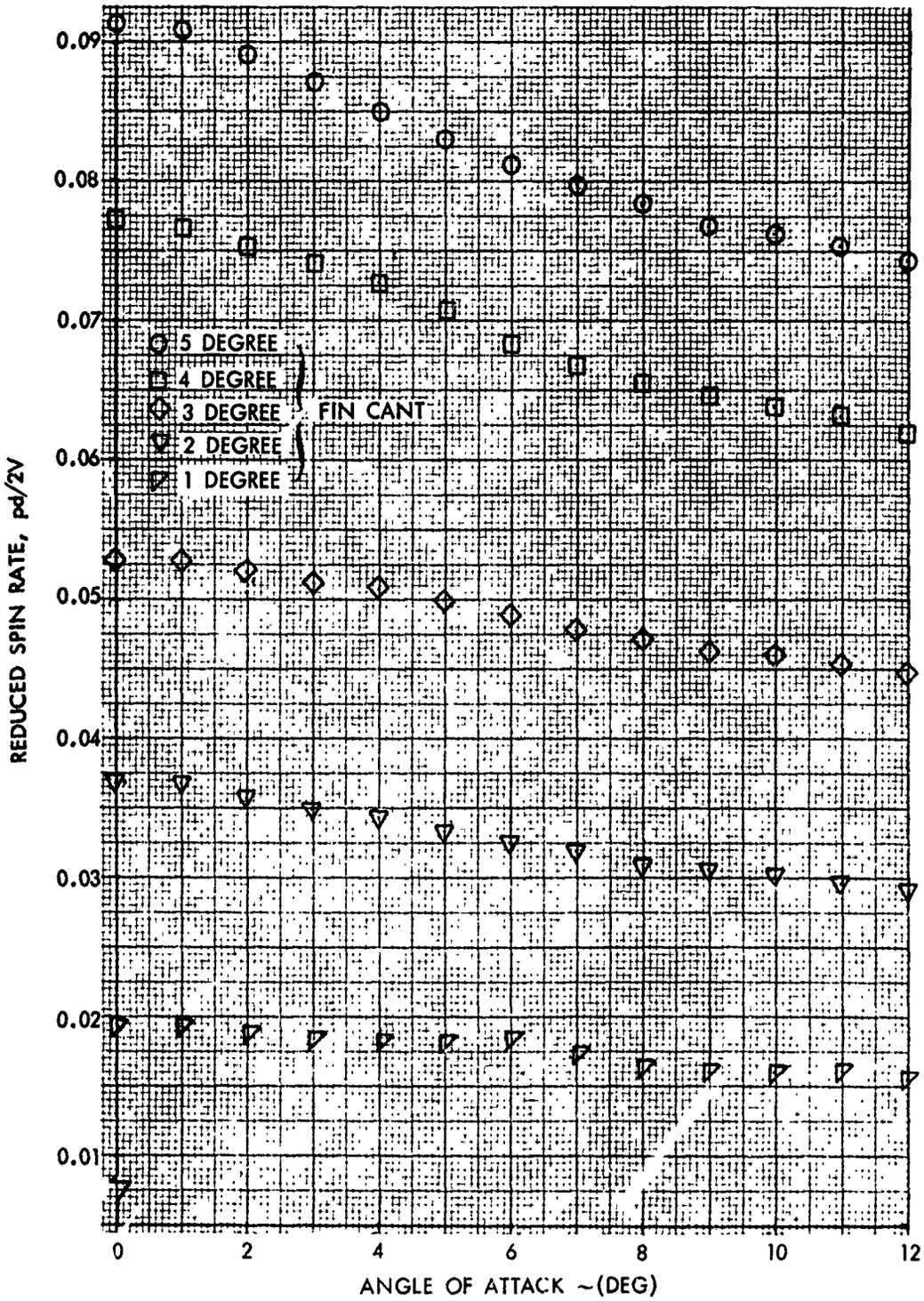

FIG. 47 REDUCED SPIN RATE VERSUS ANGLE OF ATTACK FOR THE FREELY SPINNING STABILIZER AT FIN CANTS OF 1, 2, 3, 4 AND 5 DEGREES AND A MACH NUMBER OF 1.20

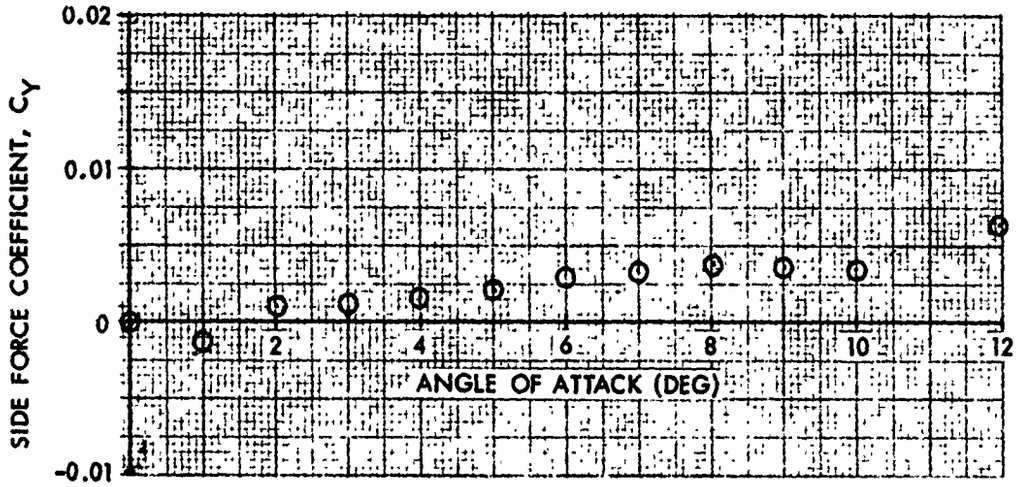

FIG. 48A SIDE FORCE COEFFICIENT VERSUS ANGLE OF ATTACK FOR THE FREELY SPINNING STABILIZER AT A FIN CANT OF 1 DEGREE AND A MACH NUMBER OF 0.60

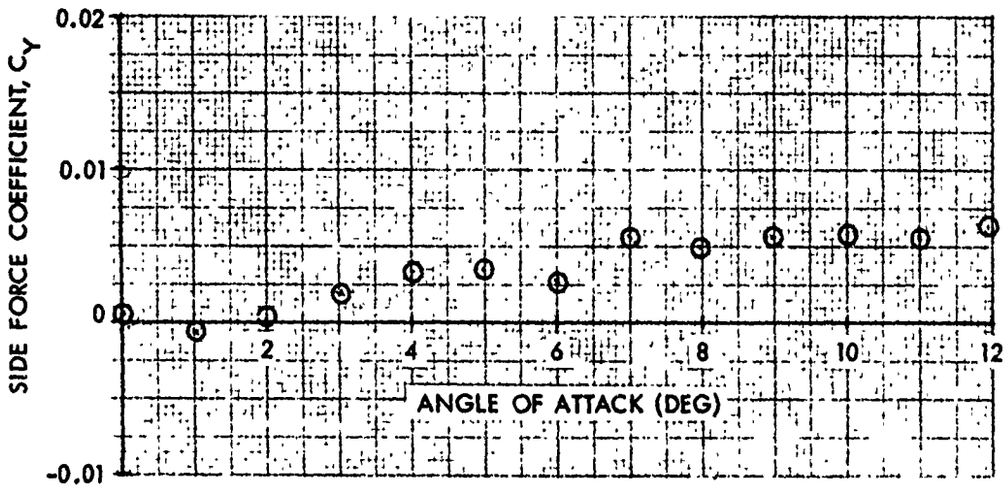

FIG. 48B SIDE FORCE COEFFICIENT VERSUS ANGLE OF ATTACK FOR THE FREELY SPINNING STABILIZER AT A FIN CANT OF 1 DEGREE AND A MACH NUMBER OF 0.70

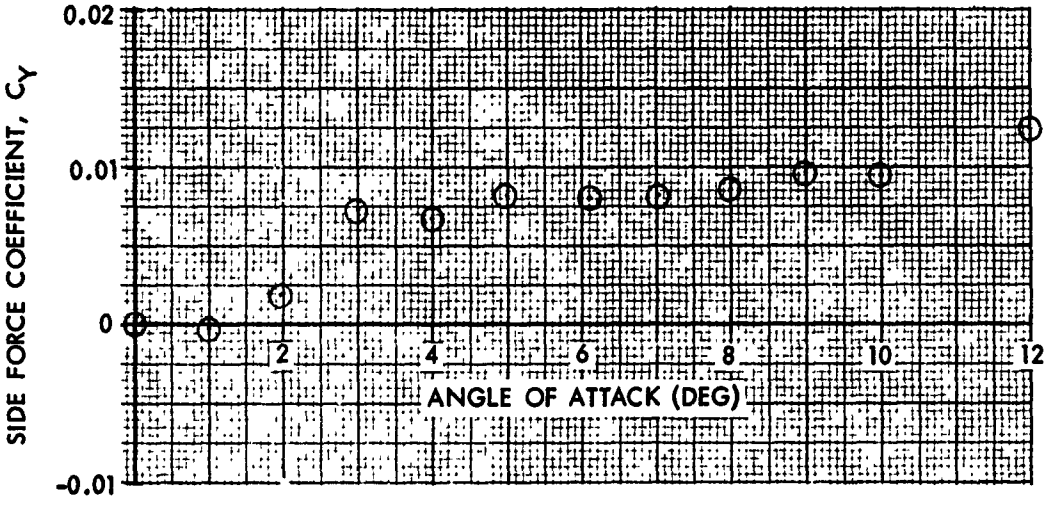

FIG. 49A SIDE FORCE COEFFICIENT VERSUS ANGLE OF ATTACK FOR THE FREELY SPINNING STABILIZER AT A FIN CANT OF 1 DEGREE AND A MACH NUMBER OF 0.74

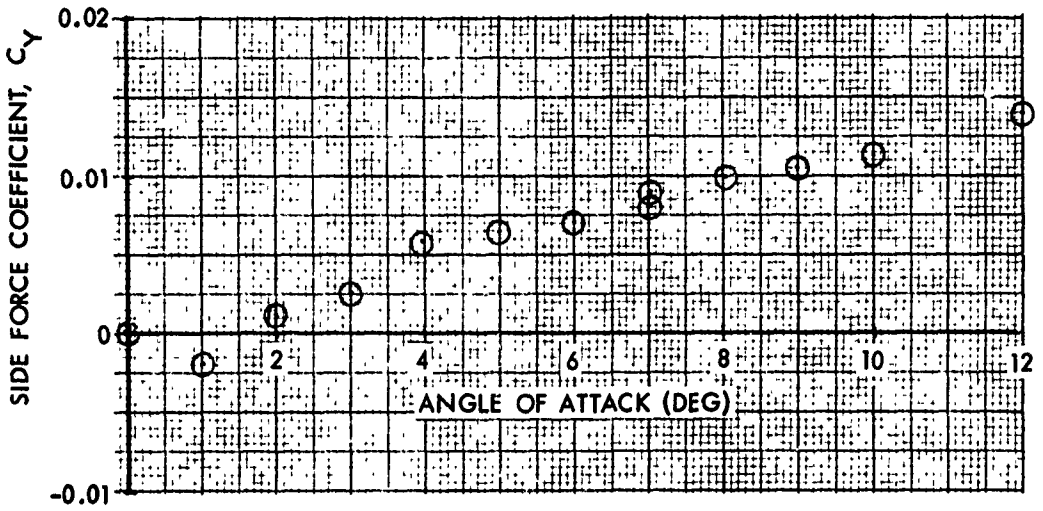

FIG. 49B SIDE FORCE COEFFICIENT VERSUS ANGLE OF ATTACK FOR THE FREELY SPINNING STABILIZER AT A FIN CANT OF 1 DEGREE AND A MACH NUMBER OF 0.83

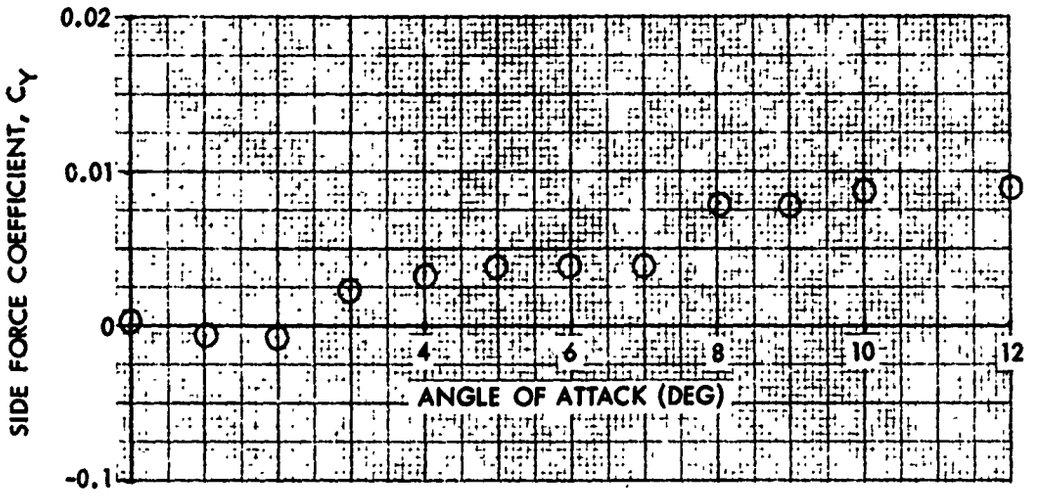

FIG. 50A SIDE FORCE COEFFICIENT VERSUS ANGLE OF ATTACK FOR THE FREELY SPINNING STABILIZER AT A FIN CANT OF 1 DEGREE AND A MACH NUMBER OF 0.89

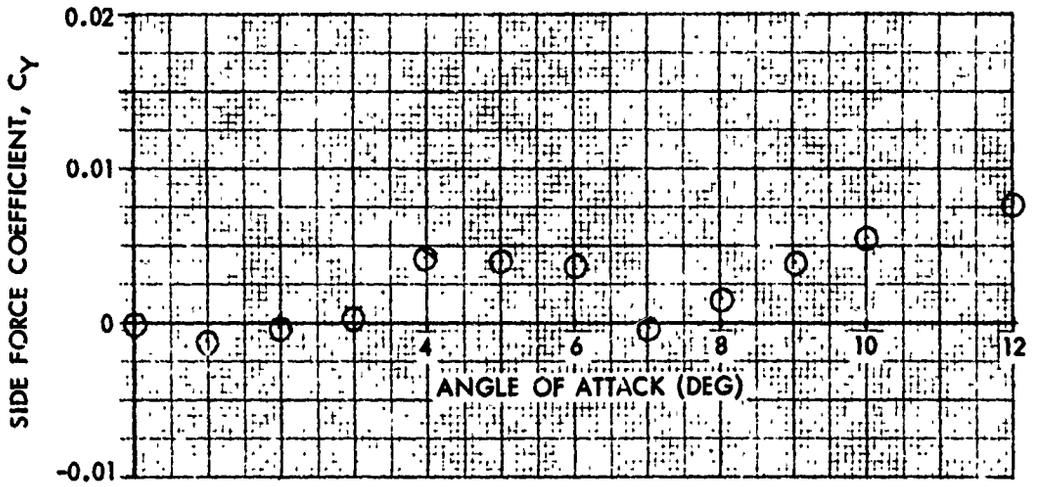

FIG. 50B SIDE FORCE COEFFICIENT VERSUS ANGLE OF ATTACK FOR THE FREELY SPINNING STABILIZER AT A FIN CANT OF 1 DEGREE AND A MACH NUMBER OF 0.94

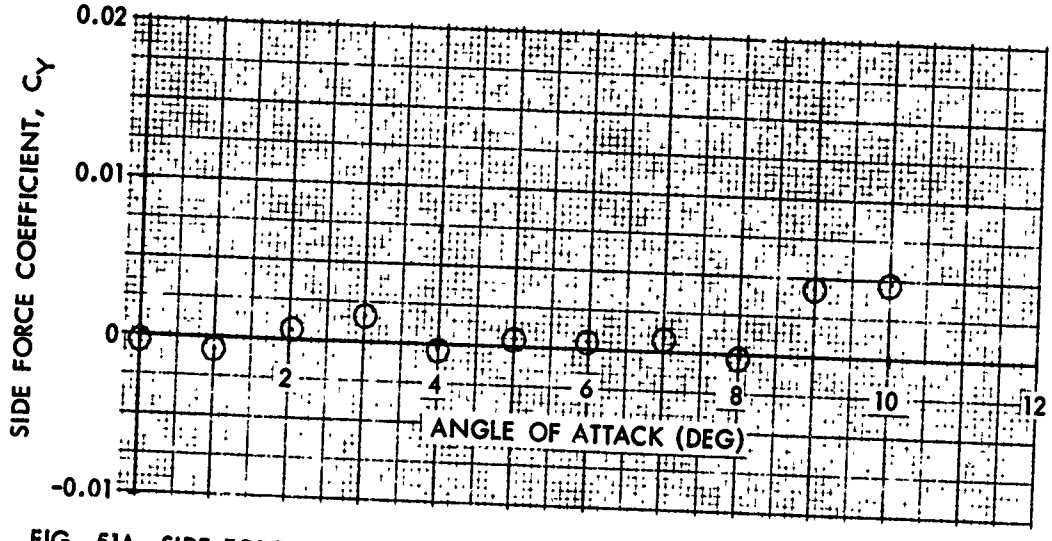

FIG. 51A SIDE FORCE COEFFICIENT VERSUS ANGLE OF ATTACK FOR THE FREELY SPINNING STABILIZER AT A FIN CANT OF 1 DEGREE AND A MACH NUMBER OF 1.10

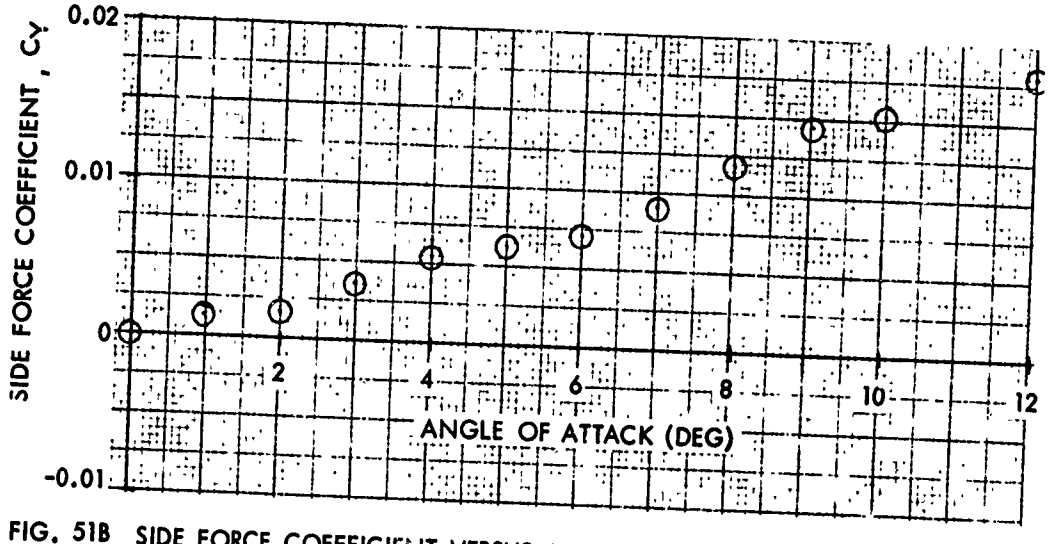

FIG. 51B SIDE FORCE COEFFICIENT VERSUS ANGLE OF ATTACK FOR THE FREELY SPINNING STABILIZER AT A FIN CANT OF 1 DEGREE AND A MACH NUMBER OF 1.19

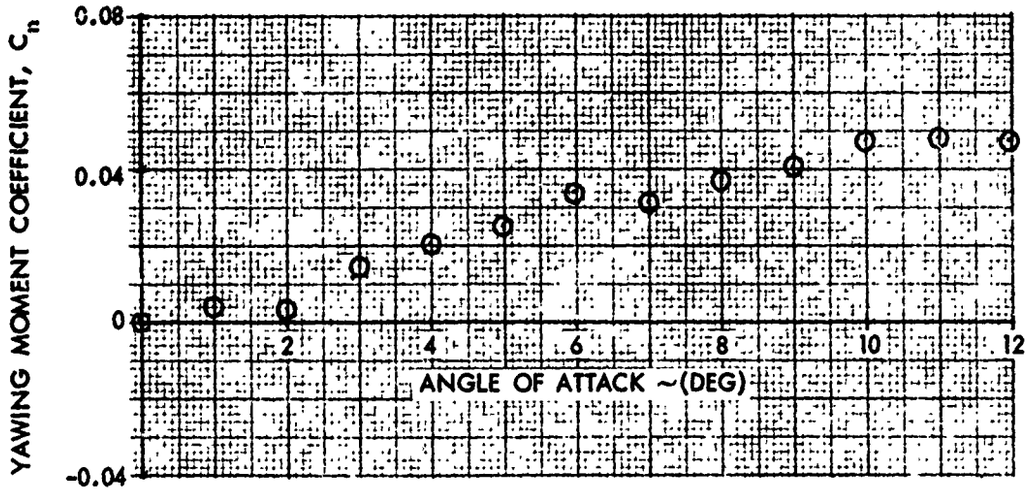

FIG. 52A YAWING MOMENT COEFFICIENT VERSUS ANGLE OF ATTACK FOR THE FREELY SPINNING STABILIZER AT A FIN CANT OF 1 DEGREE AT A MACH NUMBER OF 0.59

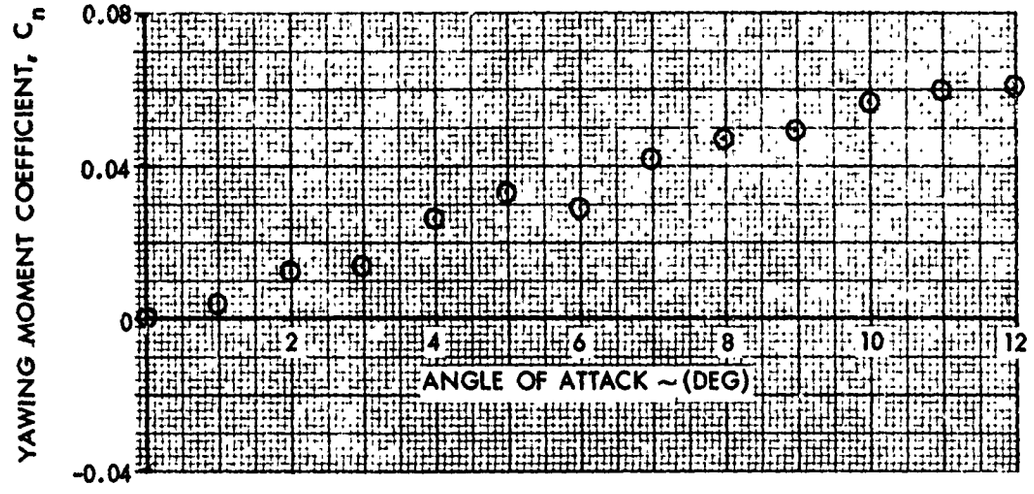

FIG. 52B YAWING MOMENT COEFFICIENT VERSUS ANGLE OF ATTACK FOR THE FREELY SPINNING STABILIZER AT A FIN CANT OF 1 DEGREE AT A MACH NUMBER OF 0.74

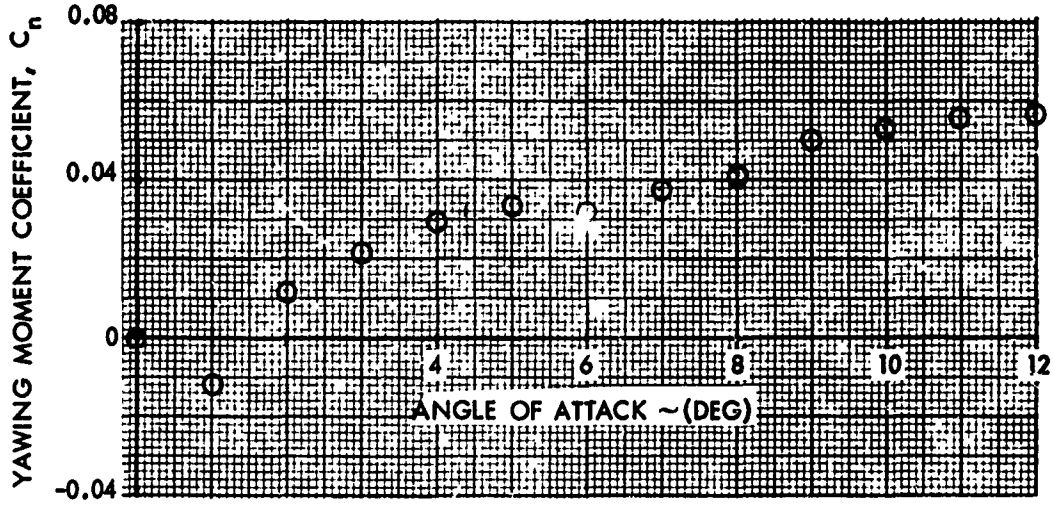

FIG. 53A YAWING MOMENT COEFFICIENT VERSUS ANGLE OF ATTACK FOR THE FREELY SPINNING STABILIZER AT A FIN CANT OF 1 DEGREE AT A MACH NUMBER OF 0.79

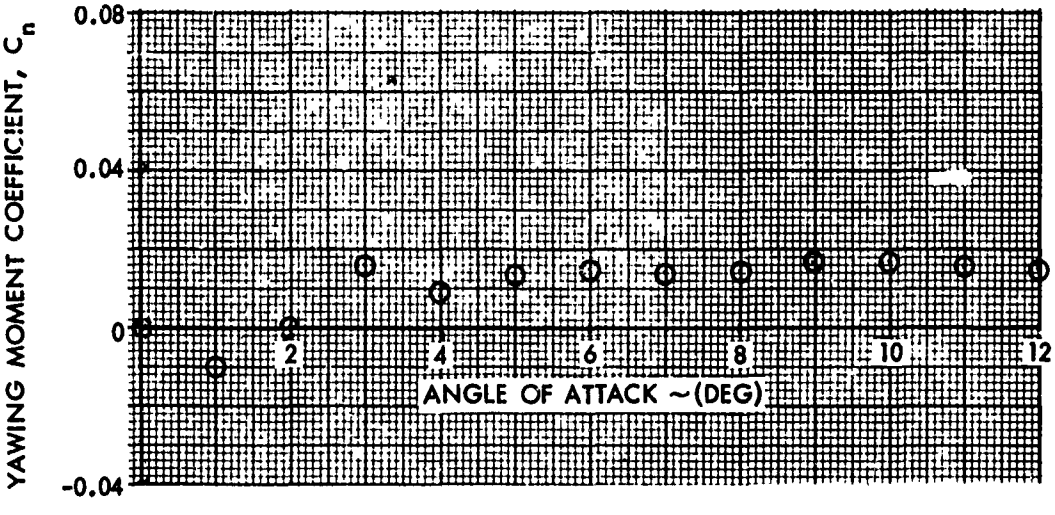

FIG. 53B YAWING MOMENT COEFFICIENT VERSUS ANGLE OF ATTACK FOR THE FREELY SPINNING STABILIZER AT A FIN CANT OF 1 DEGREE AT A MACH NUMBER OF 0.84

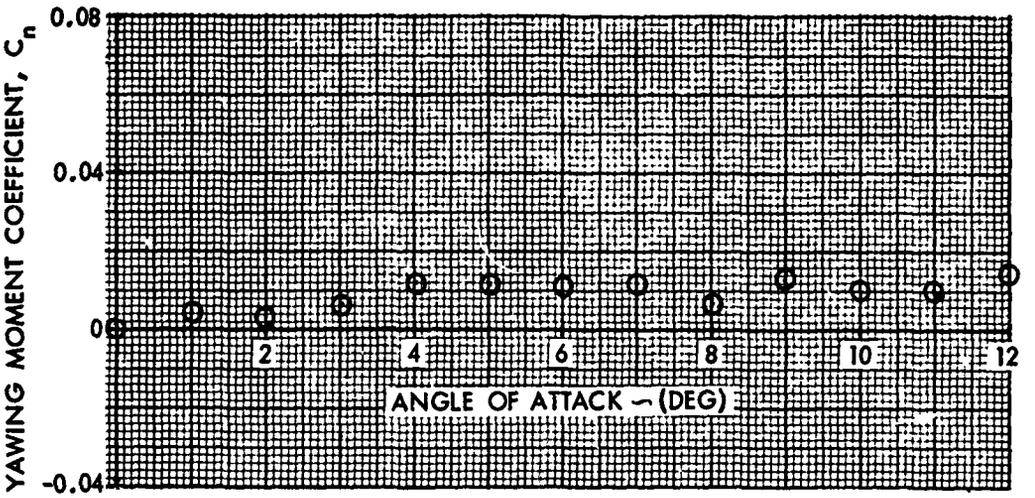

FIG. 54A YAWING MOMENT COEFFICIENT VERSUS ANGLE OF ATTACK FOR THE FREELY SPINNING STABILIZER AT A FIN CANT OF 1 DEGREE AT A MACH NUMBER OF 0.88

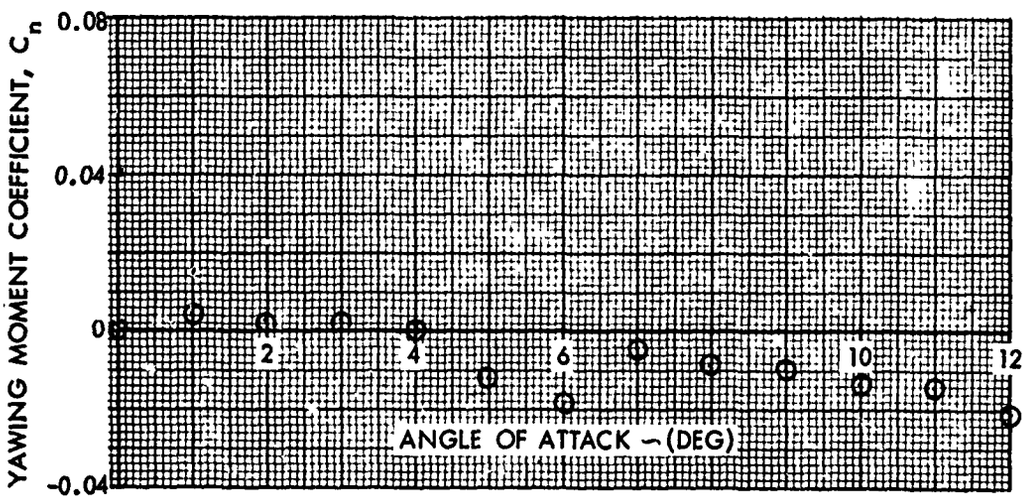

FIG. 54B YAWING MOMENT COEFFICIENT VERSUS ANGLE OF ATTACK FOR THE FREELY SPINNING STABILIZER AT A FIN CANT OF 1 DEGREE AT A MACH NUMBER OF 0.94

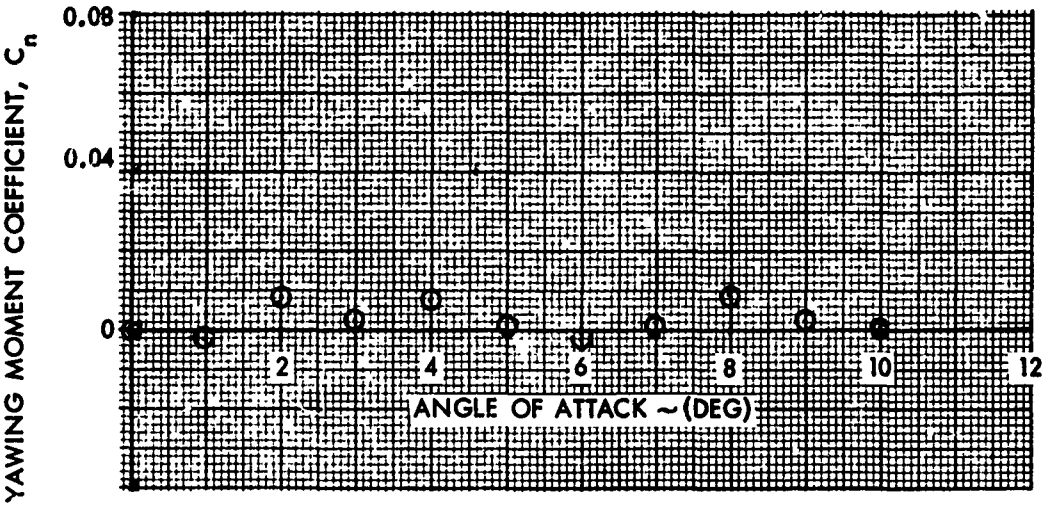

FIG. 55A YAWING MOMENT COEFFICIENT VERSUS ANGLE OF ATTACK FOR THE FREELY SPINNING STABILIZER AT A FIN CANT OF 1 DEGREE AT A MACH NUMBER OF 1.10

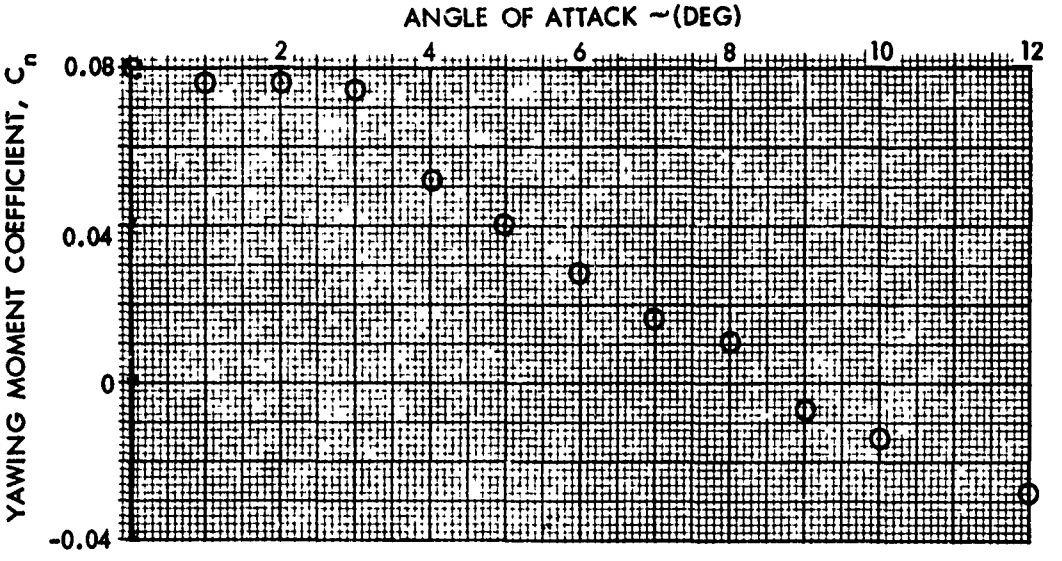

FIG. 55B YAWING MOMENT COEFFICIENT VERSUS ANGLE OF ATTACK FOR THE FREELY SPINNING STABILIZER AT A FIN CANT OF 1 DEGREE AT A MACH NUMBER OF 1.20

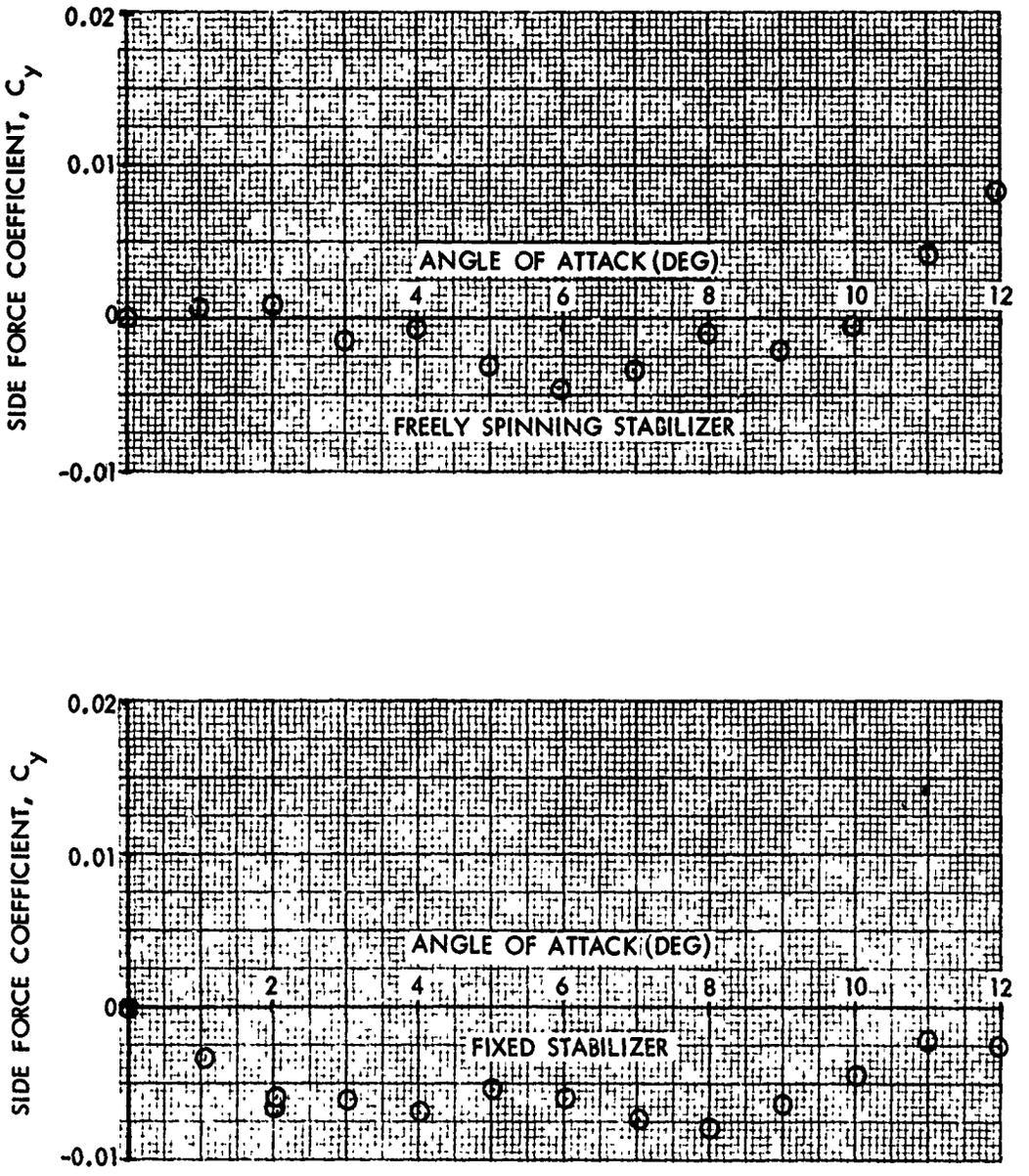

FIG. 56 SIDE FORCE COEFFICIENT VERSUS ANGLE OF ATTACK FOR THE FREELY SPINNING AND FIXED STABILIZERS AT A FIN CANT OF 2 DEGREES AND A MACH NUMBER OF 0.60

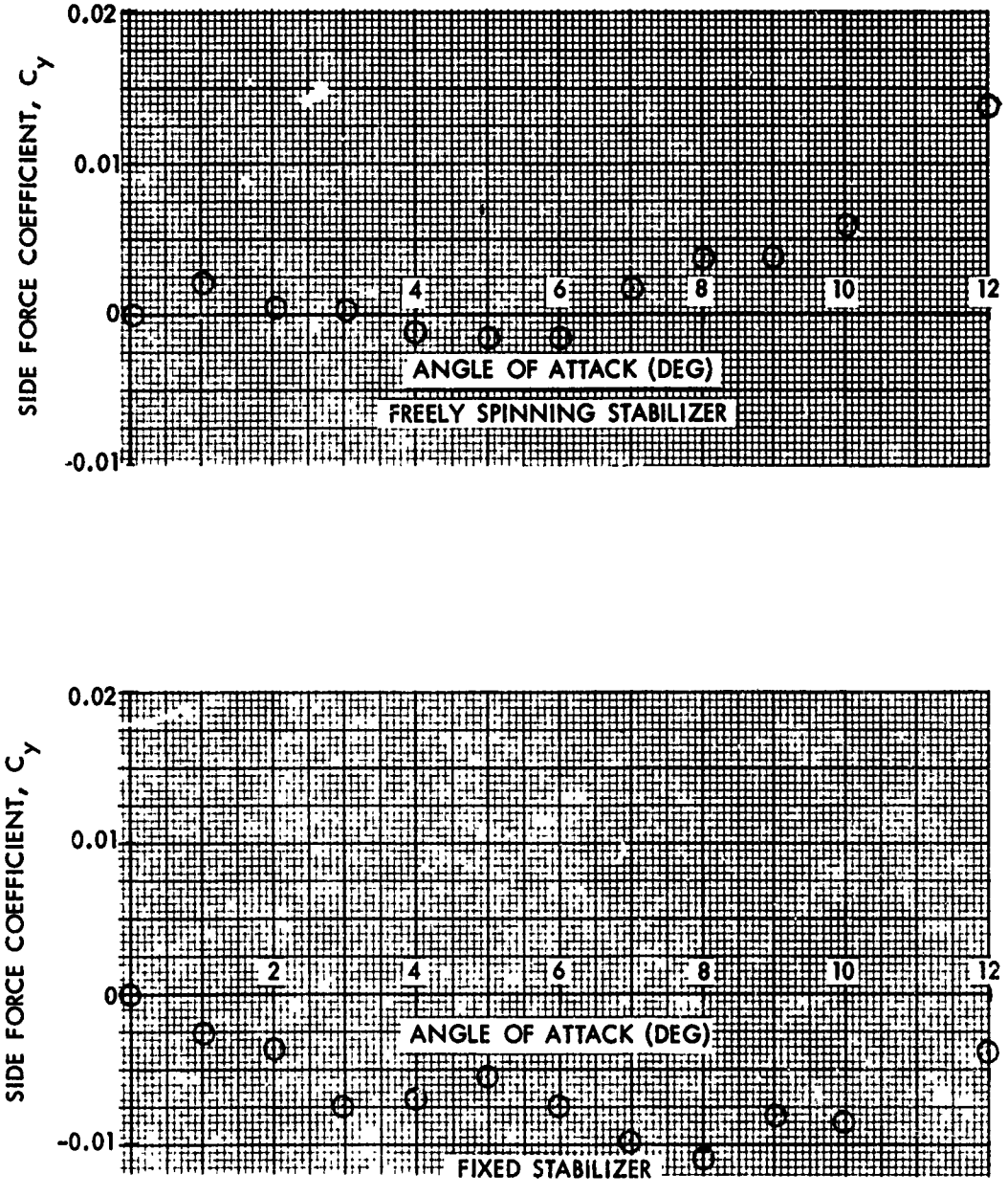

FIG. 57 SIDE FORCE COEFFICIENT VERSUS ANGLE OF ATTACK FOR THE FREELY SPINNING AND FIXED STABILIZERS AT A FIN CANT OF 2 DEGREES AND A MACH NUMBER OF 0.70

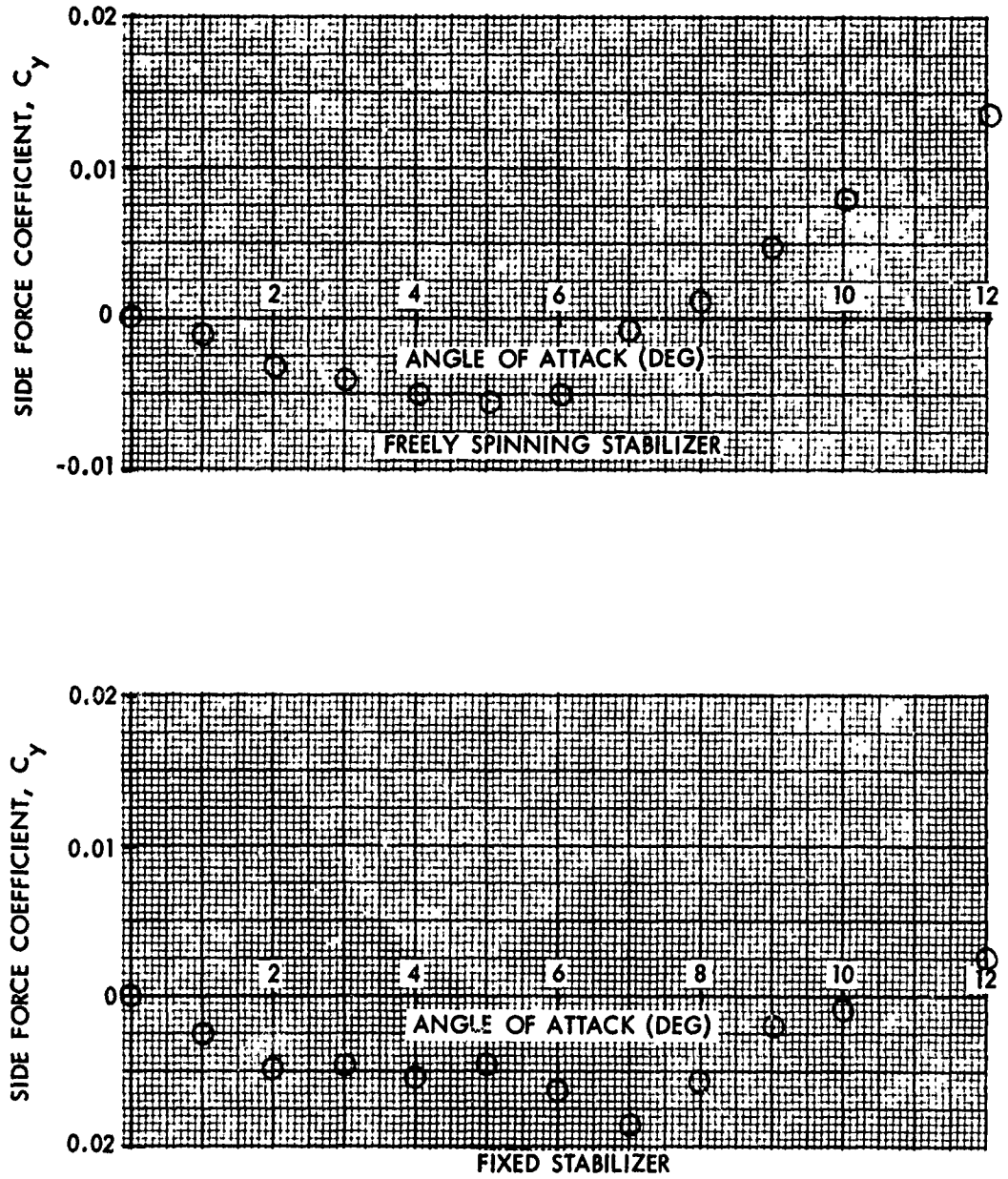

FIG. 58 SIDE FORCE COEFFICIENT VERSUS ANGLE OF ATTACK FOR THE FREELY SPINNING AND FIXED STABILIZERS AT A FIN CANT OF 2 DEGREES AND A MACH NUMBER OF 0.75

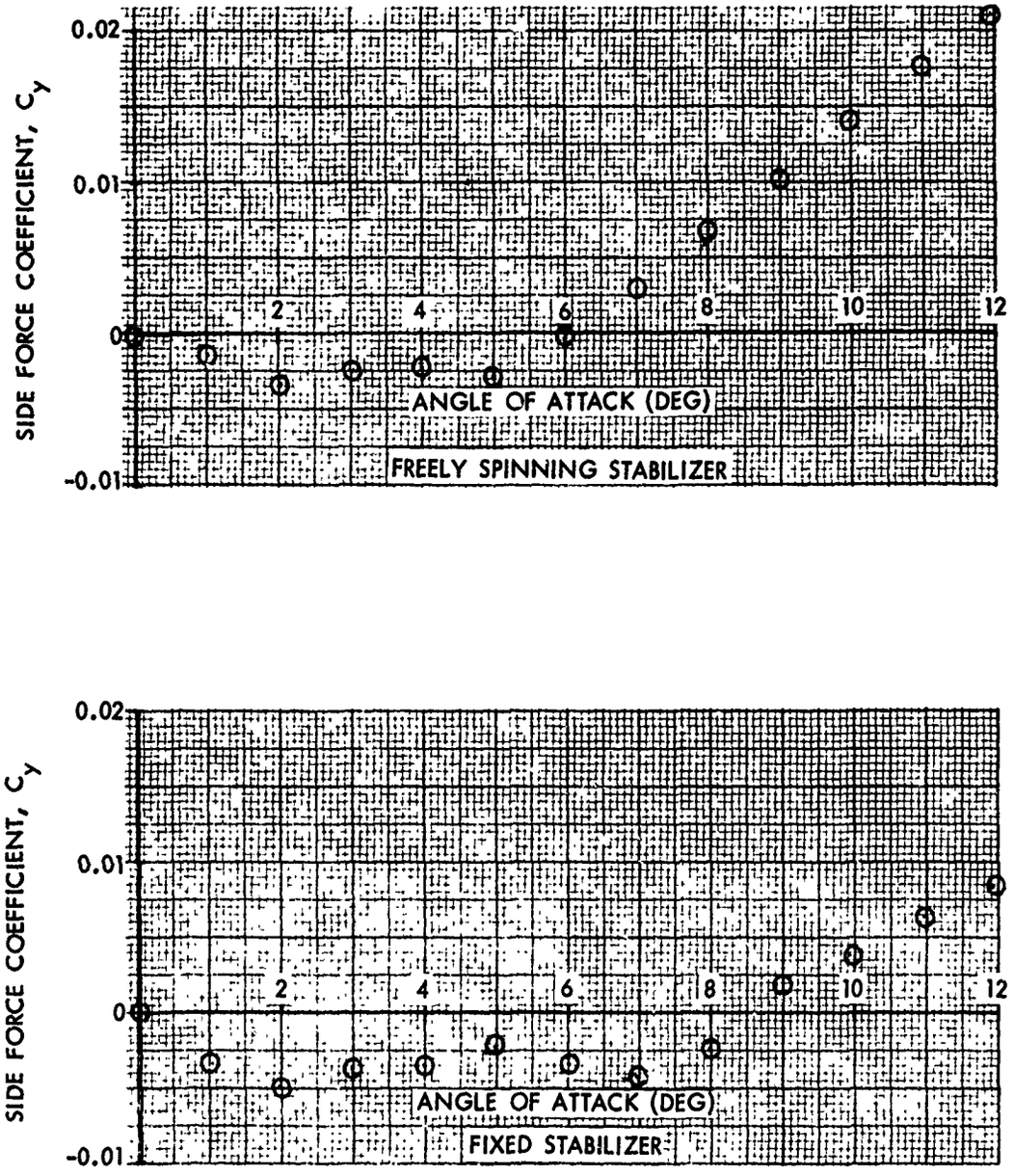

FIG. 59 SIDE FORCE COEFFICIENT VERSUS ANGLE OF ATTACK FOR THE FREELY SPINNING AND FIXED STABILIZERS AT A FIN CANT OF 2 DEGREES AND A MACH NUMBER OF 0.80

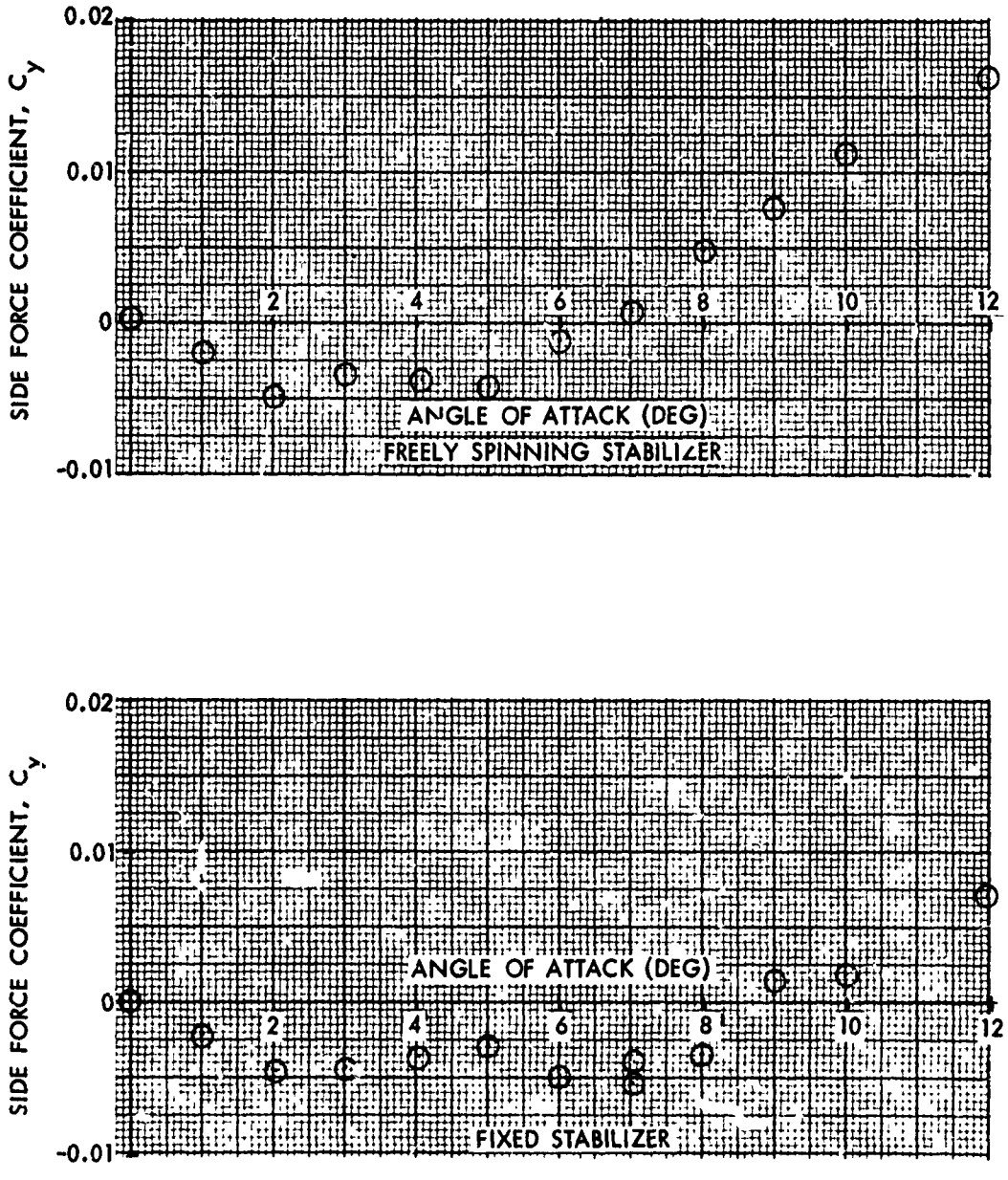

FIG. 60 SIDE FORCE COEFFICIENT VERSUS ANGLE OF ATTACK FOR THE FREELY SPINNING AND FIXED STABILIZERS AT A FIN CANT OF 2 DEGREES AND A MACH NUMBER OF 0.84

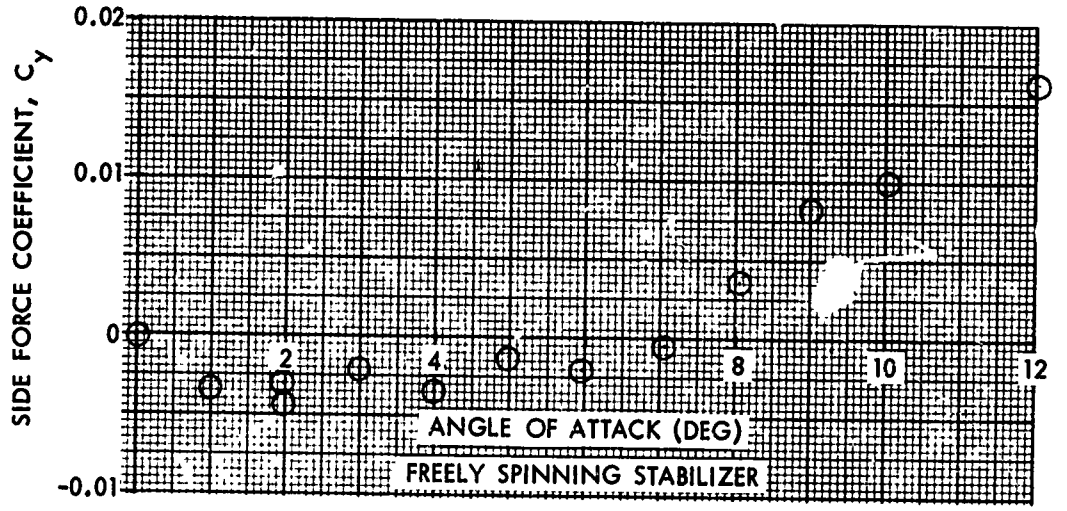

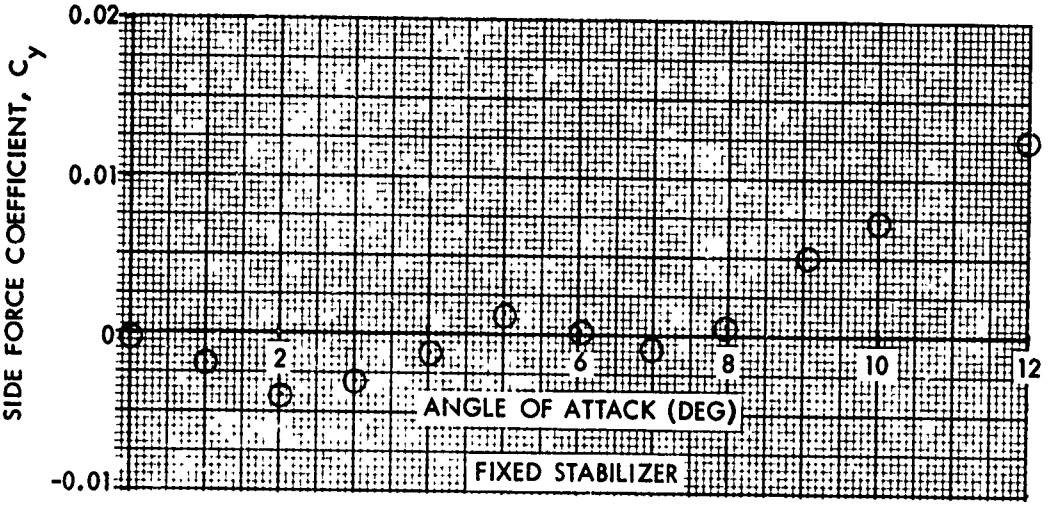

FIG. 61 SIDE FORCE COEFFICIENT VERSUS ANGLE OF ATTACK FOR THE FREELY SPINNING AND FIXED STABILIZERS AT A FIN CANT OF 2 DEGREES AND A MACH NUMBER OF 0.90

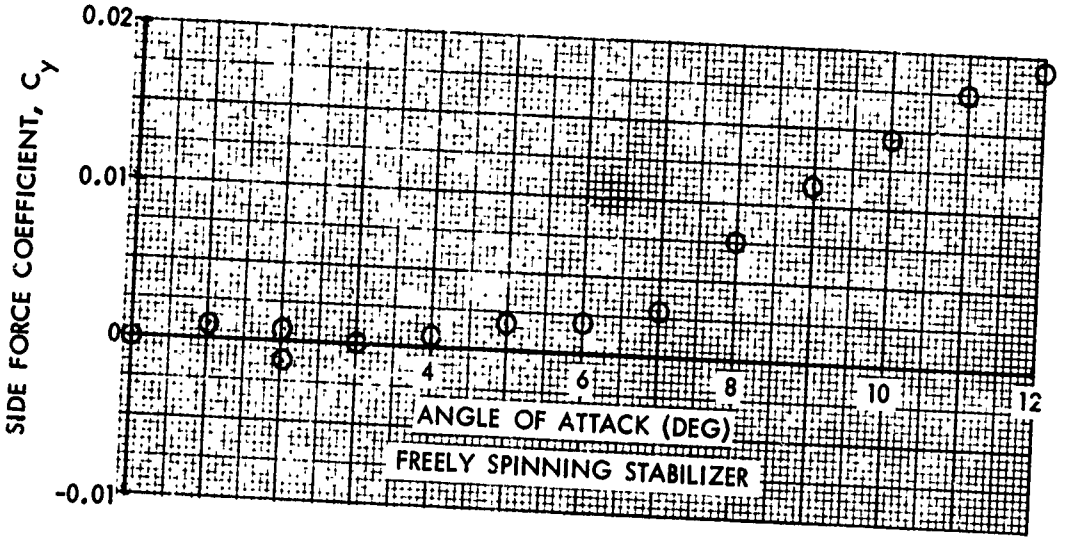

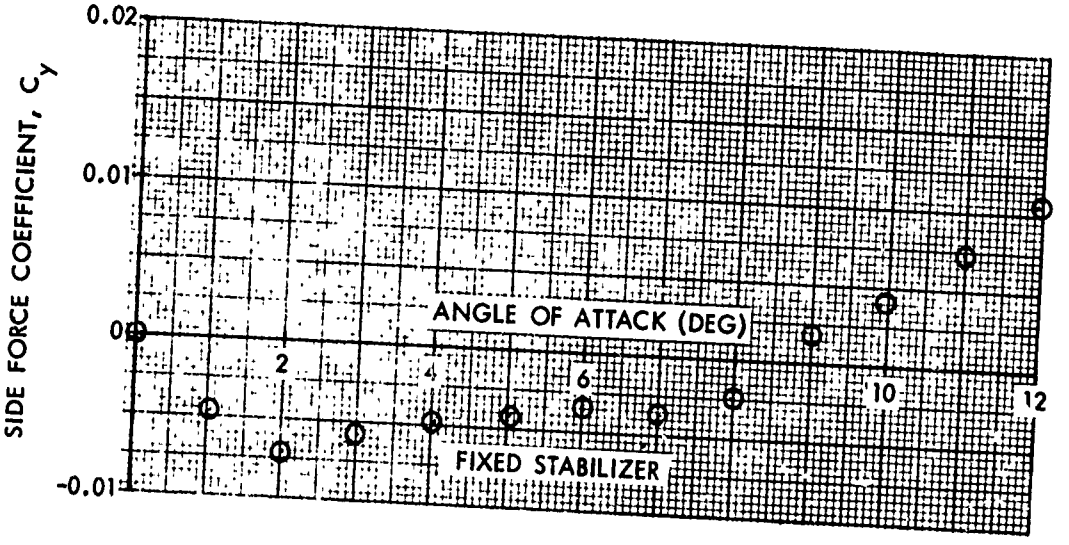

FIG. 62 SIDE FORCE COEFFICIENT VERSUS ANGLE OF ATTACK FOR THE FREELY SPINNING AND FIXED STABILIZERS AT A FIN CANT OF 2 DEGREES AND A MACH NUMBER OF 0.94

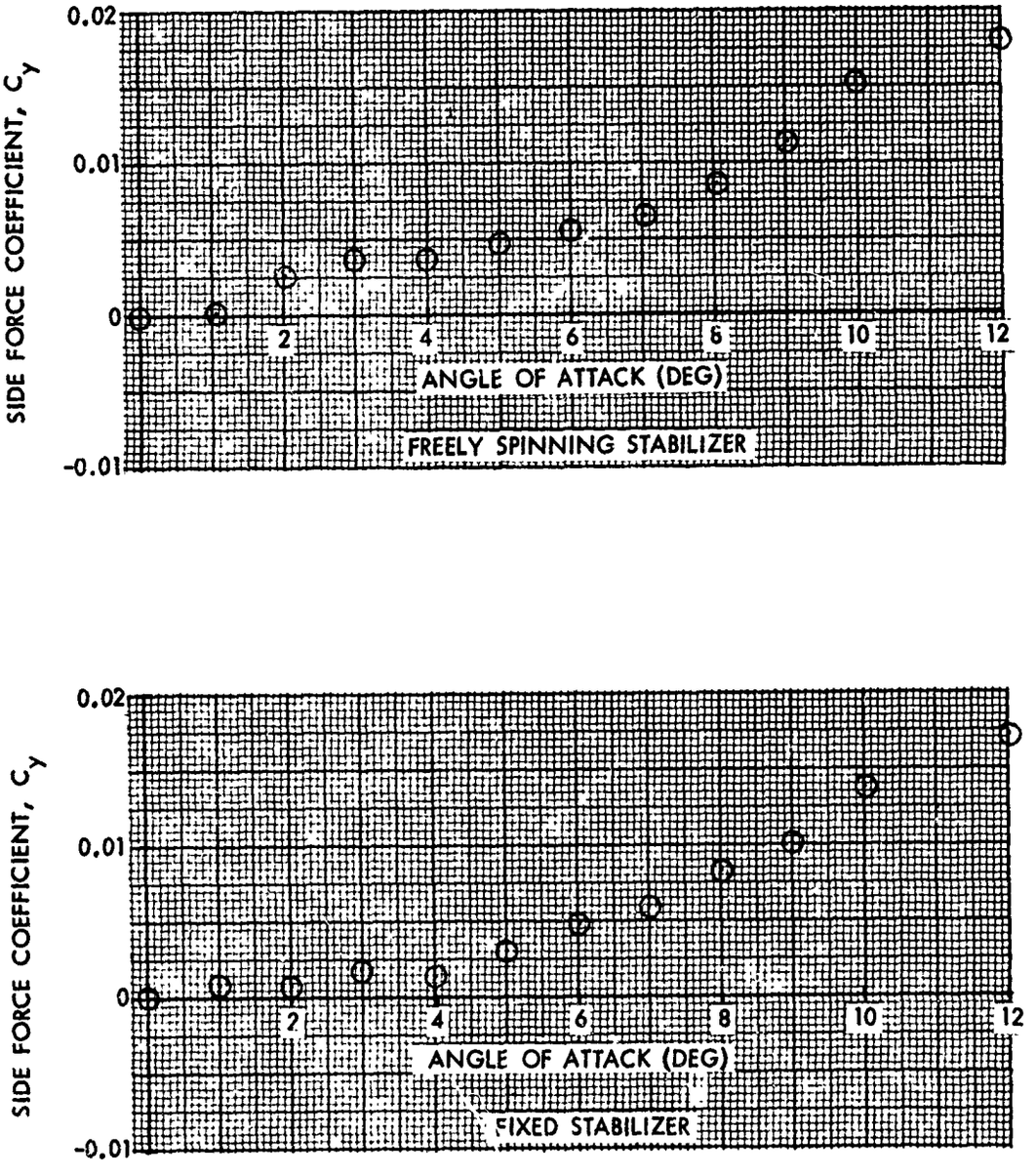

FIG. 63 SIDE FORCE COEFFICIENT VERSUS ANGLE OF ATTACK FOR THE FREELY SPINNING AND FIXED STABILIZERS AT A FIN CANT OF 2 DEGREES AND A MACH NUMBER OF 1.10

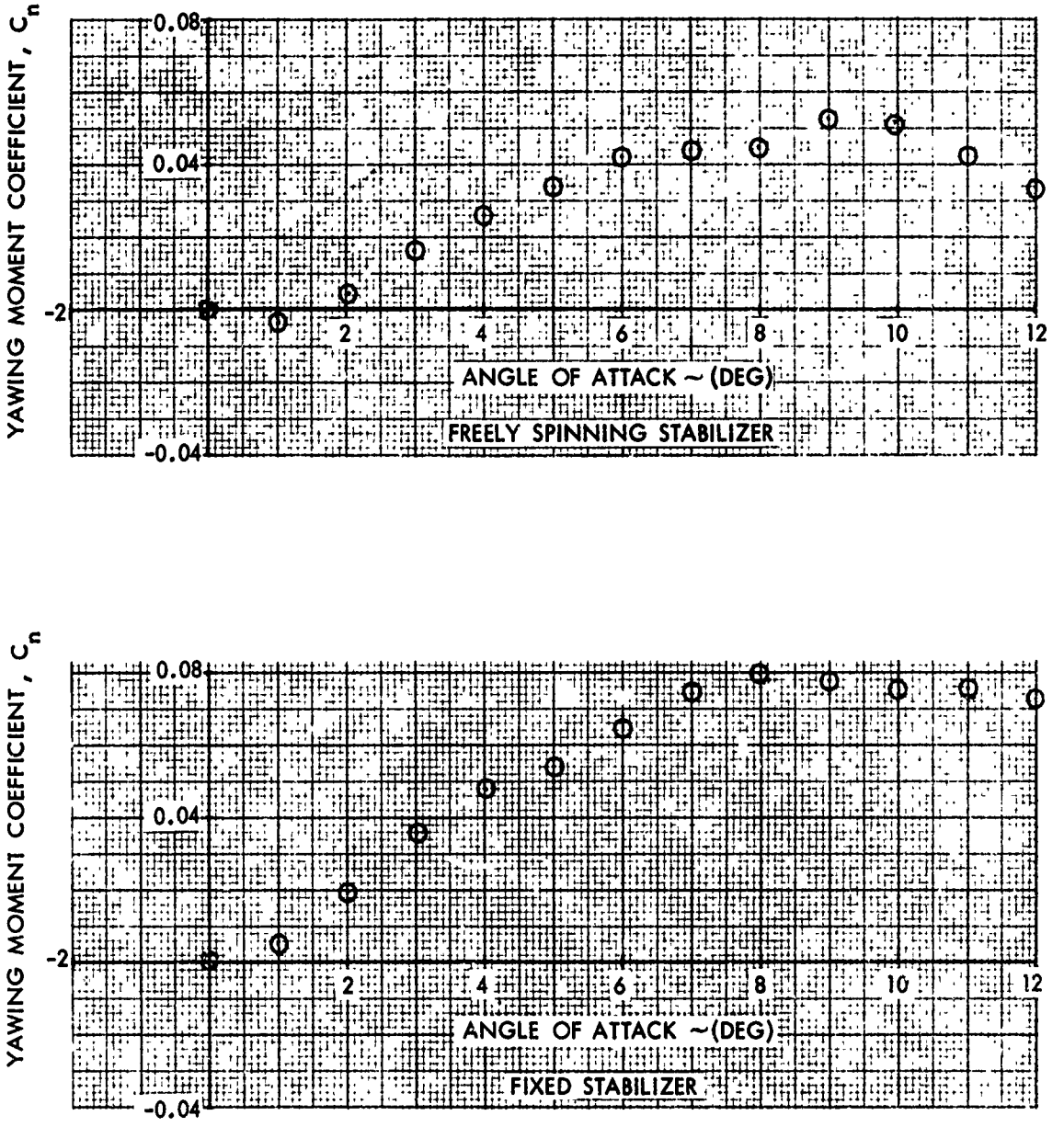

FIG. 64 YAWING MOMENT COEFFICIENT VERSUS ANGLE OF ATTACK FOR THE FIXED AND FREELY SPINNING STABILIZERS AT A FIN CANT OF 2 DEGREES AND A MACH NUMBER OF 0.60

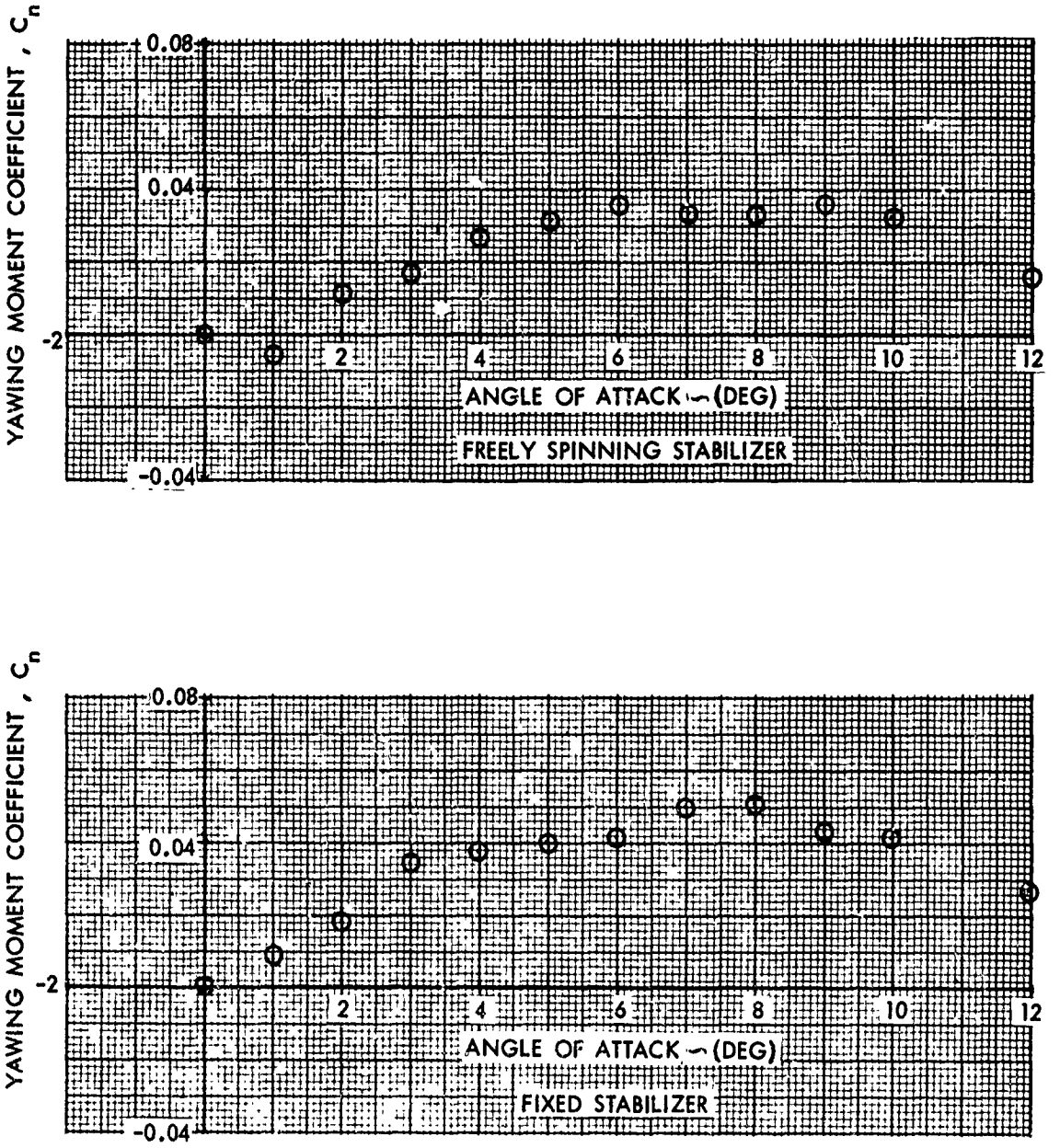

FIG. 65 YAWING MOMENT COEFFICIENT VERSUS ANGLE OF ATTACK FOR THE FIXED AND FREELY SPINNING STABILIZERS AT A FIN CANT OF 2 DEGREES AND A MACH NUMBER OF 0.69

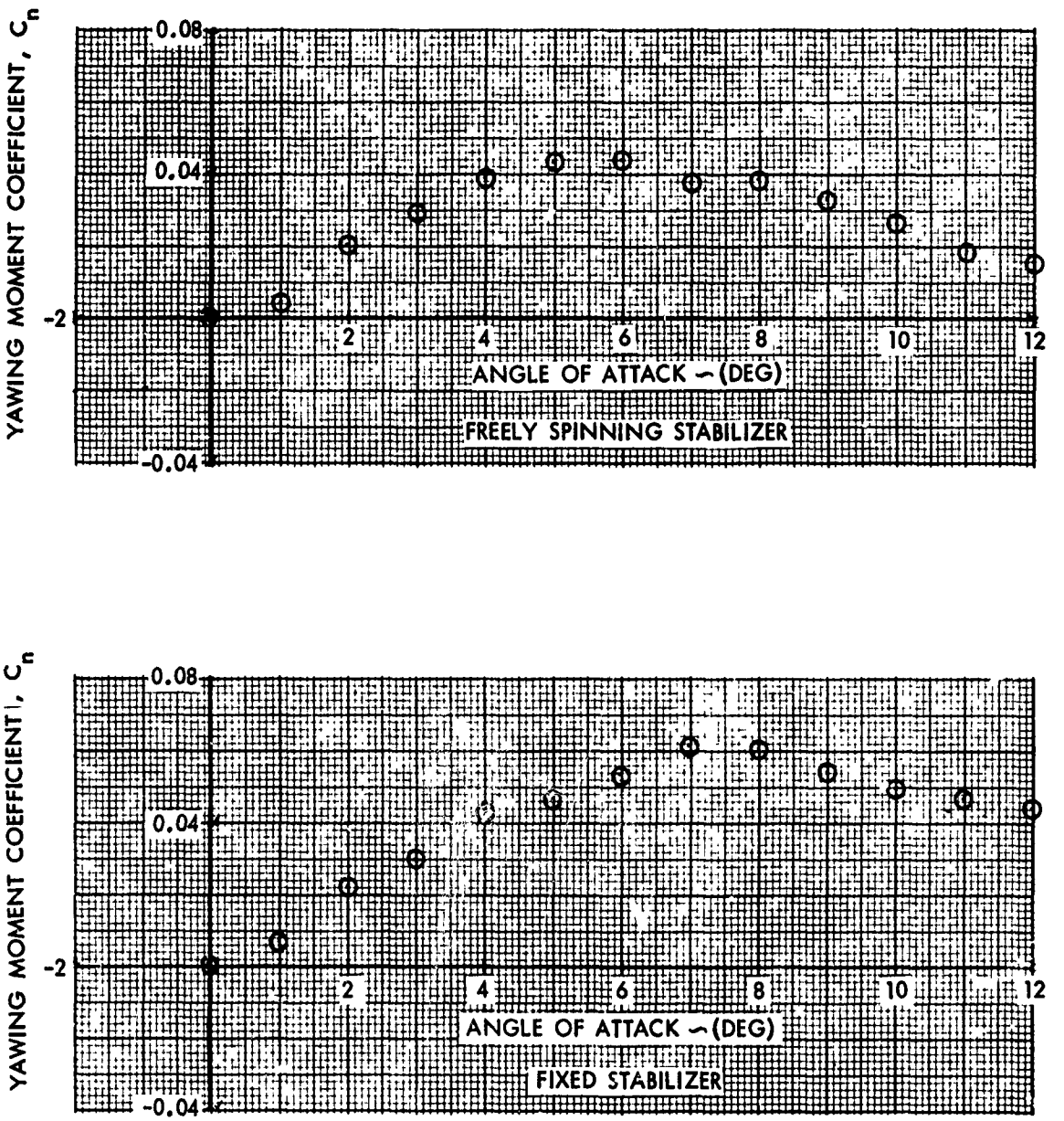

FIG. 66 YAWING MOMENT COEFFICIENT VERSUS ANGLE OF ATTACK FOR THE FIXED AND FREELY SPINNING STABILIZERS AT A FIN CANT OF 2 DEGREES AND A MACH NUMBER OF 0.74

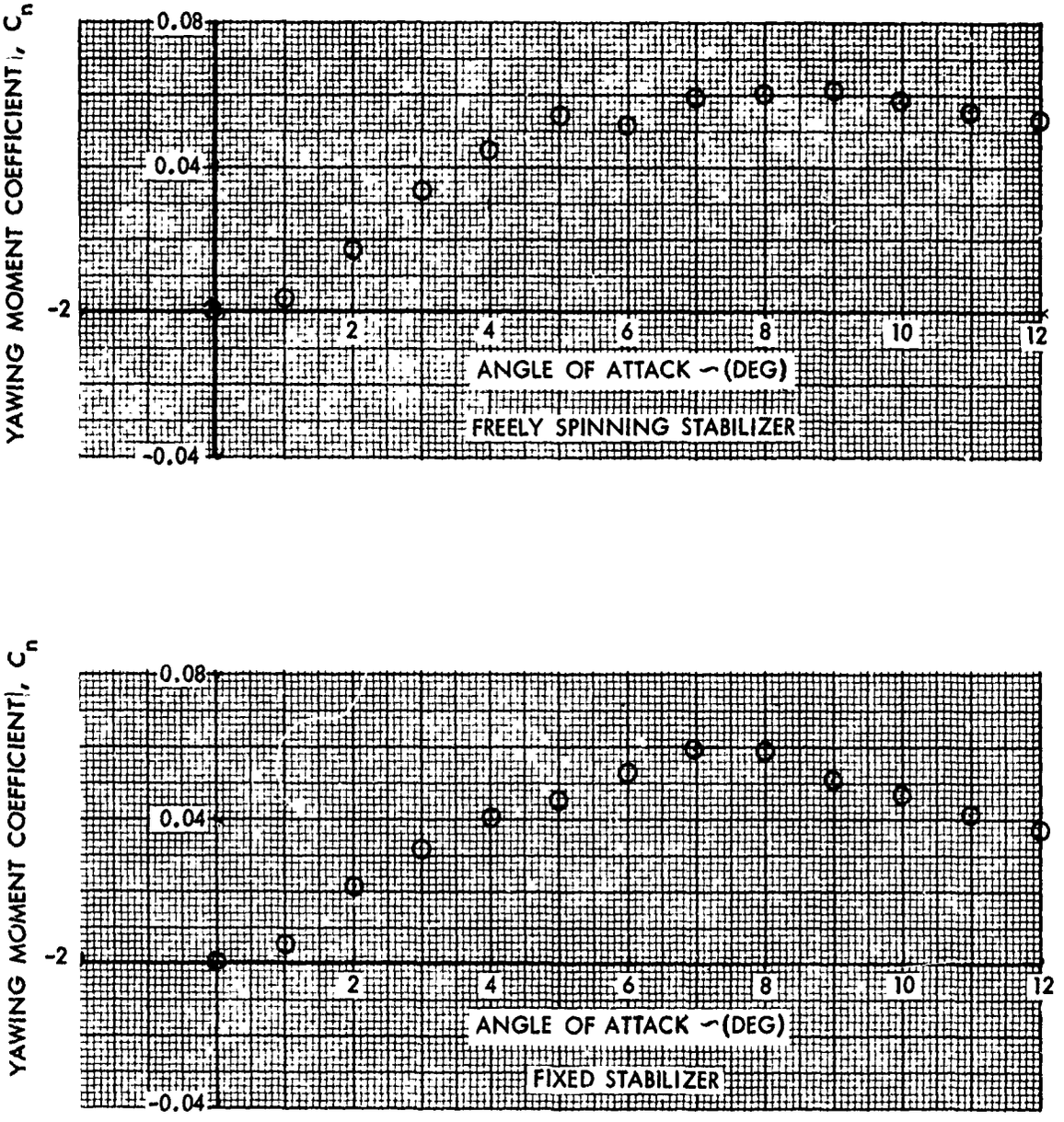

FIG. 67 YAWING MOMENT COEFFICIENT VERSUS ANGLE OF ATTACK FOR THE FIXED AND FREELY SPINNING STABILIZERS AT A FIN CANT OF 2 DEGREES AND A MACH NUMBER OF 0.80

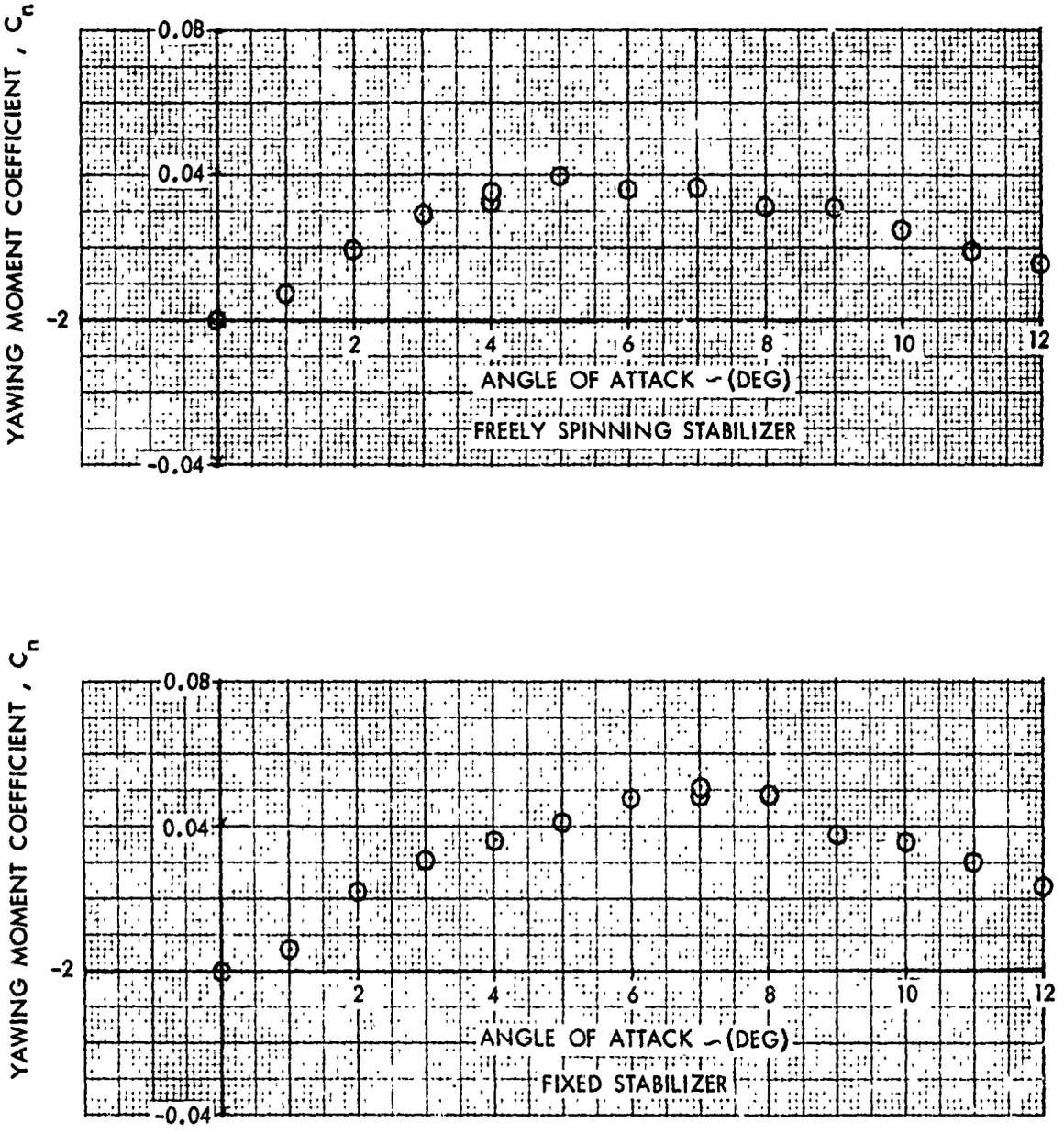

FIG. 68 YAWING MOMENT COEFFICIENT VERSUS ANGLE OF ATTACK FOR THE FIXED AND FREELY SPINNING STABILIZERS AT A FIN CANT OF 2 DEGREES AND A MACH NUMBER OF 0.84

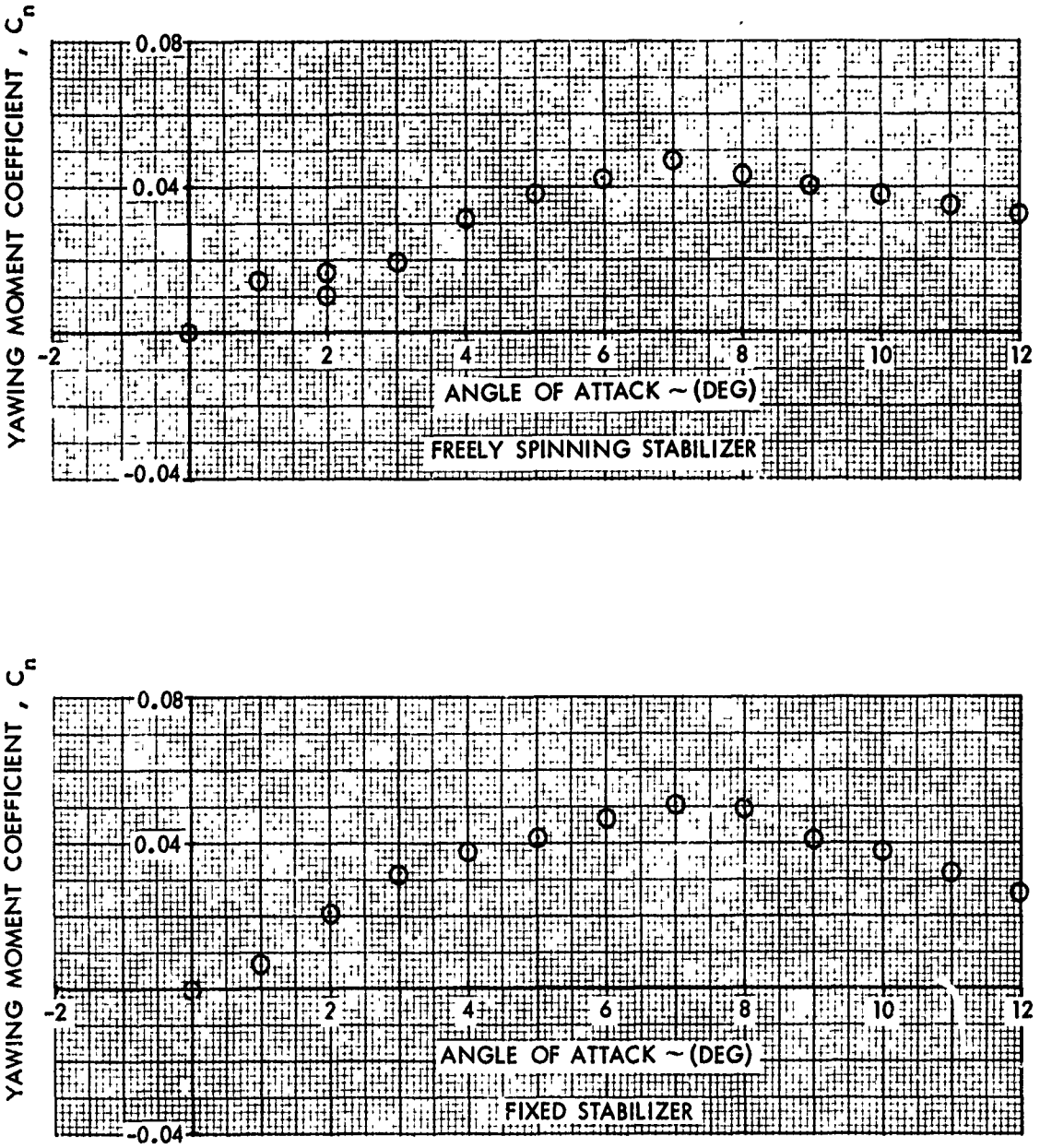

FIG. 69 YAWING MOMENT COEFFICIENT VERSUS ANGLE OF ATTACK FOR THE FIXED AND FREELY SPINNING STABILIZERS AT A FIN CANT OF 2 DEGREES AND A MACH NUMBER OF 0.89

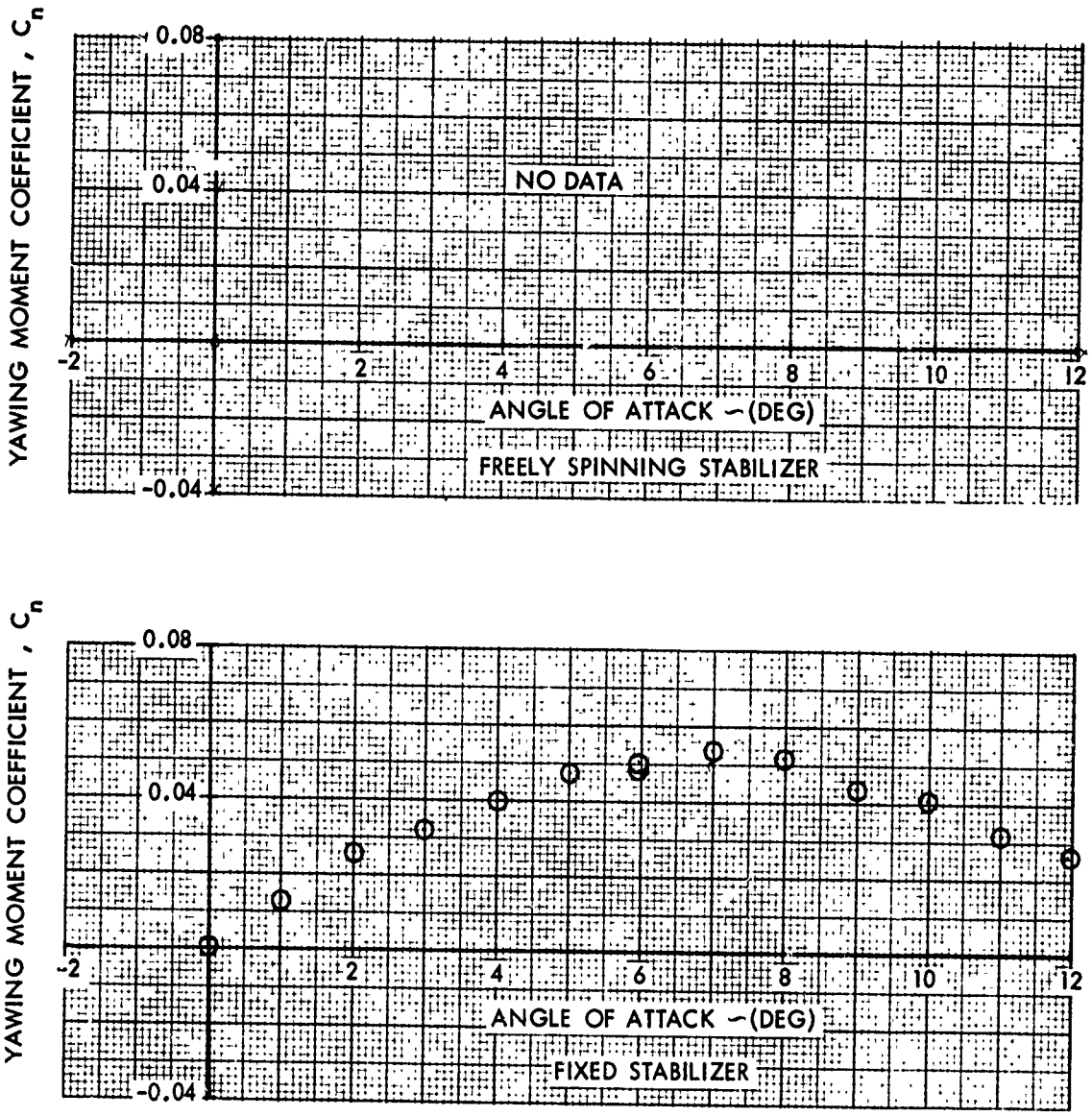

FIG. 70 YAWING MOMENT COEFFICIENT VERSUS ANGLE OF ATTACK FOR THE FIXED AND FREELY SPINNING STABILIZERS AT A FIN CANT OF 2 DEGREES AND A MACH NUMBER OF 0.94

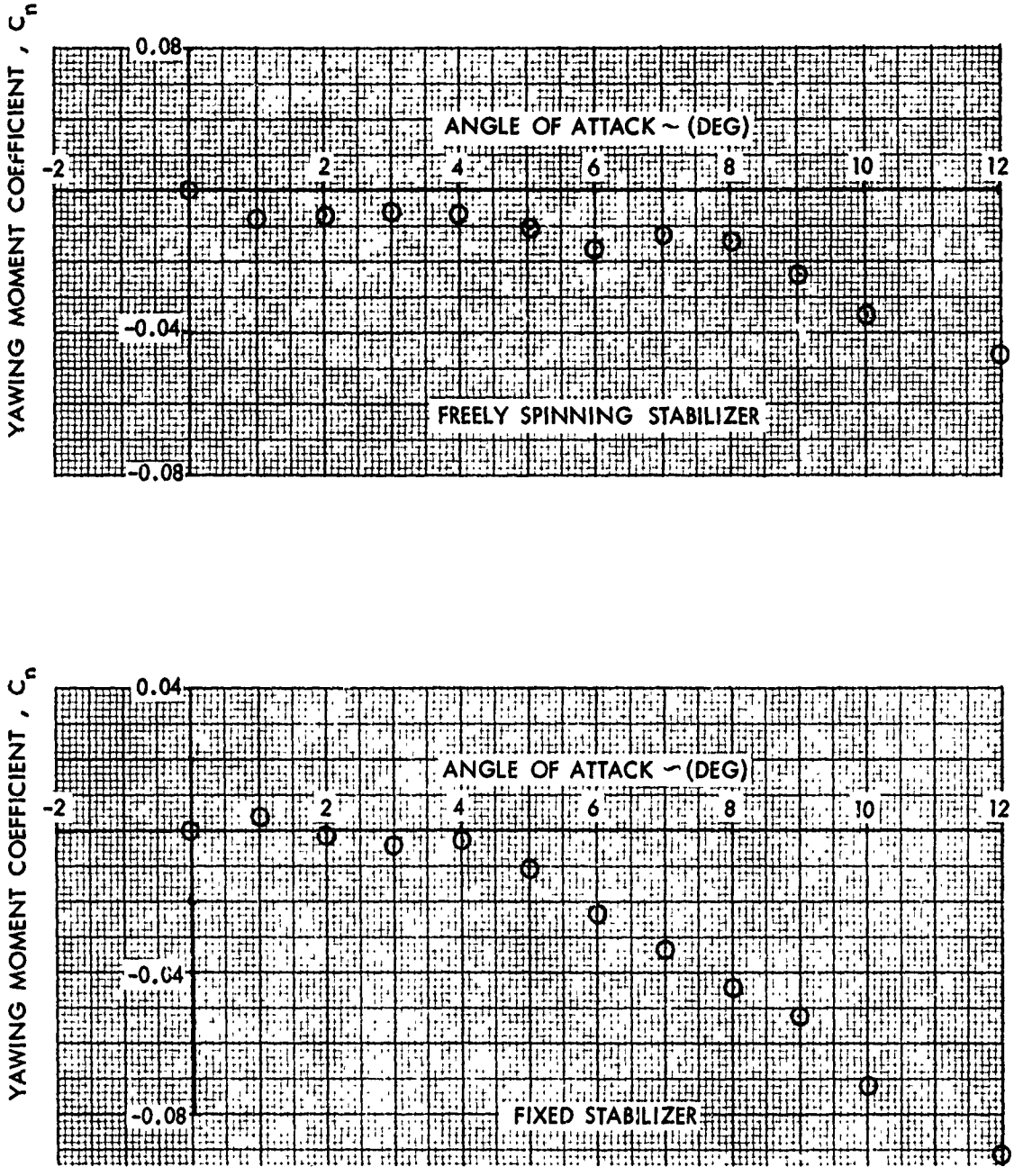

FIG. 71 YAWING MOMENT COEFFICIENT VERSUS ANGLE OF ATTACK FOR THE FIXED AND FREELY SPINNING STABILIZERS AT A FIN CANT OF 2 DEGREES AND A MACH NUMBER OF 1.11

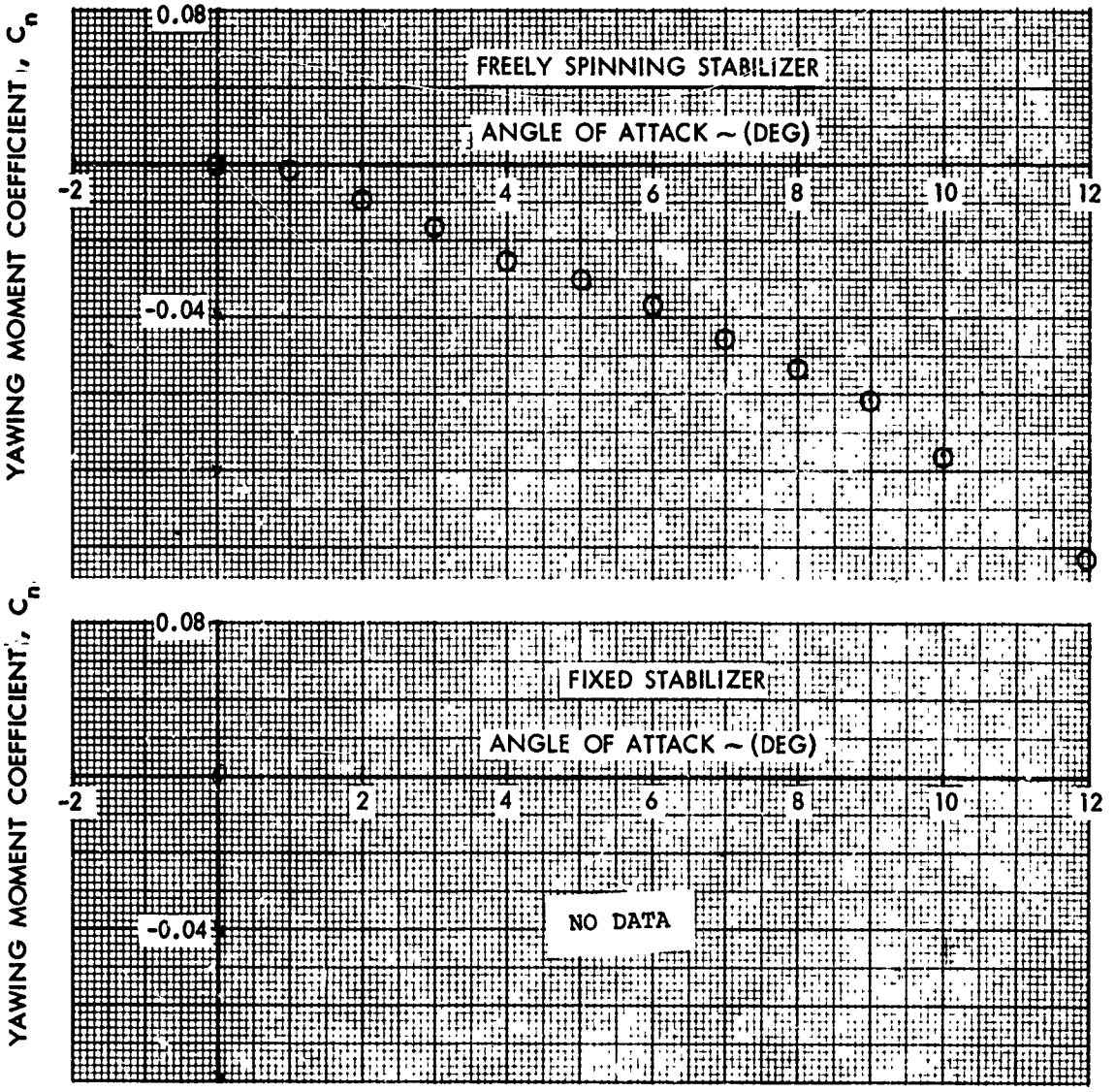

FIG. 72 YAWING MOMENT COEFFICIENT VERSUS ANGLE OF ATTACK FOR THE FIXED AND FREELY SPINNING STABILIZERS AT A FIN CANT OF 2 DEGREES AND A MACH NUMBER OF 1.20

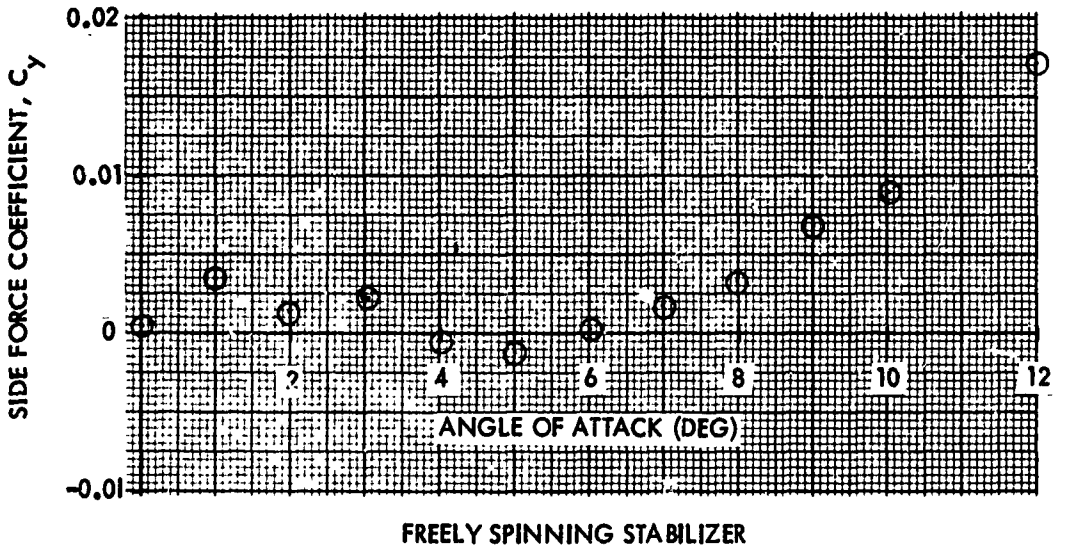

FREELY SPINNING STABILIZER

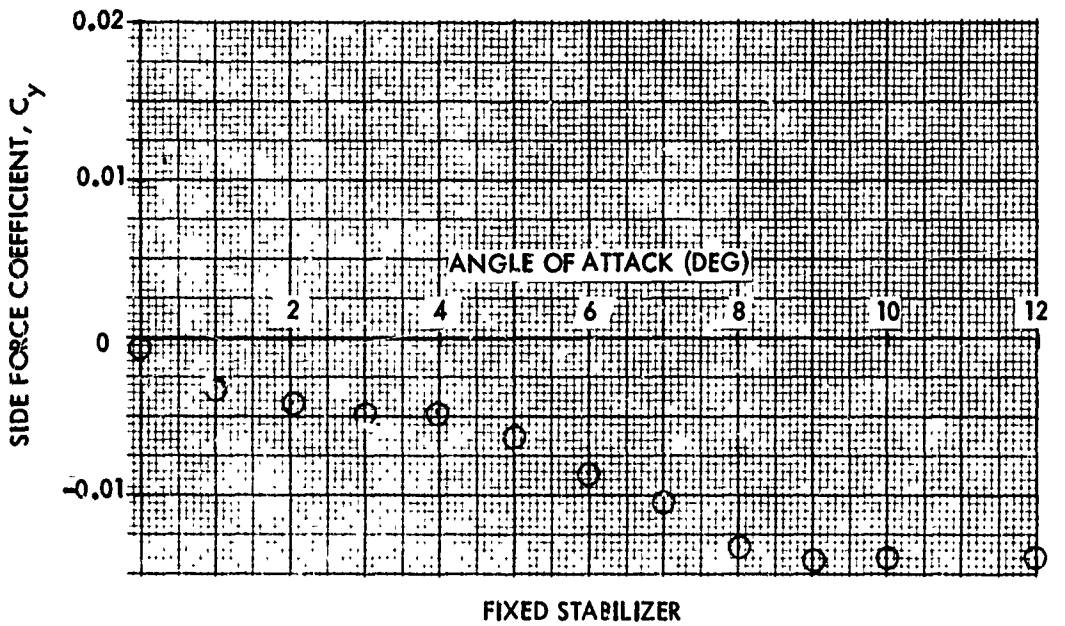

FIXED STABILIZER

FIG. 73 SIDE FORCE COEFFICIENT VERSUS ANGLE OF ATTACK FOR THE FREELY SPINNING AND FIXED STABILIZERS AT A FIN CANT OF 3 DEGREES AND A MACH NUMBER OF 0.60

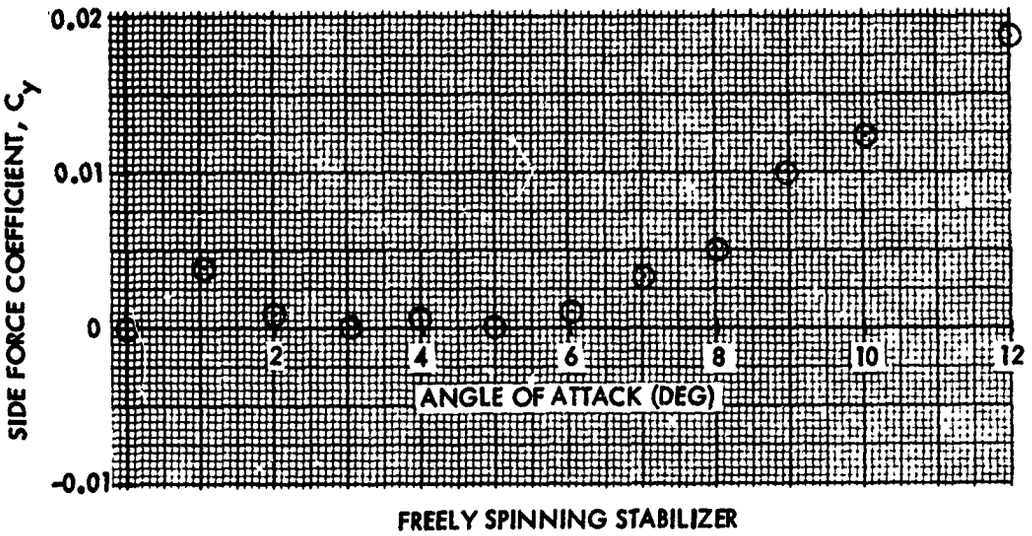

FREELY SPINNING STABILIZER

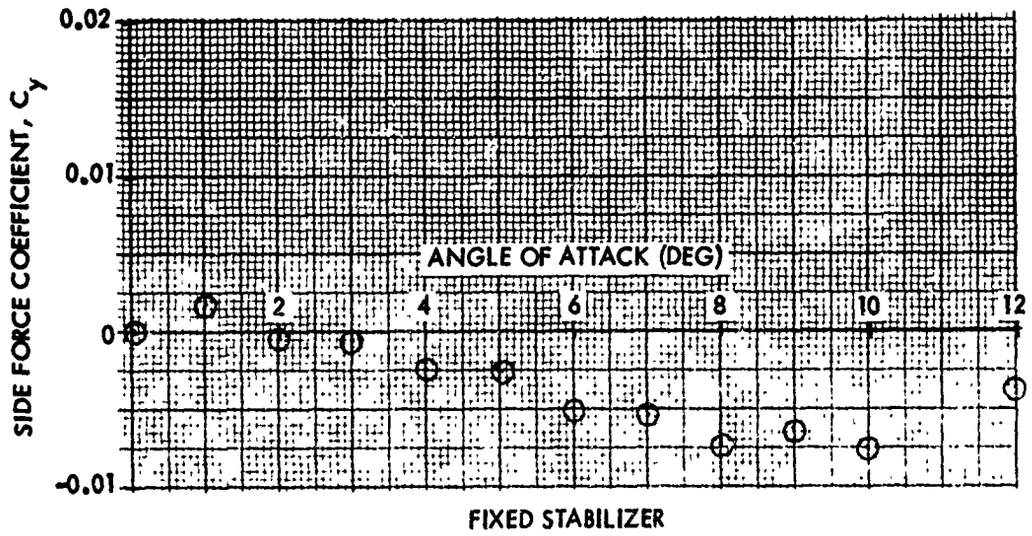

FIXED STABILIZER

FIG. 74 SIDE FORCE COEFFICIENT VERSUS ANGLE OF ATTACK FOR THE FREELY SPINNING AND FIXED STABILIZERS AT A FIN CANT OF 3 DEGREES AND A MACH NUMBER OF 0.70.

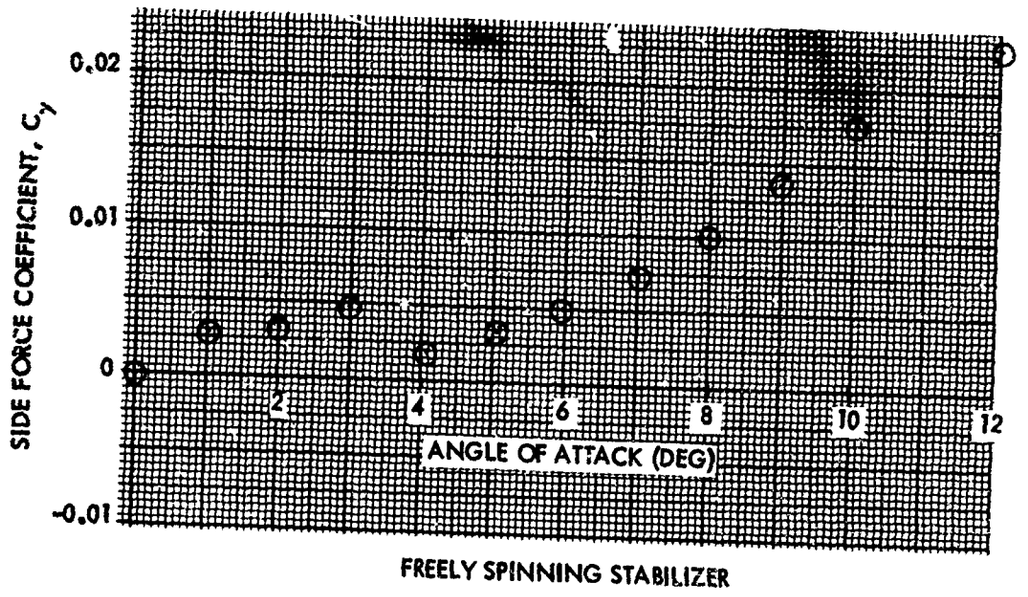

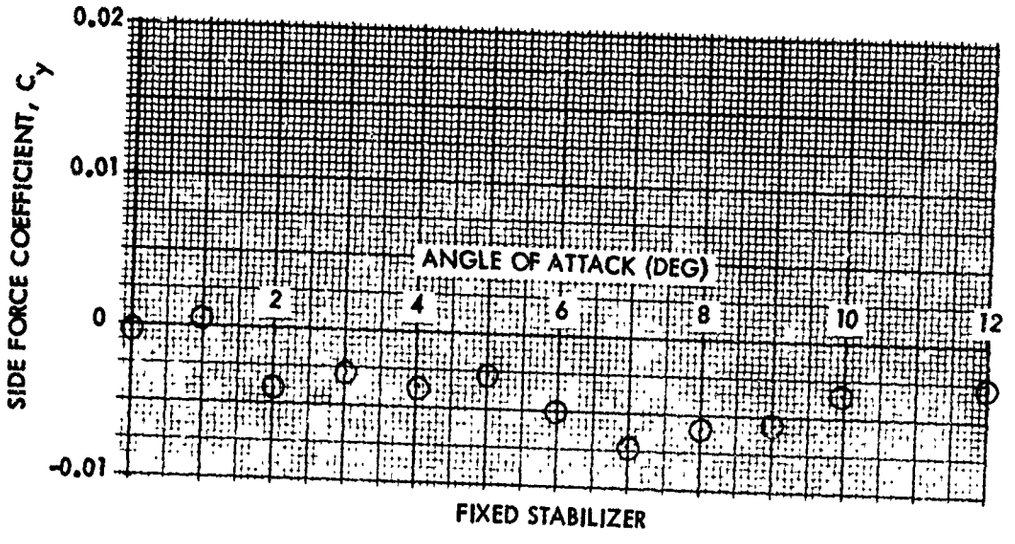

FIG. 75 SIDE FORCE COEFFICIENT VERSUS ANGLE OF ATTACK FOR THE FREELY SPINNING AND FIXED STABILIZERS AT A FIN CANT OF 3 DEGREES AND A MACH NUMBER OF 0.75

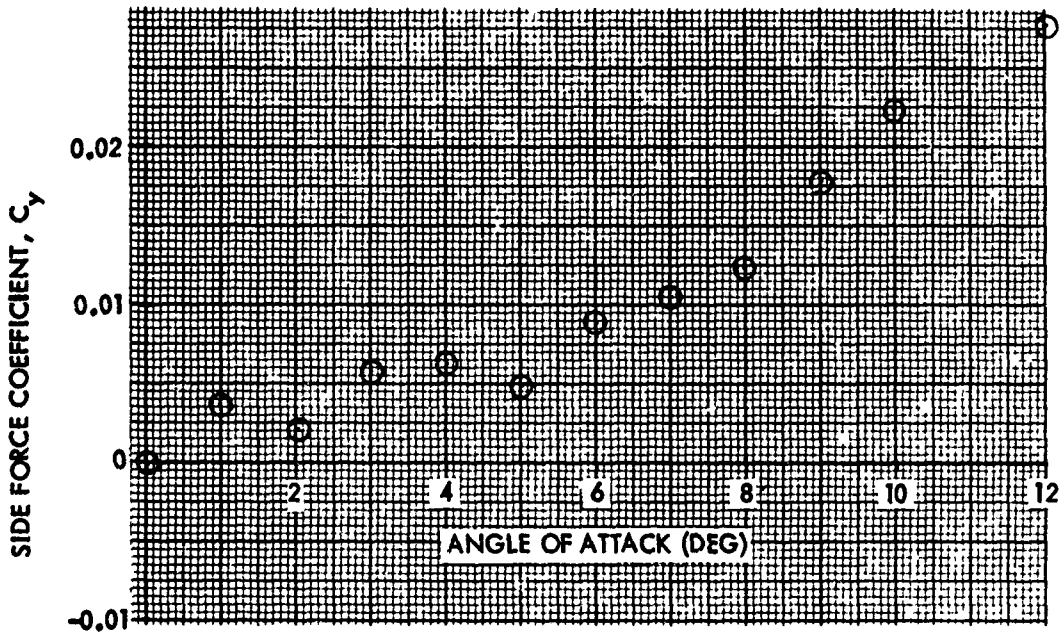

FREELY SPINNING STABILIZER

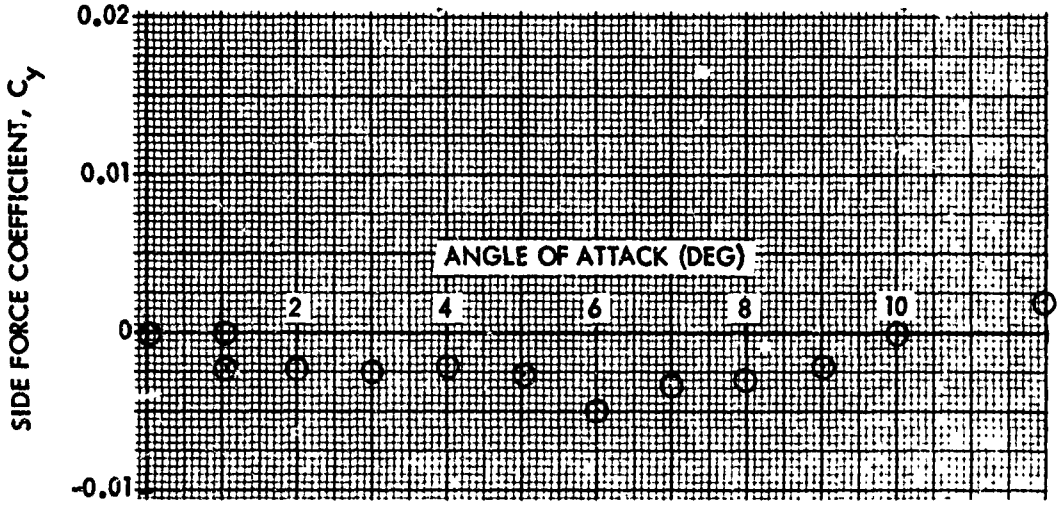

FIXED STABILIZER

FIG. 76 SIDE FORCE COEFFICIENT VERSUS ANGLE OF ATTACK FOR THE FREELY SPINNING AND FIXED STABILIZERS AT A FIN CANT OF 3 DEGREES AND A MACH NUMBER OF 0.80.

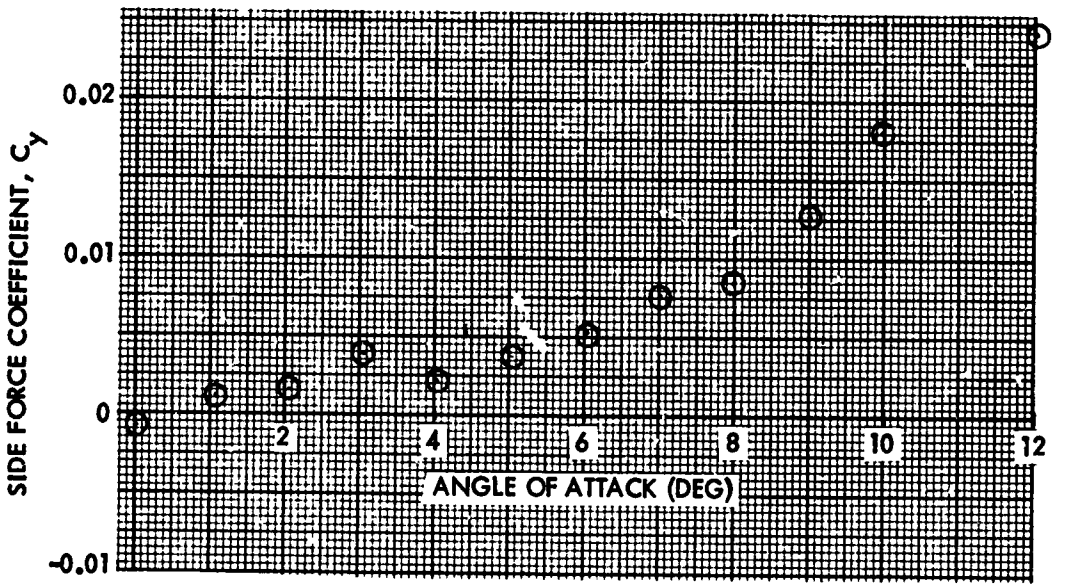

FREELY SPINNING STABILIZER

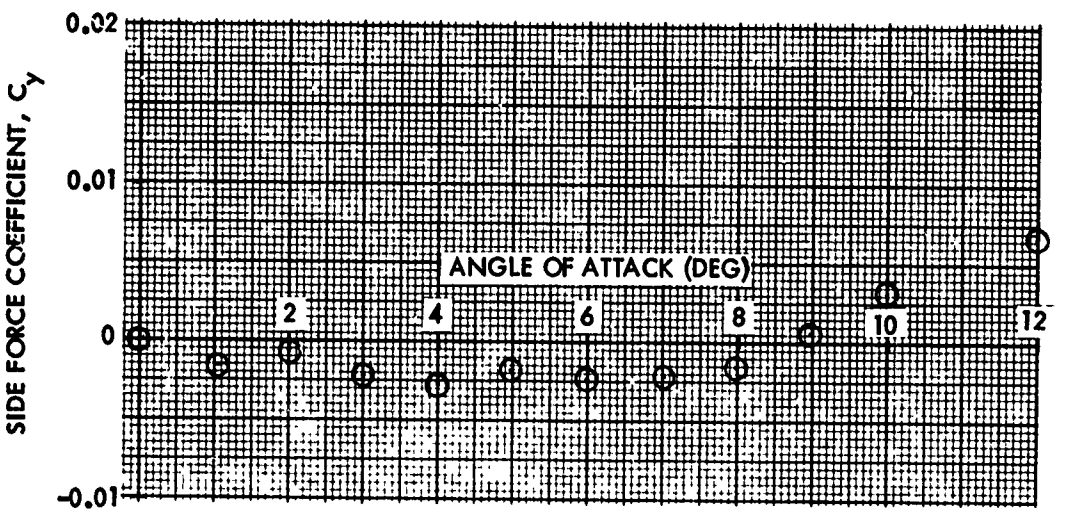

FIXED STABILIZER

FIG. 77 SIDE FORCE COEFFICIENT VERSUS ANGLE OF ATTACK FOR THE FREELY SPINNING AND FIXED STABILIZERS AT A FIN CANT OF 3 DEGREES AND A MACH NUMBER OF 0.84

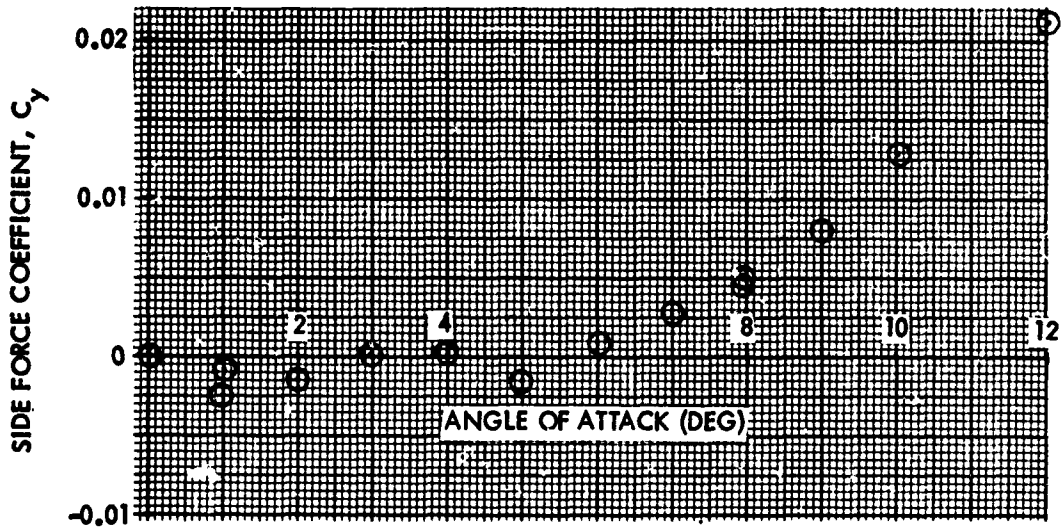

FREELY SPINNING STABILIZER

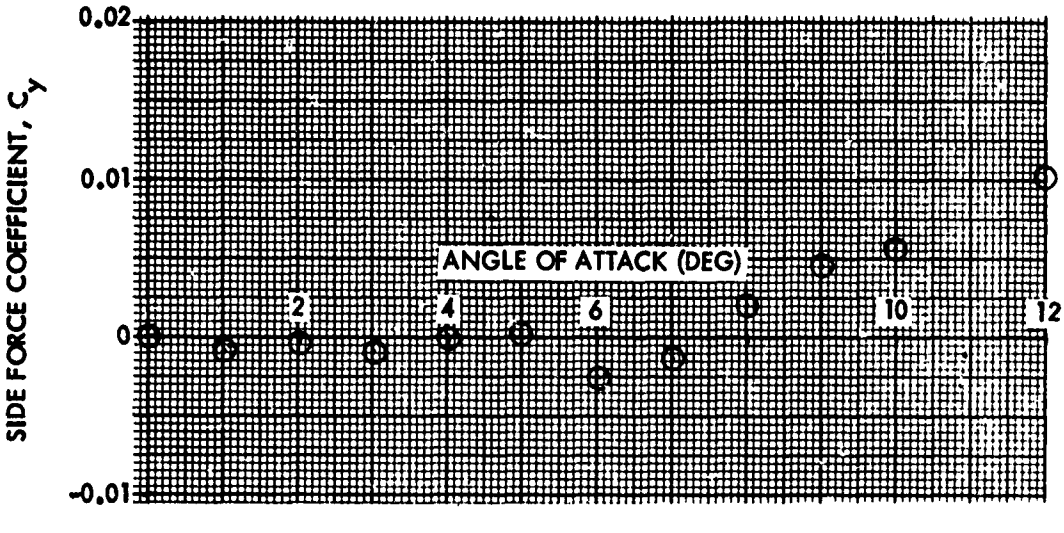

FIXED STABILIZER

FIG. 78 SIDE FORCE COEFFICIENT VERSUS ANGLE OF ATTACK FOR THE FREELY SPINNING AND FIXED STABILIZERS AT A FIN CANT OF 3 DEGREES AND A MACH NUMBER OF 0.90

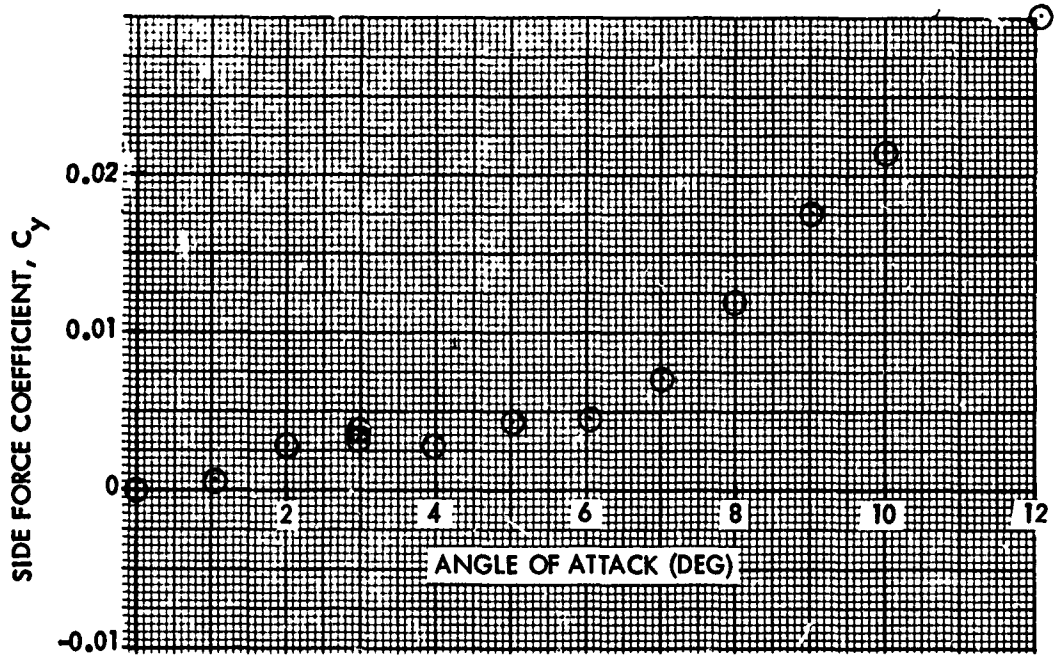

FREELY SPINNING STABILIZER

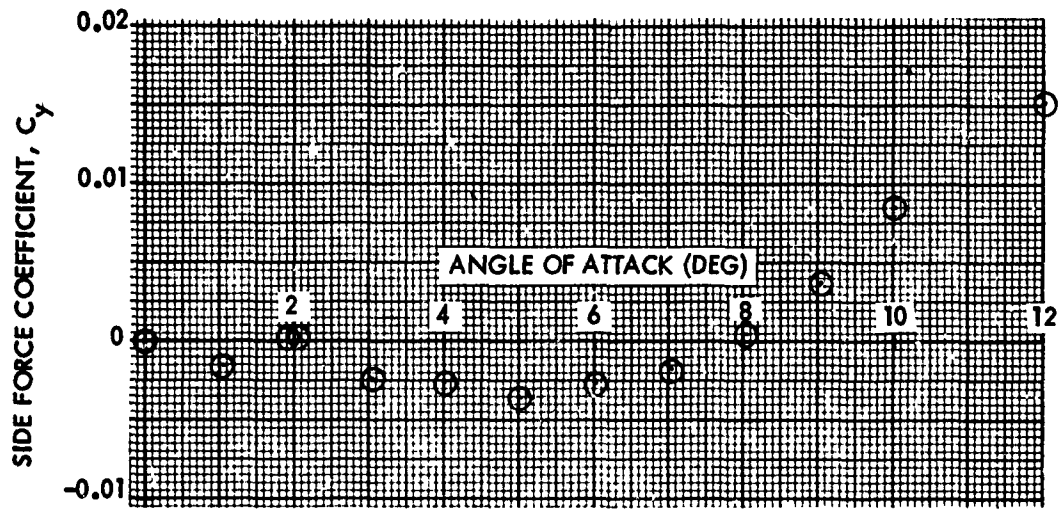

FIXED STABILIZER

FIG. 79 SIDE FORCE COEFFICIENT VERSUS ANGLE OF ATTACK FOR THE FREELY SPINNING AND FIXED STABILIZERS AT A FIN CANT OF 3 DEGREES AND A MACH NUMBER OF 0.94

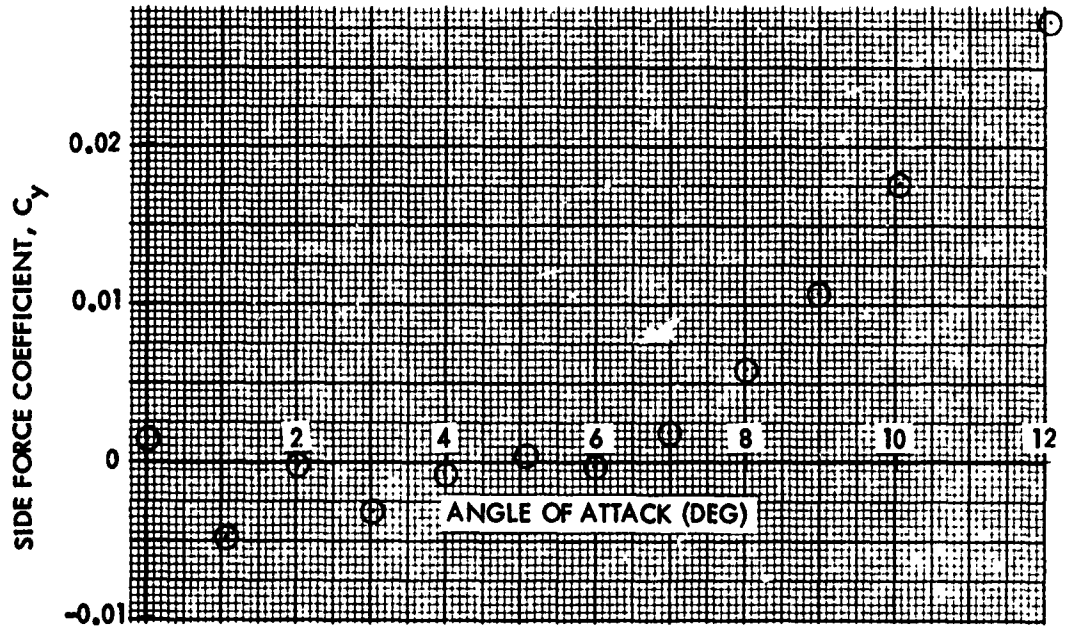

FREELY SPINNING STABILIZER

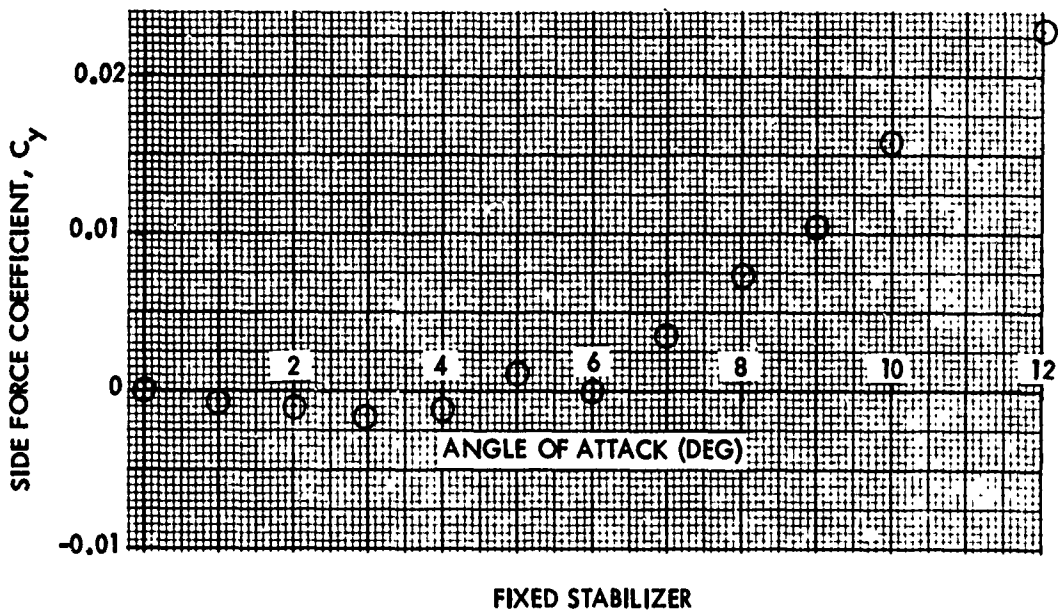

FIXED STABILIZER

FIG. 80 SIDE FORCE COEFFICIENT VERSUS ANGLE OF ATTACK FOR THE FREELY SPINNING AND FIXED STABILIZERS AT A FIN CANT OF 3 DEGREES AND A MACH NUMBER OF 1.11

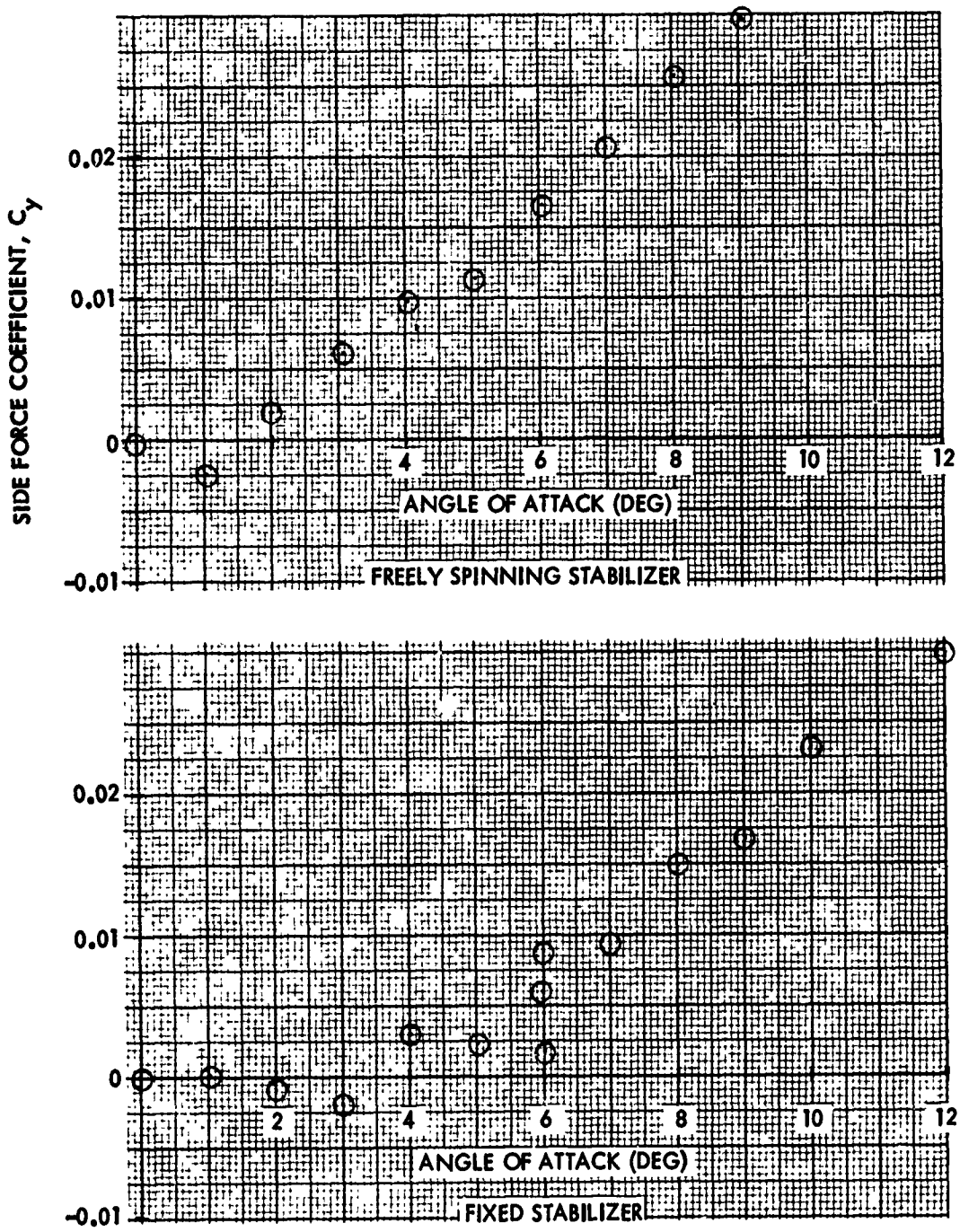

FIG. 81 SIDE FORCE COEFFICIENT VERSUS ANGLE OF ATTACK FOR THE FREELY SPINNING AND FIXED STABILIZERS AT A FIN CANT OF 3 DEGREES AND A MACH NUMBER OF 1.20

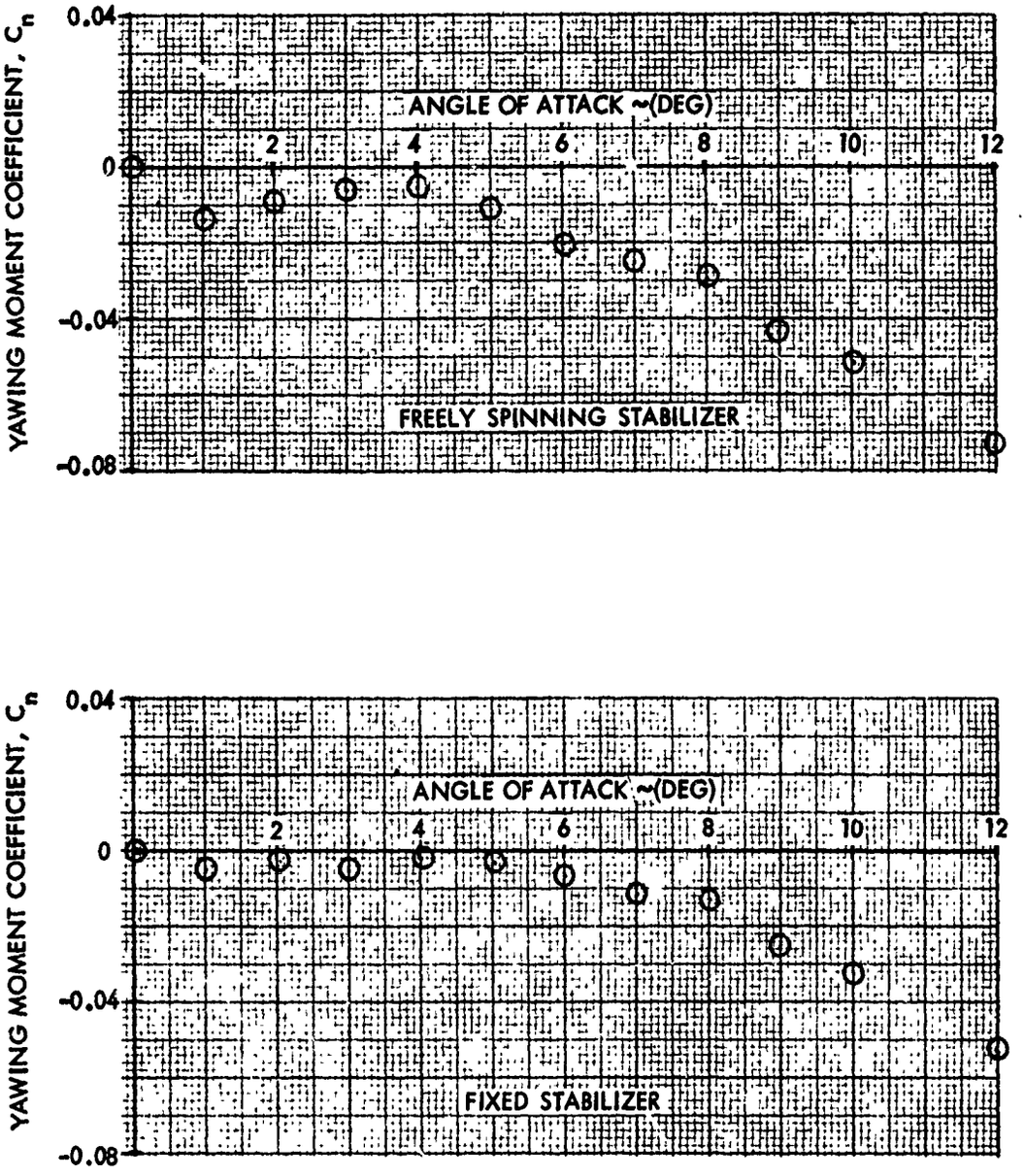

FIG. 82 YAWING MOMENT COEFFICIENT VERSUS ANGLE OF ATTACK FOR THE FIXED AND FREELY SPINNING STABILIZERS AT A FIN CANT OF 3 DEGREES AND A MACH NUMBER OF 0.69

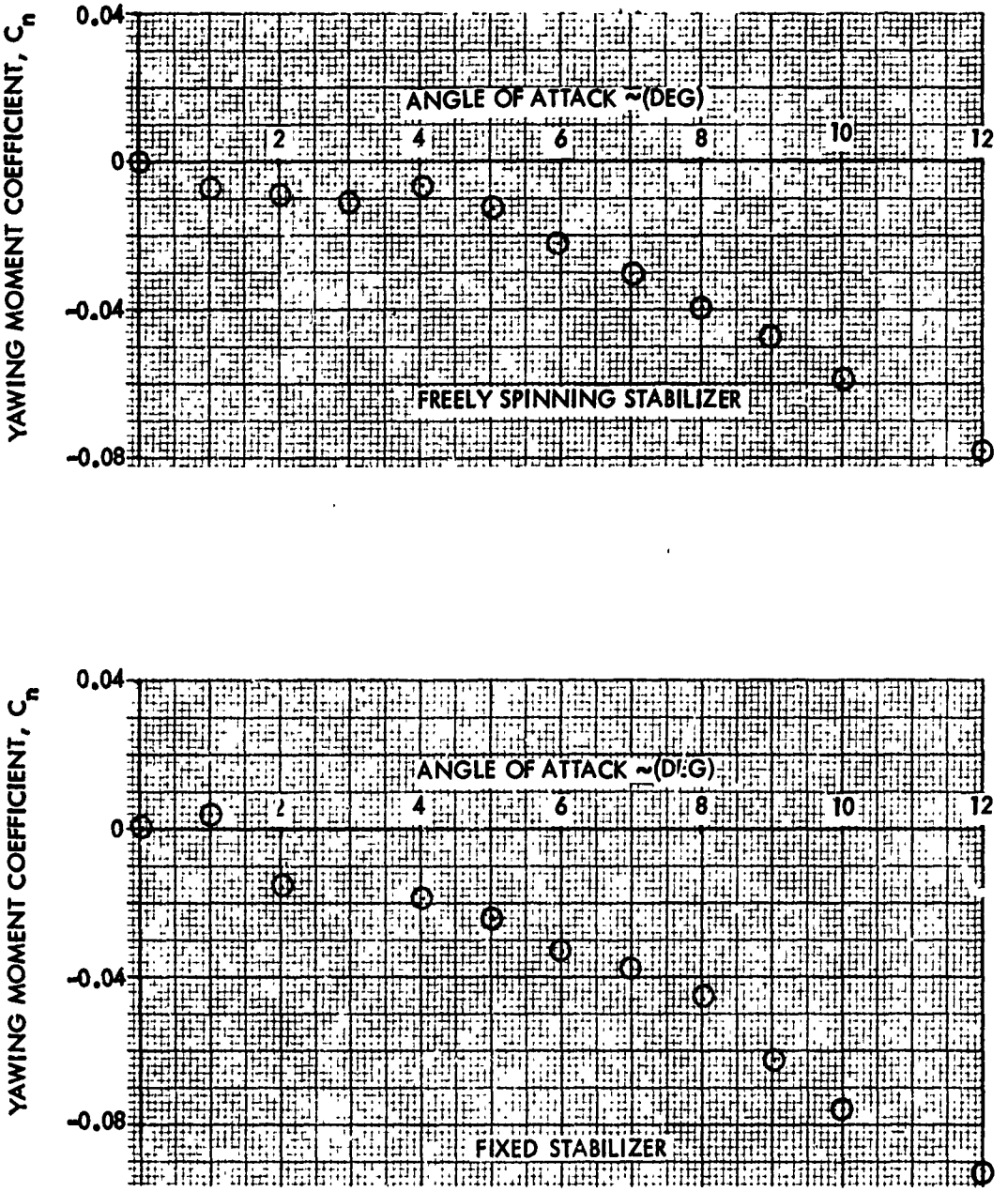

FIG. 83 YAWING MOMENT COEFFICIENT VERSUS ANGLE OF ATTACK FOR THE FIXED AND FREELY SPINNING STABILIZERS AT A FIN CANT OF 3 DEGREES AND A MACH NUMBER OF 0.74

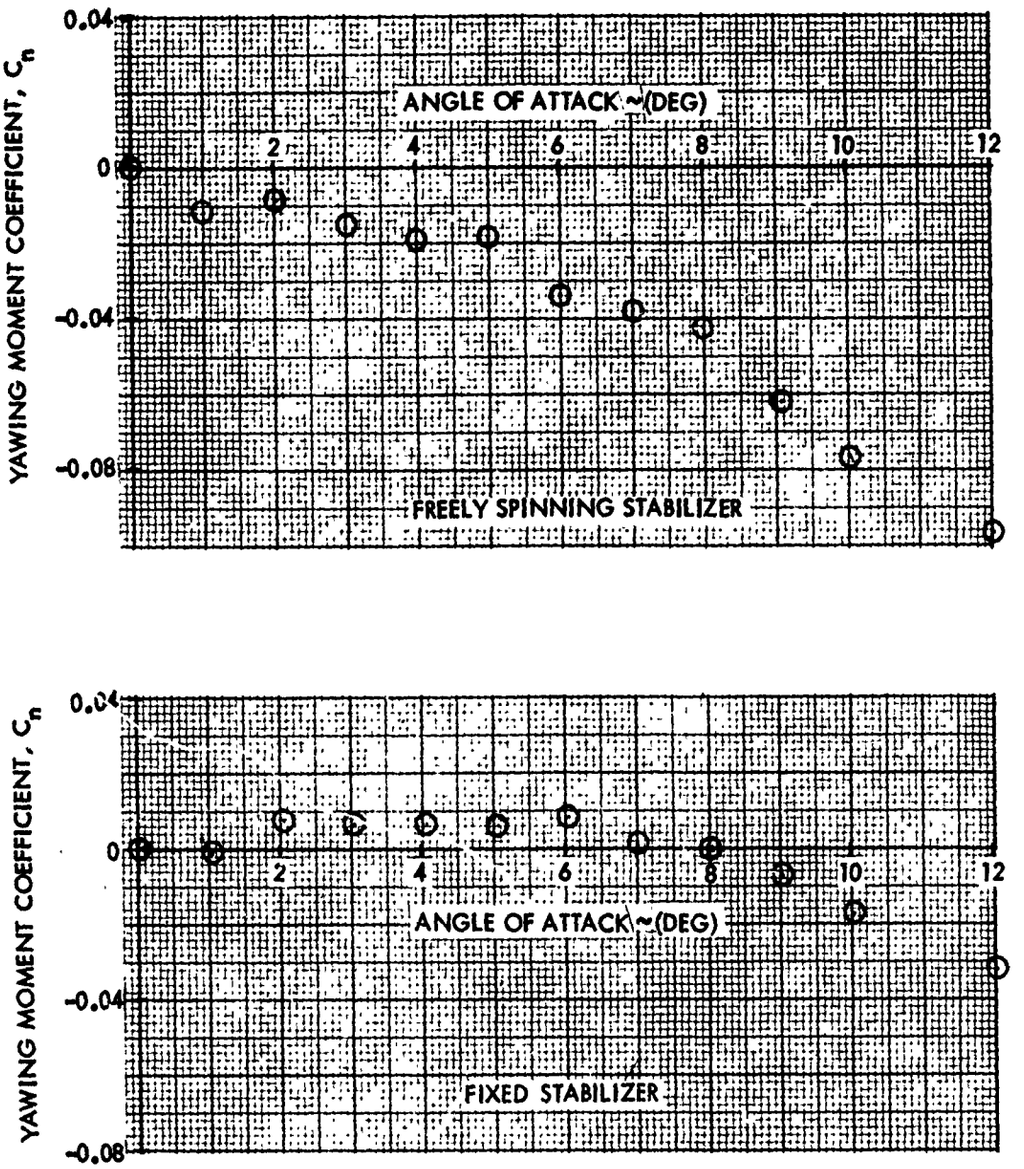

FIG. 84. YAWING MOMENT COEFFICIENT VERSUS ANGLE OF ATTACK FOR THE FIXED AND FREELY SPINNING STABILIZERS AT A FIN CANT OF 3 DEGREES AND A MACH NUMBER OF 0.79.

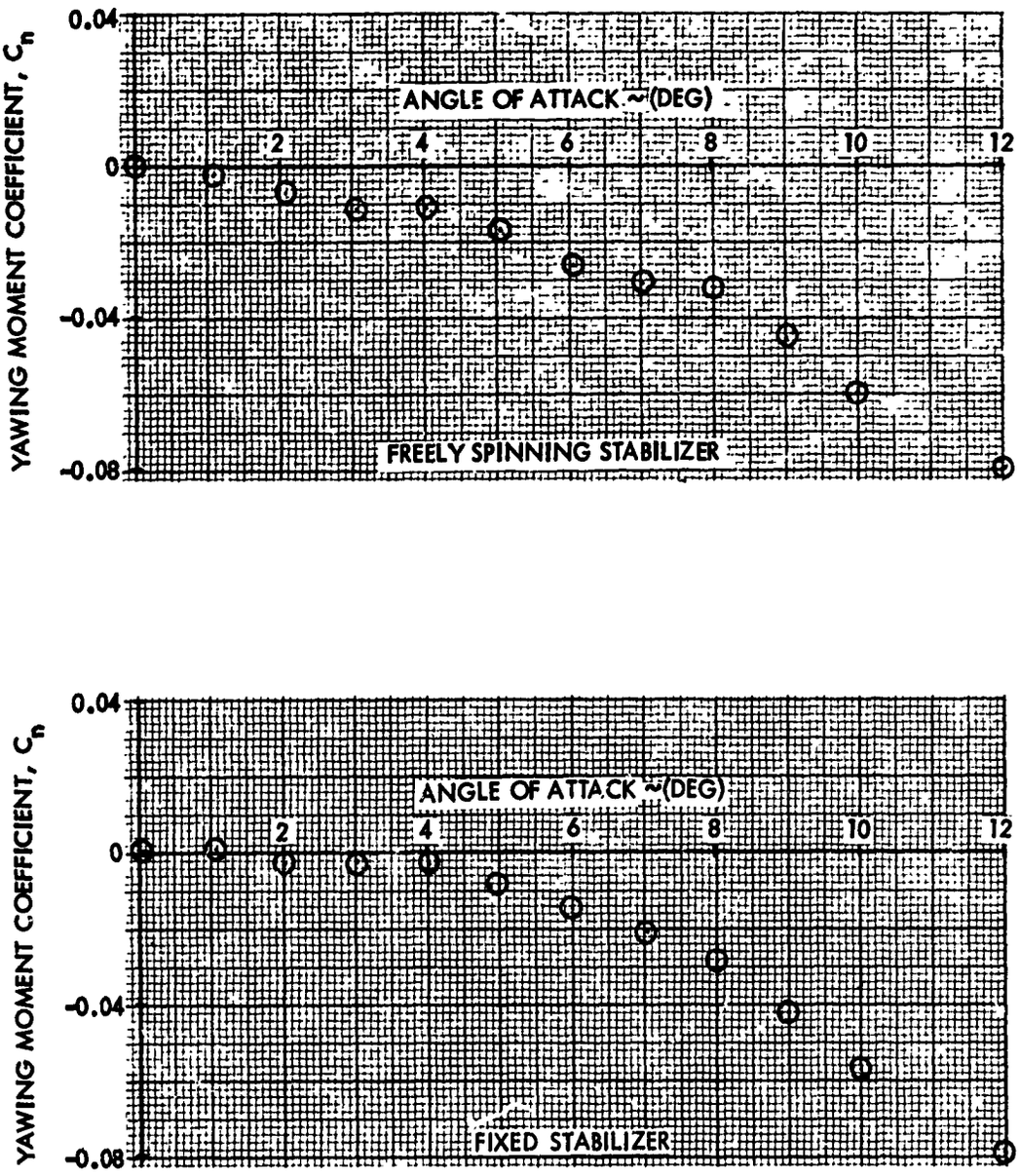

FIG. 85. YAWING MOMENT COEFFICIENT VERSUS ANGLE OF ATTACK FOR THE FIXED AND FREELY SPINNING STABILIZERS AT A FIN CANT OF 3 DEGREES AND A MACH NUMBER OF 0.84.

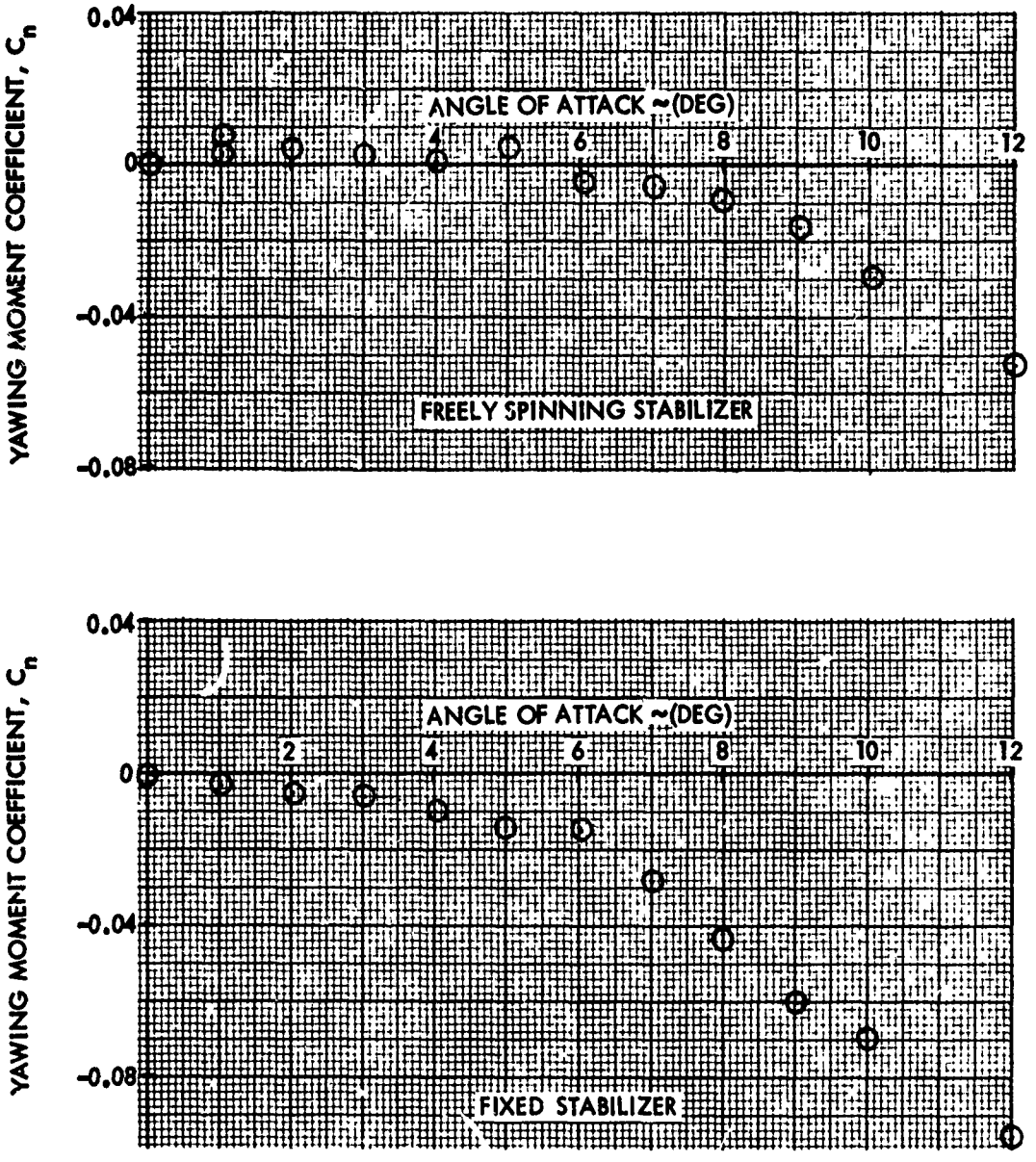

FIG. 86 YAWING MOMENT COEFFICIENT VERSUS ANGLE OF ATTACK FOR THE FIXED AND FREELY SPINNING STABILIZERS AT A FIN CANT OF 3 DEGREES AND A MACH NUMBER OF 0.89

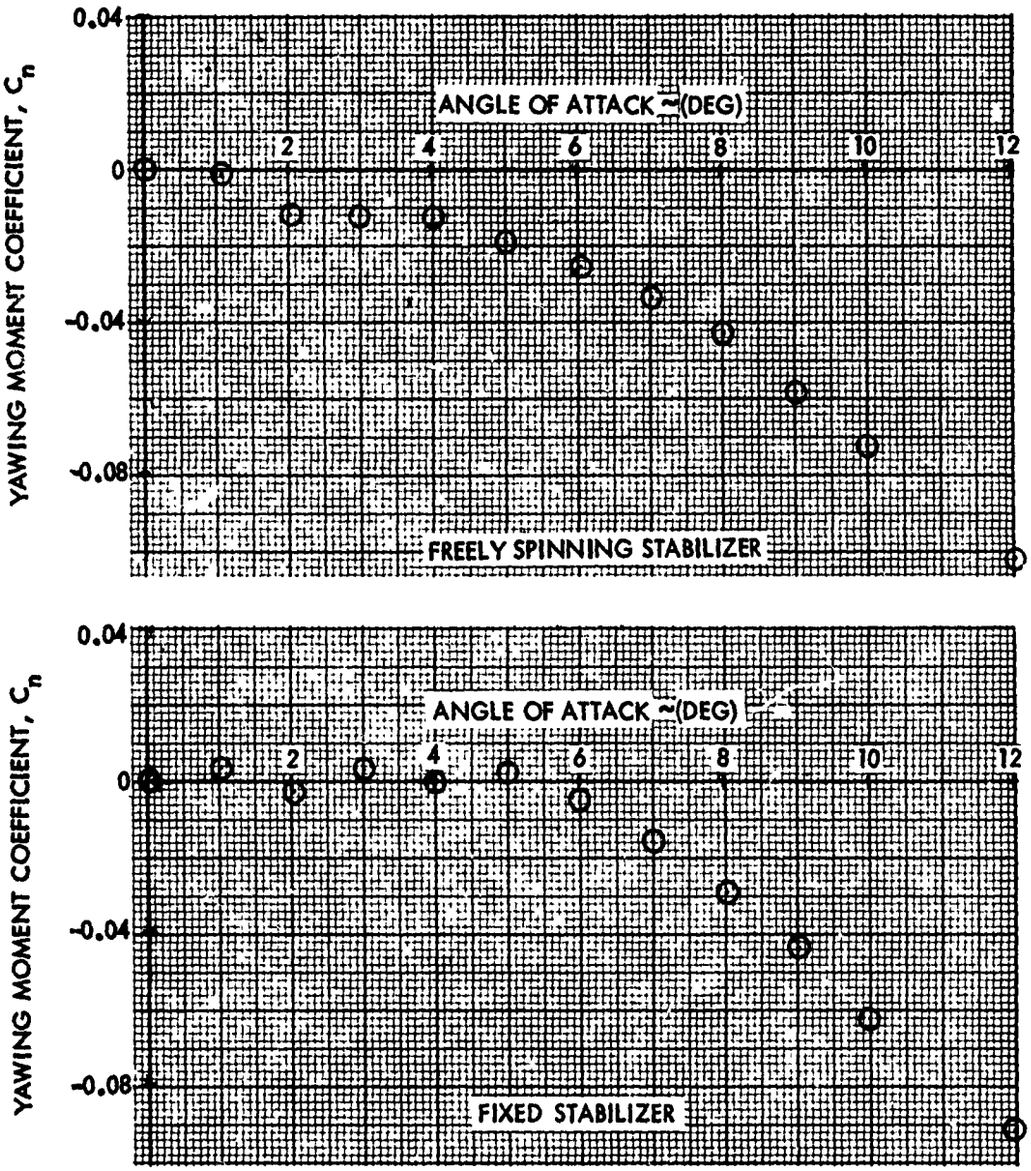

FIG. 87. YAWING MOMENT COEFFICIENT VERSUS ANGLE OF ATTACK FOR THE FIXED AND FREELY SPINNING STABILIZERS AT A FIN CANT OF 3 DEGREES AND A MACH NUMBER OF 0.94.

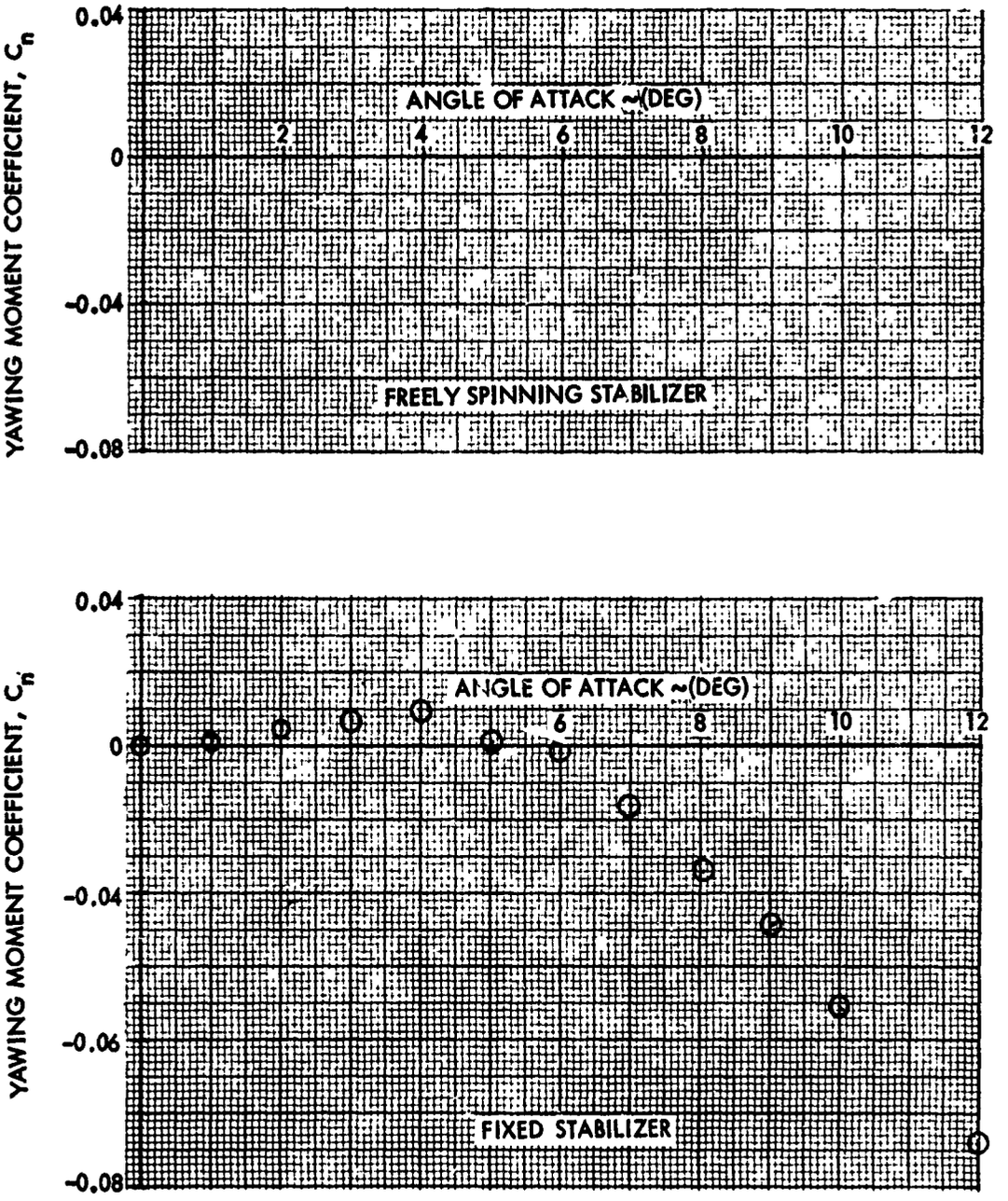

FIG. 88. YAWING MOMENT COEFFICIENT VERSUS ANGLE OF ATTACK FOR THE FIXED AND FREELY SPINNING STABILIZERS AT A FIN CANT OF 3 DEGREES AND A MACH NUMBER OF 1.11

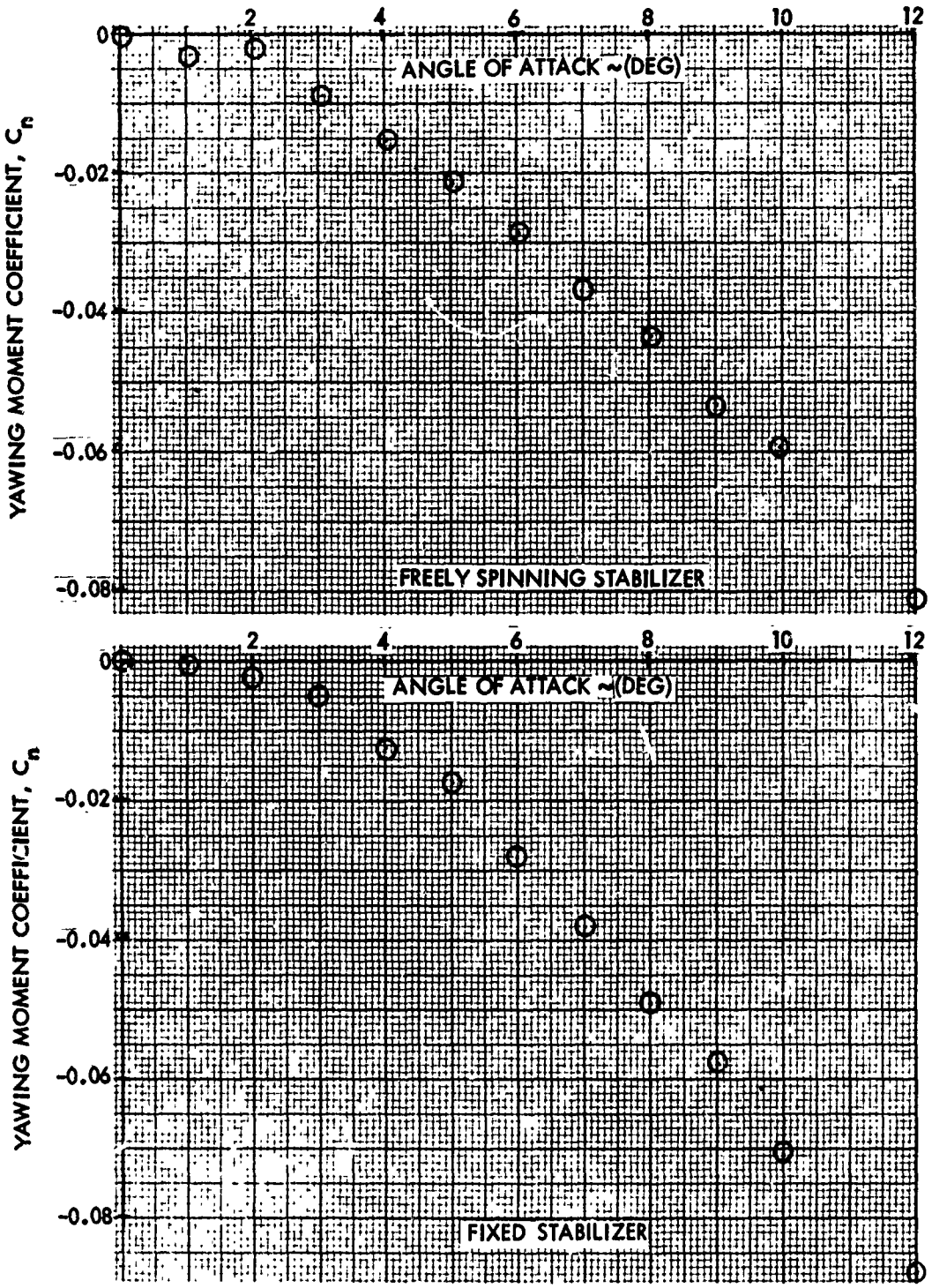

FIG. 89 YAWING MOMENT COEFFICIENT VERSUS ANGLE OF ATTACK FOR THE FIXED AND FREELY SPINNING STABILIZERS AT A FIN CANT OF 3 DEGREES AND A MACH NUMBER OF 1.20

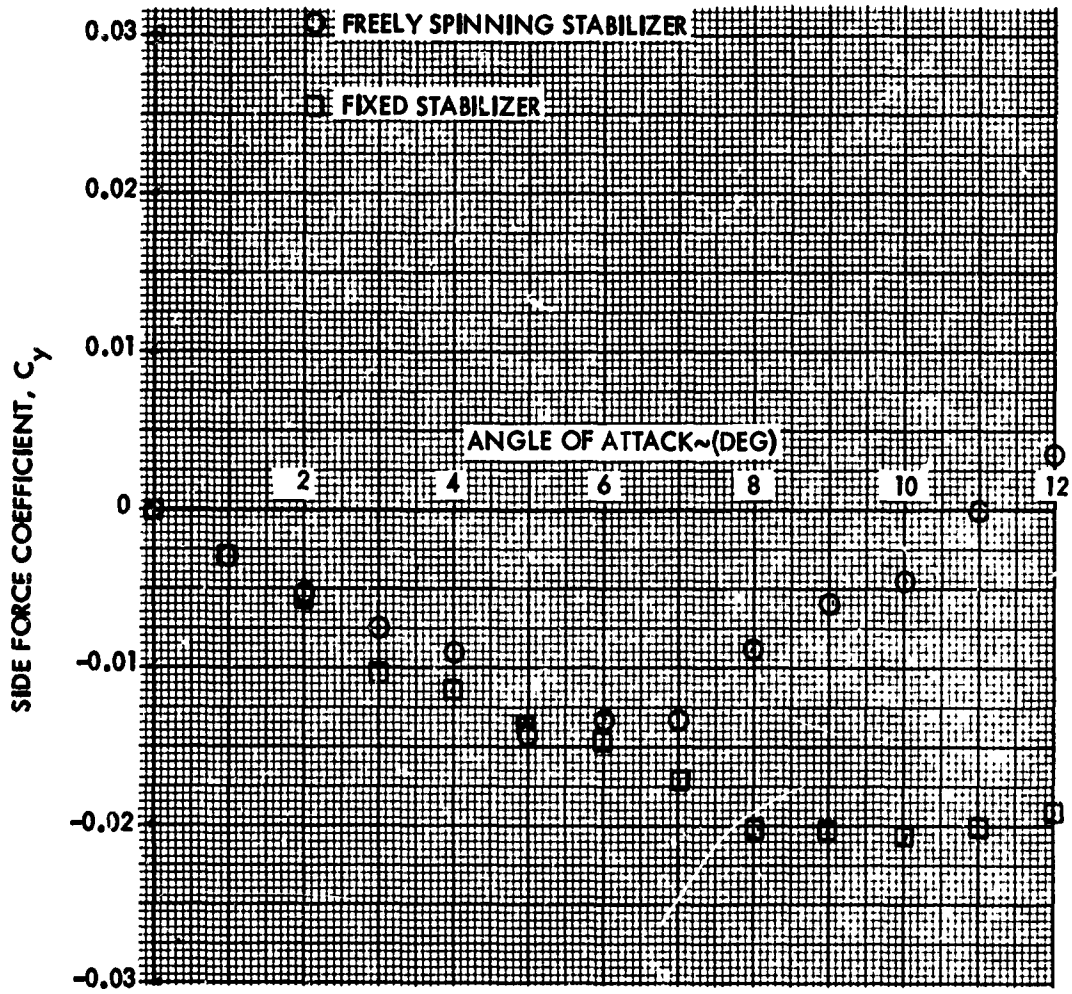

FIG. 90 SIDE FORCE COEFFICIENT VERSUS ANGLE OF ATTACK FOR THE FIXED AND FREELY SPINNING STABILIZERS AT A FIN CANT OF 4 DEGREES AND A MACH NUMBER OF 0.60

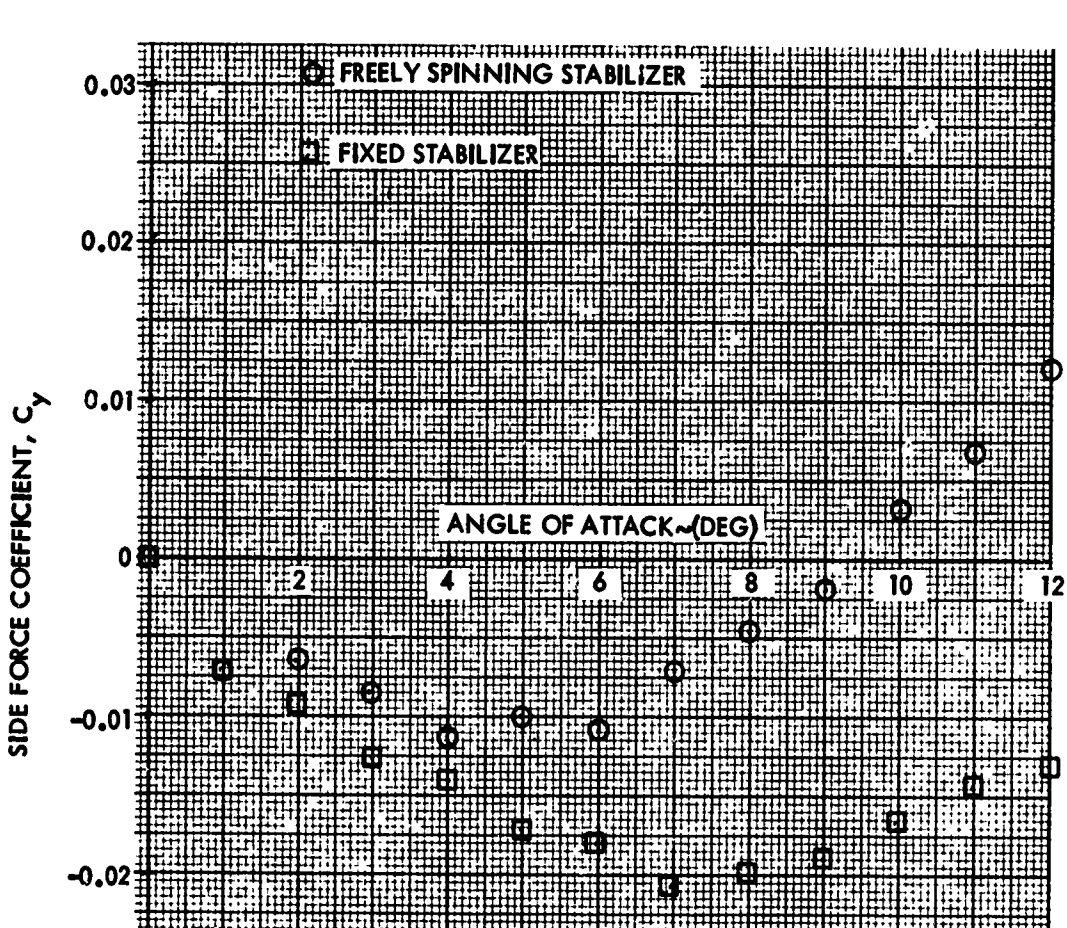

FIG. 91 SIDE FORCE COEFFICIENT VERSUS ANGLE OF ATTACK FOR THE FIXED AND FREELY SPINNING STABILIZERS AT A FIN CANT OF 4 DEGREES AND A MACH NUMBER OF 0.69

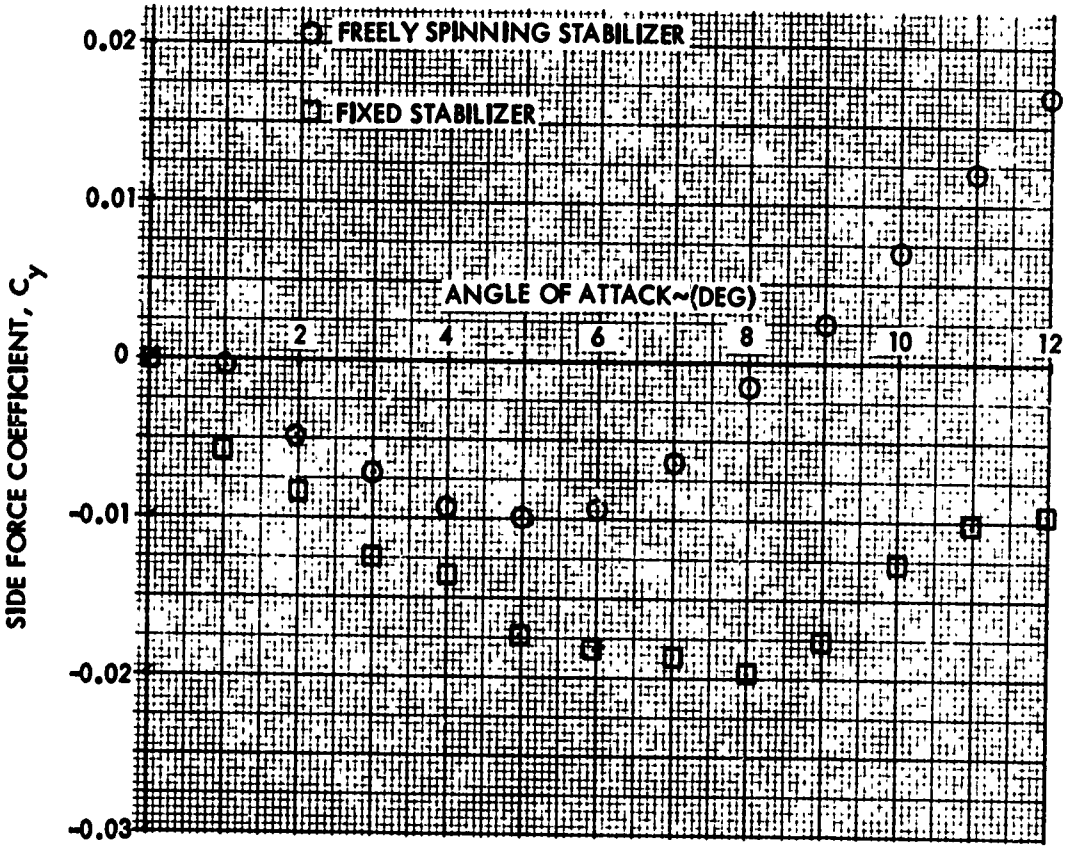

FIG. 92. SIDE FORCE COEFFICIENT VERSUS ANGLE OF ATTACK FOR THE FIXED AND FREELY SPINNING STABILIZERS AT A FIN CANT OF 4 DEGREES AND A MACH NUMBER OF 0.74.

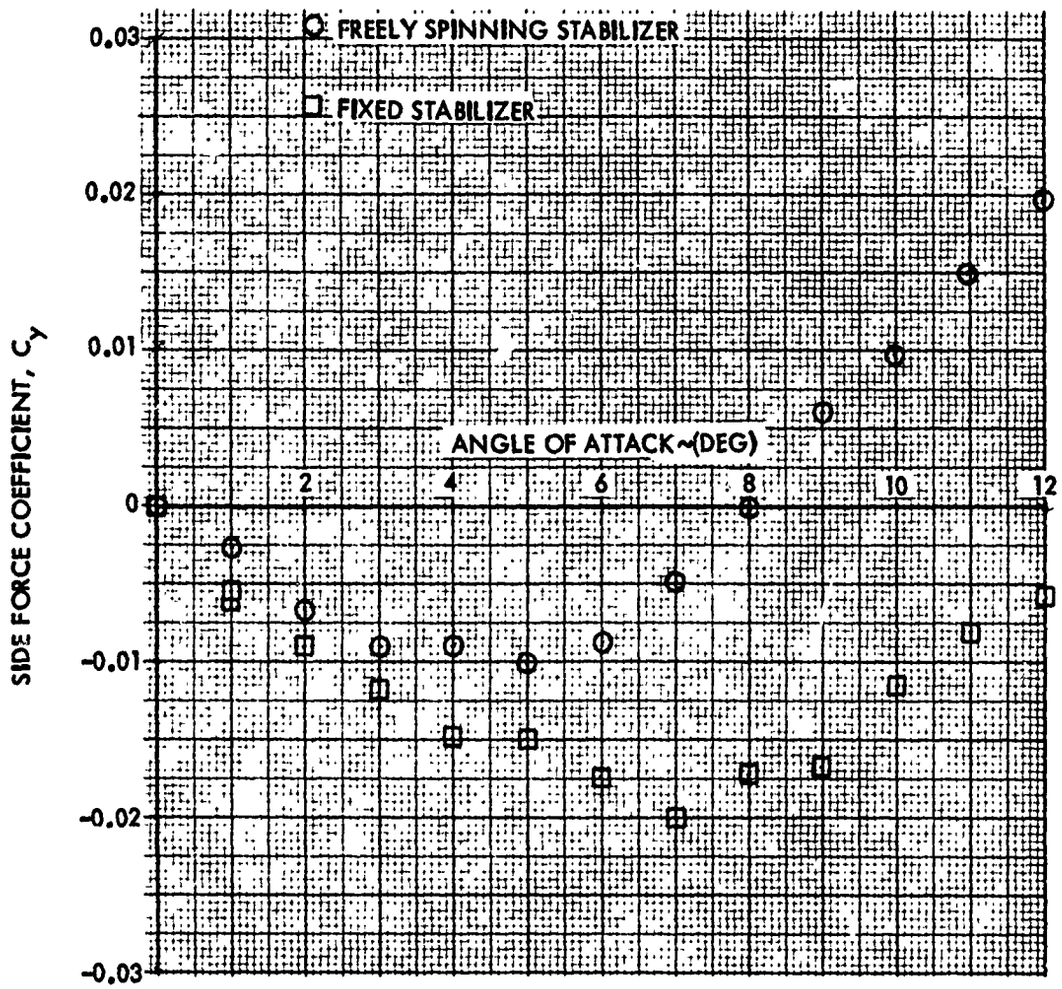

FIG. 93 SIDE FORCE COEFFICIENT VERSUS ANGLE OF ATTACK FOR THE FIXED AND FREELY SPINNING STABILIZERS AT A FIN CANT OF 4 DEGREES AND A MACH NUMBER OF 0.79

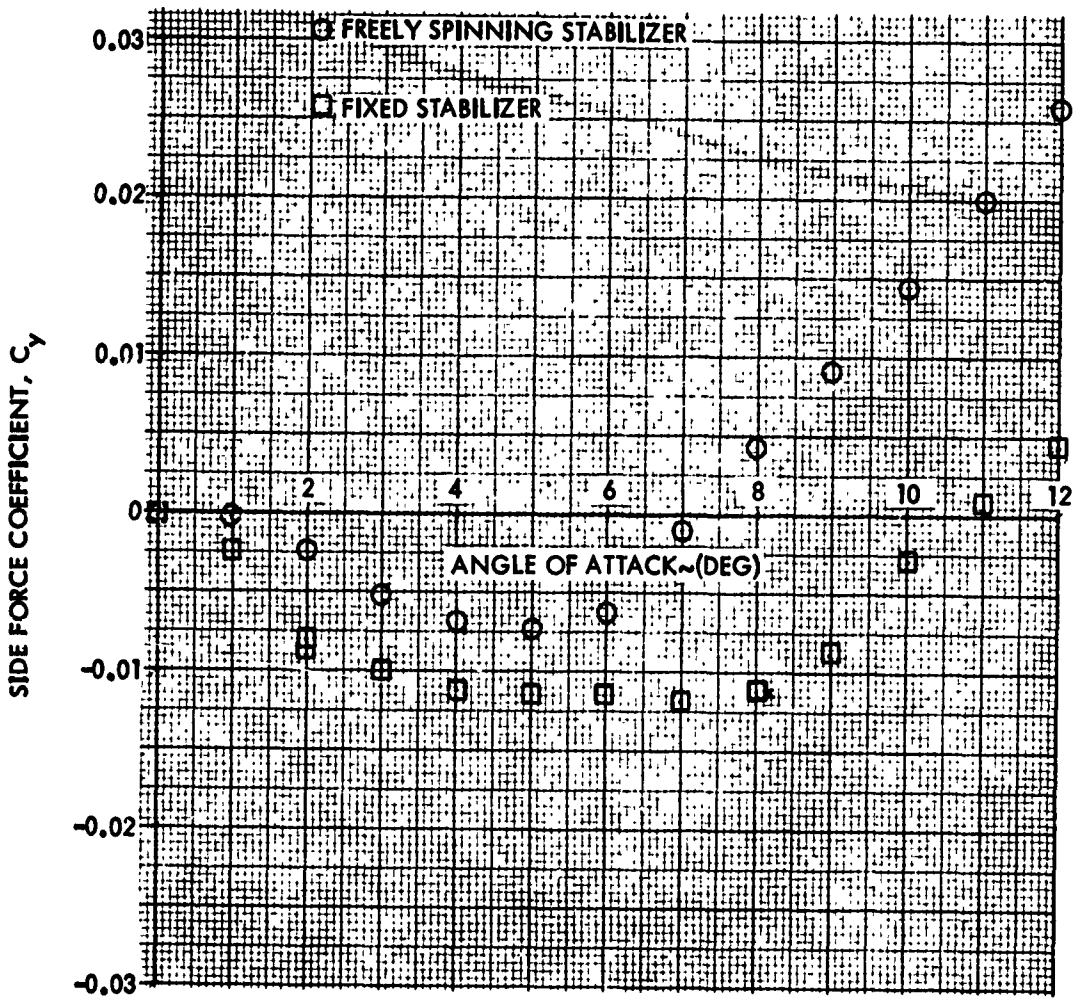

FIG. 94 SIDE FORCE COEFFICIENT VERSUS ANGLE OF ATTACK FOR THE FIXED AND FREELY SPINNING STABILIZERS AT A FIN CANT OF 4 DEGREES AND A MACH NUMBER OF 0.84

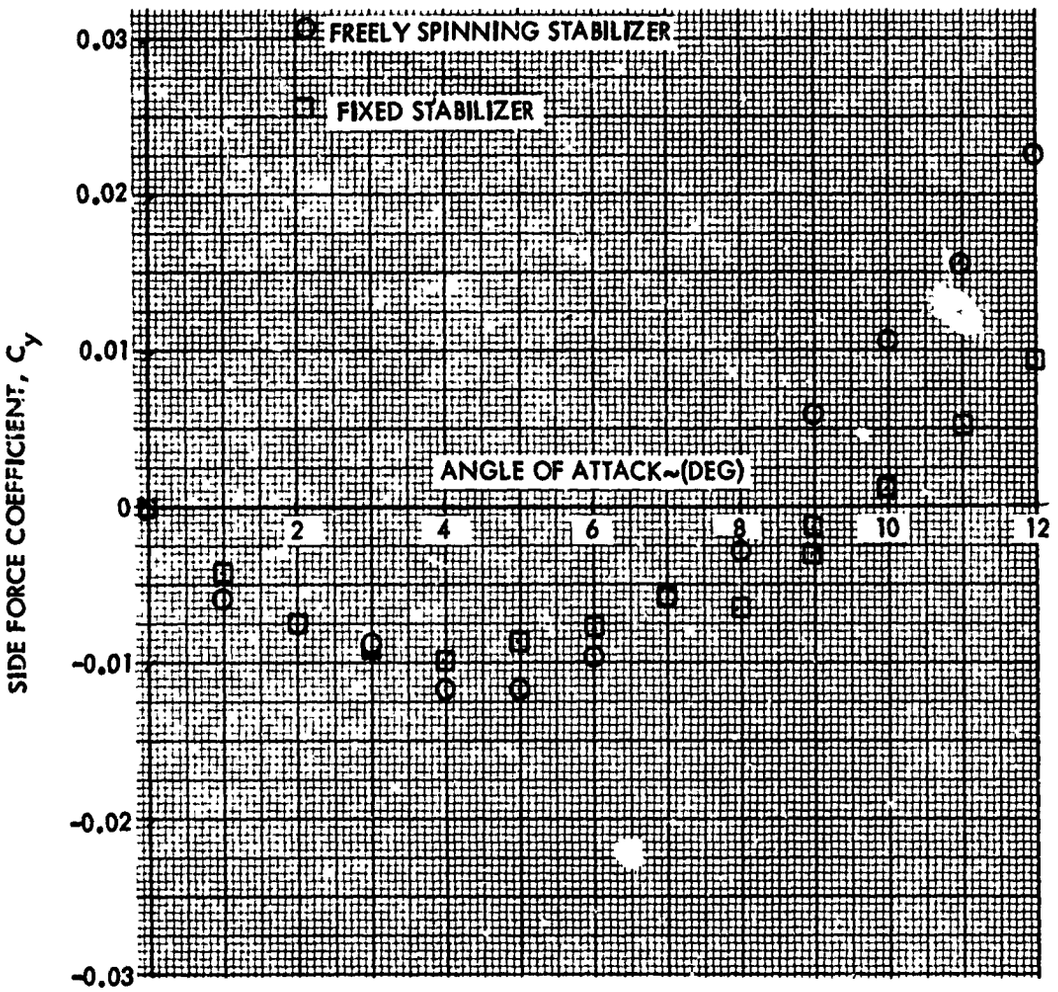

FIG. 95 SIDE FORCE COEFFICIENT VERSUS ANGLE OF ATTACK FOR THE FIXED AND FREELY SPINNING STABILIZERS AT A FIN CANT OF 4 DEGREES AND A MACH NUMBER OF 0.88

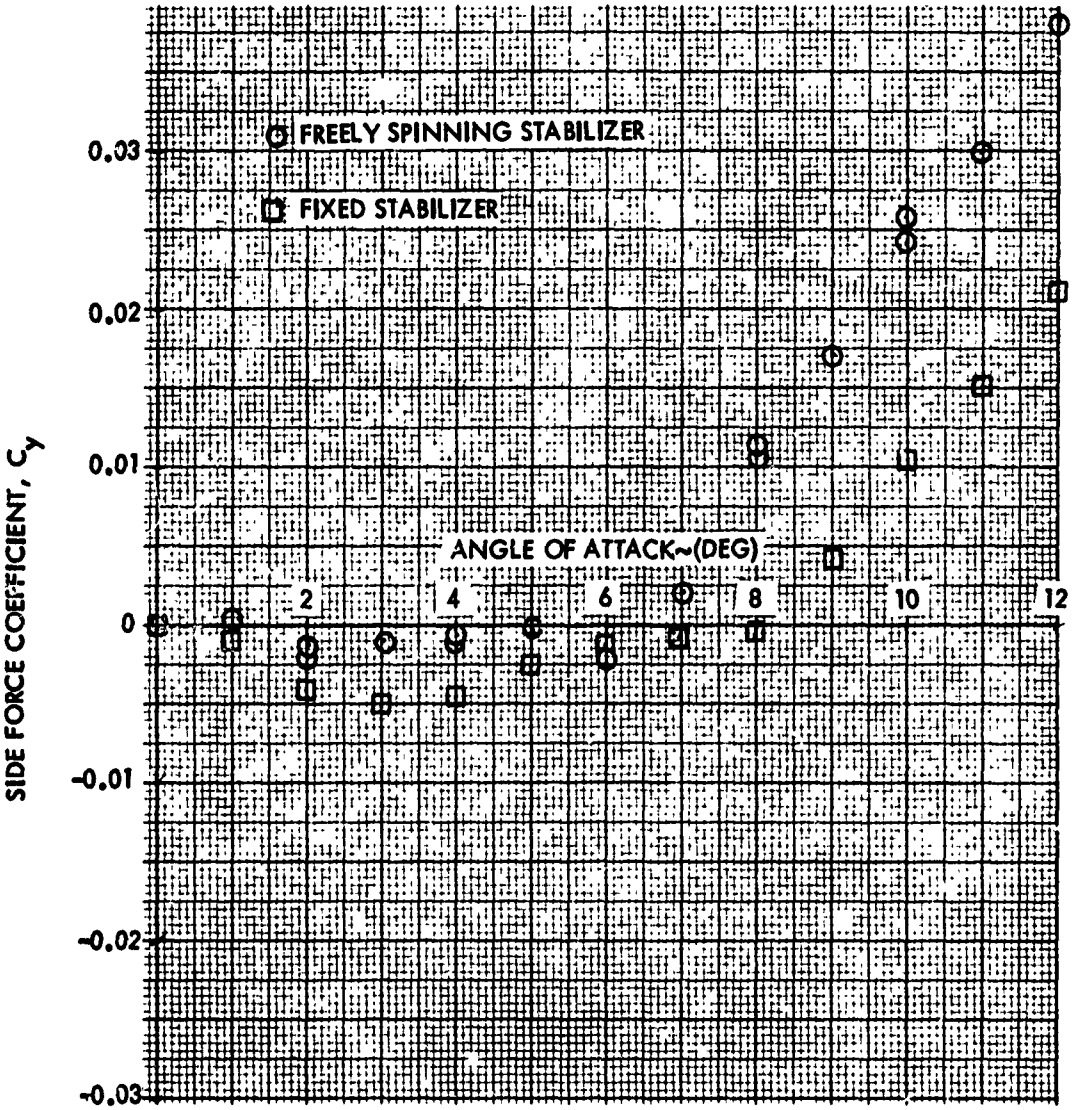

FIG. 96 SIDE FORCE COEFFICIENT VERSUS ANGLE OF ATTACK FOR THE FIXED AND FREELY SPINNING STABILIZERS AT A FIN CANT OF 4 DEGREES AND A MACH NUMBER OF 0.94

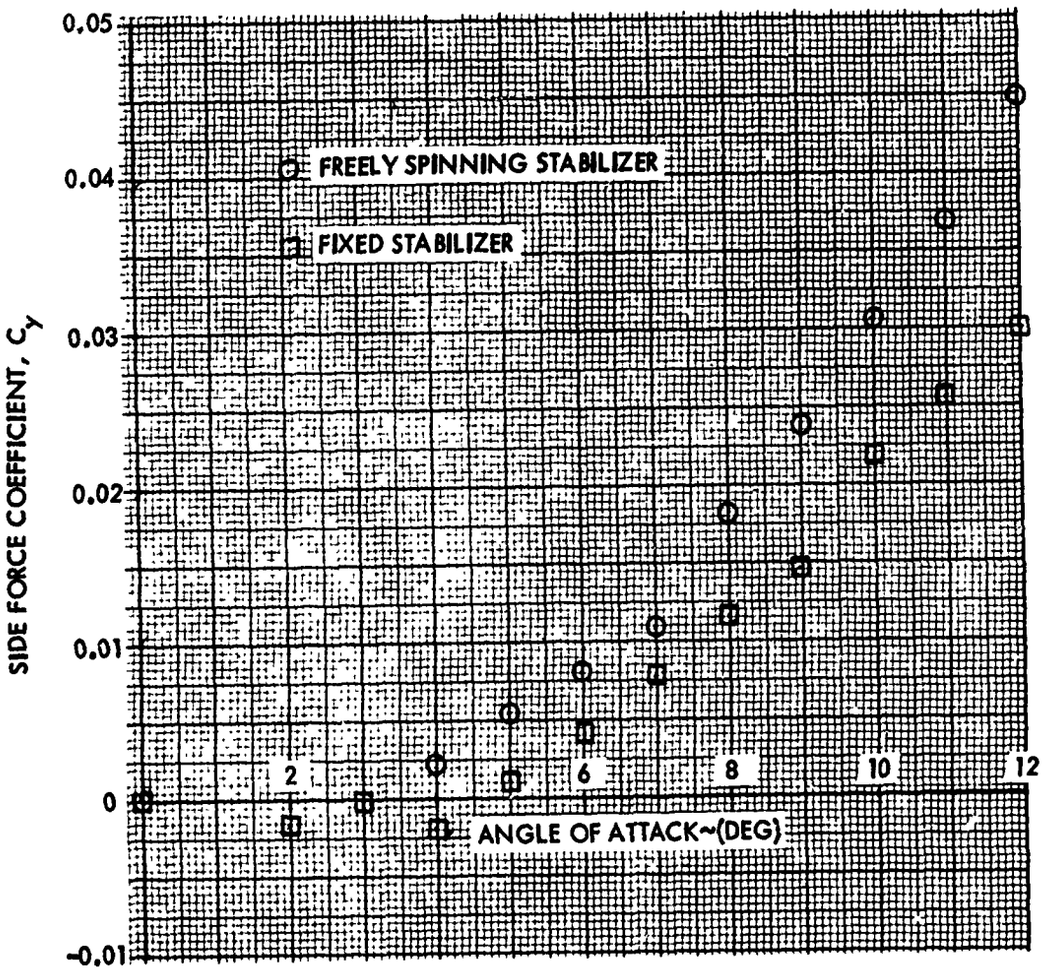

FIG. 97 SIDE FORCE COEFFICIENT VERSUS ANGLE OF ATTACK FOR THE FIXED AND FREELY SPINNING STABILIZERS AT A FIN CANT OF 4 DEGREES AND A MACH NUMBER OF 1.11

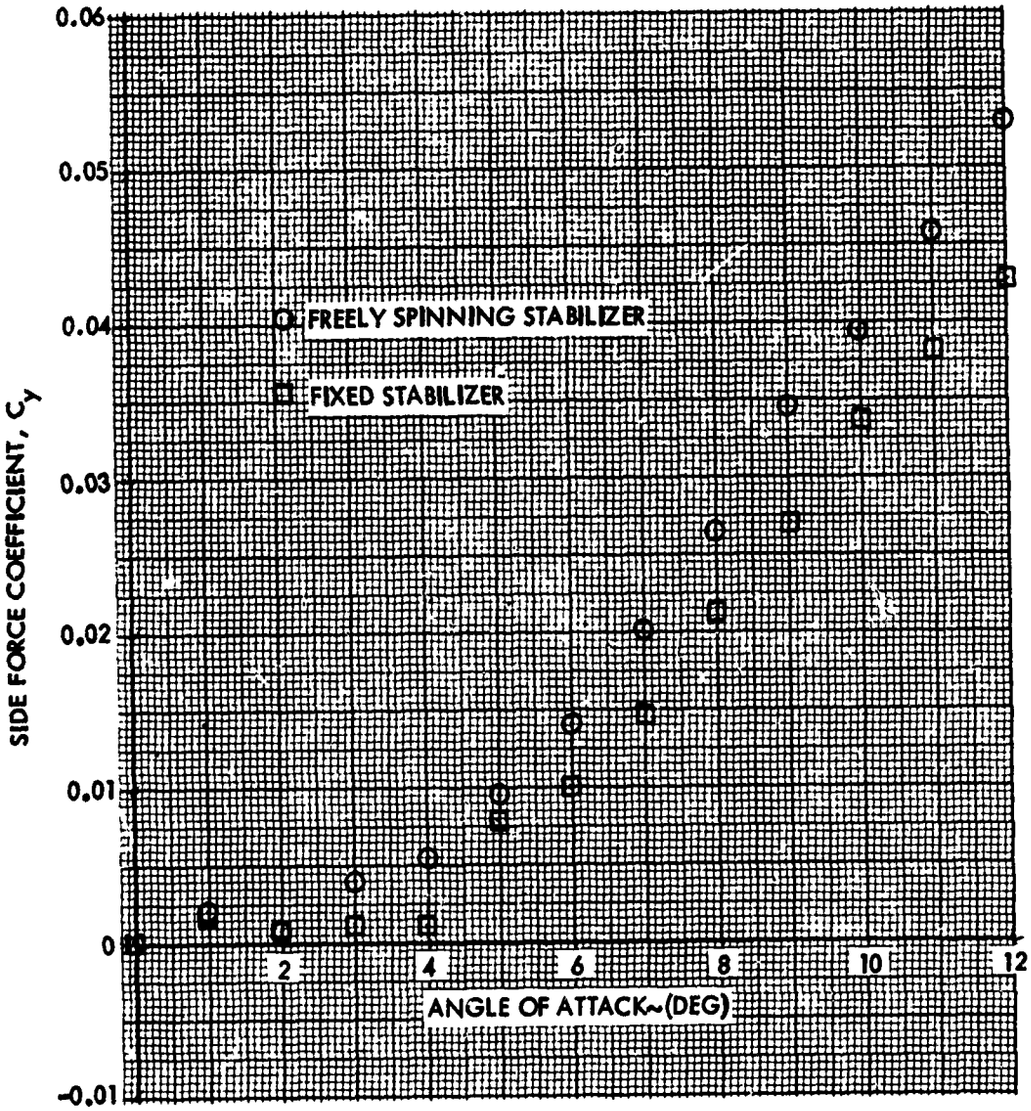

FIG. 98 SIDE FORCE COEFFICIENT VERSUS ANGLE OF ATTACK FOR THE FIXED AND FREELY SPINNING STABILIZERS AT A FIN CANT OF 4 DEGREES AND A MACH NUMBER OF 1.20

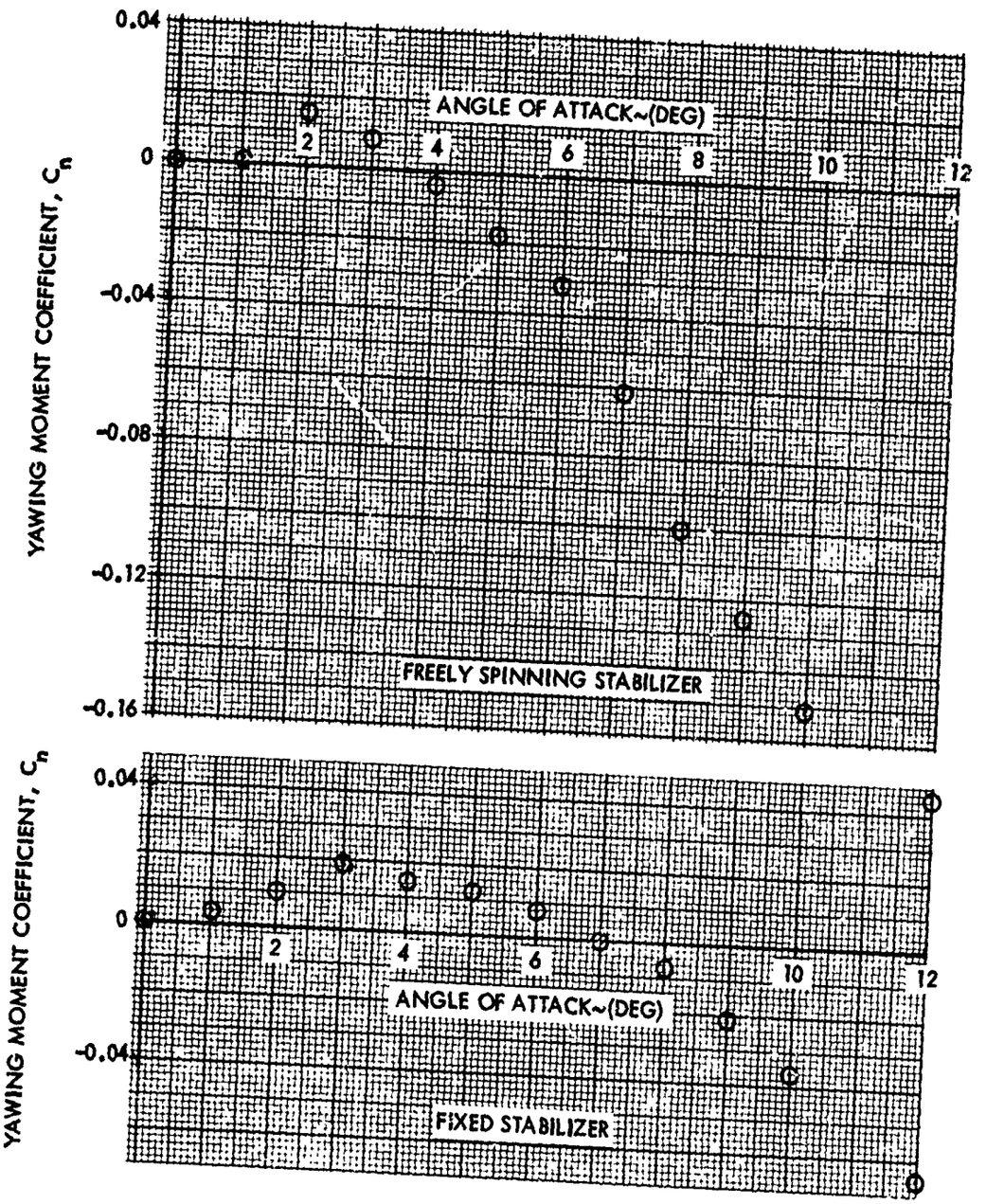

FIG. 99. YAWING MOMENT COEFFICIENT VERSUS ANGLE OF ATTACK FOR THE FIXED AND FREELY SPINNING STABILIZERS AT A FIN CANT OF 4 DEGREES AND A MACH NUMBER OF 0.60.

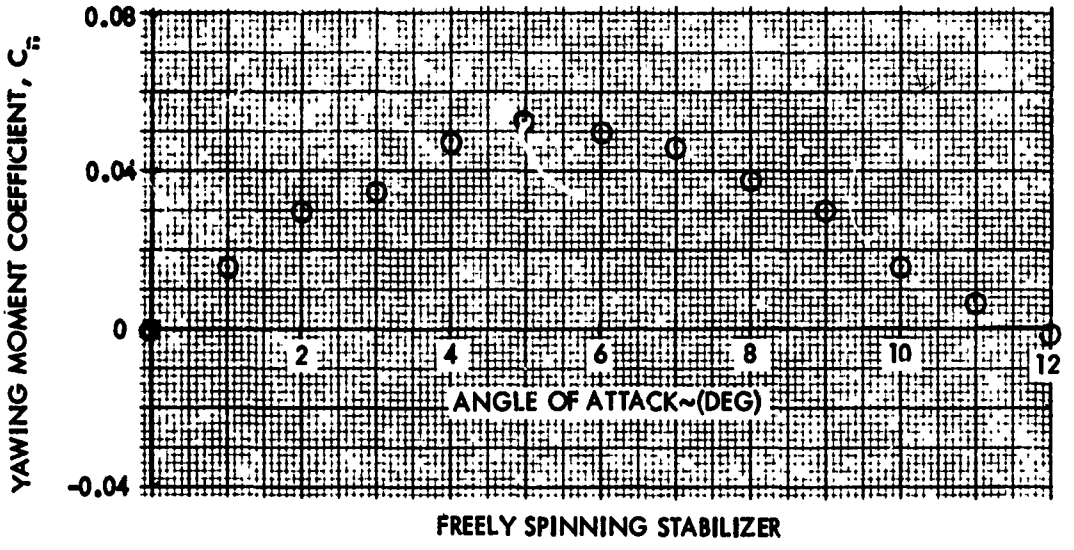

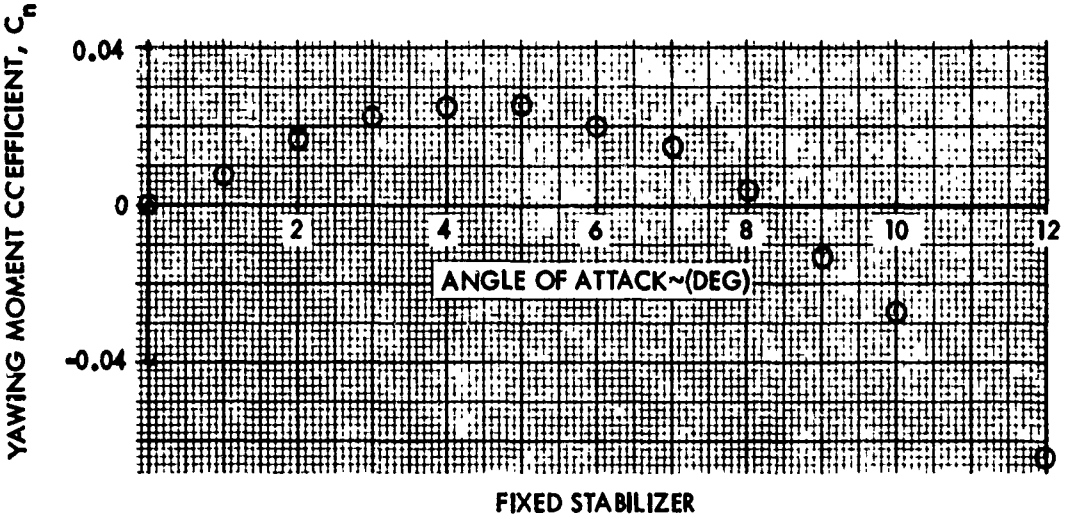

FIG. 100 YAWING MOMENT COEFFICIENT VERSUS ANGLE OF ATTACK FOR THE FIXED AND FREELY SPINNING STABILIZERS AT A FIN CANT OF 4 DEGREES AND A MACH NUMBER OF 0.69

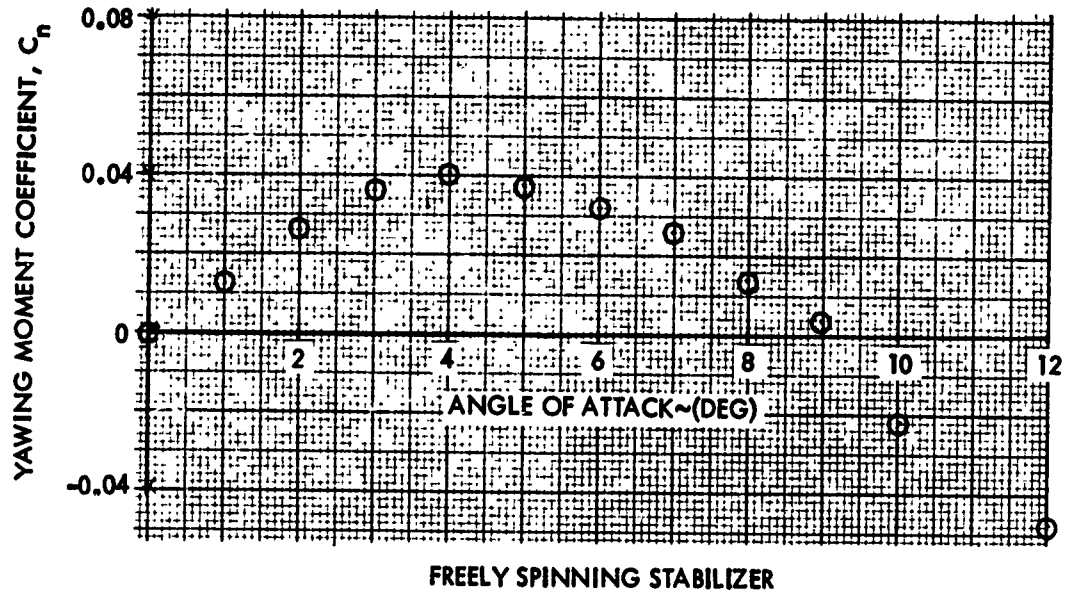

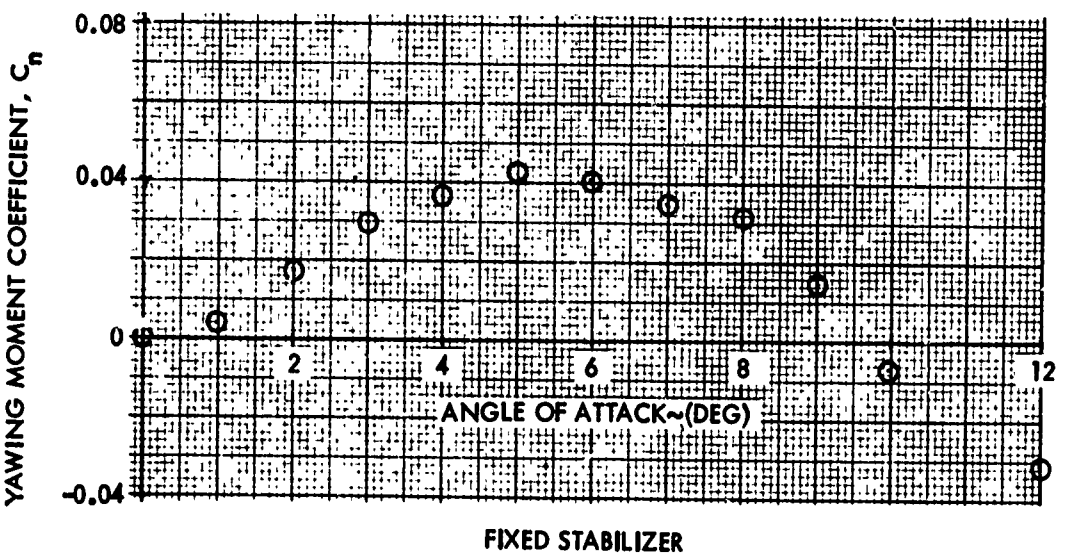

FIG. 101 YAWING MOMENT COEFFICIENT VERSUS ANGLE OF ATTACK FOR THE FIXED AND FREELY SPINNING STABILIZERS AT A FIN CANT OF 4 DEGREES AND A MACH NUMBER OF 0.74

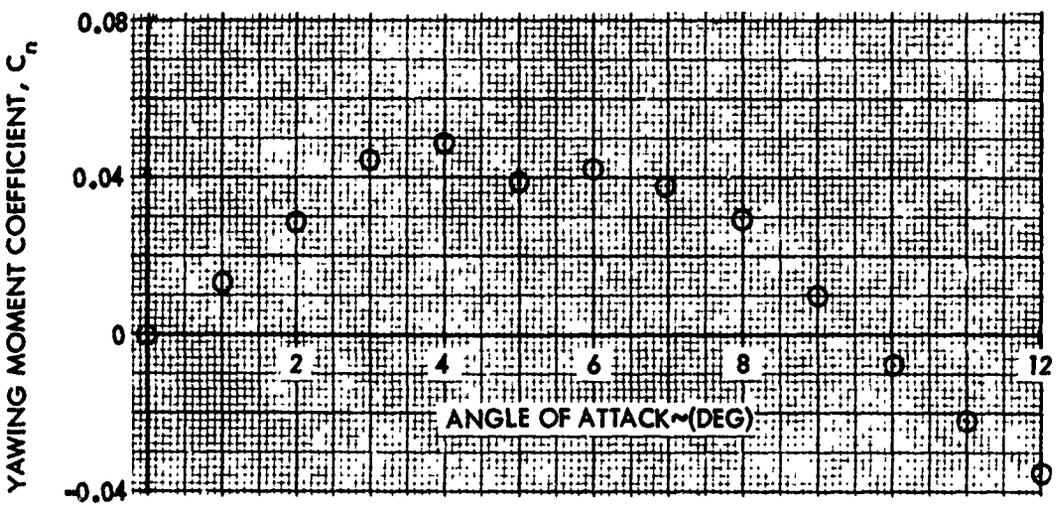

FREELY SPINNING STABILIZER

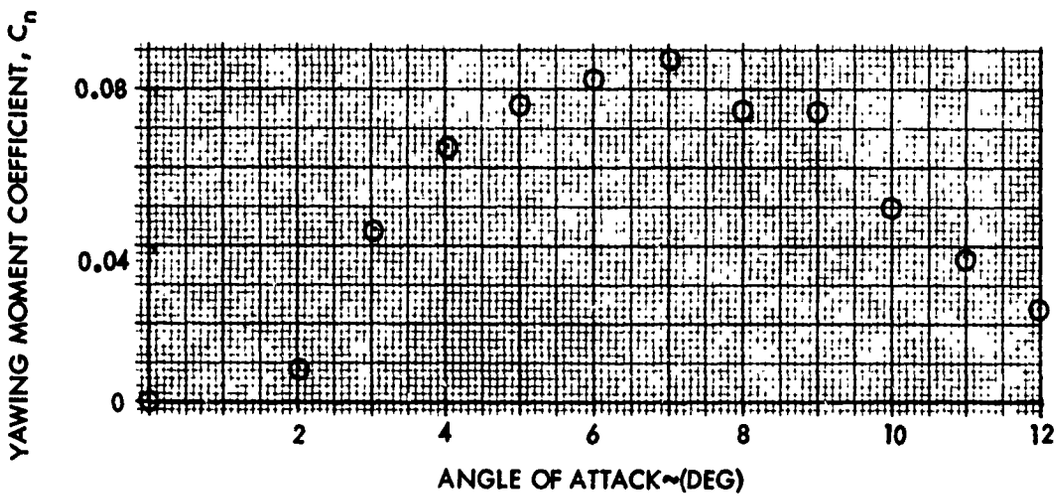

FIXED STABILIZER

FIG. 102 YAWING MOMENT COEFFICIENT VERSUS ANGLE OF ATTACK FOR THE FIXED AND FREELY SPINNING STABILIZERS AT A FIN CANT OF 4 DEGREES AND A MACH NUMBER OF 0.78

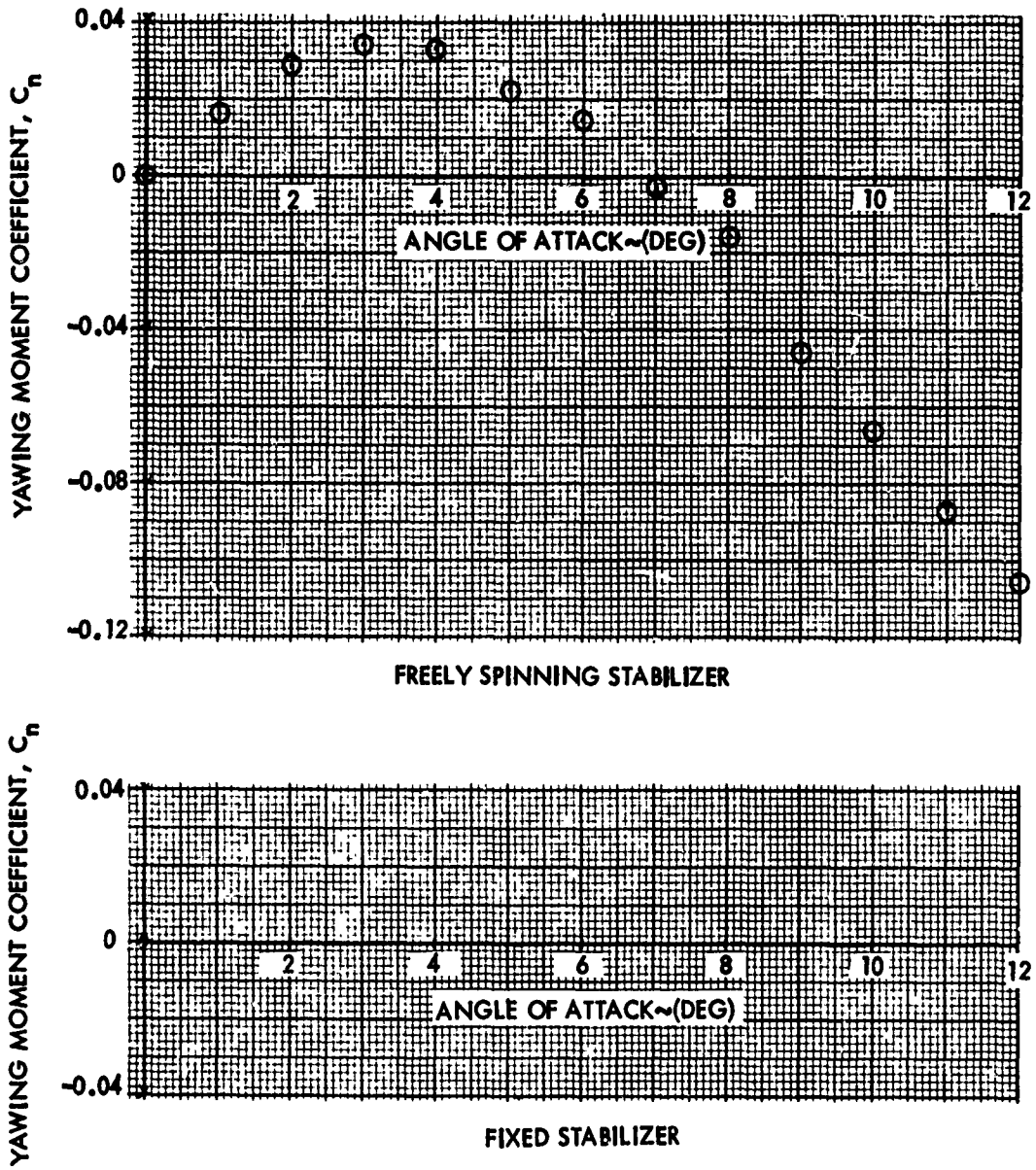

FIG. 103 YAWING MOMENT COEFFICIENT VERSUS ANGLE OF ATTACK FOR THE FIXED AND FREELY SPINNING STABILIZERS AT A FIN CANT OF 4 DEGREES AND A MACH NUMBER OF 0.84

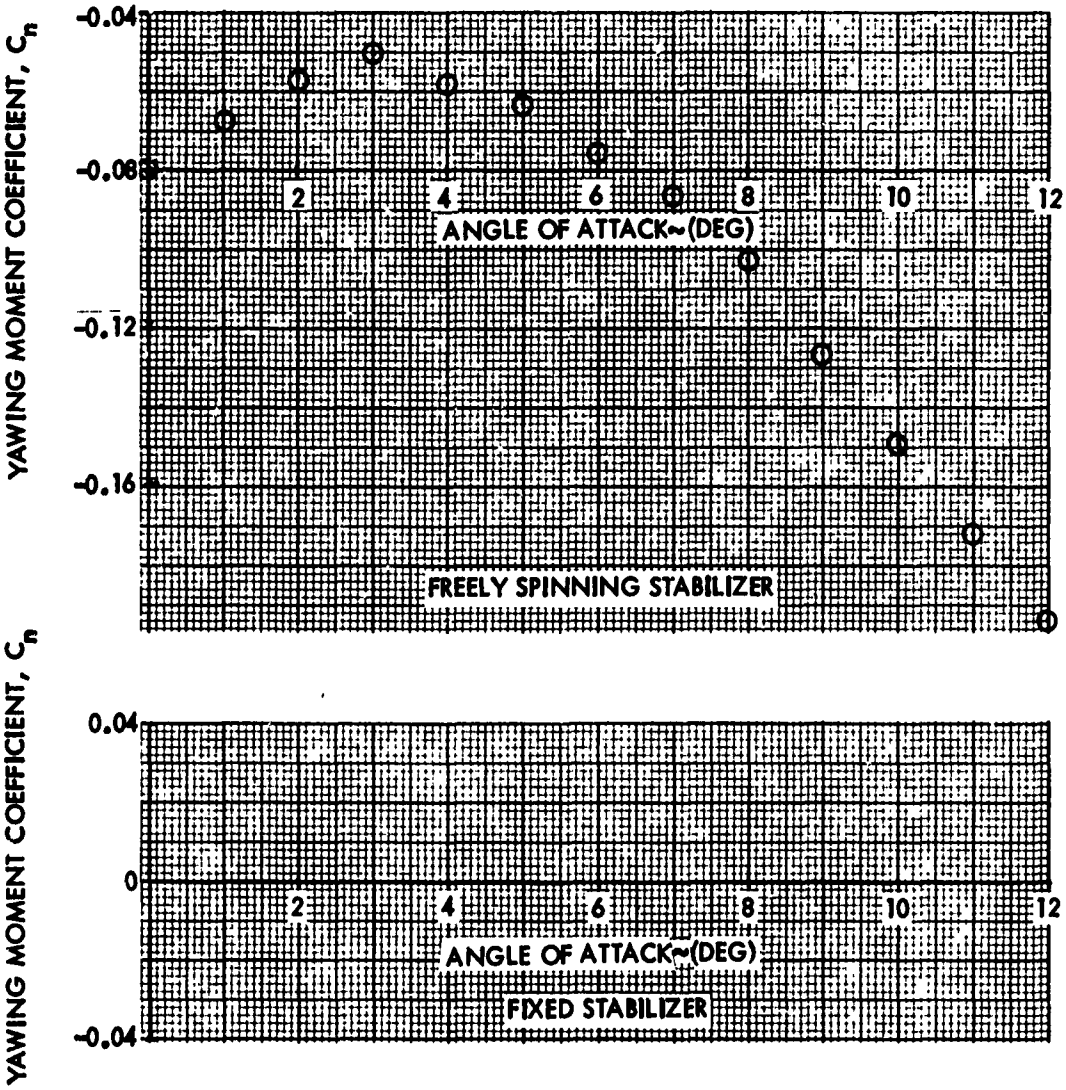

FIG. 104. YAWING MOMENT COEFFICIENT VERSUS ANGLE OF ATTACK FOR THE FIXED AND FREELY SPINNING STABILIZERS AT A FIN CANT OF 4 DEGREES AND A MACH NUMBER OF 0.89.

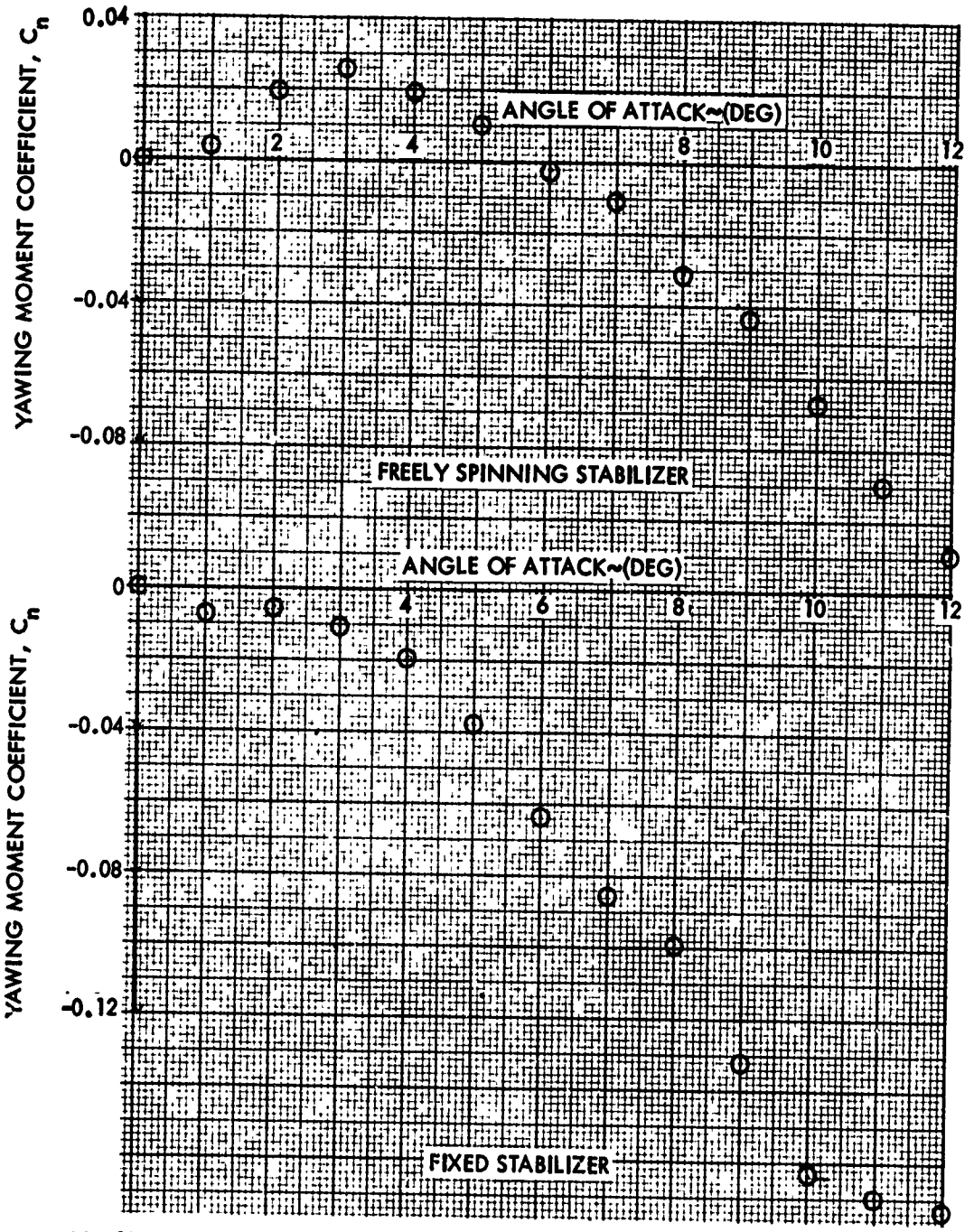

FIG. 105. YAWING MOMENT COEFFICIENT VERSUS ANGLE OF ATTACK FOR THE FIXED AND FREELY SPINNING STABILIZERS AT A FIN CANT OF 4 DEGREES AND A MACH NUMBER OF 0.94.

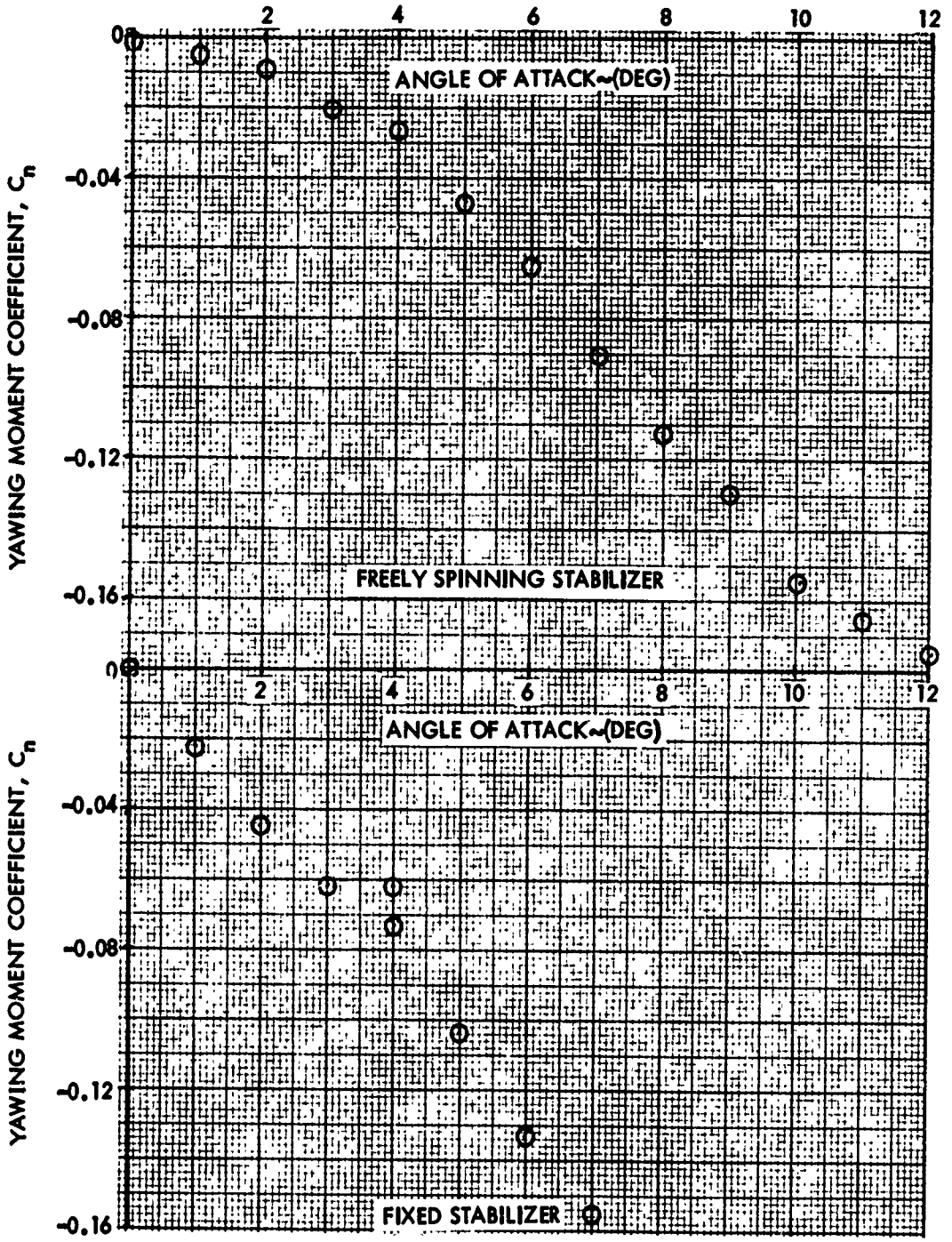

FIG. 106. YAWING MOMENT COEFFICIENT VERSUS ANGLE OF ATTACK FOR THE FIXED AND FREELY SPINNING STABILIZERS AT A FIN CANT OF 4 DEGREES AND A MACH NUMBER OF 1.2.

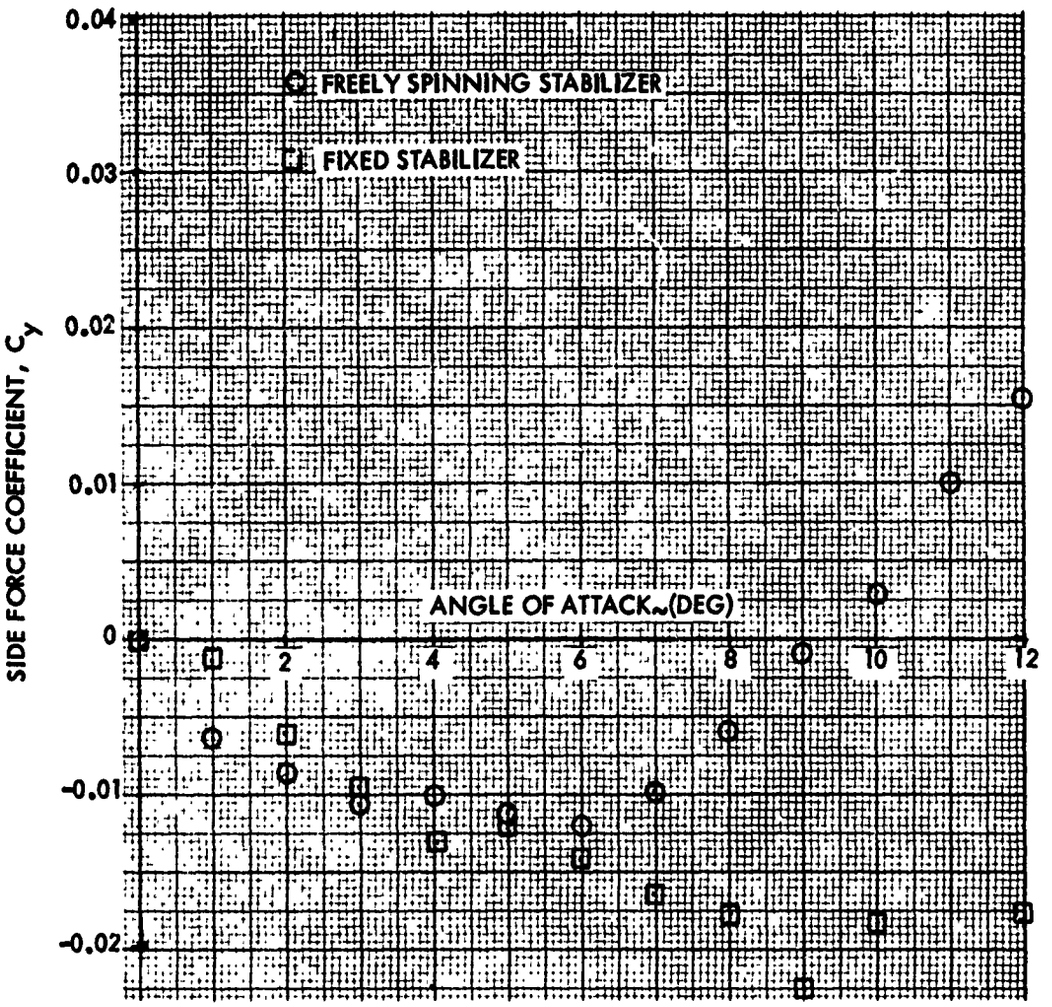

FIG. 107 SIDE FORCE COEFFICIENT VERSUS ANGLE OF ATTACK FOR THE FIXED AND FREELY SPINNING STABILIZERS AT A FIN CANT OF 5 DEGREES AND A MACH NUMBER OF 0.60

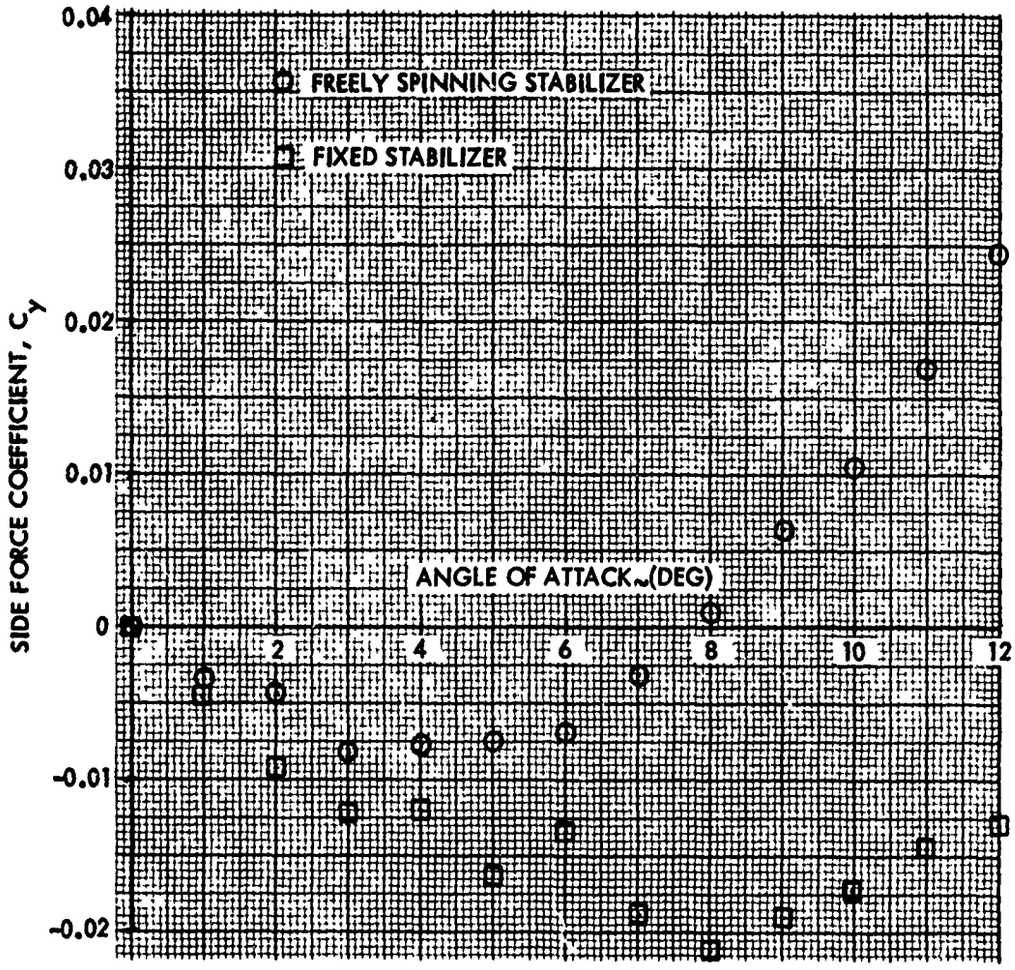

FIG. 108. SIDE FORCE COEFFICIENT VERSUS ANGLE OF ATTACK FOR THE FIXED AND FREELY SPINNING STABILIZERS AT A FIN CANT OF 5 DEGREES AND A MACH NUMBER OF 0.69.

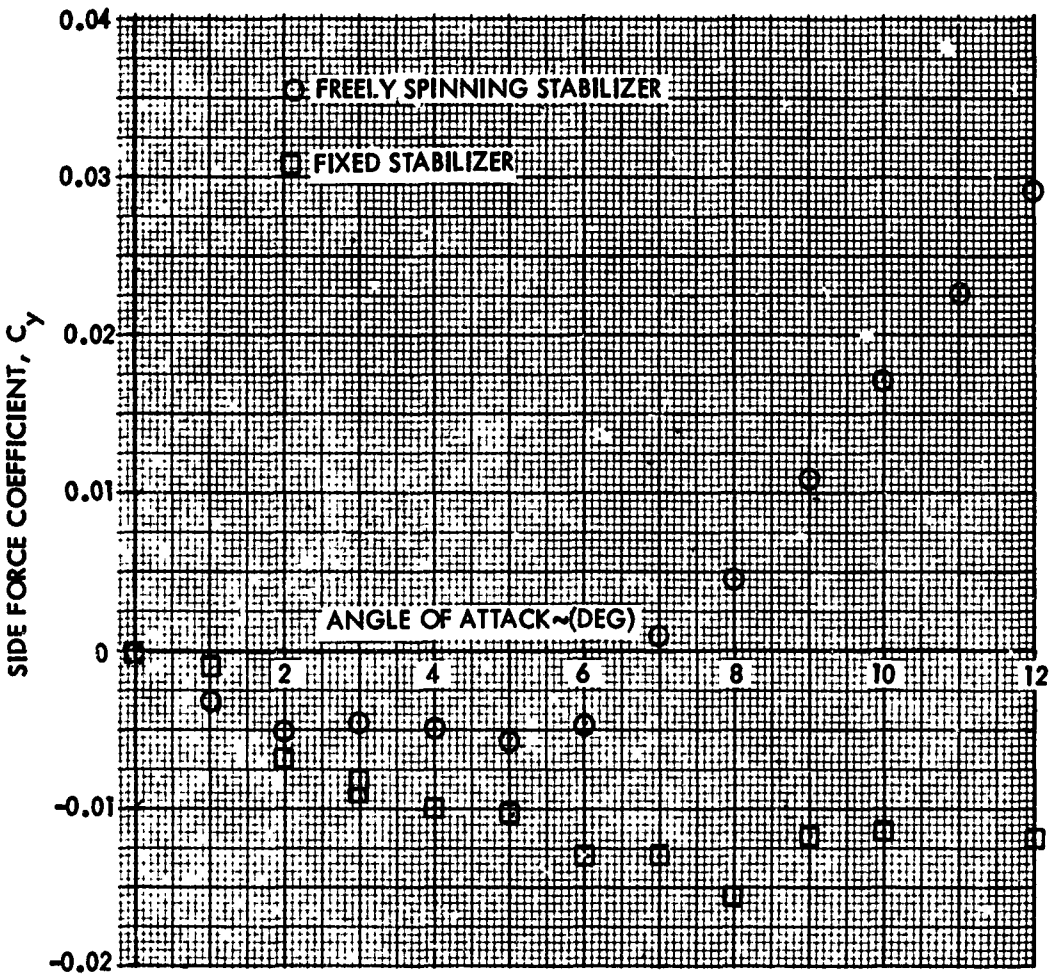

FIG. 109 SIDE FORCE COEFFICIENT VERSUS ANGLE OF ATTACK FOR THE FIXED AND FREELY SPINNING STABILIZERS AT A FIN CANT OF 5 DEGREES AND A MACH NUMBER OF 0.74

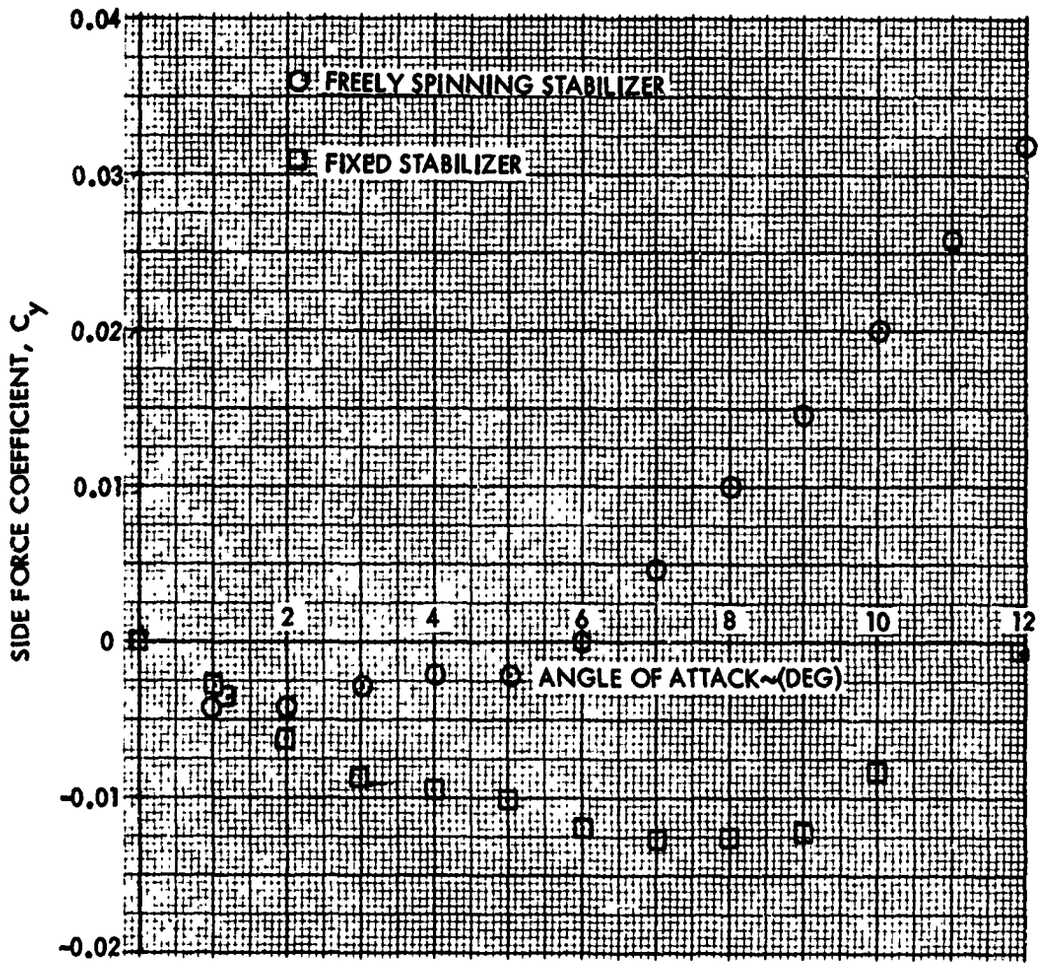

FIG. 110 · SIDE FORCE COEFFICIENT VERSUS ANGLE OF ATTACK FOR THE FIXED AND FREELY SPINNING STABILIZERS AT A FIN CANT OF 5 DEGREES AND A MACH NUMBER OF 0.79

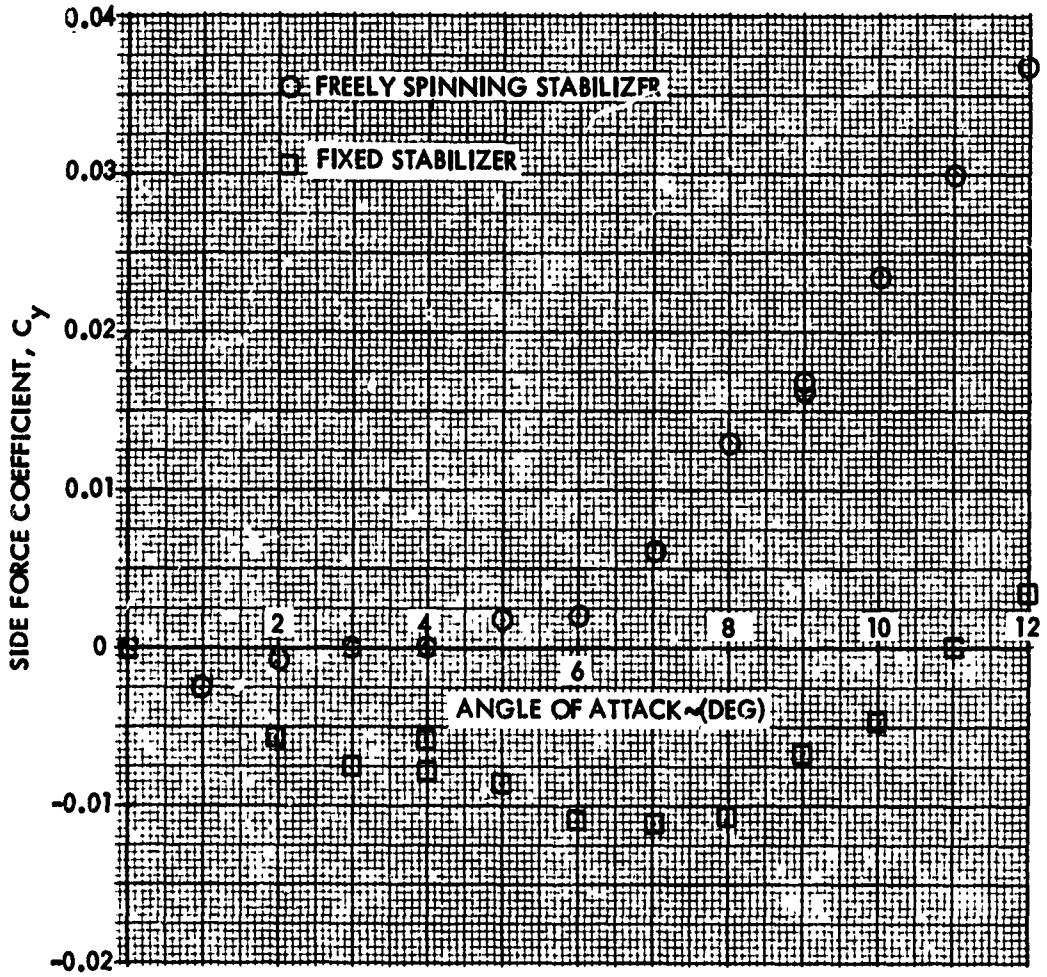

FIG. 111 SIDE FORCE COEFFICIENT VERSUS ANGLE OF ATTACK FOR THE FIXED AND FREELY SPINNING STABILIZERS AT A FIN CANT OF 5 DEGREES AND A MACH NUMBER OF 0.84

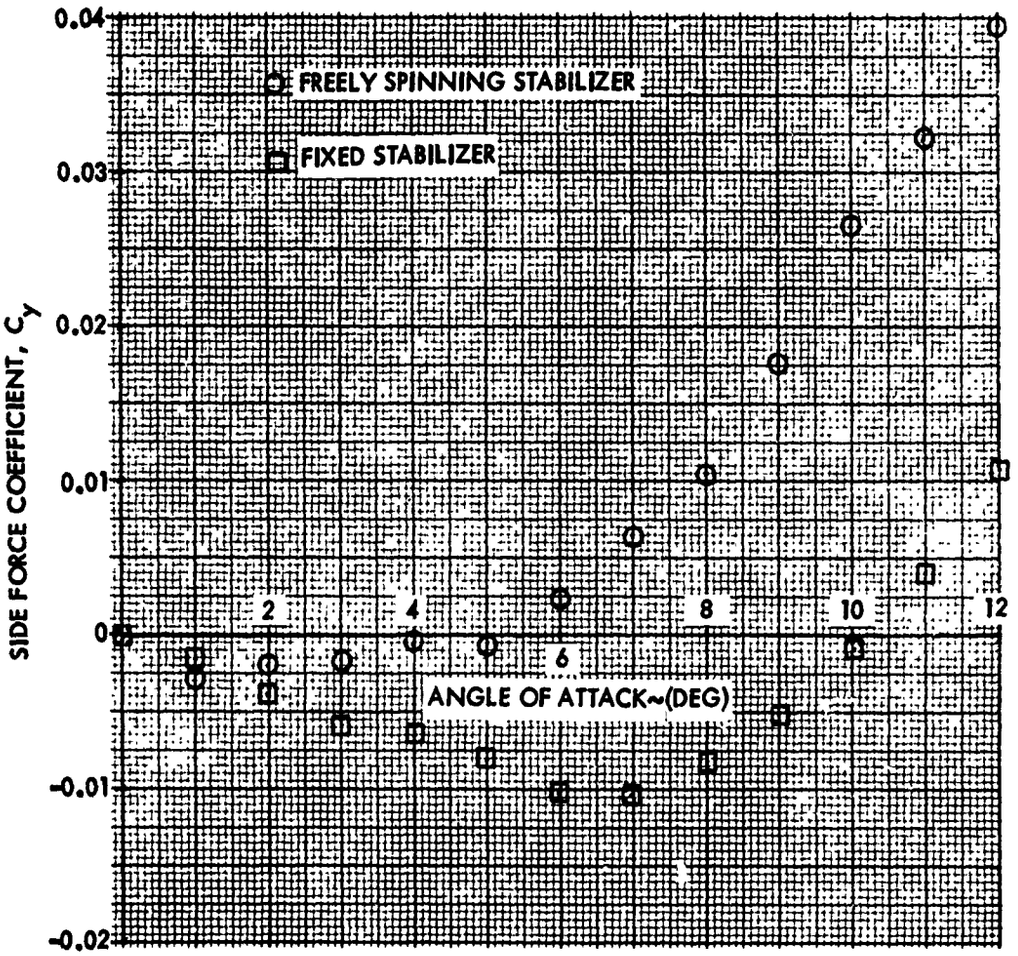

FIG. 112 SIDE FORCE COEFFICIENT VERSUS ANGLE OF ATTACK FOR THE FIXED AND FREELY SPINNING STABILIZERS AT A FIN CANT OF 5 DEGREES AND A MACH NUMBER OF 0.89

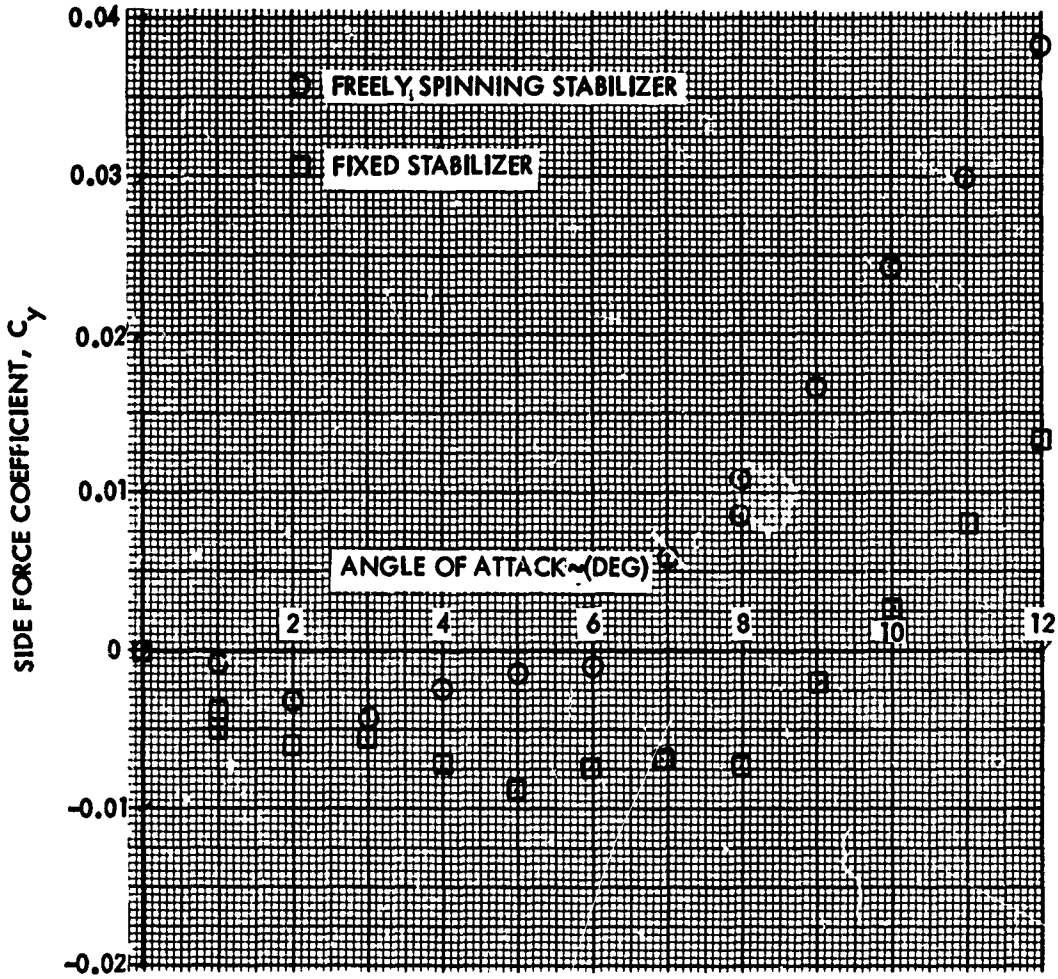

FIG. 113. SIDE FORCE COEFFICIENT VERSUS ANGLE OF ATTACK FOR THE FIXED AND FREELY SPINNING STABILIZERS AT A FIN CANT OF 5 DEGREES AND A MACH NUMBER OF 0.94.

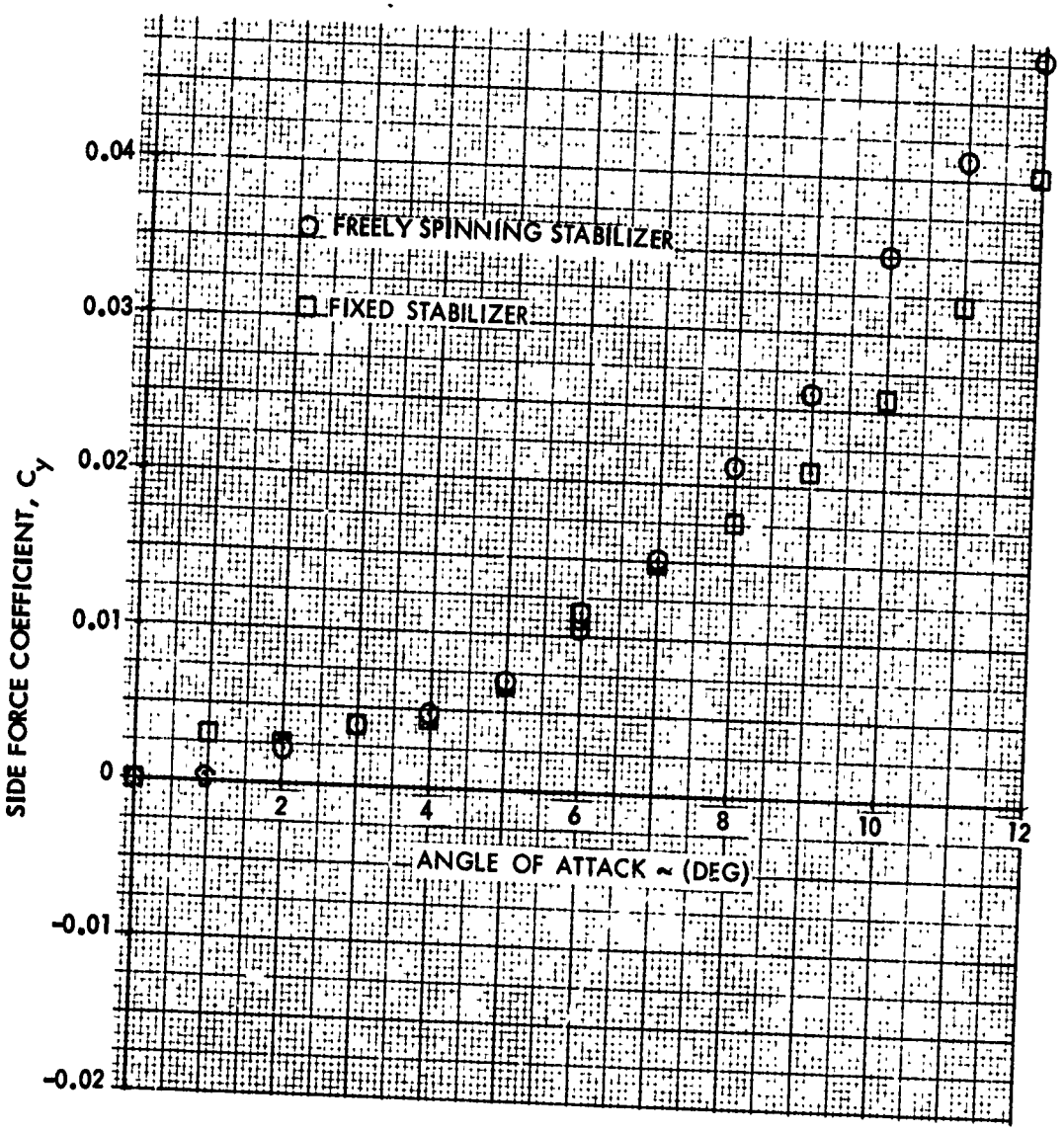

FIG. 114 SIDE FORCE COEFFICIENT VERSUS ANGLE OF ATTACK FOR THE FIXED AND FREELY SPINNING STABILIZERS AT A FIN CANT OF 5 DEGREES AND A MACH NUMBER OF 1.11

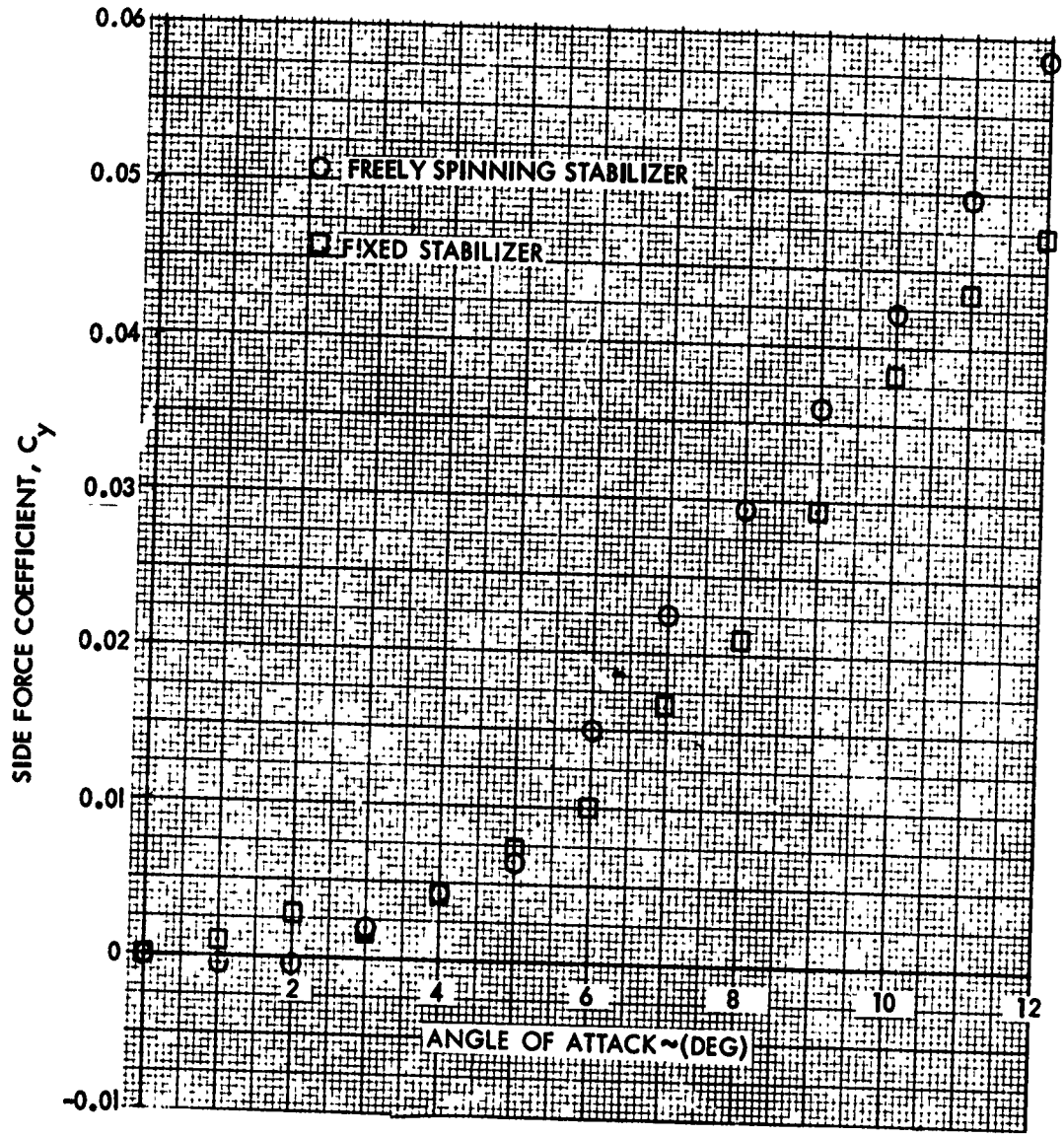

FIG. 115 SIDE FORCE COEFFICIENT VERSUS ANGLE OF ATTACK FOR THE FIXED AND FREELY SPINNING STABILIZERS AT A FIN CANT OF 5 DEGREES AND A MACH NUMBER OF 1.20

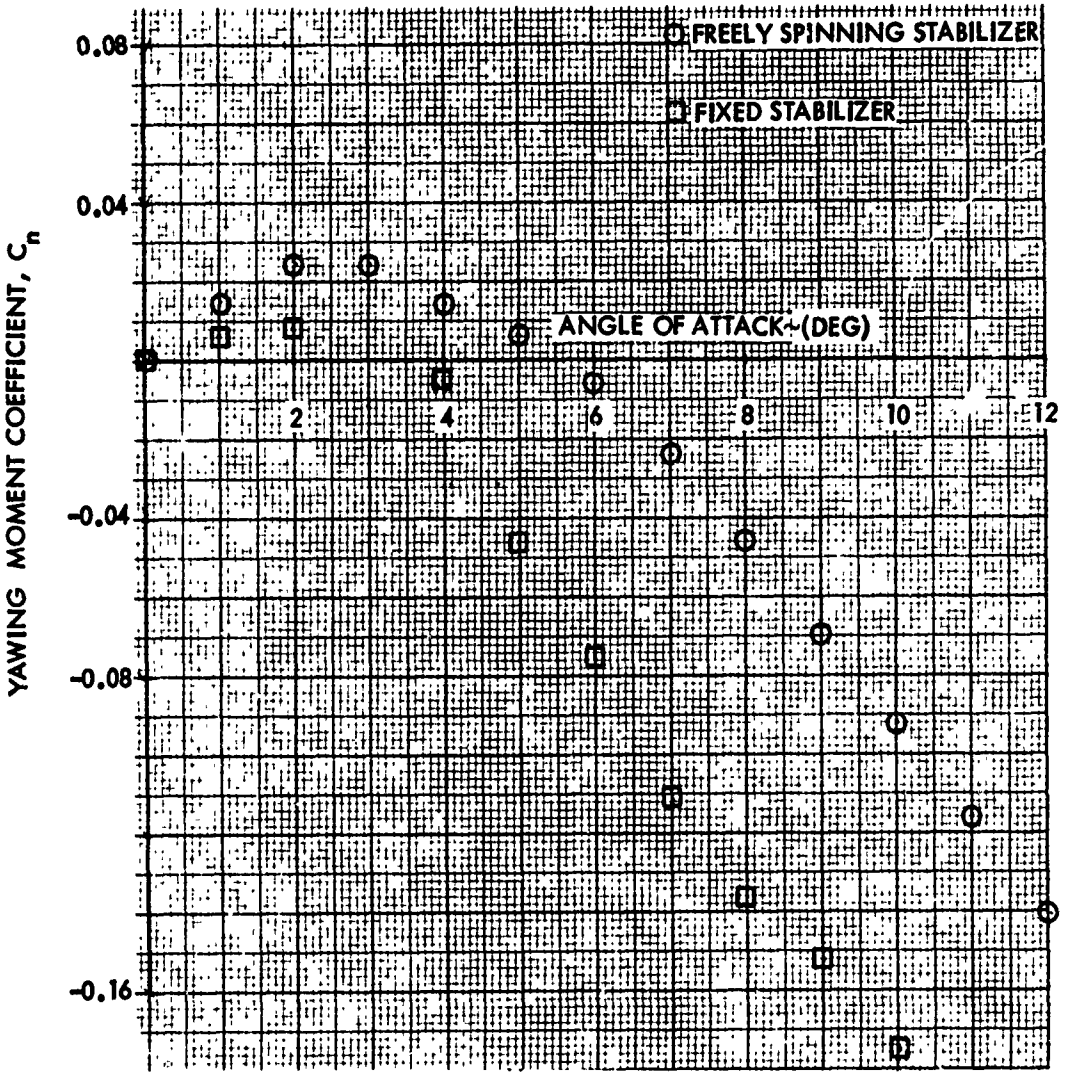

FIG. 116 YAWING MOMENT COEFFICIENT VERSUS ANGLE OF ATTACK FOR THE FIXED AND FREELY SPINNING STABILIZERS AT A FIN CANT OF 5 DEGREES AND A MACH NUMBER 0.59

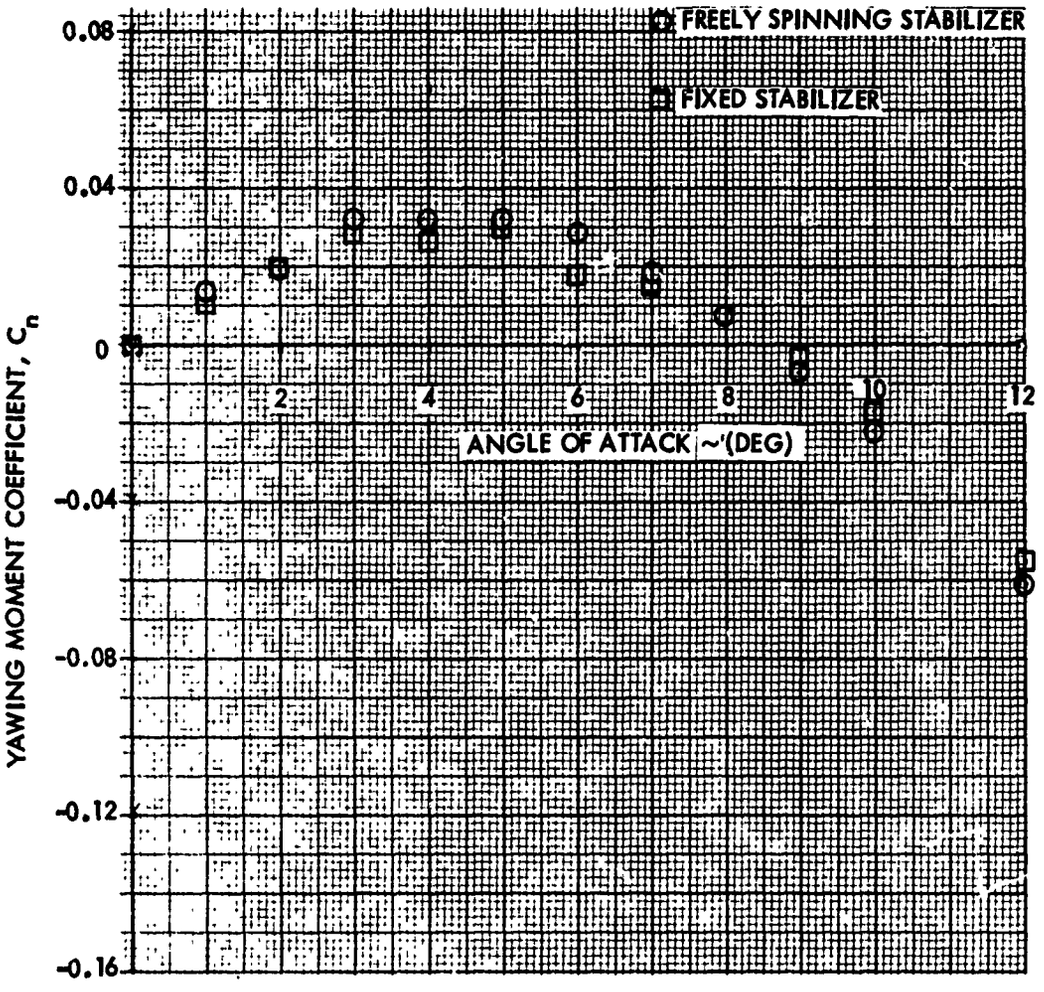

FIG. 117 YAWING MOMENT COEFFICIENT VERSUS ANGLE OF ATTACK FOR THE FIXED AND FREELY SPINNING STABILIZERS AT A FIN CANT OF 5 DEGREES AND A MACH NUMBER 0.69

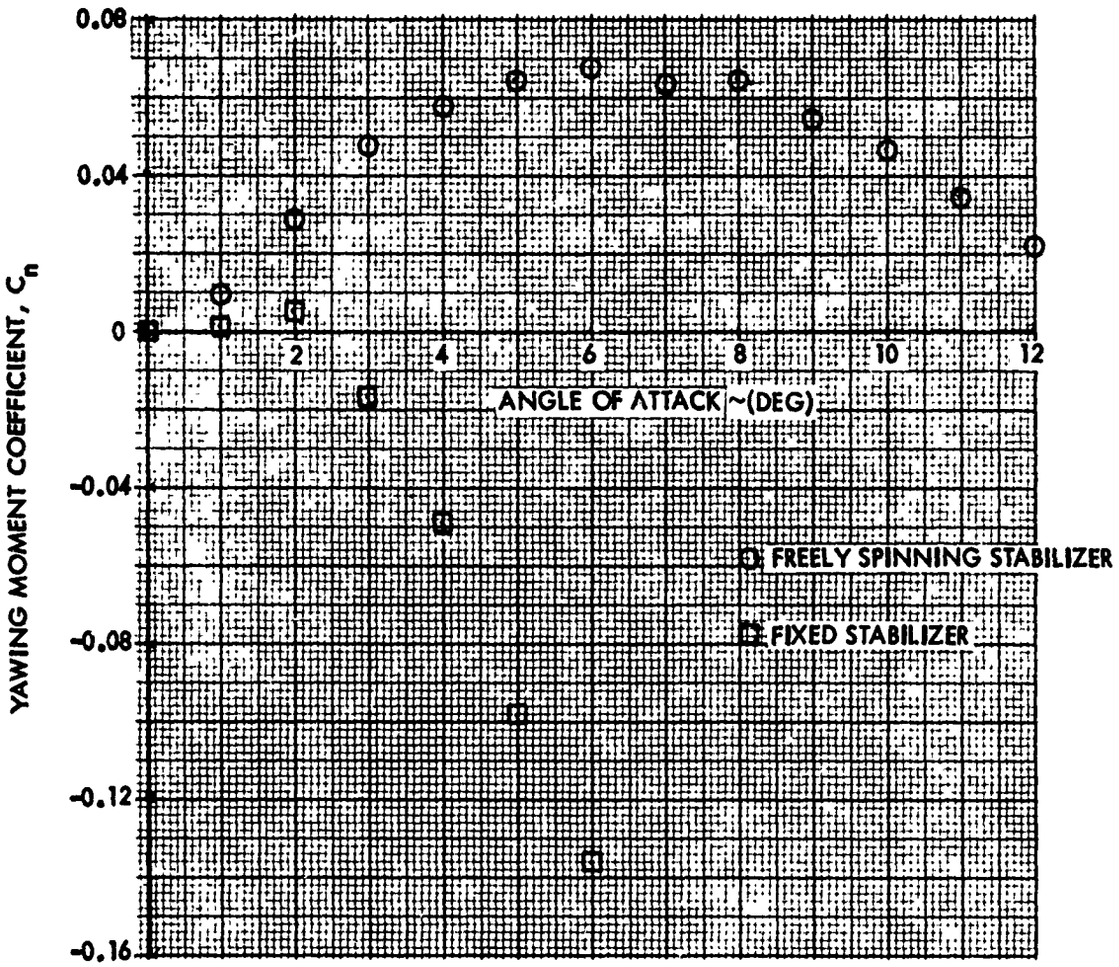

FIG. 118 YAWING MOMENT COEFFICIENT VERSUS ANGLE OF ATTACK FOR THE FIXED AND FREELY SPINNING STABILIZERS AT A FIN CANT OF 5 DEGREES AND A MACH NUMBER 0.74

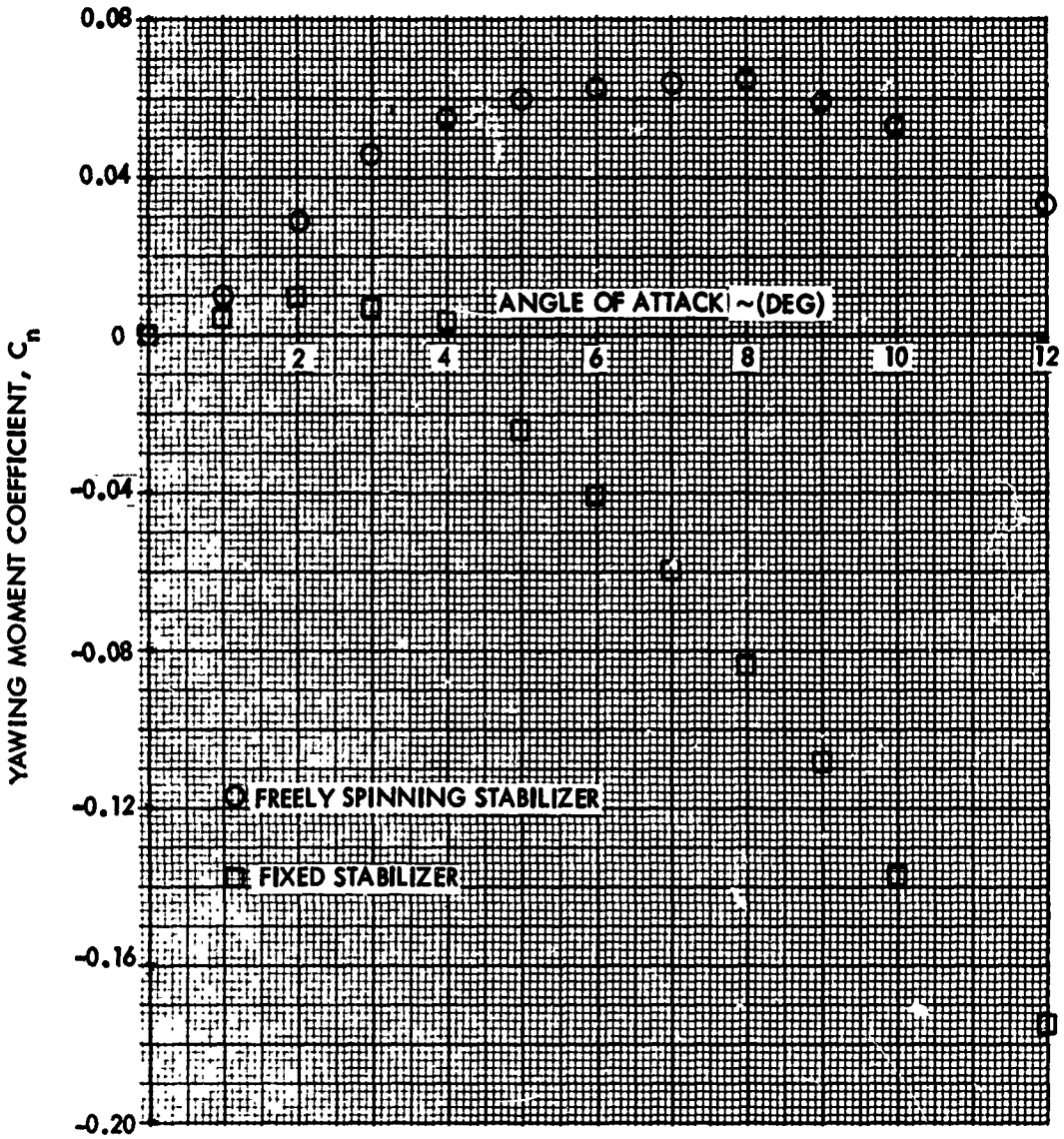

FIG. 119 YAWING MOMENT COEFFICIENT VERSUS ANGLE OF ATTACK FOR THE FIXED AND FREELY SPINNING STABILIZERS AT A FIN CANT OF 5 DEGREES AND A MACH NUMBER 0.79

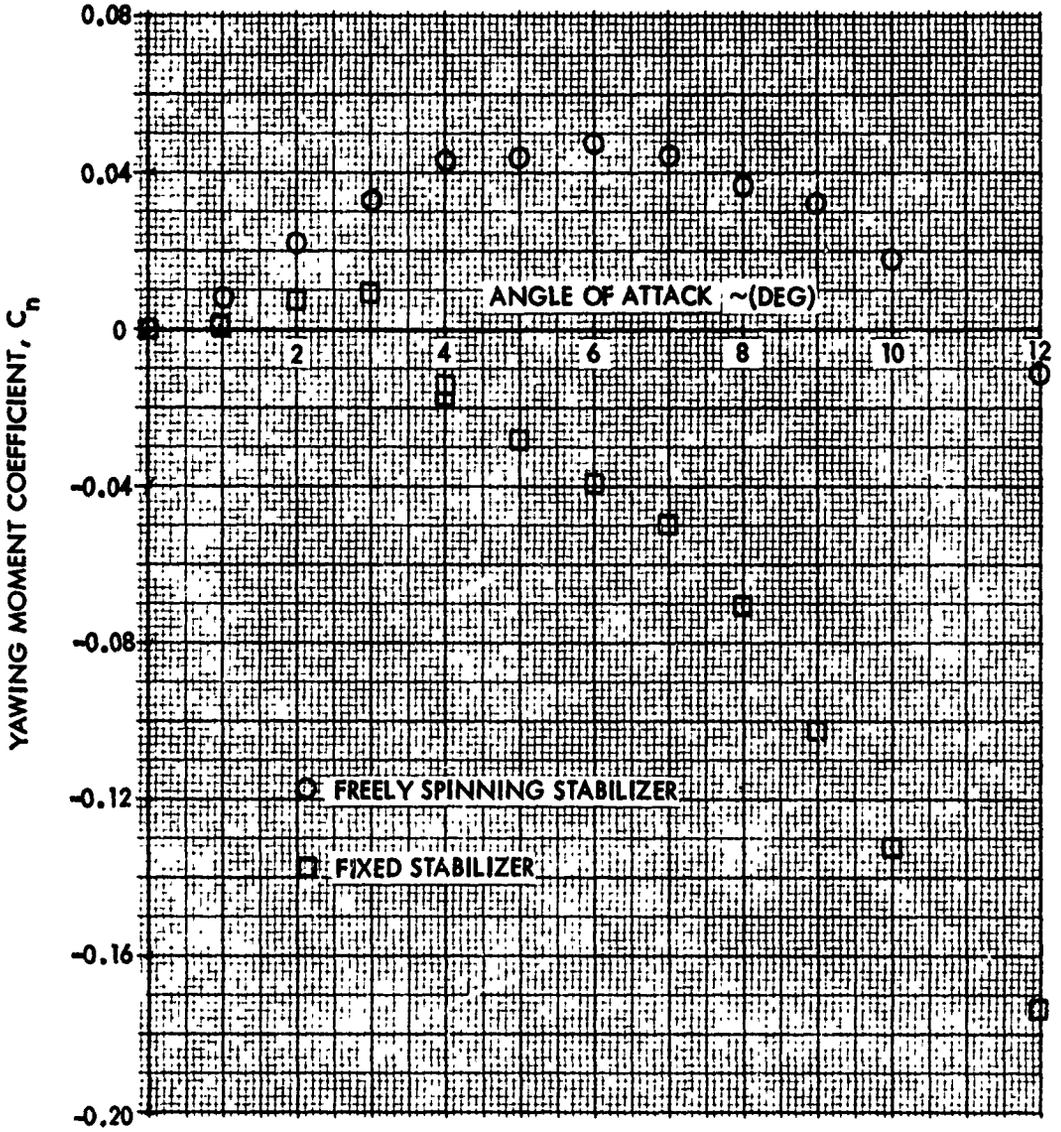

FIG. 120 YAWING MOMENT COEFFICIENT VERSUS ANGLE OF ATTACK FOR THE FIXED AND FREELY SPINNING STABILIZERS AT A FIN CANT OF 5 DEGREES AND A MACH NUMBER 0.84

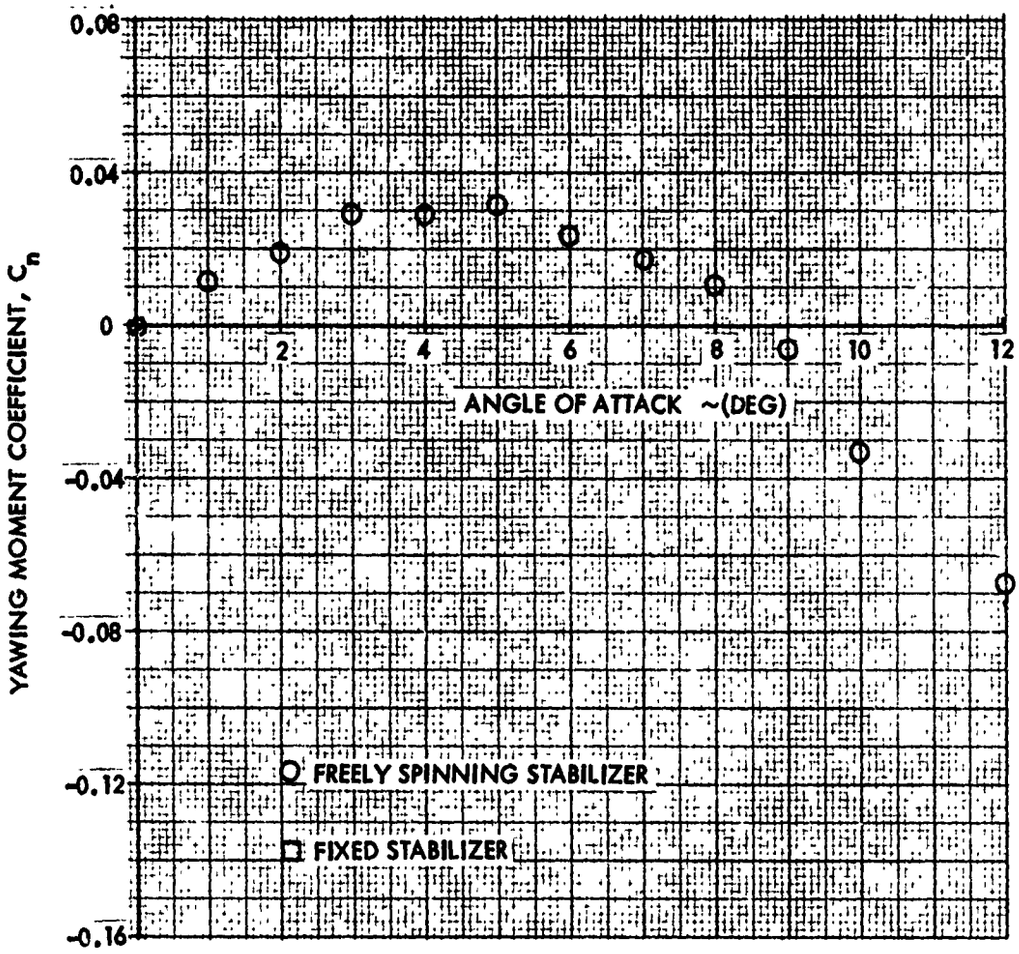

FIG. 121 YAWING MOMENT COEFFICIENT VERSUS ANGLE OF ATTACK FOR THE FIXED AND FREELY SPINNING STABILIZERS AT A FIN CANT OF 5 DEGREES AND A MACH NUMBER 0.89

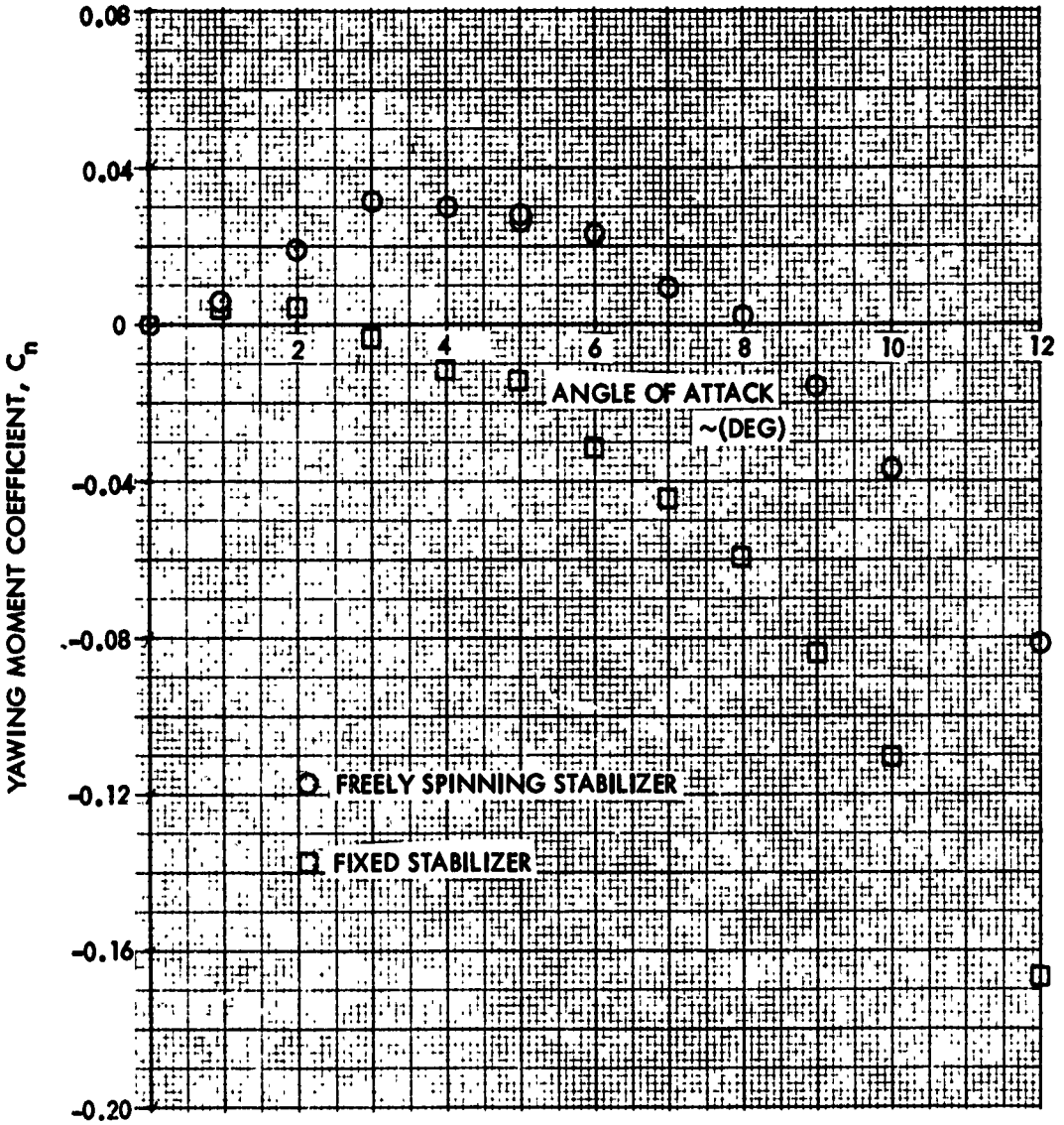

FIG. 122. YAWING MOMENT COEFFICIENT VERSUS ANGLE OF ATTACK FOR THE FIXED AND FREELY SPINNING STABILIZERS AT A FIN CANT OF 5 DEGREES AND A MACH NUMBER 0.94.

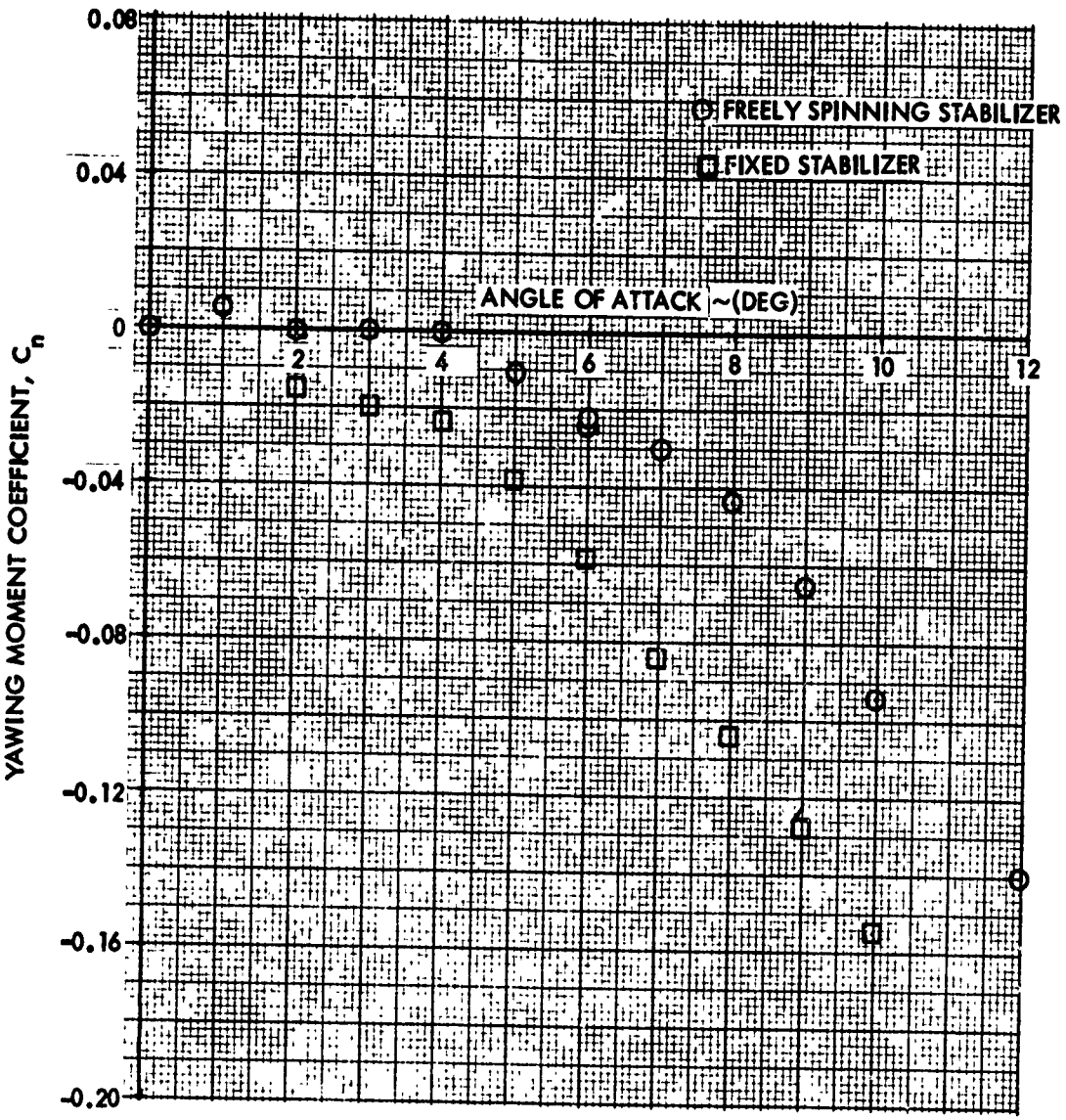

FIG. 123. YAWING MOMENT COEFFICIENT VERSUS ANGLE OF ATTACK FOR THE FIXED AND FREELY SPINNING STABILIZERS AT A FIN CANT OF 5 DEGREES AND A MACH NUMBER 1.11.

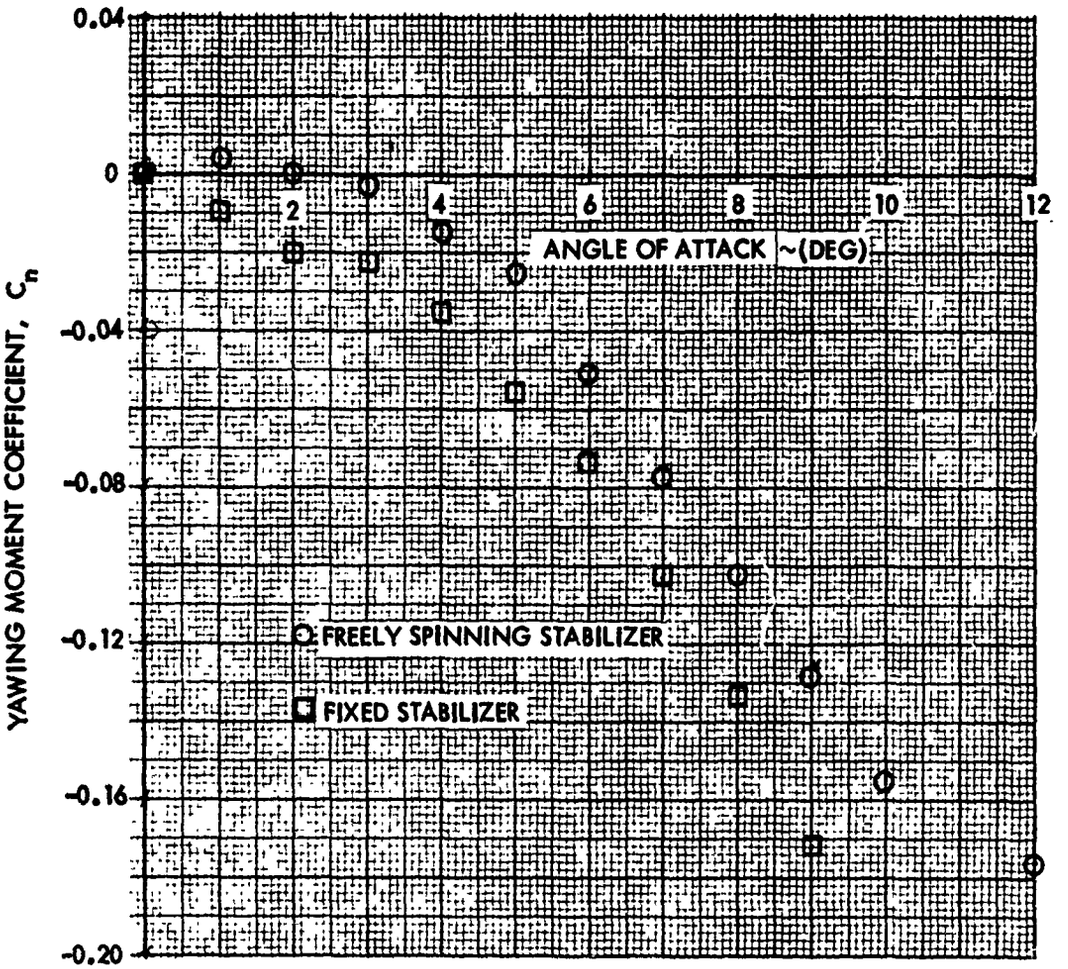

FIG. 124. YAWING MOMENT COEFFICIENT VERSUS ANGLE OF ATTACK FOR THE FIXED AND FREELY SPINNING STABILIZERS AT A FIN CANT OF 5 DEGREES AND A MACH NUMBER 1.19.

APPENDIX A

FLOW ANGULARITY CORRECTIONS TO MAGNUS MEASUREMENTS

The making of Magnus measurements poses a considerable challenge to the aerodynamic experimentalist. The nature of the Magnus effect presents two principal obstacles in the path of systematic and reliable measurements. First, measurements must be made in the presence of model spin and, secondly, the Magnus force is small and acts normal to the angle-of-attack plane. Stated in another way, this second consideration says that the Magnus force must be measured in the presence of an orthogonal force whose magnitude is much larger (about 20 times) than the Magnus force.

The first difficulty can be met only through careful model design construction and fitting to the wind-tunnel balance. The second consideration might be accepted as a balance design requirement setting the relative stiffness of the balance to yaw and pitch loads. However, the relative magnitude and direction of the Magnus and normal loads at least hints that what might appear as a superficial interaction of normal-force and yaw measurements can have a disasterous effect on the quality of the Magnus data.

The interaction of normal force and yaw loads treated in this note will be confined to flow angularities. Briefly stated, if there is an angular resolution between the flow vector and the axis-of-symmetry vector at a nominal angle-of-attack setting of zero, then there will be a nonzero yaw load measurement. In general this angular offset will prevail over the whole angle-of-attack range. In other words, even at angle of attack the true angle between the flow vector and the axis-of-symmetry vector will differ from the nominal angle-of-attack setting. In addition, the actual and nominal angle-of-attack plane will differ in orientation. This is especially important as the normal force is defined in and the Magnus force normal to the angle-of-attack plane. It will be shown subsequently that even though the angle between the nominal and actual angle-of-attack planes may be "small" the effect on the Magnus force can be significant.

It should be pointed out that effects of flow angularity gradients in space will not be considered although gradients along the model can be accounted for in an approximate fashion. Stated alternately, no consideration is given to changes in flow direction at different points in the test section flow field. Attention herein is confined to effects arising from a failure to orient the model along the flow at a nominal angle-of-attack value of zero degrees. While the failure might be attributed to operational error, tunnel flow angularities or even carelessness, such angularity exists in all wind-tunnel Magnus measurements. This angularity is apparent in the existence of non-zero normal and side loads at a nominal zero angle of attack. Actually, it appears that there is little that can be done at this time to align the model perfectly into the flow at zero angle of

attack. In this Appendix balance corrections will be developed to remove the effects of the flow angularity from the Magnus or side-load measurements.

The model is assumed mounted on a conventional axial sting. The axis of symmetry is taken along the "X" axis with the axial direction indicated by the unit vector $\bar{i}$. A conventional right-hand triad is formed by unit vectors $\bar{i}$, $\bar{j}$, $\bar{k}$, with normal force along the negative "Z" axis in the opposite direction of $\bar{k}$ and side forces along the positive "Y" axis in the direction of $\bar{j}$. These axes and vectors may be identified in Figure A-1 below:

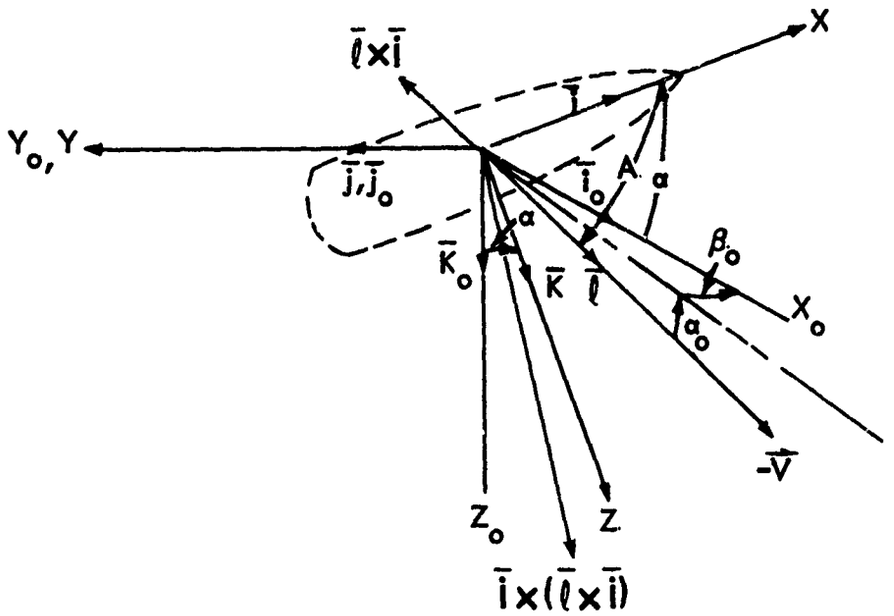

FIG. A-1

It will also be noted that when the configuration is at a nominal angle of attack of zero degrees, the {X,Y,Z} axes are coincident with the $\{X_o,Y_o,Z_o\}$ axes. Rotation in angle of attack, α, is entirely about the Y axis. Further, the velocity vector, $-\bar{V}$, is not assumed coincident with $\bar{i}_o$ but rather has direction angles $\{\alpha_o,\beta_o\}$ with respect to $\bar{i}_o$ as shown in Figure A-1. As a consequence, the true angle of attack, A, is not at any time equal in magnitude to the nominal angle of attack, α. The angle-of-attack plane obviously will not lie in the $\{X_oY_o\}$ plane. The implication of this "tilting" of the angle-of-attack plane will be pointed out subsequently.

The direction of the velocity vector, $-\bar{V}$, is designated by the unit vector, $\bar{\ell}$, which can be written in the $\{\bar{i}_o,\bar{j}_o,\bar{k}_o\}$ system as,

$$\vec{\ell} = (\cos\alpha_o \cos\beta_o)\vec{i}_o + (\cos\alpha_o \sin\beta_o)\vec{j}_o + (\sin\alpha_o)\vec{k}_o \qquad \text{(A-1)}$$

We can write $\bar{\ell}$ in terms of the $\{\bar{i},\bar{j},\bar{k}\}$ system by means of the following transformation

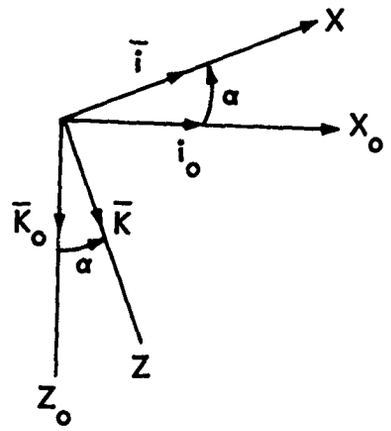

FIG. A-2

where

$$\vec{i}_o = \cos\alpha\,\vec{i} + \sin\alpha\,\vec{k} \qquad \text{(A-2a)}$$

$$\vec{j}_o = \bar{j} \qquad \text{(A-2b)}$$

$$\vec{k}_o = -\sin\alpha\,\vec{i} + \cos\alpha\,\vec{k} \qquad \text{(A-2c)}$$

Inserting Equation (A-1) into Equation (A-2) gives

$$\vec{\ell} = [\cos\alpha_o \cos\beta_o \cos\alpha - \sin\alpha_o \sin\alpha]\vec{i} + [\cos\alpha_o \sin\beta_o]\vec{j} + [\cos\alpha_o \cos\beta_o \sin\alpha + \sin\alpha_o \cos\alpha]\vec{k} \qquad \text{(A-3)}$$

It was pointed out above that the assumed angle-of-attack plane $\{i,i_o\}$ and the actual angle-of-attack plane $\{\bar{i},\bar{\ell}\}$ are not coincidental if β_o is not zero. By definition the Magnus force must lie <u>normal to</u> the angle-of-attack plane and the normal force must lie <u>in</u> the angle-of-attack plane. The wind-tunnel balance will resolve the aerodynamic

load along the $\{\bar{i},\bar{j},\bar{k}\}$ vectors; while this in itself is not incorrect, it is incorrect to identify the load along the $\bar{j}$ axis as the Magnus load.

A unit vector normal to the angle-of-attack plane may be given as

$$a\bar{\eta} = \bar{\ell} \times \bar{i} \tag{A-4}$$

where a is the magnitude of $\bar{\ell} \times \bar{i}$. Thus,

$$a\vec{\eta} = [\cos\alpha_o \sin\beta_o](-\vec{k}) + [\cos\alpha_o \cos\beta_o \sin\alpha + \sin\alpha_o \cos\alpha]\vec{j} \tag{A-5}$$

where it immediately follows that

$$a = \sqrt{[\cos\alpha_o \sin\beta_o]^2 + [\cos\alpha_o \cos\beta_o \sin\alpha + \sin\alpha_o \cos\alpha]^2} \tag{A-6}$$

or finally,

$$\vec{\eta} = \frac{1}{a}\left[(\cos\alpha_o \cos\beta_o \sin\alpha + \sin\alpha_o \cos\alpha)\vec{j} - (\cos\alpha_o \sin\beta_o)\vec{k}\right] \tag{A-7a}$$

Note that if β_o equals zero, Equation (A-7a) becomes

$$\vec{\eta} = \vec{j} \tag{A-7b}$$

It is also necessary to have a vector in the angle-of-attack plane and normal to both $\bar{i}$ and $\bar{\eta}$. This unit vector, $\bar{\xi}$, will be determined from

$$\begin{aligned} b\vec{\xi} = \vec{i} \times \vec{\eta} &= \vec{i} \times (\vec{\ell} \times \vec{i}) = \vec{\ell}(\vec{i}\cdot\vec{i}) - \vec{i}(\vec{\ell}\cdot\vec{i}) \\ &= \vec{\ell} - \vec{i}(\vec{\ell} \times \vec{i}) \end{aligned} \tag{A-8}$$

From Equation (A-3) we immediately have

$$b\vec{\xi} = [\cos\alpha_o \sin\beta_o]\vec{j} + [\cos\alpha_o \cos\beta_o \sin\alpha + \sin\alpha_o \cos\alpha]\vec{k} \tag{A-9}$$

Obviously, from Equation (A-6), b = a; thus Equation (A-9) becomes,

$$\vec{\xi} = \frac{1}{a}\left[(\mathrm{Cos}\alpha_o \mathrm{Sin}\beta_o)\vec{j} + (\mathrm{Cos}\alpha_o \mathrm{Cos}\beta_o \mathrm{Sin}\alpha + \mathrm{Sin}\alpha_o \mathrm{Cos}\alpha)\vec{k}\right] \quad \text{(A-10a)}$$

Again, as might be expected, if β_o equals zero,

$$\vec{\xi} = \vec{k} \quad \text{(A-10b)}$$

If Figure A-1 is examined it may readily be seen that the nominal angle of attack, α, is not the actual angle of attack, A. Since the angle of attack is defined as the angle between the axis of symmetry and the velocity vector, it is necessary to have a relationship between α and A. This relationship is easily obtained by first noting that,

$$\mathrm{Sin}\,A = |\vec{i} \times \vec{\ell}| = |a||\bar{\eta}| = a \quad \text{(A-11a)}$$

and

$$\mathrm{Cos}\,A = \vec{i} \cdot \vec{\ell} \quad \text{(A-11b)}$$

Since nearly all computer programs have an Arc-Tan routine, an expression is sought for Tan A. Dividing Equation (A-11a) by (A-11b) and making use of Equations (A-6) in the numerator and Equation (A-3) in the denominator results in the following expression:

$$A = \mathrm{Tan}^{-1}\left\{\frac{\left\langle[\mathrm{Cos}\alpha_o \mathrm{Cos}\beta_o \mathrm{Sin}\alpha + \mathrm{Sin}\alpha_o \mathrm{Cos}\alpha]^2 + [\mathrm{Cos}\alpha_o \mathrm{Sin}\beta_o]^2\right\rangle^{\frac{1}{2}}}{[\mathrm{Cos}\alpha_o \mathrm{Cos}\beta_o \mathrm{Cos}\alpha - \mathrm{Sin}\alpha_o \mathrm{Sin}\alpha]}\right. \quad \text{(A-12)}$$

It might be of some interest to examine the above relationship where $\alpha_o << \alpha$ and $\beta_o << \alpha$. From Equation (A-6) the expression for a becomes:

$$\begin{aligned} a &= \left\{\beta_o^2 + (\mathrm{Sin}\alpha + \alpha_o \mathrm{Cos}\alpha)^2\right\}^{\frac{1}{2}} \\ &= \left\{\beta_o^2 + \mathrm{Sin}^2\alpha + 2\alpha_o \mathrm{Sin}\alpha \mathrm{Cos}\alpha + \alpha_o^2 \mathrm{Cos}^2\alpha\right\}^{\frac{1}{2}} \end{aligned} \quad \text{(A-13)}$$

Within the above restrictions on the size of α_o and β_o relative to α, Equation (A-13) might be rewritten using the following:

$$2\alpha_o \sin\alpha \cos\alpha = \alpha_o \sin 2\alpha > \alpha_o^2 \cos^2\alpha, \beta_o^2$$

Equation (A-13) can now be further reduced as:

$$\begin{aligned} a &\cong (\sin^2\alpha)^{\frac{1}{2}} + \tfrac{1}{2}(\sin^2\alpha)^{-\frac{1}{2}}(\alpha_o \sin 2\alpha) \\ &\cong \sin\alpha + \alpha_o \cos\alpha \end{aligned} \qquad \text{(A-14)}$$

Equation (A-12) now becomes:

$$A = \tan^{-1}\left[\frac{\sin\alpha + \alpha_o \cos\alpha}{\cos\alpha - \alpha_o \sin\alpha}\right] \qquad \text{(A-15)}$$

If α_o is equal to zero (and β_o has been ignored so it is effectively "zero") Equation (A-15) becomes

$$A = \tan^{-1}\left\{\frac{\sin\alpha}{\cos\alpha}\right\} = \alpha \qquad \text{(A-16)}$$

Of course, Equation (A-16) is nothing more than a check of Equation (A-12), showing that if the flow angularity variables $\{\alpha_o, \beta_o\}$ become small and then negligible the true and nominal angles of attack A and α, respectively, become equal. Also Equation (A-15) shows (as one might expect) that for large angles of attack, the effect of α_o is second order and the effect of β_o is third order. Actually Equation (A-15) is not of much value as it cannot be used where the angle of attack, α, is of the same order as $\{\alpha_o, \beta_o\}$.

Two orthogonal axis systems have been introduced: $(\bar{i},\bar{j},\bar{k})$ and $(\bar{i},\bar{\eta},\bar{\xi})$; the first being the system into which the aerodynamic force vector is resolved by the wind-tunnel balance; the second being the system in which the aerodynamic loads are defined. For example, the Magnus load is defined normal to the angle-of-attack plane, i.e., along $\bar{\eta}$ and not along $\bar{j}$. Similarly, the normal force lies in the angle-of-attack plane (along negative $\bar{\xi}$) and not along negative $\bar{k}$. Relationships will now be developed between loads measured in these two systems.

The aerodynamic load vector, $\bar{F}$, can be expressed in both the $(\bar{i},\bar{j},\bar{k})$ and $(\bar{i},\bar{\eta},\bar{\xi})$ systems as

$$\vec{F} = G_x \vec{i} + G_y \vec{\eta} + G_z \vec{\xi} = F_x \vec{i} + F_y \vec{j} + F_z \vec{k} \qquad \text{(A-17a)}$$

Through the use of Equations (A-7a) and (A-10a) Equation (17) above may be rewritten as:

$$G_x \vec{i} + \frac{G_y}{a}\left[(\cos\alpha_o \cos\beta_o \sin\alpha + \sin\alpha_o \cos\alpha)\vec{j} - (\cos\alpha_o \sin\beta_o)\vec{k}\right]$$

$$+ \frac{G_z}{a}\left[(\cos\alpha_o \sin\beta_o)\vec{j} + (\cos\alpha_o \cos\beta_o \sin\alpha + \sin\alpha_o \cos\alpha)\vec{k}\right] \quad \text{(A-17b)}$$

$$= F_x \vec{i} + F_y \vec{j} + F_z \vec{k}$$

Equating the components in the above vector equation gives

$$F_x = G_x \quad \text{(A-18a)}$$

$$F_y = \frac{G_y}{a}\left[\cos\alpha_o \cos\beta_o \sin\alpha + \sin\alpha_o \cos\alpha\right] + \frac{G_z}{a}\left[\cos\alpha_o \sin\beta_o\right] \quad \text{(A-18b)}$$

$$F_z = -\frac{G_y}{a}\left[\cos\alpha_o \sin\beta_o\right] + \frac{G_z}{a}\left[\cos\alpha_o \cos\beta_o \sin\alpha + \sin\alpha_o \cos\alpha\right] \quad \text{(A-18c)}$$

Since it is of greater interest to express $\{G_x, G_y, G_z\}$ as functions of $\{F_x, F_y, F_z\}$, it is necessary to solve Equations (A-18) for $\{G_x, G_y, G_z\}$. It is immediately obvious that G_x equals F_x, however, such a relationship is of no practical use since axial loads are not usually measured in a Magnus test anyway. Defining the following relationships,

$$h = \cos\alpha_o \cos\beta_o \sin\alpha + \sin\alpha_o \cos\alpha \quad \text{(A-19a)}$$

$$k = \cos\alpha_o \sin\beta_o \quad \text{(A-19b)}$$

Equations (A-18b) and (A-18c) become:

$$a F_y = G_y h + G_z k \quad \text{(A-20a)}$$

$$a F_z = -G_y k + G_z h \quad \text{(A-20b)}$$

From Equation (A-6) it is obvious that

$$a^2 = h^2 + k^2 \tag{A-21}$$

Using Cramer's rule, Equations (A-20) can be rewritten as,

$$G_y = a \frac{\begin{vmatrix} F_y & k \\ F_z & h \end{vmatrix}}{\begin{vmatrix} h & k \\ -k & h \end{vmatrix}} = \frac{\begin{vmatrix} F_y & k \\ F_z & h \end{vmatrix}}{a} \tag{A-22a}$$

$$G_z = a \frac{\begin{vmatrix} h & F_y \\ -k & F_z \end{vmatrix}}{\begin{vmatrix} h & k \\ -k & h \end{vmatrix}} = \frac{\begin{vmatrix} h & F_y \\ -k & F_z \end{vmatrix}}{a} \tag{A-22b}$$

The above expressions become,

$$G_y = \frac{F_y h - F_z k}{a} \tag{A-23a}$$

$$G_z = \frac{F_z h + F_y k}{a} \tag{A-23b}$$

Equations (A-23) may now be written in coefficient form by replacing G_y, G_z, F_y, F_z by C_y^C, $-C_N^C$, C_y and $-C_N$, respectively. If this is done Equations (A-23) become:

$$C_y^C = \frac{C_y h + C_N k}{a} \tag{A-24a}$$

$$C_N^C = \frac{C_N h - C_y k}{a} \tag{A-24b}$$

The normal-force and side-force coefficients, C_N and C_y, are measured at a nominal angle of attack, α. Once these quantities are available it remains only to obtain the flow angularity variables, α_o and β_o. Before doing this it is probably of some value to point out that Equation (A-24b) is not of much practical value. It would be

expected that the corrected value of C_N, that is C_N^c, would not differ much from the measured value. The reason is that for small values of α_o and β_o, the quantity K would be nearly equal to β_o (see Eq. (A-19b)) and h no less than the order of α_o (see Eq. (A-19a)). Since the magnitude of C_y is an order of magnitude less than C_N (measured at the same angle of attack), the correction to C_N would be negligibly small. Therefore, in considering corrections to measured data, attention will be confined to the side-force equation, Equation (A-24a).

Next, consideration should be given to corrections to the moment measurements. Moment correction equations, analogous to Equations (A-24), can be written quite easily by returning to Equations (A-23). The force components $\{F_x,F_y,F_z\}$ can be thought of as the components of the aerodynamic moment resolved in the wind-tunnel balance frame, $\{\bar{i},\bar{j},\bar{k}\}$. The corrected force components $\{G_x,G_y,G_z\}$ are then the resolution of the aerodynamic moment in the $\{\bar{i},\bar{\eta},\bar{\xi}\}$ frame. The moment coefficients are introduced by replacing G_y,G_z,F_y and F_z by C_m^c, C_n^c, C_m and C_n, respectively, to get:

$$C_m^c = \frac{C_m h - C_n K}{a} \qquad \text{(A-25a)}$$

$$C_n^c = \frac{C_n h + C_m k}{a} \qquad \text{(A-25b)}$$

Using arguments similar to those offered in the case of the normal-force coefficient, the corrections to the pitching moment (Eq. (A-25a)) can be ignored. The correction equations will then be Equation (A-24a) for the side force and Equation (A-25b) for the yawing moment.

Now for the above correction equations to be of any value, there must be some means for measuring the flow angularity angles α_o and β_o. These quantities are indicated by a nonzero load measurement at a nominal zero angle of attack. In the sketch below the model is indicated to be at a nominal angle of attack of zero.

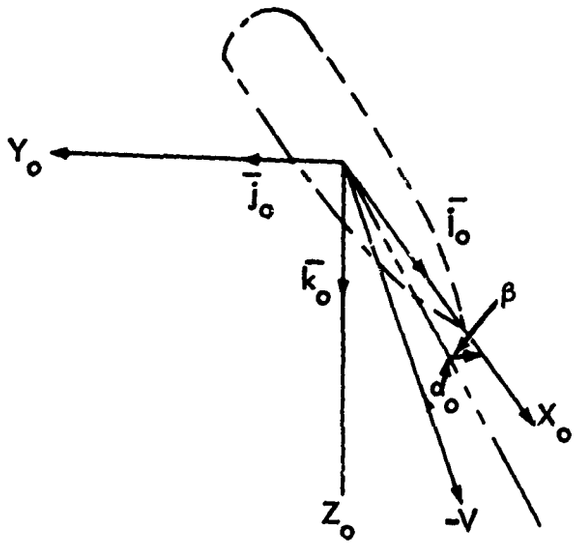

FIG. A-3

Since α_o and β_o are small, the situation seen when "looking in" along the Y_o axis along the negative direction is approximately that given in the following sketch:

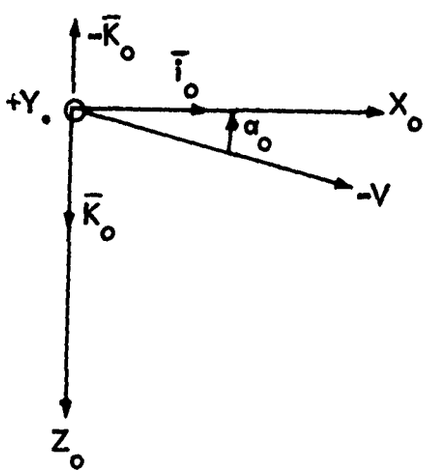

FIG. A-4

Clearly

$$C_{N_0} \cong C_{N_\alpha} \alpha$$

or

$$\alpha_0 \cong C_{N_0} / C_{N_\alpha} \qquad \text{(A-26)}$$

where C_{N_α}, the normal-force derivative at $\alpha = 0$, may be obtained in an approximate manner as

$$C_{N_\alpha} \cong [\Delta C_N / \Delta \alpha] 57.3 \qquad \text{(A-27)}$$

In this note the use of the above expression will be implemented by obtaining C_N at two and zero degrees to give

$$C_{N_\alpha} \cong \frac{(C_{N_2} - C_{N_0})}{2} 57.3 \qquad \text{(A-28)}$$

The situation seen "looking in" along the Z_o axis in the positive direction is approximately that given in the following sketch.

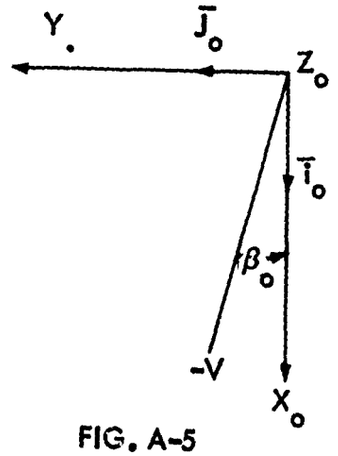

FIG. A-5

For a positive value of C_{N_α} and a positive sideslip angle, β_o, the analogy of Equation (A-26) may be written as

$$\beta_o = - C_{Y_0} / C_{N_\alpha} \qquad \text{(A-29)}$$

APPENDIX B

SPIN RATE RELATIONSHIPS

If the spinning motion of a free-fall store is assumed to have a single degree of freedom, the angular momentum in spin can be related to the applied moments as,

$$I_x \frac{dp}{dt} = \left[C_{\ell_p} \frac{pd}{2V} + C_{\ell_\delta} \delta\right] QSd \qquad \text{(B-1)}$$

where C_{ℓ_p} is the roll-damping moment derivative and C_{ℓ_δ} is the rolling moment due to fin cant. Equation (B-1) can be rearranged by replacing the spin rate, p, by the reduced spin rate, $\tilde{p}$, to give:

$$\frac{d\tilde{p}}{dt} = \left[C_{\ell_p} \tilde{p} + C_{\ell_\delta} \delta\right] \frac{QSd^2}{2VI_x} \qquad \text{(B-2)}$$

The unit of the independent variable time may be changed from seconds to the time for passage of one bomb length or

$$t/(\ell/V) = t^*$$

Equation (B-2) may now be rewritten replacing t by t*.

$$\frac{d\tilde{p}}{dt^*} = \left[C_{\ell_p} \tilde{p} + C_{\ell_\delta} \delta\right] \frac{QSd^2\ell}{2I_x V} \qquad \text{(B-3)}$$

with the axial moment of inertia replaced by the nondimensional radius of gyration $K_x = \sqrt{I_x/md^2}$ and the bomb "average" density, ρ_B, equal to $m/S\ell$, the second term on the right of Equation (B-3) becomes,

$$\frac{QSd^2\ell}{2I_x V} = \frac{\rho S \ell d^2 V^2}{4md^2 k_x^2 V^2} = \left(\frac{\rho}{\rho_B}\right)\left(\frac{1}{4k_x^2}\right)$$

Equation (B-3) now becomes:

$$\frac{d\tilde{p}}{dt^*} = \left[\tilde{p} + \frac{C_{\ell_\delta}\delta}{C_{\ell_p}}\right]\left(\frac{\rho}{\rho_B}\right)\left(\frac{C_{\ell_p}}{4K_x^2}\right) = \frac{d}{dt}\left[\tilde{p} + \frac{C_{\ell_\delta}\delta}{C_{\ell_p}}\right] \qquad \text{(B-4)}$$

where $C_{\ell_\delta}\delta/C_{\ell_p}$ may be brought inside the derivative since it is a constant. Integrating Equation (B-4) gives,

$$\left(\tilde{p} - \tilde{p}_s\right) = \left(\tilde{p}_o - \tilde{p}_s\right)\exp\left\{\left(\frac{\rho}{\rho_B}\right)\left(\frac{C_{\ell_p}}{4K_x^2}\right)t^*\right\} \qquad \text{(B-5)}$$

where the steady-state spin rate which occurs when $t^* \to \infty$ might be written as

$$\tilde{p}_\delta = -\frac{C_{\ell_\delta}\delta}{C_{\ell_p}} \qquad \text{(B-6)}$$